

INVESTIGATION OF INHIBITION, FILAMENT FORMATION, AND INTER-
DOMAIN AMMONIA CHANNELLING
OF CTP SYNTHASE

by

Gregory D. McCluskey

Submitted in partial fulfilment of the requirements
for the degree of Doctor of Philosophy

at

Dalhousie University
Halifax, Nova Scotia
March 2018

© Copyright by Gregory D. McCluskey, 2018

The Universe is under no obligation to make sense to you – Neil deGrasse Tyson

and neither is CTP Synthase – Gregory D. McCluskey

TABLE OF CONTENTS

LIST OF TABLES	viii
LIST OF FIGURES.....	ix
LIST OF SCHEMES	xiii
ABSTRACT.....	xiv
LIST OF ABBREVIATIONS USED.....	xv
ACKNOWLEDGEMENTS.....	xx
CHAPTER 1 INTRODUCTION	1
1.1 CYTIDINE-5'-TRIPHOSPHATE.....	1
1.2 GLUTAMINE AMIDOTRANSFERASES.....	1
1.3 CTP SYNTHASE OVERVIEW	5
1.4 CTPS MECHANISM.....	6
1.4.1 Glutamine Hydrolysis.....	6
1.4.2 Ammonia Tunnel	10
1.4.3 Amidoligase Reaction	15
1.5 HALF-OF-THE-SITES REACTIVITY.....	18
1.6 ROLE OF NTP LIGANDS	20
1.5.1 GTP	20
1.5.2 UTP and ATP.....	20
1.5.3 CTP.....	23
1.7 CTPS OLIGOMERIZATION AND FILAMENT FORMATION.....	24
1.7.1 CTPS Filaments in Prokaryotes.....	24
1.7.2 CTPS Filaments in Eukaryotes.....	25
1.8 POST-TRANSLATIONAL MODIFICATIONS OF CTP SYNTHASE.....	29
1.9 CTPS IN HUMAN HEALTH	31
1.10 PROJECT GOALS	35
CHAPTER 2 GENERAL METHODS.....	37
2.1 GENERAL	37
2.2 SITE-DIRECTED MUTAGENESIS	37
2.3 GENE EXPRESSION AND ENZYME PURIFICATION.....	39
2.4 UV ASSAY OF CTP GENERATION.....	39

2.5 REVERSED PHASE-HIGH PERFORMANCE LIQUID CHROMATOGRAPHY ASSAY OF GLN HYDROLYSIS	43
2.6 IC ₅₀ DETERMINATIONS	44
2.7 CIRCULAR DICHROISM SPECTROMETRY	44
2.8 GEL FILTRATION-HIGH PERFORMANCE LIQUID CHROMATOGRAPHY	44
CHAPTER 3 INHIBITION OF CTP SYNTHASE BY	
GEMCITABINE-5'-TRIPHOSPHATE	46
3.1 INTRODUCTION	46
3.2 EXPERIMENTAL	48
3.2.1 General	48
3.2.2 Assay of CTP Production	48
3.2.3 Inhibition of CTPS by dF-dCTP	50
3.2.4 <i>In Silico</i> Docking of dF-dCTP	51
3.2.5 dF-dUTP HPLC Assay	51
3.2.6 dF-dUTP UV Spectrophotometric Assay	52
3.2.7 Product Analysis for Enzymatically Generated dF-dCTP	52
3.2.8 Circular Dichroism	54
3.3 RESULTS	54
3.3.1 Inhibition of CTP Synthase by dF-dCTP	54
3.3.2 Glu 149 Substitutions	55
3.3.3 Regioisomeric Requirements for Cytidine-Dependent Inhibition	60
3.3.4 CTPS-Catalyzed Conversion of dF-dUTP into dF-dCTP	65
3.4 DISCUSSION	71
3.4.1 Potent Inhibition of CTPS by dF-dCTP	71
3.4.2 Structural Considerations for dF-dCTP Inhibition	72
3.4.3 CTPS-Catalyzed Conversion of dF-dUTP into dF-dCTP	74
3.4.4 Conclusions	78
CHAPTER 4 GEMCITABINE-5'-TRIPHOSPHATE INDUCES CTP SYNTHASE	
FILAMENT FORMATION	81
4.1 INTRODUCTION	81
4.2 EXPERIMENTAL	83

4.2.1 General	83
4.2.2 Transmission Electron Microscopy.....	83
4.2.3 Dynamic Light Scattering.....	83
4.2.4 Calculations	84
4.2.5 Effects of UTP on Filament Assembly.....	85
4.2.6 Kinetic Characterization of <i>Ec</i> CTPS Variants.....	86
4.2.7 GF-HPLC.....	87
4.2.8 Circular Dichroism.....	87
4.3 RESULTS	87
4.3.1 Effects of dF-dCTP on <i>Ec</i> CTPS Filaments	87
4.3.2 Effects of UTP on <i>Ec</i> CTPS Filaments	94
4.3.3 Structural Determinants for CTP- and dF-dCTP-Induced <i>Ec</i> CTPS Filament Formation	101
4.4 DISCUSSION	108
4.4.1 dF-dCTP Induces <i>Ec</i> CTPS Filament Formation.....	108
4.4.2 UTP Prevents Filament Formation and Disassembles Pre-Formed Filaments.....	111
4.4.3 Sensing the Cytosine Ring is Important for Filament Formation.....	113
4.4.4 Conclusions.....	120
CHAPTER 5 INVESTIGATION OF CTP SYNTHASE NH ₃ CHANNELLING	121
5.1 INTRODUCTION.....	121
5.2 EXPERIMENTAL	122
5.2.1 General	122
5.2.2 Assay of CTP production	122
5.2.3 Coupling Ratio Determinations	124
5.2.4 Assay of <i>N</i> ⁴ -OH-CTP Production	125
5.2.5 Derivatization of <i>Ec</i> CTPS with 6-Diazo-5-oxo-L-norleucine (DON).....	126
5.2.6 Dynamic Light Scattering.....	127
5.2.7 Gel Filtration-High Performance Liquid Chromatography	127
5.2.8 Tunnel Modelling and Molecular Dynamics (MD) Simulations.....	128
5.2.9 Circular Dichroism.....	129

5.3 RESULTS	129
5.3.1 NH ₃ -dependent CTP Production.....	131
5.3.2 Gln-Dependent CTP Production.....	133
5.3.3 UTP- and ATP-Dependent kinetics	135
5.3.4 GATase Activity and Coupling Efficiencies.....	135
5.3.5 Utilization of NH ₂ OH.....	140
5.3.6 Effects of Acyl-Enzyme Formation.....	142
5.3.7 Effects of Salt.....	147
5.3.8 Effects of Val 60 Substitutions on Oligomerization	149
5.3.9 Molecular Dynamics Simulations.....	153
5.4 DISCUSSION	157
5.4.1 V60A and V60C.....	162
5.4.2 V60D and V60W	163
5.4.3 V60F.....	165
5.4.4 DON-V60F	168
5.4.5 Conclusions.....	170
CHAPTER 6 ANALYSIS OF THE UTP SITE.....	173
6.1 INTRODUCTION.....	173
6.2 EXPERIMENTAL	175
6.2.1 General	175
6.2.2 Analysis of N ⁴ -OH-CTP Production	175
6.2.3 Analysis of GATase activity.....	175
6.2.4 Inhibition by ΨTP	176
6.3 RESULTS	176
6.3.1 H57A	176
6.3.2 Inhibition of <i>Ec</i> CTPS by ΨTP.....	182
6.4 DISCUSSION	185
CHAPTER 7 CONCLUSIONS	190
7.1 GEMCITABINE-5'-TRIPHOSPHATE AND CTP SYNTHASE.....	190
7.2 NH ₃ CHANNELLING	192
7.3 FUTURE WORK.....	194

REFERENCES.....	197
APPENDIX A.....	214
APPENDIX B.....	239

LIST OF TABLES

Table 2.1. Oligodeoxynucleotide primers used for site-directed mutagenesis.	38
Table 2.2. Saturating concentrations of <i>Ec</i> CTPS substrates and activators (in mM) used to determine kinetic parameters.	42
Table 3.1. Kinetic parameters for the inhibition of UTP-dependent CTP production by dF-dCTP	57
Table 3.2. Kinetic parameters for wild-type, E149D, and E149Q CTP synthases	62
Table 3.3. IC ₅₀ values for the inhibition of CTPS-catalyzed, Gln-dependent CTP production by CTP and analogues.	64
Table 3.4. Kinetic parameters for CTPS-catalyzed conversion of dF-dUTP into dF-dCTP	70
Table 4.1. Length and diffusive properties for wild-type and mutant <i>Ec</i> CTPSs equilibrated with ATP (control), and CTP or dF-dCTP.....	93
Table 4.2. Kinetic parameters for wild-type and mutant <i>Ec</i> CTPS variants.....	95
Table 4.3. IC ₅₀ values for the inhibition of wild-type and mutant <i>Ec</i> CTPS variants by CTP and dF-dCTP.....	96
Table 5.1. Relative amino acid probabilities for position 60 (<i>E. coli</i> numbering).....	132
Table 5.2. Relative amino acid probabilities for position 57 (<i>E. coli</i> numbering).....	132
Table 5.3. Kinetic parameters for exogenous and nascent NH ₃ -dependent catalysis of wild-type and Val 60-substituted <i>Ec</i> CTPS variants.....	134
Table 5.4. Kinetic parameters for NTP-dependent catalysis of wild-type and Val 60-substituted <i>Ec</i> CTPS variants.....	136
Table 5.5. Coupling efficiencies for wild-type and Val 60-substituted <i>Ec</i> CTPSs at saturating ligand concentrations.....	138
Table 5.6. Coupling efficiencies for V60F <i>Ec</i> CTPS at non-saturating ligand concentrations.....	139
Table 6.1. Kinetic parameters for wild-type and H57A <i>Ec</i> CTPS variants.....	179

LIST OF FIGURES

Figure 1.1. A general reaction mechanism for ADP-forming Class-I (triad) GATase family enzymes.....	3
Figure 1.2. 3D superposition of GATases highlighting structural features of the invariant core.....	4
Figure 1.3. Comparison between CTPS-catalyzed Gln hydrolysis (A) and alkylation by DON (B).....	8
Figure 1.4. Structural features of GATase domains from CTPS and other related enzymes.....	9
Figure 1.5. Structural features of the NH ₃ tunnels from five structurally-characterized CTPSs.....	12
Figure 1.6. Two possible orders for the amidoligase mechanism.....	16
Figure 1.7. Positional isotope exchange experiment with CTPS.....	17
Figure 1.8. Two models for half-of-the-sites reactivity in CTPS.....	19
Figure 1.9. View of the synthase NTP-binding cleft.....	22
Figure 1.10. Partial sequence alignment for some structurally- and biochemically-characterized CTPS homologues.....	28
Figure 1.11. Sequence and structural comparison of <i>Hs</i> CTPS1 and <i>Hs</i> CTPS2.....	32
Figure 1.12. Structures for small-molecule CTPS inhibitors.....	34
Figure 2.1. SDS-PAGE analysis of wild-type and mutant <i>Ec</i> CTPS variants.....	40
Figure 3.1. Structural comparison of <i>E. coli</i> and human CTP synthases.....	49
Figure 3.2. UV characterization of the conversion of dF-dUTP to dF-dCTP.....	53
Figure 3.3. Inhibition of UTP-dependent CTP formation by dF-dCTP.....	56
Figure 3.4. Protein sequence alignment and the CTP binding site.....	59
Figure 3.5. CD analysis of CTPS variants.....	61
Figure 3.6. Inhibition studies for E149D using increasing amounts of CTP.....	63
Figure 3.7. Steady-state progress curves for wild-type (A) and E149D (B) CTPS-catalyzed conversion of dF-dUTP to dF-dCTP.....	66
Figure 3.8. ESI-MS analysis of the nucleoside diphosphate species present in the E149D <i>Ec</i> CTPS reaction mixture, when dF-dUTP was employed as a substrate.....	67

Figure 3.9. INEPT proton decoupled ¹⁵ N-NMR spectrum of the E149D-catalyzed conversion of dF-dUTP to dF-dCTP (solvent = DMSO-d ₆).	68
Figure 3.10. RP-HPLC chromatograms showing wild-type CTPS-catalyzed conversion of dF-dUTP to dF-dCTP.	69
Figure 3.11. <i>Ec</i> CTPS docked with dF-dCTP in the C3'- <i>endo</i> conformation (yellow sticks) super-positioned with the C2'- <i>endo</i> conformer (cyan sticks).	75
Figure 3.12. Proposed model for gemcitabine metabolism.	79
Figure 4.1. Detection of wild-type <i>Ec</i> CTPS filaments by TEM and DLS.	89
Figure 4.2. Representative transmission electron micrograph of <i>Ec</i> CTPS aggregates in the absence of ligands.	90
Figure 4.3. GF-HPLC analysis of wild-type (A), E149D (B), F227A (C), and F227L (D) <i>Ec</i> CTPS variants.	91
Figure 4.4. ATP and UTP limit the large-scale aggregation of wild-type <i>Ec</i> CTPS.	92
Figure 4.5. Inhibition of filament formation by UTP.	98
Figure 4.6. UTP-dependent disassembly of <i>Ec</i> CTPS filaments.	99
Figure 4.7. Dilution by assay buffer does not cause <i>Ec</i> CTPS filament disassembly.	100
Figure 4.8. Detection of E149D <i>Ec</i> CTPS filaments by TEM and DLS.	102
Figure 4.9. Circular dichroism spectra for wild-type (blue), F227A (red), F227L (green) CTPS variants.	104
Figure 4.10. Detection of F227A <i>Ec</i> CTPS filaments by TEM and DLS.	106
Figure 4.11. Detection of F227L <i>Ec</i> CTPS filaments by TEM and DLS.	107
Figure 4.12. Potential mechanisms for UTP-dependent <i>Ec</i> CTPS filament disassembly.	114
Figure 4.13. Putative role for Phe 227.	116
Figure 4.14. Protein sequence alignment for structurally characterized CTP synthases.	118
Figure 5.1. Partial sequence alignment of some biochemically characterized CTPSs.	123
Figure 5.2. Catalytic mechanism and mutation strategy for inter-domain NH ₃ channelling.	130

Figure 5.3. CD analysis of Val 60 <i>Ec</i> CTPS variants.....	141
Figure 5.4. Competition between nascent NH ₃ and NH ₂ OH and the activating effects of the GATase machinery on V60F.....	144
Figure 5.5. Effects of GTP on NH ₃ -dependent CTP production catalyzed by <i>Ec</i> CTPS variants.....	146
Figure 5.6. Inhibition of Gln-dependent CTP production by salts.....	148
Figure 5.7. DLS results for Val 60 variants.....	150
Figure 5.8. GF-HPLC analysis of wild-type and Val 60 <i>Ec</i> CTPS variants.....	152
Figure 5.9. Structural model of the inter-domain NH ₃ tunnel of wild-type and V60F <i>Ec</i> CTPS variants.....	155
Figure 5.10. Surface model for the V60F homology model before and after 10 ns simulation.....	156
Figure 5.11. Snapshots of simulated wild-type and V60F <i>Ec</i> CTPS variants.....	159
Figure 5.12. Distance between Val 60 (wild-type, green) or Phe 60 (V60F, blue) and His 57.....	160
Figure 5.13. Effects of Val 60 mutation on <i>Ec</i> CTPS enzymatic properties.....	161
Figure 6.1. View of the UTP-binding site in <i>Ec</i> CTPS.....	174
Figure 6.2. (A) UTP- and (B) ATP-dependent kinetics for the H57A variant.....	178
Figure 6.3. UTP-dependent kinetics for wild-type <i>Ec</i> CTPS.....	180
Figure 6.4. Kinetic determination of the Gln- and Gln-OH-dependent GATase activity of H57A <i>Ec</i> CTPS.....	181
Figure 6.5. Proposed binding interactions with the pyrimidine ring of ΨTP at the active site of <i>Ec</i> CTPS.....	183
Figure 6.6. Inhibition of <i>Ec</i> CTPSs by ΨTP.....	184
Figure 6.7. Hypothetical mechanism for the amidoligation reaction.....	188
Figure A.1. Steady-state kinetic characterization of wild-type (A), E149D (B), and E149Q (C) <i>Ec</i> CTPS variants.....	215
Figure A.2. Inhibition of wild-type and E149Q variants by CTP and analogues.....	217
Figure A.3. Steady-state kinetic characterization of the E149D <i>Ec</i> CTPS-catalyzed conversion of dF-dUTP to dF-dCTP.....	219
Figure A.4. Steady-state kinetic characterization of wild-type (WT, red), E149D	

(green), F227A (blue), and F227L (violet) <i>Ec</i> CTPS variants.....	221
Figure A.5. Inhibition of wild-type (WT, red), F227A (blue), and F227L (violet) <i>Ec</i> CTPS variants by CTP (A and B) and dF-dCTP (C).....	223
Figure A.6. Steady-state kinetic characterization of wild-type <i>Ec</i> CTPS.	225
Figure A.7. Steady-state kinetic characterization of V60A <i>Ec</i> CTPS.....	227
Figure A.8. Steady-state kinetic characterization of V60C <i>Ec</i> CTPS.....	229
Figure A.9. Steady-state kinetic characterization of V60D <i>Ec</i> CTPS.....	231
Figure A.10. Steady-state kinetic characterization of V60W <i>Ec</i> CTPS.....	232
Figure A.11. Steady-state kinetic characterization of V60F <i>Ec</i> CTPS.....	234
Figure A.12. Steady-state kinetic characterization of DON-V60F <i>Ec</i> CTPS.....	236
Figure A.13. Kinetic determination of the GATase activity for wild-type and Val 60-substituted <i>Ec</i> CTPS variants.....	238

LIST OF SCHEMES

Scheme 3.1. Putative kinetic mechanism for parabolic competitive inhibition of <i>Ec</i> CTPS by dF-dCTP	55
---	----

ABSTRACT

Cytidine-5'-triphosphate (CTP) synthase (CTPS) catalyzes the biosynthesis of CTP from UTP using either L-glutamine or free NH₃ as a substrate. Glutamine is hydrolyzed in the glutamine amidotransferase (GATase) domain, with GTP acting as a positive allosteric effector, and nascent NH₃ is transported through a ~25-Å tunnel to the synthase domain where CTP is generated. The requirement for CTP in cell growth and proliferation has highlighted the importance of CTPS in a variety of infectious diseases, cancer, and the immune response. Consequently, CTPS is a recognized target for the development of chemotherapeutic agents.

To better understand the inhibition of CTPS by the drug metabolite gemcitabine-5'-triphosphate (dF-dCTP), we used the *Escherichia coli* variant (*EcCTPS*) as a model because of its ease of purification and similarities to human CTPS. dF-dCTP was a parabolic competitive inhibitor ($K_i = 3.0 \pm 0.1 \mu\text{M}$) that likely bound tightly through interactions between the 2'-*arabino* fluorine and an interdigitating loop in the CTP-binding site. Inhibition by dF-dCTP, but not enzymatic activity with UTP, was ablated by mutation of Glu 149 to Asp (E149D). This variant could recycle dF-dUTP, the 'inactive' catabolite of dF-dCTP, which may have consequences for gemcitabine pharmacology *in vivo*. Using dynamic light scattering and transmission electron microscopy, we showed that dF-dCTP induces *EcCTPS* filament formation, and disassembly was facilitated by UTP. E149D and variants of Phe 227 (F227A and F227L) were unable to undergo large-scale filament formation, supporting the role of Phe 227 as a 'sensor' of CTP that promotes filament formation.

Molecular gates within enzymes often play important roles in synchronizing catalytic events. The determinants of NH₃ channelling through a putative gate were investigated by site-directed mutagenesis. Point mutations at Val 60 (V60A, V60C, V60D, V60W, and V60F), at the most constricted point of the NH₃ tunnel, had varying consequences on catalysis. Notably, the V60F variant could not utilize exogenous NH₃ as a substrate, but permitted passage of glutamine-derived NH₃. Addition of Gln, or a combination of GTP with modification of V60F with 6-diazo-5-oxo-L-norleucine, enhanced NH₃ channelling, suggesting that the GATase activity promoted opening of the gate.

LIST OF ABBREVIATIONS USED

I : decay rate

λ : wavelength

τ : decay time

θ : scattering angle

η : viscosity

4-P-UTP: 4-phospho-uridine-5'-triphosphate

ADP: adenosine-5'-diphosphate

Ala: alanine

Arg: arginine

Asn: asparagine

Asp: aspartate

araC: 2'-*arabino*-cytidine

araCTP: 2'-*arabino*-cytidine-5'-triphosphate

AS: anthranilate synthase

ATP: adenosine-5'-triphosphate

CD: circular dichroism

CDP: cytidine-5'-diphosphate

CK1: casein kinase 1

CPEC: cyclopentenyl cytosine

CPEC-TP: cyclopentenyl cytidine-5'-triphosphate

CPS: carbamoyl phosphate synthase

CTP: cytidine-5'-triphosphate

CTPS: cytidine-5'-triphosphate synthase

Cryo-EM: cryo-electron microscopy

Cys: cysteine

D: self-diffusion coefficient

Da: Daltons

dCK: deoxycytidine kinase

dCTP: deoxycytidine-5'-triphosphate

dF-dC: 2',2'-difluoro-2'-deoxycytidine; gemcitabine

dF-dCDP: 2',2'-difluoro-2'-deoxycytidine-5'-diphosphate

dF-dCMP: 2',2'-difluoro-2'-deoxycytidine-5'-monophosphate

dF-dCTP: 2',2'-difluoro-2'-deoxycytidine-5'-triphosphate

dF-dU: 2',2'-difluoro-2'-deoxyuridine

dF-dUDP: 2',2'-difluoro-2'-deoxyuridine-5'-diphosphate

dF-dUMP: 2',2'-difluoro-2'-deoxyuridine-5'-monophosphate

dF-dUTP: 2',2'-difluoro-2'-deoxyuridine-5'-triphosphate

d_H: hydrodynamic diameter

DLS: dynamic light scattering

DMSO-*d*₆: deuterated dimethyl sulphoxide

DNA: deoxynucleic acid

DON: 6-diazo-5-oxo-L-norleucine

E: enzyme

EGTA: ethylene glycol-bis(β-aminoethyl ether)-N,N,N',N'-tetraacetic acid

ESI: electrospray ionization

[E]_T: total enzyme concentration

F-araCTP: 2'-*arabino*-fluoro-2'-deoxycytidine-5'-triphosphate

F-dCTP: 2'-fluoro-2'-deoxycytidine-5'-triphosphate

FGAR-AT: phosphoribosylformylglycinamide synthase II

GATase: glutamine amidotransferase

GF-HPLC: gel filtration-high performance liquid chromatography

GFP: green fluorescent protein

GlmS: glucosamine-6-phosphate synthase

Gln: glutamine

Gln-OH: L- γ -glutamyl hydroxamate

Glu: glutamate

GMPS: guanosine-5'-monophosphate synthase

GROMACS: Groningen machine for chemical simulations

GSK-3: glycogen synthase kinase 3

GTP: guanosine-5'-triphosphate

HEPES: *N*-[2-hydroxyethyl]piperazine-*N'*-[2-ethanesulphonic acid]

His: histidine

HPLC: high performance liquid chromatography

I: inhibitor

IC₅₀: inhibitor concentration that yields half-maximal velocity

ImGPS: imidazole glycerol phosphate synthase

INEPT: insensitive nuclei enhanced by polarization transfer

IPTG: isopropyl- β -D-thiogalacto-pyranoside

k_{act} : rate constant for enzyme-activator complex

k_{cat} : rate constant for turnover

k_0 : rate constant in absence of activator

K_A : apparent dissociation constant for an activator

K_i : apparent dissociation constant for an inhibitor

K_m : Michaelis constant

LB: Luria-Bertani

Leu: leucine

LINCS: linear constraint solver

Lys: lysine

n : Hill coefficient

NadE: glutamine-dependent NAD⁺ synthetase

NDPK: nucleotide diphosphate kinase

NMR: nuclear magnetic resonance

NNLS: non-negative least squares

NTP: nucleotide-5'-triphosphate

OPA: *o*-phthaldialdehyde

PDB: protein data bank

Phe: phenylalanine

P_i: inorganic phosphate

PIX: positional isotope exchange

q : scattering vector

R_I : refractive index

RNA: ribonucleic acid

RP-HPLC: reversed-phase high performance liquid chromatography

S: substrate

$[S]_{0.5}$: substrate concentration that yields half-maximal velocity

Ser: serine

SDS-PAGE: sodium dodecyl sulphate polyacrylamide gel electrophoresis

TEM: transmission electron microscopy

Thr: threonine

TK2: thymidine kinase 2

Trp: tryptophan

Tyr: tyrosine

UMP/CMPK: uridine-5'-monophosphate/cytidine-5'-monophosphate kinase

UTP: uridine-5'-triphosphate

Ψ TP: pseudouridine-5'-triphosphate

Val: valine

v_i : initial velocity

V_{\max} : maximal velocity

v_0 : initial velocity in absence of inhibitor

ACKNOWLEDGEMENTS

A lot of work goes into a Ph.D., and it takes a lot of cooperation and coordination to (successfully) produce a 250+ page thesis on a single enzyme. I would like to express my deepest gratitude to those who helped it all come together. In particular, I have to thank Prof. Stephen Bearne who risked a sizeable portion of his funding on a lowly *biologist*. Though my previous training involved studying enzymes in zebrafish and mammals, my proficiency in interpreting protein structures and inferring catalytic mechanisms had not yet developed (and there's still room for improvement!). While I have received a wealth of mentorship throughout my tenure at Dal, working with Steve changed how I think of biological processes at the molecular level, and that is probably the greatest asset I will take with me when I leave.

Of course, there are others who contributed immensely to this work. My sincere thanks go out to Drs. Jan Rainey, Aarnoud van der Spoel, and David Byers who served on my many supervisory committee meetings. Without their help this would not have been possible. I'd like to thank Drs. David Langelaan, Vanya Ewart, and Andrew Gulick for serving on my Ph.D. examining committee. Also, Dr. Hyo-Sung Ro who not only served as the Department representative for my thesis defence, but who mentored me during my M.Sc. studies. Past and present members of the Bearne lab who had to withstand lengthy group meeting presentations on a topic surely nobody else cared about, thank you for your attention and constructive feedback. Thank you, Róisín, for being my mother away from home and Paul Briggs for fostering my love of teaching.

Lastly, thank you Anto for everything. Now you're stuck with me.

CHAPTER 1 INTRODUCTION

1.1 CYTIDINE-5'-TRIPHOSPHATE

Cytidine-5'-triphosphate (CTP) is an essential pyrimidine nucleotide that plays a central role in the biosynthesis of nucleic acids (Hatse *et al.*, 1999), phospholipids (Bakovic *et al.*, 2007; Ostrander *et al.*, 1998), and sialic acid (Liu *et al.*, 2004). CTP can be incorporated directly into RNA via RNA polymerases, or DNA following ribonucleotide reductase-catalyzed conversion to 2'-deoxyCTP (dCTP) (Abeles & Beck, 1967). Like other nucleotide 5'-triphosphates, CTP can be utilized as a high-energy substrate for the synthesis of other biomolecules. CTP is converted to CDP-choline and CDP-ethanolamine by choline-phosphate cytidylyltransferase and CTP:phosphoethanolamine cytidylyltransferase, respectively (Dowhan *et al.*, 2008; Sundler & Akesson, 1975). Generation of these molecules is the rate limiting step in phosphatidylcholine (Dowhan *et al.*, 2008) and phosphatidylethanolamine synthesis (Sundler & Akesson, 1975). As such, CTP is a prerequisite for the synthesis of genetic material and phospholipid membranes in all forms of life, and is only synthesized *de novo* through the catalytic action of the glutamine amidotransferase, cytidine-5'-triphosphate synthase (CTPS) (Zalkin, 1993).

1.2 GLUTAMINE AMIDOTRANSFERASES

Glutamine amidotransferases (GATases) participate in the biosynthesis of a variety of aminated compounds such as nucleotides (Long & Pardee, 1967; Zalkin *et al.*, 1985), amino acids (Klem & Davisson, 1993), and coenzymes (Burns *et al.*, 2005). Like CTPS, many are the sole *de novo* source of such molecules (Zalkin, 1993). Because the products of GATase reactions are fundamental precursors for nucleic acids, proteins, and

phospholipid membranes (Chang & Carman, 2008; Ostrander *et al.*, 1998), the evolution of such biocatalysts was paramount for life to exist.

The GATase family comprises enzymes that couple the catalysis of glutamine (Gln) hydrolysis to the amination of an ATP-activated acceptor substrate (Figure 1.1) (Massiere & Badet-Denisot, 1998). Each enzyme has a GATase domain that is associated with a synthase (also called amidoligase) domain that can reside on the same polypeptide chain or exist as a separate subunit. Every family member contains an inter-domain NH₃ tunnel that physically connects the GATase and synthase domains to maximize catalytic efficiency (Raushel *et al.*, 1999; Raushel *et al.*, 2003; Zalkin, 1993; Zalkin & Smith, 1998). Nascent NH₃ generated during Gln hydrolysis is promptly shuttled to the synthase domain, and ligated to a phosphorylated intermediate (Figure 1.1).

The GATase family is subdivided into two main classes: the Class-I (or triad) Gln amidotransferases and Class-II (or N-terminal) Gln amidotransferases that differ in how the hydrolysis of Gln is catalyzed. Class-I GATases contain a Glu-His-Cys catalytic triad, and Class-II GATases utilize an N-terminal cysteine nucleophile (Zalkin, 1993). CTPS, carbamoylphosphate synthase (CPS), anthranilate synthase (AS), guanosine-5'-monophosphate synthase (GMPS), phosphoribosylformylglycinamide synthase II (FGAR-AT), and imidazole glycerol phosphate synthase (ImGPS) are examples of class-I GATases. These enzymes have divergent amino acid sequences and variable synthase domains that are specific to the chemistry being employed therein (Zalkin, 1993; Zalkin & Smith, 1998), but X-ray crystallography studies demonstrate the structural conservation amongst GATase domains (Figure 1.2). By and large, the catalytic cores of triad GATases are structurally invariant owing to the shared chemistry being catalyzed at this step;

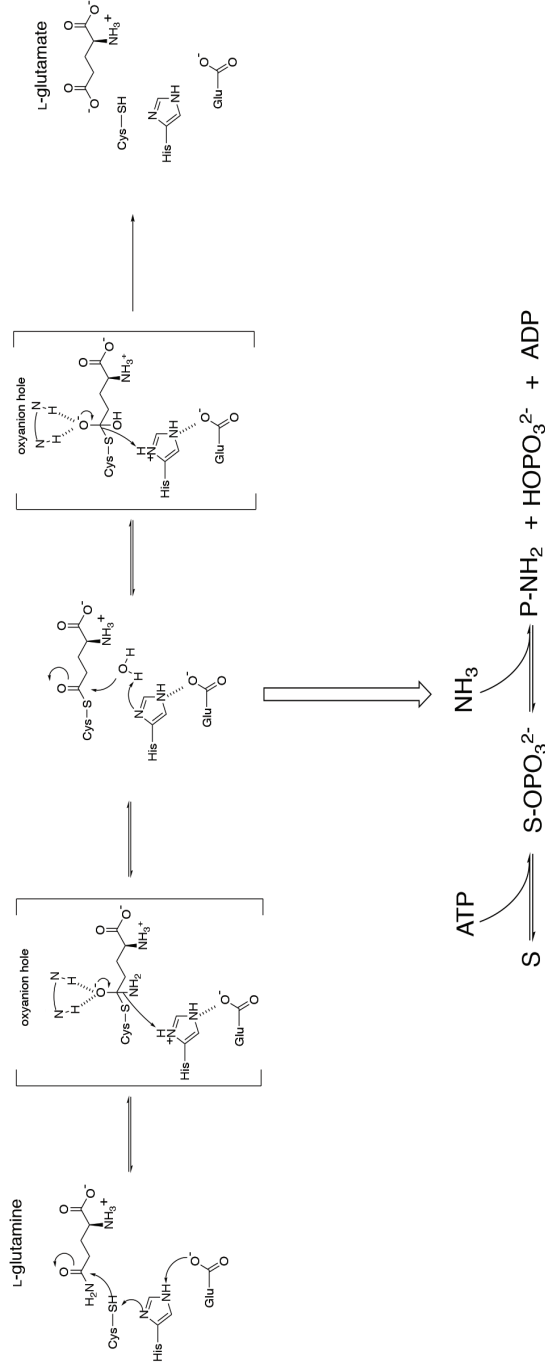


Figure 1.1. A general reaction mechanism for ADP-forming Class-I (triad) GATase family enzymes. Hydrolysis of Gln is catalyzed in the GATase domain by a Glu-His-Cys catalytic triad. Hydrolysis of the glutamyl-L-enzyme intermediate results in the production of L-glutamate. Nascent NH₃ is released following the collapse of the first tetrahedral intermediate, and transported to the synthase domain where the synthase substrate (S) is phosphorylated in an ATP-dependent manner. NH₃ then liberates the phosphate yielding the synthase product (P) and ADP + inorganic phosphate. Alternatively, some GATases (e.g., GMPS) activate the synthase substrate with pyrophosphate yielding AMP and inorganic pyrophosphate.

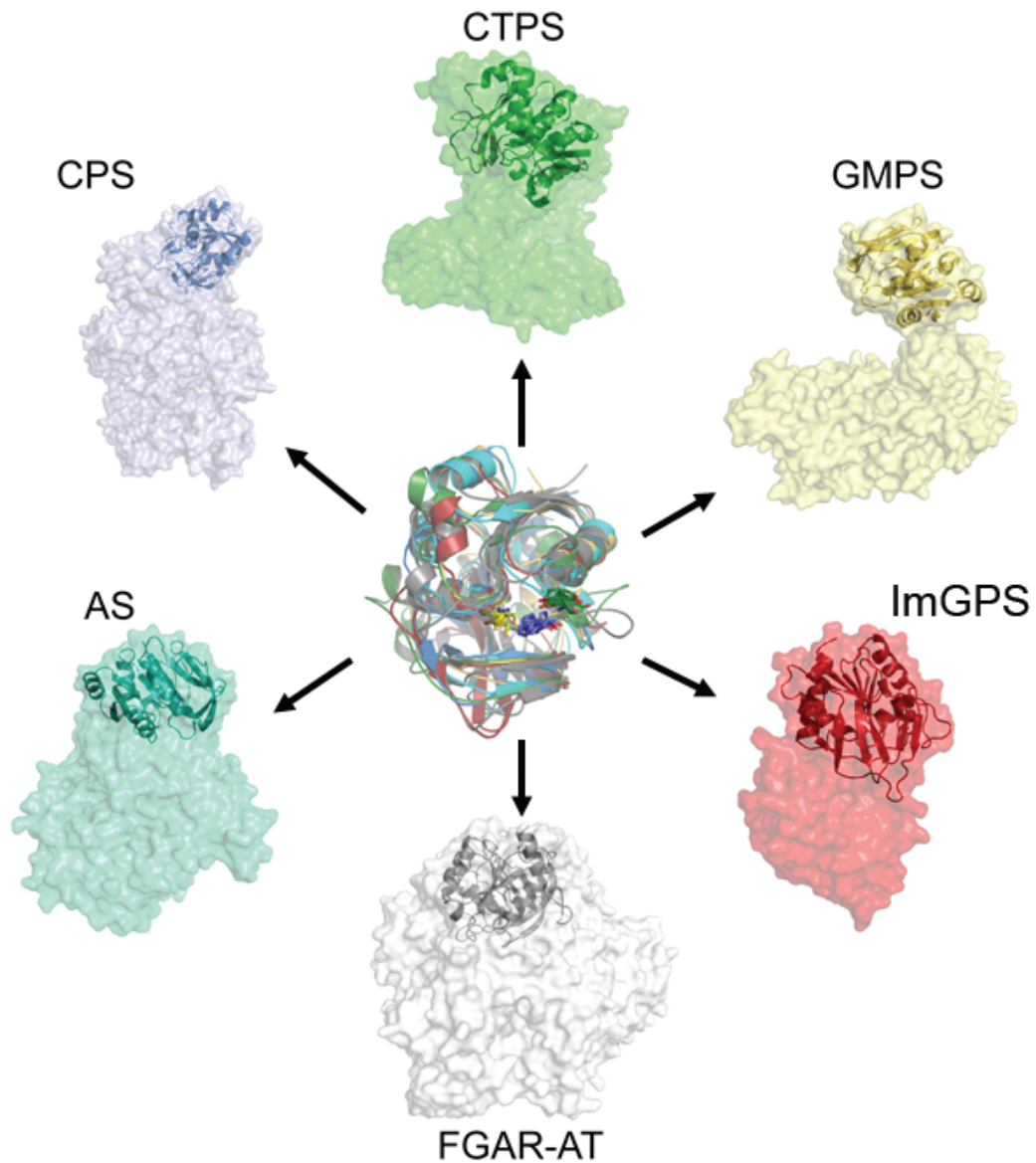


Figure 1.2. 3D superposition of GATases highlighting structural features of the invariant core. Superposition of GATase cores (cartoon) and their respective full-length structures (surface representation). The structures used were ImGPS (red; PDB: 3ZR4), FGAR-AT (grey; PDB: 1CL1), CTPS (green; PDB: 2AD5), AS (cyan; PDB: 1I1Q), GMPS (yellow; PDB: 2VXO), and CPS (blue; PDB: 1JDB). Catalytic Cys (yellow), His (violet), and Glu (green) residues are shown as sticks. Three-dimensional renderings and alignment of protein structures were constructed using PyMOL v. 1.8.2.0 (DeLano, 2002).

however, the assembly of subunits varies depending on the family member. For example, the NH₃ tunnel can reside within one bi-domain subunit (*e.g.*, CTPS) (Endrizzi *et al.*, 2004), or require more subunits to assemble a pipeline through which the nascent NH₃ can cross a multimeric assembly (*e.g.*, CPS) (Mullins & Raushel, 1999). Protomers can further assemble into supramolecular structures containing more than one catalytically active unit, enabling further allosteric regulation (Kim & Raushel, 2001; Levitzki & Koshland, 1971; Oliver *et al.*, 2014). The specificity of such interactions is determined by auxiliary insertions of amino acids stemming from the otherwise invariant catalytic core that are unique to each individual family member (Plach *et al.*, 2017). These insertions have little or no effect on glutamine hydrolysis, but presumably evolved to specify different interactions with other synthase domains (Plach *et al.*, 2017).

1.3 CTP SYNTHASE OVERVIEW

The *de novo* biosynthesis of cytidine-5'-triphosphate was first described experimentally using an extract of *Escherichia coli* (*E. coli*), in which CTP was generated from ATP, UTP, Mg²⁺, and NH₃ (Lieberman, 1956). The enzyme responsible for this reaction, CTPS, was later isolated and purified from *E. coli* (*EcCTPS*), which enabled the study of its inhibition by the product, CTP (Long & Pardee, 1967). This approach was later refined to determine that the enzyme acted in its tetrameric state, brought on by binding of UTP and ATP (Levitzki *et al.*, 1971), and that it exhibited half-sites reactivity (Levitzki & Koshland, 1972a). Furthermore, Koshland and co-workers (1972) expanded on the allosteric effects of GTP on *EcCTPS* by showing that it acts allosterically to enhance the hydrolysis of Gln. Despite these early breakthroughs, it would be several years before more details of the catalytic mechanism were delineated. Positional isotope exchange

(PIX) experiments using [γ - $^{18}\text{O}_4$]ATP demonstrated that the phosphorylation of UTP precedes ligation of NH_3 (von der Saal *et al.*, 1985). Characterization of *EcCTPS* has since provided a framework for biochemical studies on homologues from *Lactococcus lactis* (*LICTPS*) (Willemoës, 2004; Willemoës & Larsen, 2003; Willemoës & Sigurskjold, 2002), *Saccharomyces cerevisiae* (*ScCTPS*) (Chang *et al.*, 2007; Chang & Carman, 2008; Choi & Carman, 2007; Choi *et al.*, 2003; Ostrander *et al.*, 1998; Park *et al.*, 2003), and *Trypanosoma brucei* (*TbCTPS*) (Fijolek *et al.*, 2007; Hofer *et al.*, 2001; Oliveira de Souza *et al.*, 2017; Steeves & Bearne, 2011; Tamborini *et al.*, 2012). Furthermore, recent studies have demonstrated the existence of CTPS filaments in prokaryotes (Barry *et al.*, 2014; Ingerson-Mahar *et al.*, 2010) and eukaryotes (Lynch *et al.*, 2017; Noree *et al.*, 2014; Noree *et al.*, 2010; Strohlic *et al.*, 2014), with implications for a new paradigm for CTPS regulation.

1.4 CTPS MECHANISM

A single 'catalytic unit' of *EcCTPS* consists of a single 544 amino acid polypeptide chain that is organized into two discrete domains (Weng *et al.*, 1986). The N-terminal domain contains the synthase machinery which is connected to the C-terminal GATase domain by an NH_3 tunnel.

1.4.1 Glutamine Hydrolysis

Like all Class-I GATases, *EcCTPS* employs a Cys-His-Glu catalytic triad to catalyze the rate-limiting generation of nascent NH_3 via the hydrolysis of Gln (Figure 1.1) (Levitzki & Koshland, 1971, 1972b). The triad forms a network of H-bonding interactions that greatly increases the nucleophilicity of Cys 379, facilitating the attack on the γ -amide carbon of Gln (Zalkin, 1993). This results in a transient covalent γ -glutamyl thioester

adduct that is subsequently hydrolysed to yield glutamate and nascent NH_3 (Levitzki & Koshland, 1971). Cys 379 was first identified as the putative catalytic residue by affinity labelling using 6-diazo-5-oxo-L-norleucine (DON) (Levitzki & Koshland, 1971; Levitzki *et al.*, 1971). DON is a Gln analogue that irreversibly alkylates CTPS, forming an adduct that is only one methylene group longer than the cognate glutamyl-enzyme intermediate (Figure 1.3) (Levitzki & Koshland, 1971; Levitzki *et al.*, 1971). Incubation of EcCTPS with DON resulted in modification of only one of the five cysteine residues on the enzyme, suggesting that a nucleophilic cysteine was positioned near the γ -amide of Gln (Levitzki & Koshland, 1971). The resulting DON-CTPS variant was no longer able to utilize Gln as a substrate, but retained the ability to catalyze CTP production using exogenous NH_3 from bulk solvent (Levitzki & Koshland, 1971). With the advent of sequencing technologies, multiple sequence alignment later provided substantial support for Cys 379 being the catalytic residue since it was conserved amongst CTPSs, and other GATases alike (Weng & Zalkin, 1987; Zalkin, 1985, 1993). Site-directed mutagenesis confirmed this hypothesis when Ser and Ala were substituted for Cys 379, resulting in an EcCTPSs that could no longer form the thioester intermediate (Bearne *et al.*, 2001).

Naturally, all CTPSs share similar GATase domain structures with other Class-I triad GATases (Figure 1.2 and 1.4A), and these are invariant amongst structurally characterized members of the CTPS subgroup (Figure 1.4B). Furthermore, the residues comprising the catalytic triad are positioned identically within the active sites of CTPSs with solved GATase domain structures (Figure 1.4C). A second set of closely-positioned His 469 and Glu 472 (*E. coli* numbering) residues are present adjacent the active site triad that appear to help maintain this geometry *via* a salt-bridge interaction (Figure 1.4C).

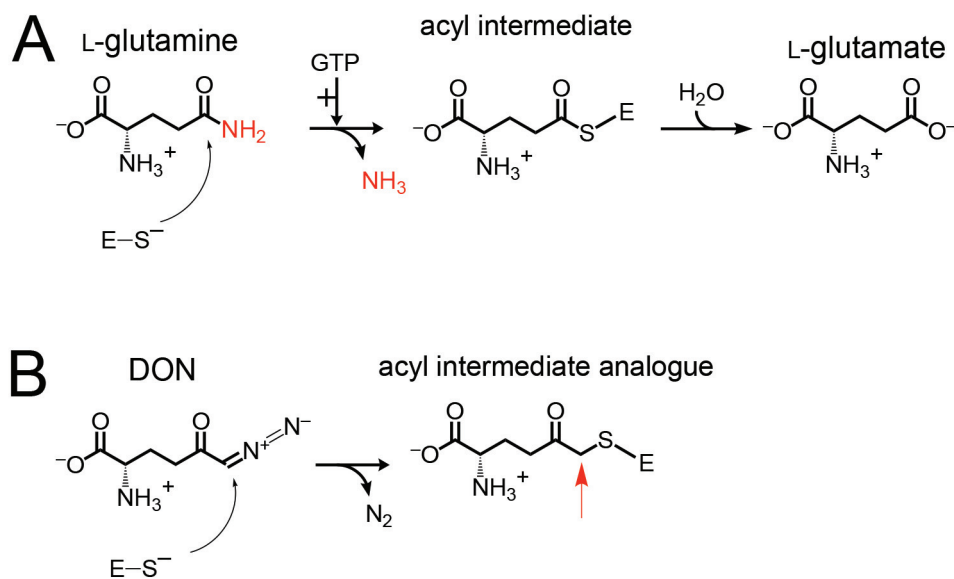


Figure 1.3. Comparison between CTPS-catalyzed Gln hydrolysis (**A**) and alkylation by DON (**B**). Nascent NH_3 that is formed during Gln hydrolysis is highlighted in red, and the extra methylene group present in the DON adduct is denoted by a red arrow.

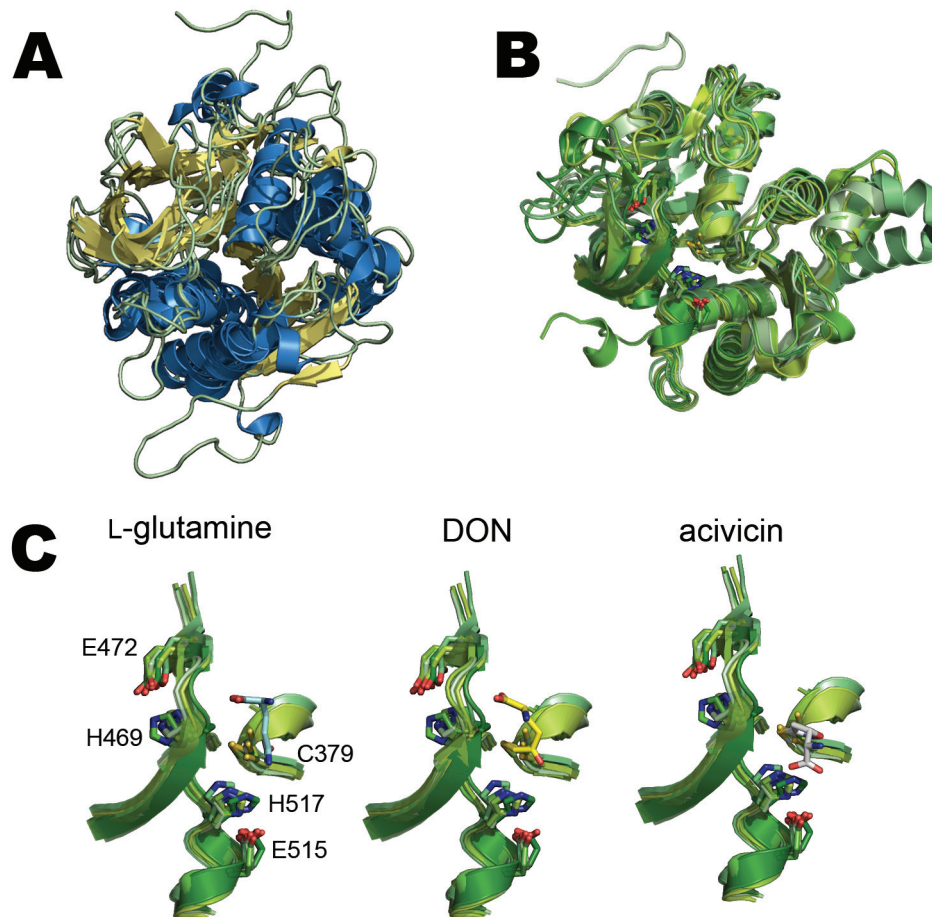


Figure 1.4. Structural features of GATase domains from CTPS and other related enzymes. (A) Structural alignment of GATase domains from ImGPS (PDB: 3ZR4), FGAR-AT (PDB: 1CL1), CTPS (PDB: 2AD5), AS (PDB: 1I1Q), GMPS (PDB: 2VXO), and CPS (PDB: 1JDB) shown in cartoon representation, coloured by secondary structure (α -helix: blue; loop: green; β -sheet: blue). Mean RMSD (relative to CPS) = 2.9 Å. (B) Structural alignment of GATase domains from CTPS homologues of *E. coli* (PDB:2AD5), *T. thermophilus* (PDB:1VCO), *S. solfataricus* (PDB:3NVA), *M. tuberculosis* (PDB:4ZDK), *Trypanosoma brucei* (PDB:5N29) and *H. sapiens* (PDB:5U03). Catalytic residues are shown in stick form, coloured by atom type. Mean RMSD (relative to *Ec*CTPS) = 1.19 Å. (C) Structural-alignment from panel B with some features removed for clarity, showing CTPS structures bound to L-Gln (cyan sticks, PDB:1VCO), DON (yellow sticks, PDB:2V4U), and acivicin (grey sticks, PDB:5N29). Active site residues are represented as green sticks, coloured by atom type, labelled with *E. coli* numbering. Three-dimensional renderings of protein structures were constructed using PyMOL v. 1.8.2.0 (DeLano, 2002)

While the catalytic machinery is structurally invariant (Figure 1.4), CTPS differs from other GATases such that Gln hydrolysis is allosterically activated by GTP (Levitzki & Koshland, 1972b). GTP was identified as a positive allosteric effector of *Ec*CTPS that increased catalytic efficiency of Gln-dependent CTP production (Levitzki & Koshland, 1972b). Alkylation of CTPS by DON was also markedly enhanced in the presence of GTP (Levitzki & Koshland, 1971, 1972b). Similarly, GTP enhanced the interaction of *Ec*CTPS with glutamate γ -semialdehyde, a transition state analogue inhibitor, suggesting that GTP induces a conformational change that stabilizes the covalent intermediate(s) formed during catalysis (Bearne *et al.*, 2001).

1.4.2 Ammonia Tunnel

All characterized GATase family enzymes have some form of inter-domain tunnel that channels NH_3 from the site of Gln hydrolysis to an activated acceptor substrate in the synthase domain. Recent crystallographic evidence has confirmed the existence of a tunnel within five structurally-characterized CTPSs (Figure 1.5). The NH_3 tunnel is comprised of several conserved residues within the synthase domain, and all homologues contain some form of constriction that was identified as a putative 'gate' (Endrizzi *et al.*, 2004). The gate corresponds to a section of the tunnel where there is a reduction in diameter caused by Pro 54 - His 57 - and Val 60 (*E. coli* numbering), and is located at the inter-domain region between GATase and synthase active sites. However, the observation that CTPS must have a mechanism for coupling the reactions without prematurely releasing NH_3 was made prior to these structural studies (Levitzki & Koshland, 1971). Exogenous NH_3 , derived from NH_4Cl , can also be used as a substrate, and Koshland and co-workers demonstrated that NH_3 , not NH_4^+ , was utilized as the substrate for the synthase reaction by examining the

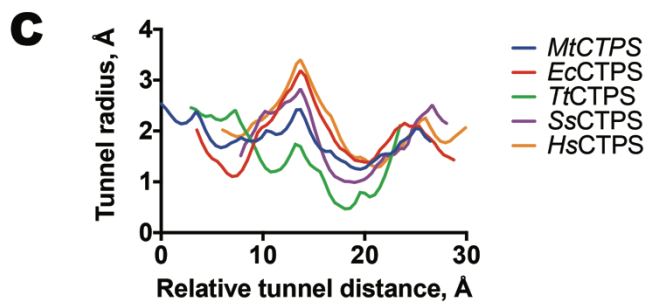
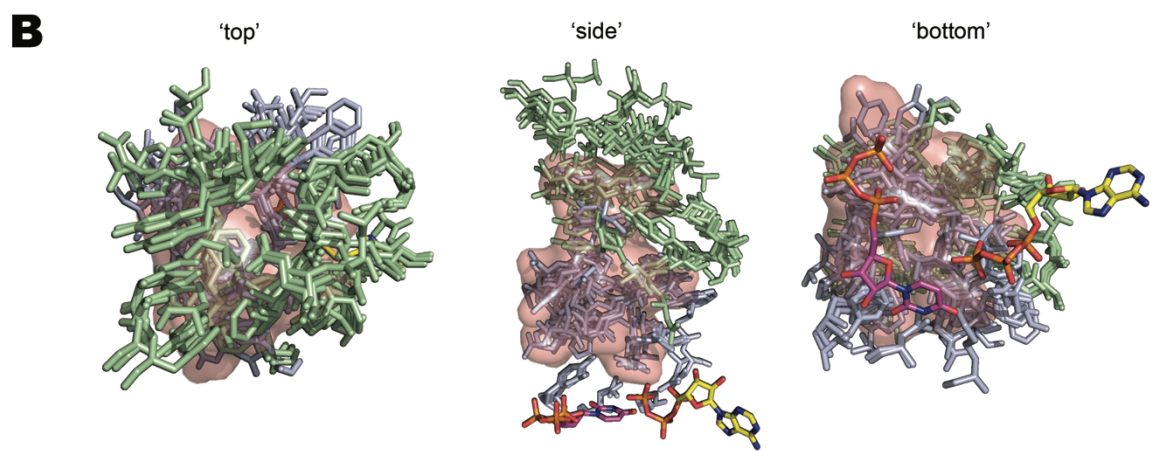
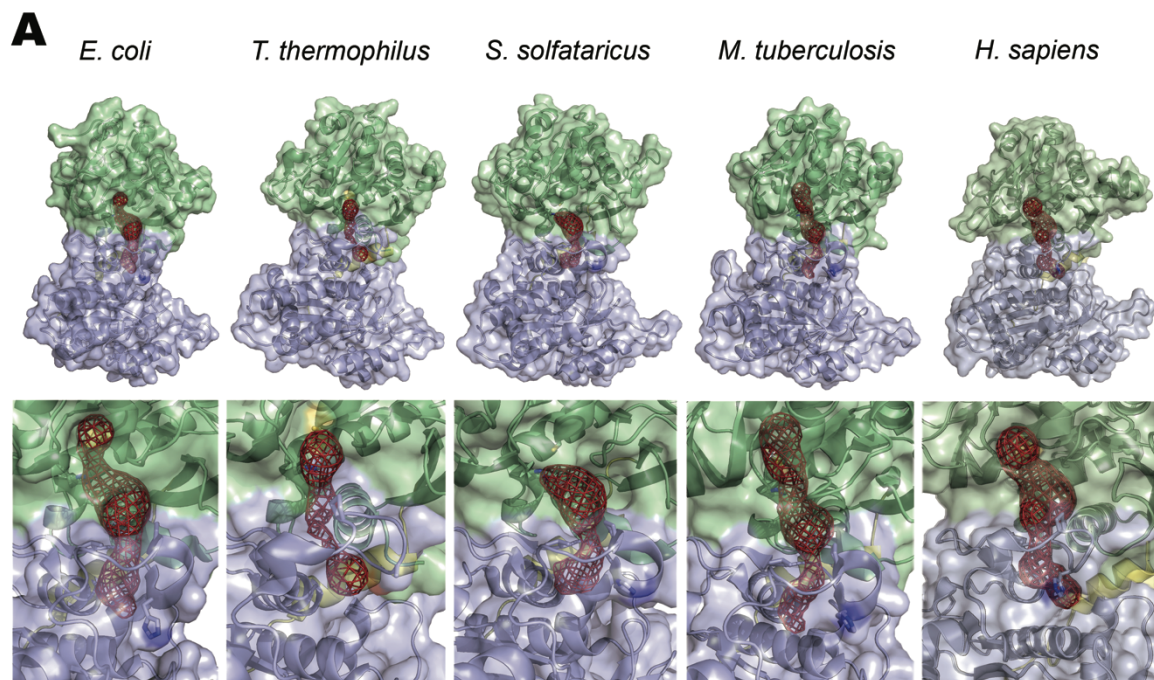


Figure 1.5. Structural features of the NH₃ tunnels from five structurally-characterized CTPSs. **(A)** Intra-subunit view of the NH₃ tunnels (red, wireframe) for *E. coli* (PDB:2AD5), *T. thermophilus* (PDB:1VCO), *S. solfataricus* (PDB:3NVA), *M. tuberculosis* (PDB:4ZDK), and *H. sapiens* (PDB:5U03). Residues comprising the catalytic triad are represented in stick form (grey, coloured by atom type). **(B)** Alignment of the structures from panel A showing the tunnel-comprising residues in stick form. Conserved residues are highlighted in red. UTP and ATP are represented in stick form, and are coloured violet and yellow, respectively. 'Top' and 'bottom' refer to views from the GATase and synthase domains, respectively. The GATase, linker, and synthase domains are shaded in green, yellow, and blue, respectively. **(C)** Measurements of each tunnel were aligned to the variant with the greatest length (*Tt*CTPS) to highlight similarities in shape. Tunnels were modelled using CAVER Analyst 1.0 (Petrek *et al.*, 2006), and 3D renderings of protein structures were constructed using PyMOL v. 1.8.2.0 (DeLano, 2002).

dependence of the enzyme-catalyzed rate on the pH of the solution (Levitzki & Koshland, 1971). A study was later performed using CPS in which only the synthase product contained ^{15}N when ^{15}N -labelled Gln was added as the NH_3 source (Rishavy *et al.*, 2000), and no $^{15}\text{NH}_4^+$ was detected in bulk solvent.

CPS was the first GATase to have its structure solved by X-ray crystallography in which an inter-domain NH_3 tunnel was directly observed (Mullins & Raushel, 1999). While the tunnel within CPS is 96-Å long, and meanders through multiple subunits, CTPS contains only one tunnel per subunit that connects the two active sites. X-Ray structures for *Ec*CTPS revealed the presence of a solvent-filled vestibule (volume $\approx 230 \text{ \AA}^3$) that interrupts the tunnel at the GATase-synthase interface (Endrizzi *et al.*, 2004). All structurally-characterized CTPS homologues contain similar tunnels, containing a large opening preceding a tight constriction (Figure 1.5). Site-directed mutagenesis of nearby residues (Arg 105, Leu 109, and Gly 110) impaired the transfer of nascent NH_3 and an L109A mutant particularly disrupted GTP-mediated allosteric activation of the GATase reaction (Iyengar & Bearne, 2003). These results suggested that the NH_3 tunnel is a dynamic feature of *Ec*CTPS, and its structure may be modulated upon binding GTP. This was further supported by the observation that GTP inhibits the utilization of exogenous NH_3 as a substrate (MacDonnell *et al.*, 2004), suggesting that GTP may bind near the tunnel.

Mutagenesis studies on NH_3 gates often reveal the sensitivity of these structures to perturbation, as was the case when mutations in CPS caused a perforation in the tunnel and caused nascent NH_3 to leak out (Kim & Raushel, 2004). An L109A substitution in *Ec*CTPS caused a constriction in the tunnel, which was revealed by substituting Gln with

L- γ -glutamyl hydroxamate (Gln-OH). *Ec*CTPS can catalyze the hydrolysis of Gln-OH yielding nascent NH₂OH, which is also a substrate for the synthase domain. Coupling between GATase and synthase activity was worse with Gln-OH than with Gln in the L109A mutant, relative to wild-type *Ec*CTPS. This indicated that the increased bulk of NH₂OH was unable to be effectively channelled past the constriction in the tunnel (Lunn & Bearne, 2004).

Though perfect coupling of GATase and synthase domains in *Ec*CTPS is observed, the mechanism is unclear. The first X-ray structural study of *apoEc*CTPS proposed that His 57 adopted two conformations; one closed over the tunnel exit and one open (Endrizzi *et al.*, 2004). A follow-up structure of *Ec*CTPS bound to products only showed His 57 in the 'open' position suggesting a gating mechanism through which the imidazole side-chain acts as a hatch that regulates NH₃ passage (Endrizzi *et al.*, 2005). Alternatively, Pro 54 and Val 60 may also play a role in gating of NH₃ passage since these two residues form the narrowest point (radius = 1.2 Å) in the tunnel. Despite the constriction being tighter than the molecular radius of NH₃ (Kammeyer & Whitman, 1972), exogenous NH₃ can be utilized readily. Nevertheless, the mechanism by which exogenous NH₃ is utilized is even less well understood than for nascent NH₃. Previous studies indicated that nascent and exogenous NH₃ competed for a similar 'binding' site; however, NH₄SO₄ was employed as the NH₃ source without controlling for the ionic strength (Levitzki & Koshland, 1971). While exogenous NH₃ appeared to inhibit utilization of nascent NH₃, later attempts to validate this result with NH₄Cl maintained at a constant ionic strength did not yield significant inhibition of Gln-dependent CTP formation (Bearne *et al.*, 2001). Rudimentary modelling of GTP into the *Ec*CTPS crystal structure revealed a putative GTP binding site

over the top of the 'vestibule' near the gate (Endrizzi *et al.*, 2004), though this has never been directly observed in any CTPS X-ray crystallographic or cryo-EM study thus far. Inhibition of NH₄Cl-dependent CTP production by GTP (MacDonnell *et al.*, 2004) in combination with the GTP-bound model suggested that exogenous NH₃ may enter the *Ec*CTPS tunnel via the vestibule.

1.4.3 Amidoligase Reaction

The N-terminal synthase domain catalyzes the amidoligase reaction using UTP and ATP as substrates. The phosphorylation of UTP was discovered by detection of ¹⁸O-labelled inorganic phosphate that was released during the CTPS-catalyzed reaction when [4-¹⁸O]UTP was used as a substrate (Levitzki & Koshland, 1971). Positional isotope exchange (PIX) experiments further demonstrated that CTPS catalyzes the ATP-dependent phosphorylation of UTP in the absence of an NH₃, indicating that the 4-P-UTP intermediate is generated prior to Gln hydrolysis (von der Saal *et al.*, 1985). Previously, two mechanisms had been proposed for the amidoligase reaction: one in which phosphorylation occurs before the attack of NH₃ and one in which NH₃ attacks and the C-4-oxygen is liberated by subsequent phosphorylation (Figure 1.6). In brief, CTPS catalyzed the transfer of ¹⁸O in the bridging position between the γ - and β -phosphates of ATP to a non-bridging position in the absence of NH₃, which indicated that there was reversible phosphorylation of UTP (Figure 1.7). However, this mechanism assumes that there is no phospho-enzyme intermediate as a positive PIX result would also occur if a residue on CTPS were reversibly phosphorylated but no archetypal phosphorylation sites (*e.g.*, Ser, Thr, or Tyr) are present near the γ -phosphate of ATP. That a phosphoryl transfer reaction is catalyzed by CTPS in

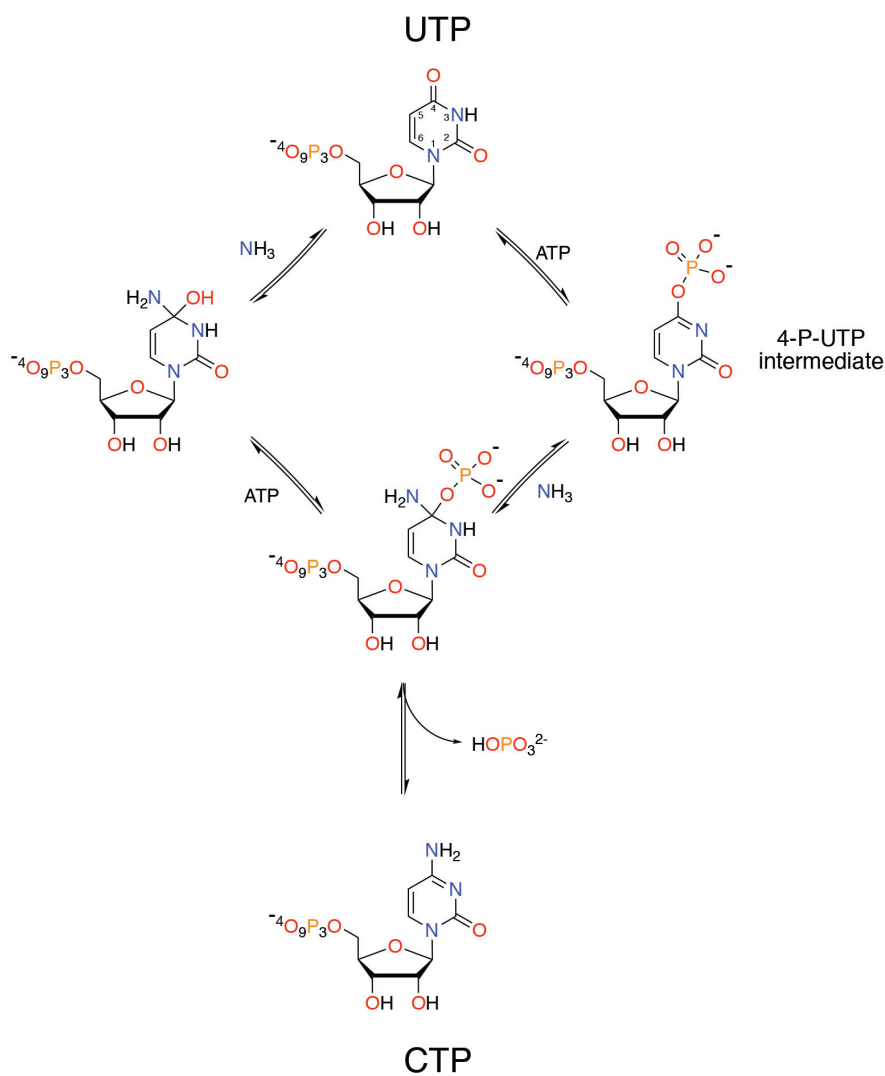


Figure 1.6. Two possible orders for the amidoligase mechanism. An initial attack by NH_3 on the C-4 position, forming a tetrahedral carbinol amine intermediate (left), was initially proposed. Reaction of the carbinol and ATP would then yield a phosphorylated intermediate followed by elimination of inorganic phosphate. Alternatively, phosphorylation of the C-4 carbonyl (right) can precede the attack by NH_3 , yielding the same tetrahedral intermediate. Figure is adapted from von der Saal *et al.*, 1985.

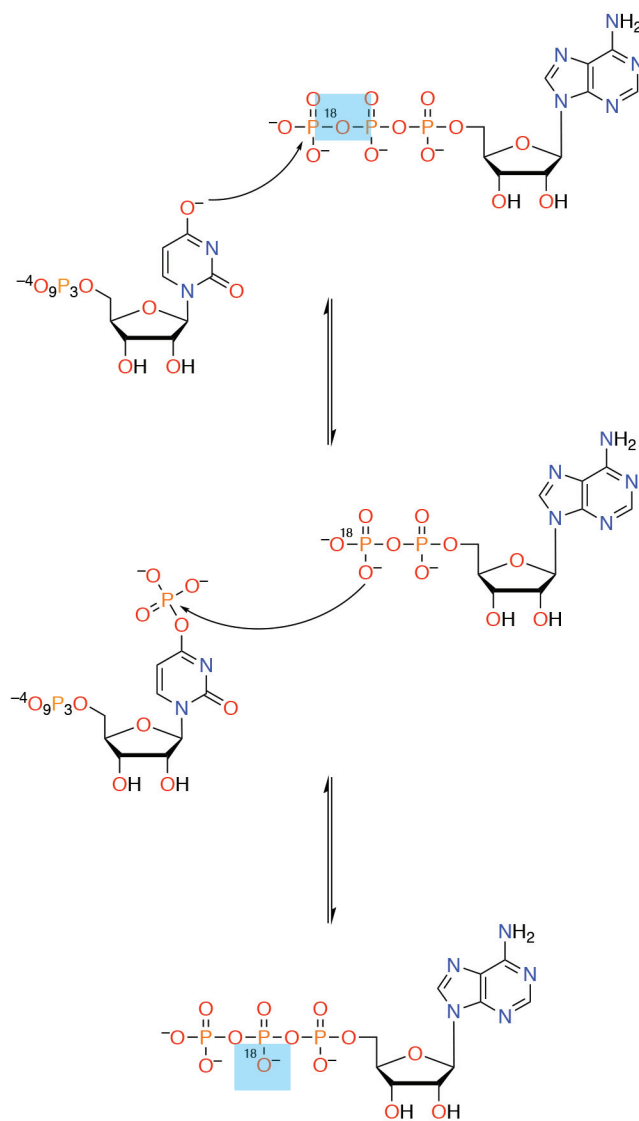


Figure 1.7. Positional isotope exchange experiment with CTPS. Phosphorylation of the O-4 position of UTP involves the attack of UTP on the γ -phosphate of ATP (top). Attack by any of the non-bridging oxygens on the β -phosphate can reverse the process (middle). If the ^{18}O does not attack (highlighted in blue), then it will end up in a non-bridging position (bottom) indicating that there was phosphorylation of UTP despite the absence of NH_3 , and that phosphorylation likely precedes attack by NH_3 . Adapted from von der Saal (1985).

the absence of NH₃ is the best evidence that phosphorylation of UTP occurs prior to Gln hydrolysis, or NH₃ channelling.

1.5 HALF-OF-THE-SITES REACTIVITY

CTPS is active as a homo tetramer; it has four GATase sites, four NH₃ tunnels, and four synthase sites. Intriguingly, affinity labelling experiments with DON revealed an unusual property of CTPS in which only two GATase active sites were modified (Levitzki *et al.*, 1971). Moreover, modification of two sites was sufficient for complete inactivation of CTPS suggesting that modification, or substrate binding, at an active site on one subunit can influence the structure of other subunits such that they are unable to catalyze a reaction (Levitzki *et al.*, 1971). Koshland's seminal work on the theory of half-of-the-sites reactivity provided a framework that described how a multimeric protein with n subunits may only bind (or react) with $n/2$ ligands, even at apparently saturating conditions (Koshland *et al.*, 1966). This cross-subunit regulation represents a form of negative cooperativity, whereby binding of a ligand at one site impairs the ability of the enzyme to bind a ligand at another site. In this instance, the ligands and sites would be the same, meaning occupation of an active site on one subunit allosterically blocks reactivity at a cognate site on another subunit (Figure 1.8, top). How such negative cooperativity is transduced across subunit interfaces can often be indistinguishable from the protein asymmetry model presented by Seydoux, Malhotra, and Bernhard (Seydoux *et al.*, 1974). The latter model describes the possibility of multimeric proteins adopting inter-subunit asymmetry upon oligomerization that would induce a conformational change in $n/2$ binding sites (Figure 1.8, bottom), which has been observed for insulin (Bloom *et al.*, 1997). However, CTPS is an enzyme that exhibits extensive nucleotide triphosphate(NTP)-

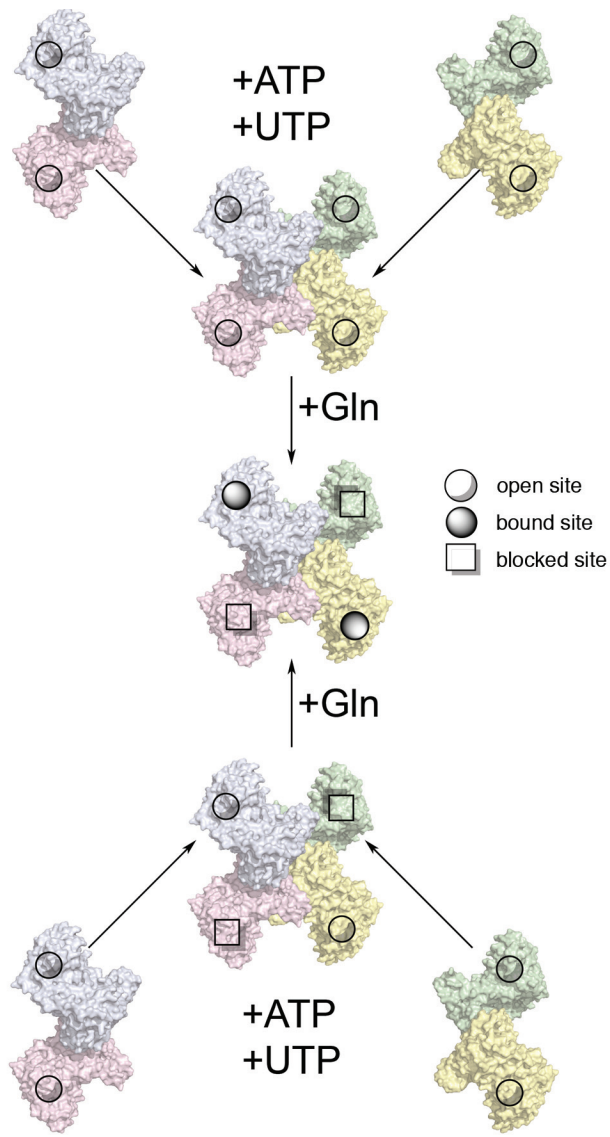


Figure 1.8. Two models for half-of-the-sites reactivity in CTPS. Two models can explain why CTPS exhibits only half-sites reactivity: one in which binding, or reacting, of Gln (or analogues) allosterically blocks the site on an adjacent subunit (top), and one in which tetramerization of two dimers with open sites results in two sites being unreactive in the absence of Gln (bottom). The top model, proposed by Levitzki and Koshland (Levitzki *et al.*, 1971), involves negative cooperativity whereby binding of Gln induces a conformational change that makes the same sites on other subunits less reactive. The bottom model, proposed by Seydoux and co-workers (1974), suggests that oligomerization can induce conformational changes that blocks half of the sites in the absence of the cognate ligand. Both models have the same result, and it can be difficult to discern which is correct in the absence of detailed kinetic and structural data.

dependent cooperativity, and structural studies on CTPSs argue that Koshland's model accurately describes half-site reactivity in this enzyme (Endrizzi *et al.*, 2004; Goto *et al.*, 2004).

1.6 ROLE OF NTP LIGANDS

1.5.1 GTP

CTPS has a basal ability to catalyze Gln hydrolysis that is markedly enhanced upon binding GTP at an unidentified site (Levitzki & Koshland, 1972b). Binding of GTP enhances the affinity and reactivity of CTPS with Gln, but inhibits the utilization of exogenous NH₃. Alkylation of CTPS by DON is also promoted by GTP, suggesting that it directly affects glutamylation in the initial half-reaction of the GATase domain (Levitzki & Koshland, 1971, 1972b). Further support for the notion that GTP specifically activates the glutamylation step was presented thirty years later using the transition state analogue inhibitor, glutamate γ -semialdehyde (Bearne *et al.*, 2001). Enhanced binding of this analogue in the presence of GTP was consistent with GTP inducing a conformational change to more effectively stabilize the oxyanion of the glutamyl tetrahedral intermediate. That GTP inhibits the utilization of NH₄Cl-derived NH₃ suggests that it binds near the putative entry site for exogenous NH₃ (Endrizzi *et al.*, 2004; MacDonnell *et al.*, 2004). GTP is not normally consumed when acting as an allosteric effector; however, it can substitute for ATP as a phosphate donor in the amidoligase reaction if [GTP] \gg [ATP] (Kizaki *et al.*, 1982; Levitzki & Koshland, 1971).

1.5.2 UTP and ATP

The binding site for ATP has been identified by X-ray crystallography and cryo-EM studies, but the exact location of the UTP binding site is ambiguous. ATP binds in a

cleft such that the γ -phosphate is positioned at the exit of the NH_3 tunnel (Endrizzi *et al.*, 2005; Lynch *et al.*, 2017) (Figure 1.9). X-Ray crystal structures of CTPS from *Mycobacterium tuberculosis* (*Mt*CTPS) identified a UTP binding site (Mori *et al.*, 2015) that overlaps with that of CTP (discussed further in **section 1.5.3**), but mutations that obviate CTP binding often have little impact on UTP binding (Barry *et al.*, 2014; Endrizzi *et al.*, 2005; Whelan *et al.*, 1993; Whelan *et al.*, 1994). Moreover, the O-4 of UTP was positioned such that it was 17 Å from the γ -phosphate of ATP (Mori *et al.*, 2015), making a mechanistic explanation of how CTP is generated in this manner difficult to rationalize. Solution of a 6.1-Å resolution cryo-EM structure of human CTPS (*Hs*CTPS) later showed electron density near the NH_3 tunnel exit, consistent with UTP positioned to accept the γ -phosphate of ATP (Lynch *et al.*, 2017). This latest structure supported the assumption derived from modelling of UTP into the active site in the same group's earlier X-ray studies of *Ec*CTPS (Endrizzi *et al.*, 2004, 2005). Together the *Mt*CTPS and *Hs*CTPS structures suggest that UTP may bind in two distinct orientations although it is possible that certain binding modes may be specific to different CTPS homologues (Figure 1.9)

Binding of UTP and ATP results in marked enhancements in the rate of GATase activity compared to the rate when these NTP substrates are absent, despite ostensibly only being required for production of CTP (Levitzki & Koshland, 1971). Binding of UTP and ATP caused an apparent conformational change that increased the rate of Gln hydrolysis, which was later found to be partly due to an increase in tetramerization (Levitzki & Koshland, 1972a). However, incubation of CTPS with UTP and either a non-hydrolyzable ATP analogue (AMPNP) or a slowly-hydrolyzable analogue (ATP- γ S) also increased GATase activity, but to a lesser extent (Levitzki & Koshland, 1971; Willemoës &

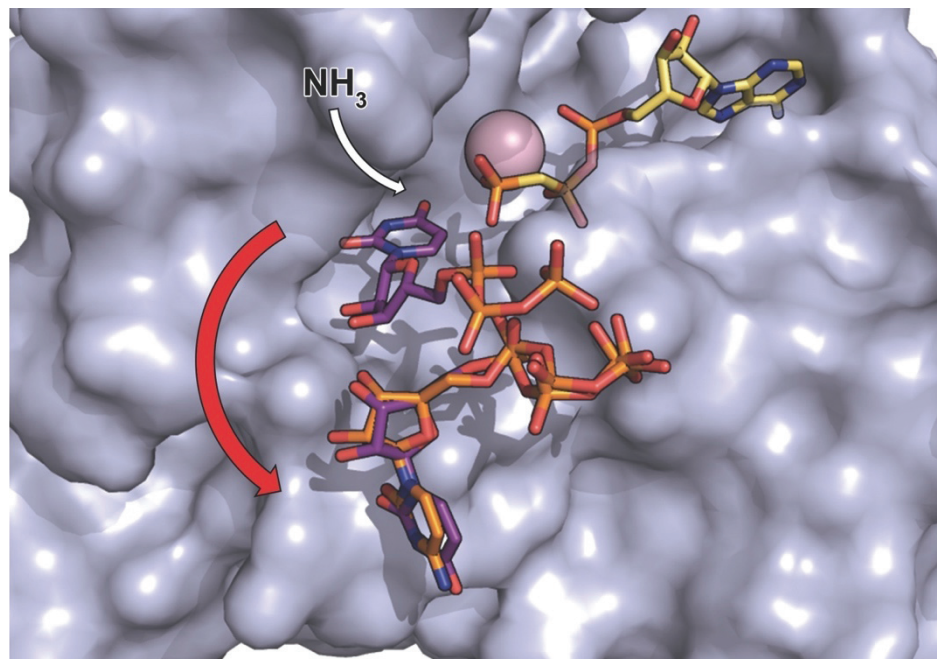


Figure 1.9. View of the synthase NTP-binding cleft. Alignment of the UTP- and AMPCP-bound *Hs*CTPS cryo-EM structure (light blue, surface; PDB: PDB:5U03), the UTP-bound *Mt*CTPS X-ray crystal structure (PDB:4ZDK), and the CTP-bound *Ec*CTPS X-ray crystal structure (PDB:2AD5). The proposed rotation of UTP (violet sticks) following amidoligase catalysis is shown as a red arrow. CTP (orange) and AMPCP (yellow) are shown in stick representation, and Mg^{2+} is shown as a pink sphere. The path of NH_3 is indicated by a white arrow. Three-dimensional renderings of protein structures were constructed using PyMOL v. 1.8.2.0 (DeLano, 2002)

Sigurskjold, 2002). These results indicated that UTP and ATP binding induce tetramerization, and generation of the 4-P-UTP intermediate following the initial γ -phosphoryl transfer reaction further activated the distal GATase domain (Willemoës & Sigurskjold, 2002). Each binding site for UTP and ATP is formed by the intersection of three subunits of the tetramer (Endrizzi *et al.*, 2004, 2005; Willemoës & Sigurskjold, 2002), but how the GATase domain is affected remains somewhat mysterious. More so, the activation of the GATase domain by the 4-P-UTP intermediate is more effective in the presence of GTP, suggesting that NTP levels play a significant physiological role in CTPS regulation *in vivo* (Willemoës & Sigurskjold, 2002).

1.5.3 CTP

Aside from being the product of CTPS catalysis, CTP inhibits the amidoligase reaction by competing with UTP (Long & Pardee, 1967). Like the binding sites for UTP and ATP, CTP is bound at the intersection of three subunits of the CTPS tetramer and can induce tetramerization of *ScCTPS* (Pappas *et al.*, 1998). CTP and UTP vie for the same 5'-triphosphate binding site, thus discrimination between the two NTPs is likely mediated by their respective nucleoside moieties (Endrizzi *et al.*, 2005; Long & Pardee, 1967; Lynch *et al.*, 2017). While the apparent binding orientations of UTP and CTP differ, they are bound by CTPS with similar affinities (Scheit & Linke, 1982) which makes CTP-dependent feedback inhibition an important regulatory mechanism for maintaining NTP pool homeostasis *in vivo* (Barry *et al.*, 2014). If CTP levels are substantial enough to out-compete UTP, *EcCTPS* polymerizes into inactive filaments to further slow CTP generation (Barry *et al.*, 2014).

1.7 CTPS OLIGOMERIZATION AND FILAMENT FORMATION

In the absence of ligands, *apo*CTPS exists as a homodimer under physiological conditions (Koshland & Levitzki, 1974) that can dissociate at temperatures lower than 37 °C, or when subjected to size-exclusion chromatography conditions (Anderson, 1983). *Apo*CTPS is otherwise detected as a distribution of monomers, dimers, and tetramers under equilibrium conditions (Robertson, 1995). While dimers maintain some GATase activity, tetramerization is required for CTP production (Levitzki & Koshland, 1972a). ATP and UTP act synergistically to induce tetramerization, though high concentrations of either NTP substrate alone can induce oligomerization in the absence of the other (Levitzki & Koshland, 1972a). CTP also induces tetramerization of the *Sc*CTPS homologue (Pappas *et al.*, 1998), but causes a more extreme polymerization of bacterial CTPS variants (Barry *et al.*, 2014; Ingerson-Mahar *et al.*, 2010; Lynch *et al.*, 2017).

1.7.1 CTPS Filaments in Prokaryotes

CTPS filaments were first discovered in *Caulobacter crescentus*, wherein CTPS can act as a cytoskeletal protein that prevents excessive membrane curvature (Ingerson-Mahar *et al.*, 2010). As their name implies, *C. crescentus* cells are typically crescent-shaped, but knock-down and over-expression of *Cc*CTPS resulted in highly curved and rod-like phenotypes, respectively (Ingerson-Mahar *et al.*, 2010). Self-assembling filaments were detected upon heterologous expression of mCherry-*Cc*CTPS in *Schizosaccharomyces pombe* and *E. coli* cells (Ingerson-Mahar *et al.*, 2010). Mutation of the catalytic Cys to Gly resulted in disassembly of *Cc*CTPS filaments, as did treatment of heterologously-expressed mCherry variants in *S. pombe* and *E. coli* treated with DON, suggesting that GATase activity was required for filament nucleation (Ingerson-Mahar *et*

et al., 2010). It wasn't until the determinants of filament formation by *EcCTPS* were studied that the mechanism of filament formation became clearer. A combined cryo-EM and kinetic study determined that prokaryotic CTPS filaments are induced upon binding of CTP to the enzyme (Barry *et al.*, 2014; Lynch *et al.*, 2017). Previously recombinant '*EcCTPS* filaments' were detected by TEM; however, the particles observed were strikingly similar to cotton-derived crystals (Ingerson-Mahar *et al.*, 2010; Kaushik *et al.*, 2015). Later, different-looking CTP-induced *EcCTPS* filaments were observed by the same group (Barry *et al.*, 2014), presenting new evidence for an additional feedback mechanism that extended beyond CTP competing with UTP. *EcCTPS* formed elongated CTP-induced filaments upon depletion of UTP pools and a concomitant build-up of CTP that locked the enzyme into an inactivated conformation (Barry *et al.*, 2014). Cryo-EM studies showed that the filament consists of tightly interlocked, tetrameric enzyme that prevents conformational dynamics that might aid in catalysis (Barry *et al.*, 2014; Lynch *et al.*, 2017). In hindsight, the hypothesis as to why GATase activity was required for *CcCTPS* polymerization was incomplete. The most likely explanation for GATase inactivation leading to filament disassembly is that inhibition of CTPS depleted intracellular CTP pools, thus diminishing CTP-dependent filament formation. While the cytoskeletal role appears to be exclusive to *C. crescentus*, there is support that CTPS filament formation may be important for regulation of NTP pools *in vivo* (Barry *et al.*, 2014). Replacement of wild-type *EcCTPS* with a variant that cannot bind CTP (E277R) ablated filament detection, and disrupted cell growth and NTP homeostasis (Barry *et al.*, 2014).

1.7.2 CTPS Filaments in Eukaryotes

Filaments have also been detected for the *ScCTPS* (Noree *et al.*, 2014; Noree *et al.*, 2010), *Drosophila melanogaster* (*DmCTPS*) (Strochlic *et al.*, 2014), and *HsCTPS* (Chang

et al., 2017; Lynch *et al.*, 2017) homologues. Unlike the previously characterized prokaryotic CTPS filaments, the determinants of filament formation in eukaryotes are less clear. *HsCTPS* filaments form when bound to UTP and ATP, and disassemble after depletion of NTP substrates unlike the prokaryotic CTPS homologues (Lynch *et al.*, 2017). While the physiological role of *HsCTPS* filaments is not yet known, polymerization increased activity relative to a filament-defective mutant (Lynch *et al.*, 2017). Indeed, *EcCTPS* and *HsCTPS* filaments differ significantly in structure as *HsCTPS* filaments do not interlock, which appears to provide more conformational freedom (Lynch *et al.*, 2017). *HsCTPS* also contains a short, helical C-terminal insertion that mediates contacts between the tetramers in the filamentous state (Lynch *et al.*, 2017). This helical insertion contains a His residue (355) that is required for polymerization, and substitution of His 355 with Ala (H355A) resulted in a 6-fold decrease in the rate of CTP production (Lynch *et al.*, 2017).

A significant amount of study has been focused on the role of CTPS in *Drosophila* sp. development because NTP pools are critically important during embryogenesis. Elongated intracellular filaments were first detected using GFP-tagged CTPS, and termed 'cytoophidia' meaning 'cell serpents' (Liu, 2010). Though the name has not gained traction amongst other researchers, studies on *DmCTPS* filaments make up the bulk of eukaryotic CTPS filament investigation. Interestingly, inosine monophosphate dehydrogenase (IMPDH), required for GTP biosynthesis, co-localizes to CTPS filaments in *Drosophila* embryos suggesting a co-scaffolding effect brought on to further regulate NTP pools (Chang *et al.*, 2015). The activity of these filaments has not been demonstrated, but treatment of *Drosophila* cells with DON results in *DmCTPS* and IMPDH filament

formation. That DON can induce CTPS polymerization in these cells is in accord with the effects observed for *HsCTPS* following depletion of CTP (Chen *et al.*, 2011; Lynch *et al.*, 2017).

DmCTPS polymerization may be regulated, in part, by phosphorylation as an inactivating mutation of the Ack kinase resulted in reduced numbers of filaments in *Drosophila* germline cells. Though *DmCTPS* filaments have been detected by immunofluorescence, many of these experiments were performed using CTPS-GFP fusion proteins that bear a curious resemblance to incidental GFP-membrane complexes that form when GFP is over-expressed in cell culture (Snapp *et al.*, 2003). The requirement for CTPS in phospholipid membrane biosynthesis may explain the possible co-localization of CTPS filaments to membranes, but the lack of control for this phenomenon casts doubt on the interpretation of many of the conclusions for these studies.

Similar to CTPSs from humans and *Drosophila*, *ScCTPS* also contains the helical insertion required to form active, substrate-bound filaments. However, mutations of the CTP-binding and allosteric sites disrupted filament formation, suggesting that *ScCTPS* requires CTP similarly to *EcCTPS* (Noree *et al.*, 2014). Furthermore, these *ScCTPS* filaments were suggested to be inactive, but this result requires further biochemical validation (Noree *et al.*, 2014). The helical insertion is apparently characteristic of some eukaryotic CTPS homologues, but is not present in all eukaryotic CTPS sequences. For example, CTPS from *Trypanosoma brucei* (*TbCTPS*) does not contain the insertion (Figure 1.10), and though the ability of this homologue to form filaments is unknown it would be unwise to assume *all* eukaryotic CTPS filaments are active if the insertion is distinctive for this phenomenon. Indeed, it may be the case that CTPSs from multicellular eukaryotes

```

EcCTPS  glknrvsvniklidsqdve--trg-----v-eilkgldailvpggfgyrgvegmitt  364
TtCTPS  giknrarvevkvwdaesle--aad-----ldeafrdvsgilvpggfgvrgiegkvra  376
SsCTPS  sayigvrpkliwiestdlesdtkn-----lneilgnvngiivlpfgfsgaegkika  371
MtCTPS  gfkhrakveicwvasdgcet-tsg-----aaaalgdvhgvlipggfgirgiegkiga  378
HsCTPS1 alainhkleikyidsadlepitsqepvryheawqklcsahgvlvpggfgvrgtegiqa  384
DmCTPSC alavnrklelvfiesclleeetlhsepskyhkewqklcdshgilvpggfgsrgmegkira  384
ScCTPS1 smkcrkldikwveatdlepeagesnktkfheawnmvstadgilipggfgvrgtegmvla  389
TbCTPS  qialqvrldilyvdseelegpnad-----earkallgcdgifvpggfgnrgvdgkcaa  404

```

Figure 1.10. Partial sequence alignment for some structurally- and biochemically-characterized CTPS homologues. Amino acid sequence alignment of a portion of 8 representative CTPSs with the 'helical insertion' (or lack thereof) highlighted in blue. In descending order the proteins included in the alignment are as follows: *Escherichia coli* (taxid:562), *Thermus thermophilus* (taxid:274), *Sulfolobus solfataricus* (taxid:2287), *Mycobacterium tuberculosis* (taxid:83332), *Homo sapiens* (taxid:9606), *Drosophila melanogaster* (taxid:7227), *Saccharomyces cerevisiae* (taxid:4932), and *Trypanosoma brucei* (taxid:5691). Alignment rendering was conducted using Clustal Omega (Sievers & Higgins, 2014).

(*HsCTPS* and *DmCTPS*) form active filaments, but unicellular homologues (*ScCTPS* and, assuming the insertion is critical, *TbCTPS*) do not.

1.8 POST-TRANSLATIONAL MODIFICATIONS OF CTP SYNTHASE

The activity of eukaryotic CTPSs can be regulated by post-translational modifications (Higgins *et al.*, 2007; Kassel *et al.*, 2010; W. L. Yang, & Carman, G.M., 1996). Phosphorylation of *ScCTPS* by protein kinases A and C enhances UTP- and ATP-dependent tetramerization, and de-phosphorylation correlates with lowered CTPS activity (Pappas *et al.*, 1998; Yang *et al.*, 1994). Interestingly, phosphorylation appears to limit product inhibition suggesting that a conformational change is induced upon phosphorylation that prevents the binding of *ScCTPS* to CTP (W. L. Yang, & Carman, G.M., 1996; W. L. Yang, Bruno, M.E., & Carman, G.M., 1996). Specifically, five serine residues (Ser 36, Ser 330, Ser 354, Ser 424, and Ser 454; *S. cerevisiae* numbering) in *ScCTPS* have been identified as phosphorylation sites. Phosphorylation of any site except for Ser 330 leads to increased *ScCTPS* activity (Choi *et al.*, 2003; Park *et al.*, 1999), and phosphorylation of Ser 36, 354, and 454 stimulates phospholipid synthesis via the Kennedy pathway (Choi *et al.*, 2003; Park *et al.*, 2003). On the other hand, phosphorylation of Ser 330 inhibits enzymatic activity and correlates with decreased utilization of the Kennedy pathway (Park *et al.*, 2003).

Filament formation by *ScCTPS* (Noree *et al.*, 2010) and *DsCTPSs* (Strochlic *et al.*, 2014) is stimulated by phosphorylation and may serve to increase CTPS activity (Strochlic *et al.*, 2014; Wang *et al.*, 2015). This effect bears similarities to the formation of active *HsCTPS* filaments, and may account for the increased CTPS filamentation and Kennedy pathway activity observed for *ScCTPS*. Unlike *ScCTPS*, however, *HsCTPS1* and

HsCTPS2 are not confirmed targets of protein kinase A or C. Instead, investigation into *HsCTPS1* and *HsCTPS2* phosphorylation revealed them to be phosphorylated by glycogen synthase kinase 3 (GSK-3) and casein kinase 1 (CK1), respectively (Higgins *et al.*, 2007; Kassel *et al.*, 2010). Mass spectrometry was used to detect isotopically-labelled phosphates ($^{32}\text{PO}_4^{2-}$) ligated to Ser 574 and 575 of *HsCTPS1*, and Ser 571 and 568 of *HsCTPS2* (Higgins *et al.*, 2007; Kassel *et al.*, 2010). Inhibition of these kinases or mutation of the phosphorylated residues led to increased CTPS activity in cells suggesting that phosphorylation at these residues inhibits both human CTPS paralogues (Higgins *et al.*, 2007; Kassel *et al.*, 2010). The exact mechanism for how phosphorylation impacts CTPS activity hasn't been delineated, but glutamine-dependent activity was more inhibited by phosphorylation than when exogenous NH_3 was employed as the substrate indicating that the GATase domain was specifically affected (Kassel *et al.*, 2010). Unlike the *ScCTPS* homologues, no link between phosphorylation and filament formation has been established for human CTPS variants.

Ubiquitination may also regulate CTPS activity, but has only been studied in the context of filament formation by *DsCTPS* (Wang *et al.*, 2015). Knock-down of Cbl, an E3 ubiquitin ligase, correlated with decreased *DsCTPS* filaments and impaired the replication of genomic material in *D. melanogaster* larvae (Wang *et al.*, 2015). Furthermore, over-expression of *DsCTPS* reversed the developmental defects caused by the knock-out of Cbl (Wang *et al.*, 2015). Though the mechanism is unclear, ubiquitination may present a new mechanism for inducing the formation of CTPS filaments, especially since ubiquitination of *DsCTPS* did not target the protein for degradation (Wang *et al.*, 2015). Because Cbl is a proto-oncogene linked to development of lymphoma (Langdon *et al.*, 1989), the

regulation of CTPS by ubiquitination could be linked to the incidence of CTPS-related immunopathies in humans.

1.9 CTPS IN HUMAN HEALTH

Lowered CTPS activity has been attributed to a variety of pathologies in humans. Both human CTPS paralogues have nearly identical amino acid sequences, and the structures that have been solved for both show no significant differences (Figure 1.11). Consequently, both CTPS1 and 2 ostensibly fulfil similar intracellular duties, though the tissue-specific expression patterns for each have not been clearly delineated. Despite the similarities between the two variants, homozygous mutations causing C-terminal truncation of only CTPS1 leads to severe immunodeficiency and persistent infection by Epstein-Barr virus (Martin *et al.*, 2014). Lowered CTP levels due to the inactivation of CTPS1 caused impaired T- and B-cell proliferation following T-cell receptor activation (Martin *et al.*, 2014). Residual CTP generation catalyzed by CTPS2 was unable to compensate for the loss of CTPS1, and surviving patients required bone marrow transplantations from healthy CTPS1 carriers to restore immune function (Kucuk *et al.*, 2016; Martin *et al.*, 2014; Trück *et al.*, 2016).

Elevated levels of CTPS expression and/or activity are also associated with immune dysfunction and cell proliferation. Increased CTPS activity has been described for acute lymphocytic leukaemia, myeloid leukaemia, non-Hodgkin's lymphoma, and also a host of epithelial tissue cancers (Kaufman, 1984; Verschurr, 2007; Williams *et al.*, 1978). CTP is the least abundant nucleotide in cells (de Korte *et al.*, 1985), and is required for RNA, DNA, and phospholipid biosynthesis - all of which are required *en masse* for cell proliferation. Thus, it is no wonder that CTPS is critical for immunity and cancer

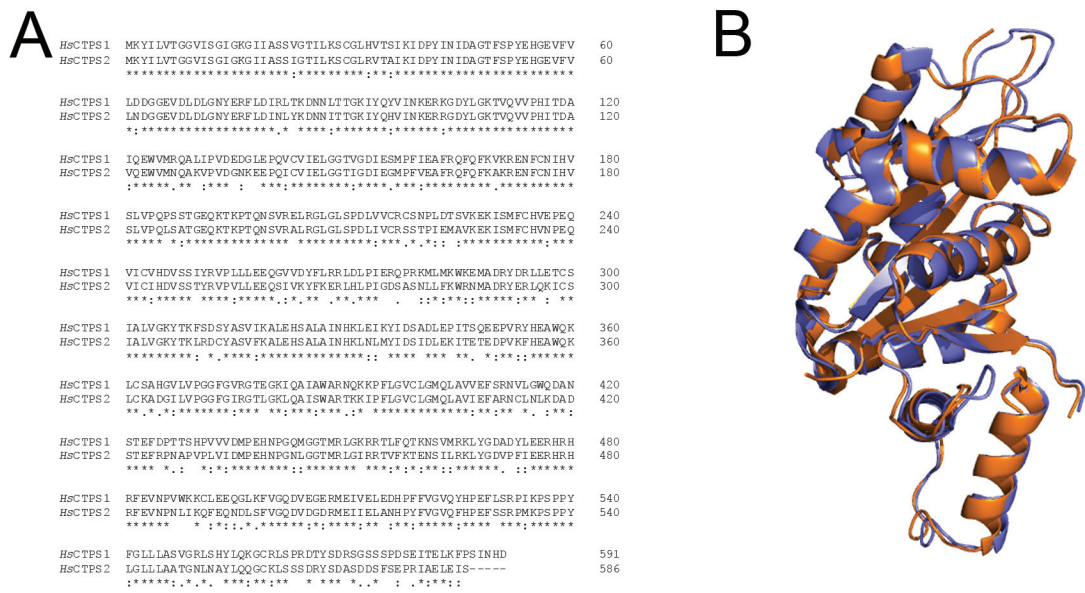


Figure 1.11. Sequence and structural comparison of *HsCTPS1* and *HsCTPS2*. **(A)** Protein sequence alignment of two human CTPSs conducted using Clustal Omega (Sievers & Higgins, 2014). Invariant residues (*) and residues showing conservation between groups of strongly (:) or weakly (.) properties are indicated. **(B)** Structural alignment of the synthase domains of *HsCTPS1* (PDB: 2VO1) and *HsCTPS2* (PDB:3IHL). Only the synthase domains are shown since there is a lack of X-ray structure data available at this time for *HsCTPSs*. Alignment and 3D rendering was performed using PyMOL 1.8.2.0 (DeLano, 2002).

progression, considering it is the sole *de novo* source of intracellular cytidine (Zalkin, 1993). One effective anticancer strategy involves depleting intracellular CTP and dCTP pools, resulting in growth arrest or apoptosis (Politi *et al.*, 1995; Verschuur *et al.*, 2000). Consequently, several CTP-based drugs have been developed to varying degrees of pharmacological success. Cyclopentenyl cytosine (CPEC), *arabino* cytosine (araC), and gemcitabine are a few cytosine-based drugs that have been developed as anti-cancer or anti-infectious agents (Heinemann *et al.*, 1995; Kang *et al.*, 1989; Schimmel *et al.*, 2007; Whelan *et al.*, 1994). Each drug is introduced as a nucleoside pro-drug that requires phosphorylation *in vivo* at the 5'-OH for cytotoxic activity (Figure 1.12). CPEC-triphosphate is an effective CTPS inhibitor with an $IC_{50} \approx 6 \mu\text{M}$ (Kang *et al.*, 1989; Schimmel *et al.*, 2007), and was a potential anti-tumour drug until severe cardiovascular toxicity was discovered to be a side-effect (Kang *et al.*, 1989; Schimmel *et al.*, 2007). AraC, which is phosphorylated to araCTP, is a safer alternative that is used to treat solid tumours, though treatment of Chinese hamster ovary cells selected for CTPS mutants that could not be product-inhibited (Whelan *et al.*, 1993). This resulted in the mass production of CTP that could theoretically compete with the drug for its intracellular targets resulting in drug resistance (Whelan *et al.*, 1993). Alternatively, gemcitabine is employed as a first-line treatment of pancreatic cancer, and the triphosphorylated form depleted intracellular CTP levels, potentially limiting the amount of competing intracellular CTP (Heinemann *et al.*, 1995). Unfortunately, resistance to gemcitabine is rapidly conferred by cytidine deaminase (Bergman *et al.*, 2002), and intra-tumoural bacteria with elevated cytidine deaminase activities can provide resistance as well (Geller *et al.*, 2017). CTP-based therapies tend to select for CTPS mutants that cannot bind CTP, increasing the intracellular

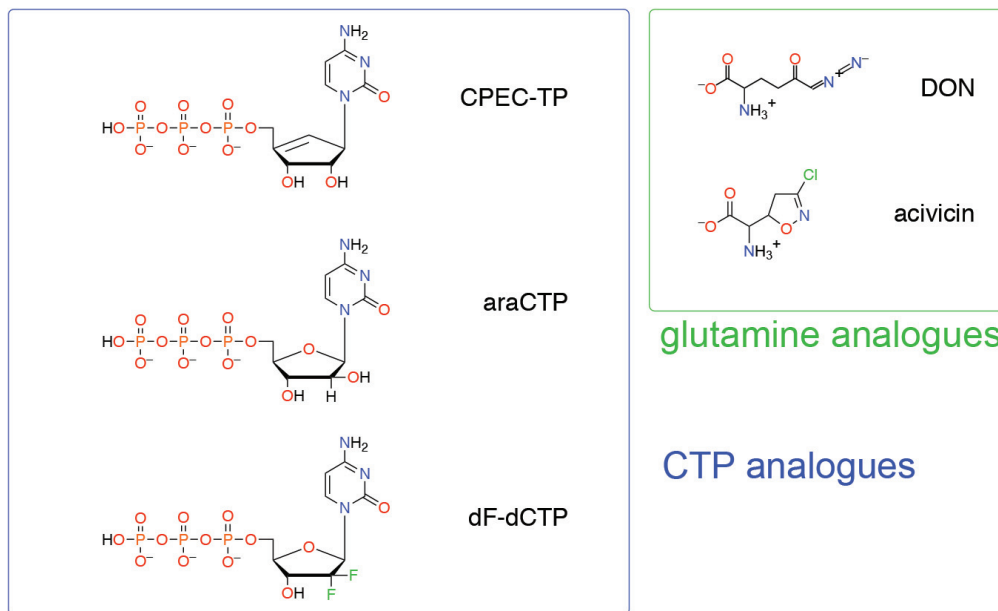


Figure 1.12. Structures for small-molecule CTPS inhibitors. Cyclopentenyl cytosine-5'-triphosphate (CPEC-TP), 2'-*arabino*-cytidine-5'-triphosphate (araCTP), and gemcitabine-5'-triphosphate (dF-dCTP) are inhibitors of the amidoligase reaction (blue box). 6-Diazo-5-oxo-L-norleucine (DON) and acivicin are mechanistic inhibitors of the GATase reaction (green box).

CTP pools and out-competing the drugs (Ostrander *et al.*, 1998; Whelan *et al.*, 1993; Whelan *et al.*, 1994).

GATase-based inhibitors constitute another stream of CTPS inhibitors that were originally developed as antiprotozoal and antiviral agents. DON and acivicin (Figure 1.12) are both Gln analogues that inactivate CTPS by alkylation of the catalytic Cys residue in the GATase domain (Chittur *et al.*, 2001; Goto *et al.*, 2004; Kemp *et al.*, 1986; Oliveira de Souza *et al.*, 2017; Zalkin & Smith, 1998). As a result, DON and acivicin reduced intracellular CTP levels in leukaemia cells (Kemp *et al.*, 1986) and effectively treated *Trypanosoma brucei* infection in mice (Hofer *et al.*, 2001). *T. brucei* lack a mechanism for salvaging cytidine, thus CTPS activity is required for trypanosome survival (Ali *et al.*, 2013; Fijolek *et al.*, 2007; Hofer *et al.*, 2001). Drawbacks to these inhibitors include a lack of specificity, resulting in cell-wide irreversible inhibition of all triad GATase enzymes due to the high conservation between members of this subclass (Chittur *et al.*, 2001). As such, there is increased importance on developing new classes of CTPS inhibitors. Phage display and high-throughput screening methods have isolated high-affinity inhibitors that bind to the ATP site of CTPS, but have not been tested exhaustively *in vivo* (Mori *et al.*, 2015; Sakamoto *et al.*, 2017).

1.10 PROJECT GOALS

Here, we used the present knowledge of CTPS regulation to investigate how EcCTPS (i) is inhibited by gemcitabine-5'-triphosphate (dF-dCTP), (ii) forms filaments, and (iii) coordinates multiple reactions while channelling NH₃ between domains. We determined that dF-dCTP is a potent parabolic, competitive inhibitor with respect to UTP, and established a structure-activity relationship describing how it is bound with high

affinity. Furthermore, these studies provide a framework for understanding inhibitor-mediated *EcCTPS* filament formation. Transmission electron microscopy (TEM) and dynamic light scattering (DLS) were used to investigate the structural determinants for CTP- and dF-dCTP-induced *EcCTPS* filament formation, and site-directed mutagenesis revealed the requirement for Phe 227 for filament elongation. Additionally, mutations that blocked CTP and dF-dCTP from binding to *EcCTPS* also prevented filament formation suggesting that the mechanism for *EcCTPS* polymerization is likely the same for both CTP analogues.

A greater mechanistic understanding of inter-domain NH₃ channelling and coupling between GATase and synthase domains was sought using a combination of site-directed mutagenesis and covalent enzyme modification. Our experiments on this topic revealed a region of the enzyme that was involved in allosteric regulation of *EcCTPS*, and the necessity of a conserved residue comprising part of the putative NH₃ gate. Specifically, substitution of Val 60, at the region between GATase and synthase domains, with Phe created a constriction in the tunnel that was relieved upon addition of Gln or formation of an alkyl-enzyme intermediate following treatment of *EcCTPS* with DON. Mutations of Val 60 also affected Gln hydrolysis, GTP-binding, and amidoligase activity and highlighted the importance of the inter-domain region in mediating many CTPS activities.

CHAPTER 2 GENERAL METHODS

2.1 GENERAL

All chemicals, unless otherwise stated, were purchased from commercial sources. The pET-15b expression system (Novagen) and HisBind resin (Novagen) were purchased from EMD Millipore (Etobicoke, ON, Canada). Synthetic DNA oligonucleotides for site-directed mutagenesis were purchased from Integrated DNA Technologies (Coralville, IA, USA). Plasmid preparations for site-directed mutagenesis and bacterial transformations were conducted using QIAprep Spin Mini-prep Kits (Qiagen, Toronto, ON, Canada). For high performance liquid chromatography experiments, a Waters 510 pump and 680 controller were used for solvent delivery, and injections were carried out with a Rheodyne 7725i sample injector fitted with a 20- μ L injection loop. Analytes were detected with a Waters 474 scanning fluorescence detector or a Waters 486 absorbance detector, as indicated. Circular dichroism studies were carried out using a JASCO J-810 spectropolarimeter.

2.2 SITE-DIRECTED MUTAGENESIS

The pET-15b-CTPS1 plasmid (Bearne *et al.*, 2001), containing the *Ec*CTPS open reading frame, was used as the template for site-directed mutagenesis. Site-directed mutagenesis was conducted using the QuickChange Site-Directed Mutagenesis Kit (Stratagene Inc., La Jolla, CA, USA) with KAPA HiFi DNA polymerase (Kapa Biosystems, Wilmington, MA, USA). The synthetic oligodeoxynucleotide primers are given in Table 2.1. DH5 α *E. coli* cells were transformed with the mutant plasmid, which was later purified using conventional protocols (Sambrook & Russell, 2006). The entire

Table 2.1. Oligodeoxynucleotide primers used for site-directed mutagenesis.^a

Substitution	Sequence (5'-3')	T _m (°C)
E149A (forward)	CAGTAGGTGATATCG CA TCCTTGCCGTTCTCG	65.2
E149A (reverse)	CGAGGAACGGCAAGGAT TGC GATATCACCTACTG	65.2
E149D (forward)	CAGTAGGTGATATCG ACT TCCTTGCCGTTCTCG	64.7
E149D (reverse)	CGAGGAACGGCAAGG AGT CGATATCACCTACTG	64.7
E149Q (forward)	CAGTAGGTGATATC CAA TCCTTGCCGTTCTCG	63.8
E149Q (reverse)	CGAGGAACGGCAAGG ATTG GATATCACCTACTG	63.8
F227A (forward)	CGTGCGAAGATTGCATTG GCCT GTAATGTTCCGG	66.4
F227A (reverse)	CCGGAACATTAC AGGC CAATGCAATCTTCGCACG	66.4
F227L (forward)	CGTGCGAAGATTGCATTG TGT GTAATGTTCCGG	64.0
F227L (reverse)	CCGGAACATTAC CAA CAATGCAATCTTCGCACG	64.0
V60A (forward)	CAATCCAACACGGGG AAGCG TTCGTTACTGAAG	64.7
V60A (reverse)	CTTCAGTAACGA ACG CTTCCCCGTGTTGGATTG	64.7
V60C (forward)	CAATCCAACACGGGG AATGC TTCGTTACTGAAG	63.4
V60C (reverse)	CTTCAGTAACGA AGCA TTCCCCGTGTTGGATTG	63.4
V60D (forward)	CAATCCAACACGGGG AAGAT TTCGTTACTGAAG	61.9
V60D (reverse)	CTTCAGTAACGA AATC TCCCCGTGTTGGATTG	61.9
V60W (forward)	CAATCCAACACGGGG AATGG TTCGTTACTGAAG	63.3
V60W (reverse)	CTTCAGTAACGA ACCA TTCCCCGTGTTGGATTG	63.3
V60F (forward)	CAATCCAACACGGGG AATTC TTCGTTACTGAAG	61.9
V60F (reverse)	CTTCAGTAACGA AGAA TTCCCCGTGTTGGATTG	61.9
H57A (forward)	GAGCCAATCCA AGCC GGGGAAAGTGTTCG	67.6
H57A (reverse)	CGAACACTTCCCC GGC TTGGATTGGGCTC	67.6

^a Mutated codons and base changes are underlined and bolded, respectively.

plasmid open reading frame was commercially sequenced (Robarts Research, London, ON, Canada) to verify that no other mutations in the nucleotide sequence were introduced.

2.3 GENE EXPRESSION AND ENZYME PURIFICATION

Wild-type and mutant forms of recombinant *Ec*CTPS were purified from *E. coli* BL21(DE3) cells transformed with the pET-15b-CTPS1, pET-15b-E149A, pET-15b-E149D, pET-15b-E149Q, pET-15b-H57A, pET-15b-CTPSV60A, pET-15b-CTPSV60C, pET-15b-CTPSV60D, pET-15b-CTPSV60W, or pET-15b-CTPSV60F plasmids as described previously (Bearne *et al.*, 2001). Soluble CTPS variants bearing an N-terminal His₆-tag were purified by metal ion affinity chromatography using established protocols (Bearne *et al.*, 2001) and dialyzed against assay buffer (70 mM HEPES, pH 8.0, 10 mM MgCl₂ and 0.5 mM EGTA). Recombinant enzyme preparations were > 98% pure as determined using 8%-SDS-PAGE analysis (Figure 2.1). The His₆-tag was not removed from the recombinant enzymes since the tag does not affect the activity of the enzyme (Bearne *et al.*, 2001). The concentration of each CTPS variant was determined from its absorbance at 280 nm using an extinction coefficient of 40340 M⁻¹cm⁻¹ for all *Ec*CTPSs (except V60W = 45840 M⁻¹cm⁻¹) bearing the His₆-tag, which was calculated using the ProtParam tool available on the ExPASy server (<http://web.expasy.org/protparam>) (Wilkins *et al.*, 2005).

2.4 UV ASSAY OF CTP GENERATION

The rate of CTPS-catalyzed conversion of UTP to CTP was determined at 37 °C by following the change in absorbance at 291 nm ($\Delta\epsilon = 1338 \text{ M}^{-1}\text{cm}^{-1}$) (Long & Pardee, 1967). The reaction mixture contained *Ec*CTPS in assay buffer (70 mM HEPES, pH 8.0, 10 mM MgCl₂, and 0.5 mM EGTA) and what was determined to be the saturating

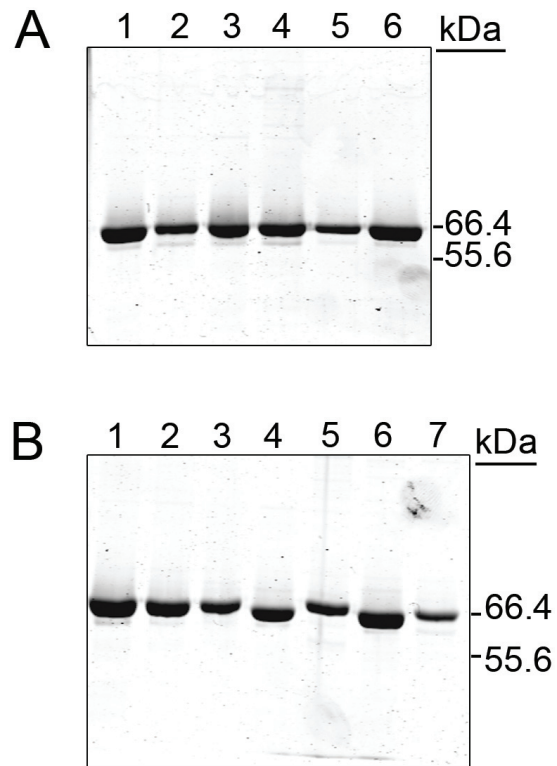


Figure 2.1. SDS-PAGE analysis of wild-type and mutant *EcCTPS* variants. SDS-PAGE (8%) analysis of recombinant His₆-tagged (**A**) wild-type (lane 1, both gels), E149A (lane 2), E149D (lane 3), E149Q (lane 4), F227A (lane 5), F227L (lane 6) and (**B**) V60A (lane 2), V60C (lane 3), V60D (lane 4), V60W (lane 5), V60F (lane 6), and H57A (lane 7). Both gels were loaded with 5 μ L of the indicated enzyme and stained with Coomassie G-250.

concentrations of ligand (Table 2.2), unless otherwise stated. Enzymes and nucleotides were pre-incubated at 37 °C followed by the addition of the NH₃ source (NH₄Cl, NH₄OAc, or Gln) to initiate the reaction. For reactions using NH₄Cl or NH₄OAc, KCl and NaOAc were used to maintain the ionic strength at 0.15 M, respectively. The [NH₃] present at pH 8.0 was calculated using a p*K*_a (NH₄⁺) of 9.24 (*i.e.*, [NH₃] = 0.0575 · [NH₄Cl]_{total}) (Iyengar & Bearne, 2003). For reactions using Gln, GTP was present at concentrations that afforded maximal activation, unless otherwise stated (Table 2.2). The values of *k*_{cat} and *K*_m were determined by fitting eqn. 2.1 to the initial velocity (*v*_i) data as a function of the concentration of substrate ([S]) using non-linear regression analysis and the program *KaleidaGraph* v. 4.02 from Synergy Software (Reading, PA). GTP was varied to determine the kinetic parameters for GTP-dependent CTP production using a saturating concentration of Gln as the NH₃ source, except where inactivity with Gln necessitated the use of NH₄OAc. The values of *K*_A, *k*_{act}, and *k*_o were estimated using non-linear regression analysis in accord with eqn 2.2. When the activation by GTP was assayed, a 0.1 cm light path was used to avoid exceeding absorbance readings > 0.7 AU, which can cause falsely lower kinetic rates in UV assays due to the high absorbance by GTP at 291 nm. UTP- and ATP-dependent CTP production were monitored similarly, but eqn 2.3 was fitted to the data to account for the cooperative behaviour of these nucleotides. Values of *V*_{max}/*[E]*_T, [S]_{0.5}, and the Hill number (*n*) were determined using non-linear regression analysis. All kinetic parameters were determined in triplicate and average values are reported ± the standard deviations (SD).

$$v_i = \frac{k_{\text{cat}}[E]_{\text{T}}[S]}{K_m + [S]} \quad (2.1)$$

Table 2.2. Saturating concentrations of *Ec*CTPS substrates and activators (in mM) used to determine kinetic parameters.

Ligand	wild-type	CTPS variant										
		E149D	E149Q	F227A	F227L	V60A	V60C	V60D	V60W	V60F	DON-V60F	
NH ₄ Cl	150	150	150	150	150	150	150	150	150	150	150	150
NH ₄ OAc	150	150	150	150	150	150	150	150	150	150	150	150
Gln	6	6	6	6	6	6	6	6	N/A	50	N/A	N/A
GTP	0.25	0.25	0.25	0.25	1	1	1	1	N/A	1	1	1
ATP	1	1	1	1	1	1	2	2	1	1	1	1
UTP	1	1	5	1	1	1	2	3	3	3	3	3

$$v_i = k_o + \frac{k_{act}[E]_T[GTP]}{K_A + [GTP]} \quad (2.2)$$

$$v_i = \frac{k_{cat}[E]_T[S]^n}{[S]_{0.5}^n + [S]^n} \quad (2.3)$$

2.5 REVERSED PHASE-HIGH PERFORMANCE LIQUID CHROMATOGRAPHY ASSAY OF GLN HYDROLYSIS

Rates of Gln hydrolysis by *Ec*CTPS variants were determined by measuring the levels of Gln and Glu derivatized by *o*-phthaldialdehyde (OPA) and β -mercaptoethanol using RP-HPLC as described previously (Iyengar & Bearne, 2002; Lunn & Bearne, 2004). *Ec*CTPS reactions were conducted in assay buffer (70 mM HEPES, pH 8.0, 10 mM MgCl₂, 0.5 mM EGTA) containing the indicated amounts of ligands in a total volume of 1.0 mL at 37 °C. At time points of 0, 1, 3, 5, and 7 min, 20- μ L aliquots were mixed with an equal volume of OPA reagent (40 mM when [Gln] \leq 20 mM; 100 mM when [Gln] \geq 20 mM). OPA reagent was prepared by dissolving OPA (27 mg) in absolute ethanol (500 μ L), followed by addition of 4.5 mL of borate buffer (0.4 M, pH 9.3) and β -mercaptoethanol (20 μ L). Following a 1 min incubation at ambient temperature, the reaction was neutralized and stopped by addition of 160 μ L NaOAc (0.1 M, pH 6.2). Injection volumes of 20 μ L were resolved on a Synergi Fusion-RP column (4 μ m; 80 Å; 50 x 4.6 mm; Phenomenex, Torrance, CA, USA). Elution was performed under isocratic conditions using a degassed 0.1 M NaOAc (pH 6.2):methanol:THF (800:190:10 v/v/v) mobile phase at a flow rate of 1.5 mL/min. Derivatives of Gln and Glu were detected using a Waters 474 scanning fluorescence detector (λ_{ex} = 343 nm; λ_{em} = 440 nm). Peak areas were determined by integration of chromatograms using PeakSimple (Mandel Scientific; Guelph, ON, Canada). The concentration of Glu produced was calculated using a standard curve prepared by

derivatization of solutions of Glu standards (0, 1.5, 3.0, 6.0, 12.5, 25.0, 75.0, and 175.0 μM).

2.6 IC₅₀ DETERMINATIONS

IC₅₀ values were determined by monitoring the rate of Gln- or exogenous NH₃-dependent CTP production in the presence of increasing amounts of inhibitor. Typically, all ligands were maintained at saturating concentrations (Table 2.2), unless otherwise stated. Inhibitor concentrations that yielded $\geq 50\%$ inhibition were used, except where 50% inhibition could not be practically obtained. In these cases, the highest concentration of inhibitor that was compatible with the assay was employed such that A₂₉₁ < 0.7 AU. Data are the average of three independent experiments \pm SD. Relative velocity data (v_i/v_o) were fitted with curves in accord with eqn. 2.4 to obtain values for IC₅₀ and n .

$$\frac{v_i}{v_o} = \frac{\text{IC}_{50}^n}{\text{IC}_{50}^n + [I]^n} \quad (2.4)$$

2.7 CIRCULAR DICHROISM SPECTROMETRY

Circular dichroism (CD) spectra for *EcCTPS* variants (0.2 mg/mL in 2 mM TrisSO₄, pH 8.0, 10 mM MgSO₄) were obtained using a JASCO J-810 spectropolarimeter and a quartz cuvette with a 0.1 cm light path. CD spectra were recorded over a wavelength range of 190–260 nm in triplicate. For each *EcCTPS* variant, the average ellipticity of a buffer blank was subtracted from the observed average of ellipticity values. Measurements were performed at a constant temperature of 37 °C except where noted otherwise.

2.8 GEL FILTRATION-HIGH PERFORMANCE LIQUID CHROMATOGRAPHY

Wild-type and mutant *EcCTPS*s (0.5 mg/mL) were analyzed using GF-HPLC. A Yarra SEC-3000 column (3 μm , 7.80 x 300 mm; Phenomenex, Torrance CA) was used to

assess the oligomerization state(s) of each variant at ambient temperature (McCluskey *et al.*, 2016). Elution was under isocratic conditions (flow rate of 0.5 mL/min) with degassed assay buffer (70 mM HEPES, pH 8.0, 10 mM MgCl₂, 0.5 mM EGTA), typically containing saturating concentrations of ATP and UTP (Table 2.2), and the protein was detected by intrinsic protein fluorescence using a Waters 474 scanning fluorescence detector ($\lambda_{\text{ex}} = 285$ nm, $\lambda_{\text{em}} = 335$ nm). Alternatively, CTP or a permutation of Gln and GTP was added to examine the effects of other ligands on oligomerization, where indicated.

CHAPTER 3 INHIBITION OF CTP SYNTHASE BY GEMCITABINE-5'- TRIPHOSPHATE

Reproduced in part with permission from – McCluskey, G.D., Mohamady, S., Taylor, S.D., Bearne, S.L. (2016) "Exploring the Potent Inhibition of CTP Synthase by Gemcitabine-5'-Triphosphate" ChemBioChem 17(23): 2240-2249. Copyright 2016 John Wiley & Sons.

3.1 INTRODUCTION

Gemcitabine (2',2'-difluoro-2'-deoxycytidine, dF-dC) is a potent chemotherapeutic agent that induces cell death through multiple different mechanisms, thus is clinically effective in treating solid tumours (Toschi *et al.*, 2005). Uptake of dF-dC into the cell is mediated by the human concentrative and equilibrative nucleoside transporters, and dF-dC subsequently enters a cascade of phosphorylation reactions that 'activate' the drug (Mini *et al.*, 2006). Gemcitabine is phosphorylated to yield its 5'-monophosphate (dF-dCMP) through the action of deoxycytidine kinase (Kroep *et al.*, 2002) and thymidine kinase 2 (S. Veltkamp *et al.*, 2008), and subsequently to its 5'-diphosphate (dF-dCDP) and 5'-triphosphate forms (dF-dCTP) by the action of UMP/CMP kinase and nucleoside diphosphate kinase, respectively (Mini *et al.*, 2006). dF-dCDP depletes dNTP pools by inhibiting ribonucleotide reductase, and dF-dCTP also inhibits the biosynthesis of nucleic acids and membrane phospholipids (Baker *et al.*, 1991; Heinemann *et al.*, 1992; Wang *et al.*, 2007). dF-dCTP is the most abundant dF-dC metabolite in treated cells, comprising 85-90% of the intracellular gemcitabine-derived species (Heinemann *et al.*, 1995; Plunkett *et al.*, 1996), and is incorporated into genomic DNA and RNA (Plunkett *et al.*, 1996; Richardson *et al.*, 2004; Ruiz van Haperen *et al.*, 1993). Incorporation into genetic material inhibits DNA polymerases α and ϵ , resulting in premature strand termination during replication (Huang *et al.*, 1991). However, free dF-dCTP can interact with a host of other

CTP-binding enzymes such as CTP:phosphocholine cytidyltransferase, which catalyzes dF-dCTP into a cytotoxic gemcitabine-choline metabolite that inhibits membrane synthesis (Bapiro *et al.*, 2014).

The deamination product, 2',2'-difluoro-2'-deoxy-UMP, depletes intracellular dTTP levels by inhibiting thymidylate synthase (Honeywell *et al.*, 2015), but 2',2'-difluoro-2'-deoxyuridine (dF-dU) is 500-fold less cytotoxic than gemcitabine and is often considered the 'inactivated' form of the drug (Rudin *et al.*, 2011). As a result, deamination of gemcitabine in tumours, catalyzed by cytidine deaminase, is linked to gemcitabine resistance (Bergman *et al.*, 2002). Studies have also demonstrated that resistance to gemcitabine can be conferred by intratumoural bacteria if they exhibit higher-than-normal cytidine deaminase activity (Geller *et al.*, 2017). Alternatively, depletion of CTP pools in Chinese hamster ovary cells, as well as solid tumour and leukaemia cell lines treated with gemcitabine, suggested that dF-dCTP exerts some of its chemotherapeutic effects by inhibiting CTPS, but direct inhibition was not demonstrated (Heinemann *et al.*, 1995). CTPS has also been associated with resistance to other cytidine-based therapies, such as arabinocytidine (araC) and gemcitabine, in which elevated CTPS activity is thought to increase the pool of CTP that out-competes the triphosphorylated forms of these two drugs (*i.e.*, araCTP and dF-dCTP) (Ostrander *et al.*, 1998; Whelan *et al.*, 1993; Whelan *et al.*, 1994). Mutations that disrupt feedback inhibition by CTP (and by extension CTP-derived drugs) have been observed in cells treated with araC (Whelan *et al.*, 1993), and elevated CTPS protein levels have been detected in gemcitabine-resistant pancreatic adenocarcinoma leading to decreased survival (Shukla *et al.*, 2017).

We investigated the mechanism by which dF-dCTP is purported to inhibit CTPS using *Ec*CTPS because of the high degree of structural identity between the human and *E. coli* CTP synthases (Figure 3.1). dF-dCTP was a competitive inhibitor of *Ec*CTPS with respect to UTP, but had a much higher affinity than the cognate ligand, CTP. Site-directed mutagenesis and several CTP and dF-dCTP analogues were then utilized to delineate a structure-activity relationship in which the 2'-*arabino* substituent imparted the lion's share of the inhibitor's potency. A single amino acid substitution also prevented inhibition by all CTP analogues tested, providing a valuable platform for the discovery of a new CTPS substrate that suggests a potential new role for CTPS in gemcitabine pharmacology.

3.2 EXPERIMENTAL

3.2.1 General

Gemcitabine-5'-triphosphate and *arabino*cytidine-5'-triphosphate (araCTP) were purchased from Jena Bioscience (Jena, Germany), and 2'-fluoro-2'-deoxycytidine (F-dCTP) was purchased from TriLink Biotechnologies (San Diego, CA, USA). 2'-Fluoro-2'-deoxy*arabino*cytidine-5'-triphosphate (F-araCTP), and additional F-dCTP, were generously provided by Dr. Masad Damha (McGill University, Montreal, QC, Canada). dF-dUTP was synthesized and provided by Dr. Samy Mohamady (The British University in Egypt, Cairo) and Dr. Scott D. Taylor (University of Waterloo, Waterloo, ON, Canada).

3.2.2 Assay of CTP Production

*Ec*CTPS activity was measured using the continuous spectrophotometric assay and data were analyzed as described in **section 2.4**. Unvaried ligands were kept at saturating concentrations in accord with Table 2.2, unless otherwise stated. *Ec*CTPS (10-30 µg/mL) was pre-incubated at 37 °C for 2 min with saturating concentrations of every ligand, except

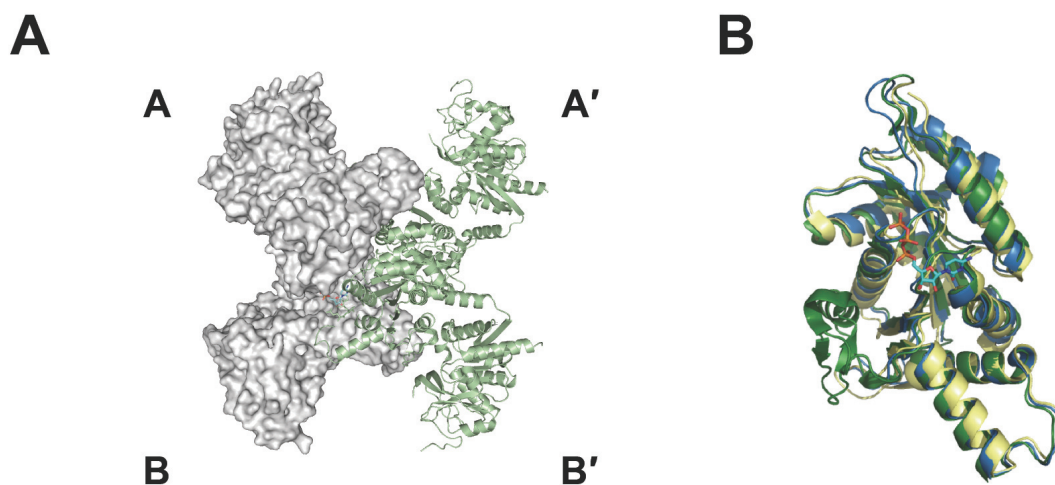


Figure 3.1. Structural comparison of *E. coli* and human CTP synthases. (A) The tetrameric *EcCTPS* structure (A-B dimer: great surface; A' -B' dimer: green cartoon) (B) The CTP-bound synthase domain from *E. coli* (green, PDB 2AD5) was super-positioned against the synthase domains from human CTPS1 (blue, PDB 2VO1), and human CTPS2 (yellow, PDB 3IHL). CTP bound in the *E. coli* CTPS structure is shown as cyan sticks. The image was rendered using PyMOL v. 1.8.2.0 (DeLano, 2002).

when one of NH₄Cl (0 – 150 mM), Gln (0 – 6.0 mM), GTP (0 – 0.8 mM), or UTP (0 – 1.5 mM for wild-type and E149D; 0 – 5.0 mM for E149Q) were varied. Data represent the average value from three independent experiments ± the standard deviations (SD).

3.2.3 Inhibition of CTPS by dF-dCTP

The inhibition of wild-type CTPS by dF-dCTP was determined by monitoring the Gln-dependent (6.0 mM) production of CTP from UTP in the presence of dF-dCTP. Initial velocity versus [UTP] plots were constructed at various fixed concentrations of dF-dCTP (0, 3, 6, 15, and 20 μM), and eqn. 3.1 (in which [S], the concentration of the substrate, is raised to the power of the Hill number *n*) was fitted to the data using nonlinear regression analysis. The apparent $[S]_{0.5}^n/V_{max}$ values, obtained from fitting the initial velocity versus [UTP] data, were re-plotted against the indicated concentration of dF-dCTP in accordance with eqn. 3.2.

$$v_i = \frac{k_{cat}[E]_T[S]^n}{[S]_{0.5}^n(1 + \frac{[I]^2}{K_i^2}) + [S]^n} \quad (3.1)$$

$$\left(\frac{[S]_{0.5}^n}{V_{max}}\right)^{app} = \left(\frac{[S]_{0.5}^n}{V_{max}}\right) + \left(\frac{[S]_{0.5}^n}{V_{max}}\right)\left(\frac{[I]^2}{K_i^2}\right) \quad (3.2)$$

IC₅₀ values were determined by monitoring the rate of Gln-dependent CTP production at a fixed concentration of UTP (0.05 mM and 0.2 mM for wild-type, 1.0 mM for E149Q) and the indicated concentrations (for wild-type and E149Q) of either CTP (5.0 – 75 μM and 5.0 – 75 μM), dF-dCTP (0.25 – 2.0 μM and 0.25 – 2.0 μM), F-dCTP (5.0 – 200 μM and 5.0 – 75 μM), araCTP (100 – 1000 μM and 100 – 1000 μM), or F-araCTP (2.5 – 50 μM and 2.5 – 50 μM). IC₅₀ determinations with E149D were conducted with

0.25 – 2.0 μM CTP and 20.0 – 200 μM dF-dCTP. Eqn. 2.4 was fitted to the inhibition data by nonlinear regression analysis to obtain the IC_{50} and n values.

3.2.4 *In Silico* Docking of dF-dCTP

The wild-type CTPS 3D coordinates, derived from an X-ray crystal structure of *E. coli* CTPS in a NTP-bound conformation (PDB: 2AD5), was docked with a 3D model of dF-dCTP using AutoDock Vina v. 1.1.2 (Trott & Olson, 2010). Co-crystallized solvent molecules and ligands were removed prior to docking of either a C2'-*endo* dF-dCTP conformer constructed using PyMOL ver 1.8.2.0, or a C3'-*endo* conformer retrieved from ChemSpider (ID: 115568) (Pence & Williams, 2010). No constraints were placed on rotatable bonds, and hydrogen atoms were added to both enzyme and ligand by use of AutoDock Tools v. 1.5.6. A search space ($40 \times 28 \times 40 \text{ \AA}$, grid spacing = 1.0 \AA) was positioned over the synthase domain near the CTP/UTP binding cleft ($x = 11.6$, $y = 5.0$, $z = -8.7$), and a random searching seed was used with an exhaustiveness level set at 50. All other AutoDock Vina parameters were kept as the default parameters. Docked dF-dCTP conformations with the highest predicted binding affinities, determined by AutoDock Vina, with respect to our positive control (CTP-docked CTPS) were selected.

3.2.5 dF-dUTP HPLC Assay

The ability of CTPS to convert dF-dUTP into dF-dCTP was initially assessed using reversed-phase HPLC. Wild-type CTPS ($377 \mu\text{g/mL}$) was incubated with ATP (1.0 mM), dF-dUTP (1.0 mM), and NH_4Cl (150 mM) at $37 \text{ }^\circ\text{C}$. Aliquots of the reaction components obtained at 0, 2.5, 5, 10, and 90 min were resolved using a Synergi Polar-RP column ($4 \mu\text{m}$, 80 \AA , $250 \times 4.60 \text{ mm}$, Phenomenex, Torrance, CA, USA) under isocratic conditions with phosphate buffer (20 mM , pH 2.7) as the eluent at a flow rate of 1.0 mL/min . The UV absorbance at 291 nm was measured with a Waters 486 absorbance detector. dF-

dUTP, dF-dCTP, and ATP eluted with retention times of 3.4, 3.3, and 3.7 min, respectively. No significant change in absorbance for dF-dUTP was observed at 291 nm over time. dF-dCTP concentrations were determined using a standard curve prepared with solutions of dF-dCTP (50, 100, 500, and 1000 μM) in assay buffer.

3.2.6 dF-dUTP UV Spectrophotometric Assay

The kinetic parameters for the conversion of dF-dUTP into dF-dCTP catalyzed by wild-type and E149D CTPSs were determined by UV spectrophotometry by measuring the changes in absorbance at 291 nm over time ($\Delta\epsilon = 1726 \text{ M}^{-1}\text{cm}^{-1}$). The extinction coefficient for dF-dUTP at pH 8.0 was $79 \text{ M}^{-1}\text{cm}^{-1}$, and that of dF-dCTP was $1805 \text{ M}^{-1}\text{cm}^{-1}$ (Figure 3.2). Strong product inhibition was observed when the reaction was carried out with wild-type CTPS, so E149D was utilized for kinetic experiments instead. To determine the affinity of E149D (20-30 $\mu\text{g}/\text{mL}$) for dF-dUTP, the enzyme was incubated with saturating concentrations of either Gln (6.0 mM) or NH_4Cl (150 mM), and varying amounts of dF-dUTP (0.1 – 2.0 mM). Alternatively, the Gln dependence of the reaction was determined by maintaining dF-dUTP at a saturating concentration (1.0 mM) and varying Gln (0.1 – 4.0 mM). KCl was used to maintain the ionic strength at 0.15 M when NH_4Cl was used as a substrate, and GTP (1.0 mM) was added when Gln was used as a substrate. The kinetic data were analyzed as previously described in **section 2.4**.

3.2.7 Product Analysis for Enzymatically Generated dF-dCTP

The CTPS-catalyzed conversion of dF-dUTP to dF-dCTP was confirmed by ESI-MS and ^{15}N NMR spectroscopy. For mass spectrometry analysis, E149D CTPS (60 $\mu\text{g}/\text{mL}$) was incubated with dF-dUTP (2.0 mM) for 2 h at 37 °C in the presence of ATP (2.0 mM) and NH_4Cl (150 mM). The enzyme was removed by centrifugation through a 10-kDa cut-off filter (Millipore), and the flow-through was lyophilized. The sample was

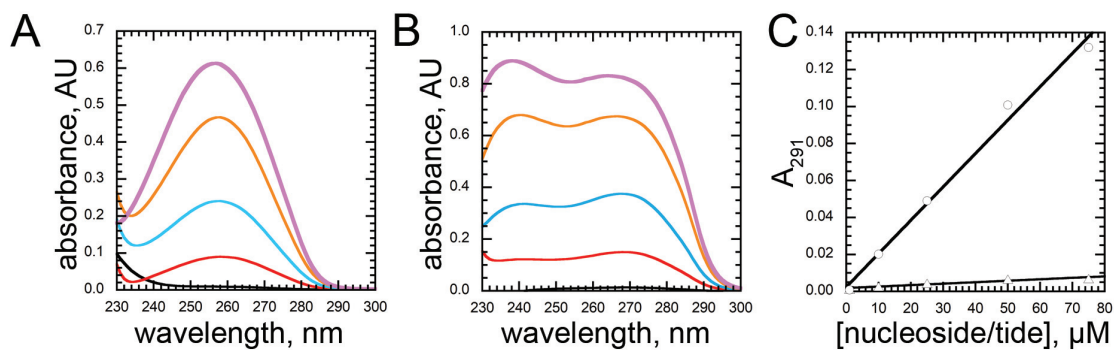


Figure 3.2. UV characterization of the conversion of dF-dUTP to dF-dCTP. $\Delta\epsilon$ was determined for dF-dCTP formation at $\lambda = 291$ nm using 1 (black), 10 (red), 25 (blue), 50 (orange), and 75 (violet) μM standard solutions of dF-dU (A) and dF-dCTP (B). (C) The resulting A_{291} for dF-dU (Δ) and dF-dCTP (\circ) plotted against concentration. Slopes for ΔA_{291} for [dF-dCTP] and [dF-dU] are 1805 and $79 \text{ M}^{-1}\text{cm}^{-1}$, respectively.

washed once with methanol (100%), followed by three washes in ethanol (80%, v/v) before being lyophilized again. For ESI-MS, the sample was reconstituted in HCl (0.1 M, 50 μ L). Acquisition was conducted using a Bruker microTOF mass spectrometer in negative ion mode. For ^{15}N NMR experiments, the sample was prepared similarly, but with the following changes. $^{15}\text{NH}_4\text{Cl}$ (150 mM) was employed as the nitrogen source for detection of ^{15}N -labelled dF-dCTP by ^{15}N NMR spectroscopy. Following the initial lyophilization step, the sample was reconstituted in 50 μ L of 1X CutSmart buffer (New England Biolabs, Ipswich, MA, USA), and calf intestinal alkaline phosphatase (2 U, New England Biolabs) was added. The solution was incubated for 2 h at 37 $^{\circ}\text{C}$ to remove the 5'-triphosphates and aid in dissolution of the sample in DMSO- d_6 . Excess salts and enzyme were removed as described for the ESI-MS analysis, the sample was lyophilized, and the residue was reconstituted in DMSO- d_6 (500 μ L). NMR analysis was carried out using a Bruker Avance (AV500) NMR spectrometer at ambient temperature.

3.2.8 Circular Dichroism

Circular dichroism (CD) spectra for wild-type, E149A, E149D, and E149Q *EcCTPS* variants (0.2 mg/mL in 2 mM Tris SO_4 , pH 8.0, 10 mM MgSO_4) were obtained as described in **section 2.7**. Measurements were performed at a constant temperature of 25 $^{\circ}\text{C}$.

3.3 RESULTS

3.3.1 Inhibition of CTP Synthase by dF-dCTP

Inhibition of *EcCTPS* by dF-dCTP was measured by monitoring the rates of Gln-dependent CTP production in the presence of increasing amounts of dF-dCTP (Figure 3.3). A competitive inhibition pattern was observed with respect to UTP upon replotting the

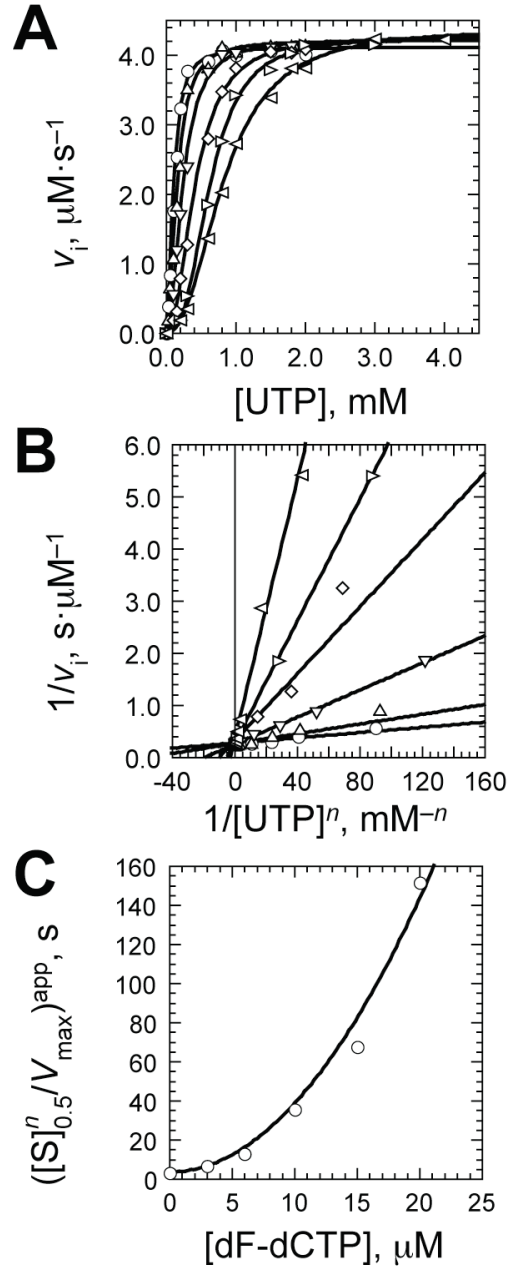


Figure 3.3. Inhibition of UTP-dependent CTP formation by dF-dCTP. **(A)** Representative plot of Gln-dependent CTP production catalyzed by wild-type CTPS. The rates of CTP production were measured at the indicated UTP concentrations in the presence of 0 (\circ), 3 (Δ), 6 (∇), 10 (\diamond), 15 (\triangleright), and 20 μM (\triangleleft) dF-dCTP. Eqn 3.1 was fit to the initial velocity data (see **section 3.2.3**), providing values for $[\text{S}]_{0.5}$, V_{max} , and n that can be found in Table 3.1. **(B)** Double-reciprocal plot showing competitive inhibition for the inhibition of CTPS-catalyzed CTP production by dF-dCTP. **(C)** Apparent $[\text{S}]_{0.5}^n / V_{\text{max}}$ values re-plotted against the concentration of dF-dCTP. The parabolic curve is a representative fit to eqn. 3.2 (see **section 3.2.3**) and the average K_i value was $3.0 \pm 0.1 \mu\text{M}$.

Table 3.1. Kinetic parameters for the inhibition of UTP-dependent CTP production by dF-dCTP

[dF-dCTP], μM	Kinetic parameter		
	$[S]_{0.5}$, mM	V_{\max} , μMs^{-1}	n
0	0.11 ± 0.01	4.10 ± 0.05	2.0 ± 0.1
3	0.16 ± 0.01	4.20 ± 0.08	2.0 ± 0.2
6	0.24 ± 0.01	4.22 ± 0.06	2.1 ± 0.1
10	0.43 ± 0.01	4.27 ± 0.08	2.2 ± 0.1
15	0.64 ± 0.01	4.25 ± 0.07	2.8 ± 0.2
20	0.84 ± 0.02	4.38 ± 0.07	2.3 ± 0.1

A

	114 116	149	
EcCTPS	rgdylgktvq ^v iphitnaikervlegge-----ghdvvlveiggtvgdieslpflea	156	
TbCTPS	qggflgktvqlvphftndvvesifrvsqspvdesgaqpeicmielggtvgdmesqpivea	187	
CgCTPS	rgeylgktvq ^v iphitdeikarilsmgepda--hgnapdvvisveggtvgdiesqpivea	169	
LlCTPS	kgeylgktvq ^m vphvtmnlkekikraattt-----dadiiitevgtvgdmeslpflea	158	
TtCTPS	rgeylsqtvq ^v iphitdeikerirkvaeeq-----kaeiVVveggtvgdieslpflea	167	
CtCTPS	ngeflgstvq ^v iphvtneiinvigscadh-----kpdiliveiggtvgdieslpflea	158	
HsCTPS1	kgdylgktvq ^v vphitdaigewmrqalipvdedglepqvcvieiggtvgdiesmpflea	162	
HsCTPS2	rgdylgktvq ^v vphitdavqewmnqakvpvgnkeepqicvieiggtvgdiegmfpivea	162	
CcCTPS	rgdylgktvq ^v iphvtneikdfvlspamdet--gekavdflvveiggtvgdieglpfivea	161	
BsCTPS	rgdylggtvq ^v iphitnelkdrvyragket-----nadvviteiggtvgdieslpflea	157	
SsCTPS	egkylggtvq ⁱ iphvtdqikdmiryaskin-----naeitlveiggtvgdieslpflea	158	
RnCTPS1	kgdylgktvq ^v vphitdaigewmrqalipvdedglepqvcvieiggtvgdiesmpflea	162	
DsCTPSC	tgeylgktvq ^v vphitdaigewvervaqtpvqgs-skpqvcvieiggtvgdiegmfpivea	161	
ScCTPS1	kgdylgktvq ^v iphltnaiqdwiervakipvddtgmpdvciielggtvgdiesapflea	162	
ScCTPS2	rgdylgktvq ^v iphltnaiqdwigrvskipvddtglepdcvieielggtvgdiesapflea	162	
SpCTPS	rgdylgktvq ^v iphvtneiQdwwervaripvdqsgeepdvciielggtvgdiesaaivea	162	
	* * * * *	* * * * *	

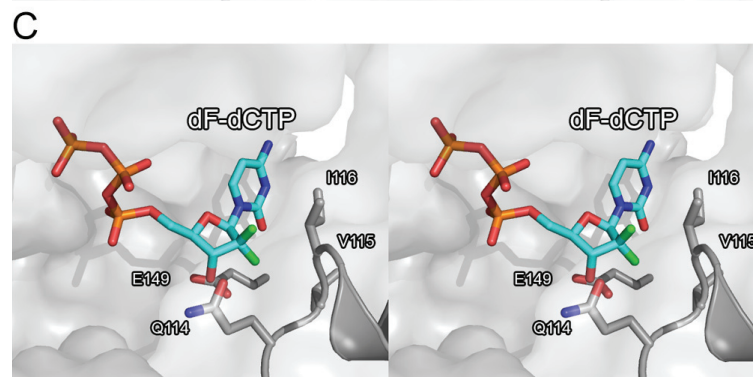
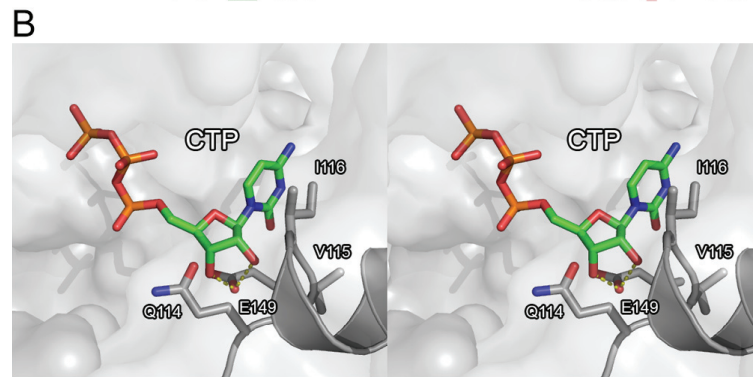


Figure 3.4. Protein sequence alignment and the CTP binding site. **(A)** Alignment of the amino acid sequences of CTP synthases from several organisms in descending order: *Escherichia coli* (taxid:562), *Trypanosoma brucei* (taxid:5691), *Corynebacterium glutamicum* (taxid:1718), *Lactococcus lactis* (taxid:1358), *Thermus thermophilus* (taxid:274), *Chlamydia trachomatis* (taxid:813), *Homo sapiens* (taxid:9606), *Caulobacter crescentus* (taxid:155892), *Bacillus subtilis* (taxid:1423), *Sulfolobus solfataricus* (taxid:2287), *Rattus norvegicus* (taxid:10116), *Drosophila melanogaster* (taxid:7227), *Saccharomyces cerevisiae* (taxid:4932), and *Schizosaccharomyces pombe* (taxid:4896). The alignment was prepared using Clustal Omega. Invariant residues (*), residues with strongly similar properties (:), and residues with weakly similar properties (.) are indicated. Residues of the Q114-V115-I116 loop (green) and Glu 149 (red) are highlighted. **(B)** Stereoview of the *EcCTPS* crystal structure (PDB 2AD5) with bound CTP showing the C2'-endo conformation of the ribose and its interaction with Glu 149 (Endrizzi *et al.*, 2004, 2005). **(C)** Stereoview of dF-dCTP (cyan, sticks) modeled in the position of CTP in the A subunit of the A-A' dimer (grey, surface representation), which is associated with the B-B' dimer (green, cartoon representation). The B' interdomain contact loop, containing the Q114-V115-I116 motif (sticks), is positioned within 3.5 Å of the 2'-F-arabino modification.

in *Ec*CTPS by substituting Glu 149 with Ala (E149A), Asp (E149D), and Gln (E149Q). Circular dichroism spectra revealed no gross changes in secondary structure between the mutant and wild-type *Ec*CTPSs (Figure 3.5); however, the E149A variant was inactive under our assay conditions. E149Q catalyzed both NH₃- and Gln-dependent CTP production, but the k_{cat}/K_m was decreased 2-fold with respect to wild-type *Ec*CTPS for both reactions (Table 3.2). The affinity of E149Q for UTP was reduced 20-fold, suggesting that the substitution had a detrimental effect on the synthase active site. E149D also exhibited 6-fold less catalytic efficiency when NH₃ was employed as the nitrogen source, but was as efficient as the wild-type enzyme ($k_{cat}/K_m = 25 \pm 1 \text{ mM}^{-1}\text{s}^{-1}$) when Gln was used ($k_{cat}/K_m = 20 \pm 4 \text{ mM}^{-1}\text{s}^{-1}$) (Table 3.2). Unlike E149Q, the affinity of E149D for UTP ($[S]_{0.5} = 0.31 \pm 0.03 \text{ mM}$) was only slightly reduced compared to the wild-type enzyme ($[S]_{0.5} = 0.11 \pm 0.01 \text{ mM}$) (Table 3.2).

Despite E149D having greater affinity for UTP than E149Q, the Asp substitution inhibited binding of CTP and dF-dCTP (Figure 3.6). Paradoxically, E149Q was inhibited by CTP and dF-dCTP similarly to wild-type *Ec*CTPS (Table 3.3) even though the UTP-dependent kinetics suggested that the active site was 'damaged'. That E149Q, but not E149D, could bind CTP and dF-dCTP demonstrated that Glu 149 was important in CTP recognition but can be substituted for a polar, isosteric residue.

3.3.3 Regioisomeric Requirements for Cytidine-Dependent Inhibition

While the inability of E149D to bind CTP and dF-dCTP demonstrated the importance of an isosteric side-chain in this position, it did not provide a conclusive reason as to why dF-dCTP binds with higher affinity than CTP. Consequently, we performed inhibition experiments on wild-type and E149Q *Ec*CTPSs using 2'-modified CTP analogues to determine which of the 2'-fluorines of dF-dCTP is more important for binding.

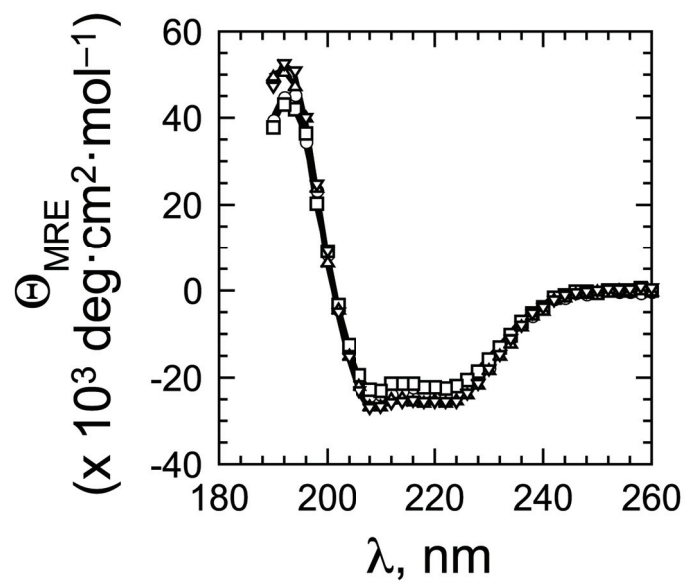


Figure 3.5. CD analysis of CTPS variants. Circular dichroism spectra for wild-type (\circ), E149D (\square), E149Q (Δ), and E149A (∇) CTPS variants were obtained at 25 °C using purified recombinant enzyme (0.2 mg/mL in 2 mM Tris-SO₄ buffer, pH 8.0, containing 10 mM MgSO₄) between 190 and 260 nm with a 0.1-cm light-path. Spectra were truncated at 194 nm where the buffer lacked transparency.

Table 3.2. Kinetic parameters for wild-type, E149D, and E149Q CTP synthases^a

Experiment	Kinetic parameter ^b	CTPS variant ^c		
		Wild-type	E149D	E149Q
NH ₃ -dependent CTP formation	K_m (mM)	2.15 ± 0.14	1.9 ± 0.9	0.21 ± 0.06
	k_{cat} (s ⁻¹)	9.50 ± 0.53	1.2 ± 0.3	0.37 ± 0.02
	k_{cat}/K_m (mM ⁻¹ s ⁻¹)	4.43 ± 0.12	0.73 ± 0.39	1.9 ± 0.6
L-Glutamine-dependent CTP formation	K_m (mM)	0.24 ± 0.02	0.15 ± 0.03	0.11 ± 0.03
	k_{cat} (s ⁻¹)	6.0 ± 0.4	2.9 ± 0.3	1.3 ± 0.1
	k_{cat}/K_m (mM ⁻¹ s ⁻¹)	25 ± 0.7	20 ± 4	12 ± 3
GTP-dependent CTP formation ^d	K_A	0.03 ± 0.01	0.14 ± 0.03	0.05 ± 0.01
	k_{act}	7.1 ± 0.3	3.66 ± 0.1	1.31 ± 0.08
	k_o	0.5 ± 0.09	0.4 ± 0.03	0.4 ± 0.06
UTP-dependent CTP formation ^d	$[S]_{0.5}$ (mM)	0.11 ± 0.01	0.31 ± 0.03	2.15 ± 0.017
	$V_{max}/[E]_T$ (s ⁻¹)	4.2 ± 0.2	4.2 ± 0.3	1.8 ± 0.1
	n	1.8 ± 0.1	0.7 ± 0.1	0.9 ± 0.1

^a See Appendix Figure A.1 for corresponding initial velocity plots.

^b Values are the averages of three experiments ± SD.

^c The activity of E149A was too low to be reliably measured.

^d See Table 2.2 for saturating ligand concentrations.

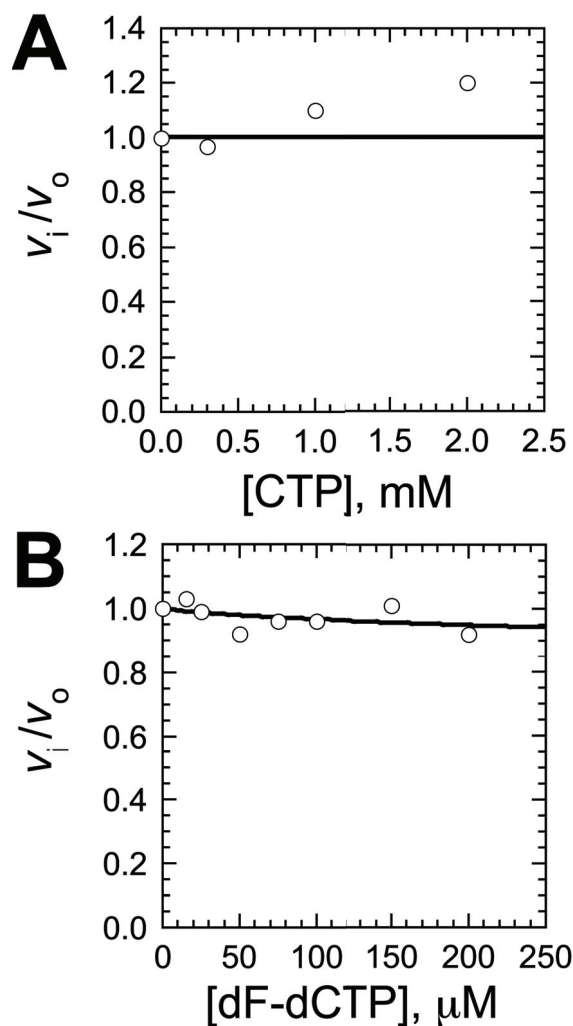
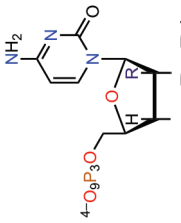


Figure 3.6 Inhibition studies for E149D using increasing amounts of CTP. (A) and dF-dCTP (B). Values of v_i/v_o were determined from the observed velocity in the presence of the inhibitor (v_i) relative to the velocity in the absence of inhibitor (v_o). Samples contained ATP, UTP, GTP (all at 1.0 mM), and the indicated concentration of inhibitor in assay buffer (70 mM HEPES, pH 8.0, 10 mM MgCl_2 , 0.5 mM EGTA). Reactions were initiated using Gln (6.0 mM) as the substrate. Eqn. 2.4 was fit to the relative velocity data.

Table 3.3. IC₅₀ values for the inhibition of CTPS-catalyzed, Gln-dependent CTP production by CTP and analogues.^a

inhibitor	 $4\text{-O}_9\text{P}_3\text{O}$	CTPS variant ^b					
		wild-type		E149Q		E149Q	
R, R'	[UTP] = 0.05 mM ^c	[UTP] = 0.2 mM ^d	[UTP] = 1.0 mM ^e	IC ₅₀ (μM)	IC ₅₀ (μM)	IC ₅₀ (μM)	n
CTP	H, OH	0.97 ± 0.25	260 ± 30	0.94 ± 0.14	52 ± 7.1	0.95 ± 0.2	n
araCTP	OH, H	> 1000 ^e	> 1000 ^e	–	> 1000 ^e	–	–
F-dCTP	H, F	109 ± 7	600 ± 100	0.94 ± 0.16	37.7 ± 9.0	1.5 ± 0.3	n
F-araCTP	F, H	35 ± 5	43 ± 5	1.03 ± 0.06	18.3 ± 2.5	1.1 ± 0.1	n
dF-dCTP	F, F	1.21 ± 0.10	3.9 ± 0.15	1.47 ± 0.01	1.5 ± 0.09	2.2 ± 0.2	n

^a See Appendix Figure A.2 for corresponding v_i/v_0 plots.

^b Values are the averages of three experiments ± SD

^c [UTP] = [UTP]_{0.5}/2

^d [UTP] = 2 × [UTP]_{0.5}

^e no significant inhibition observed

Wild-type *Ec*CTPS exhibited a 3-fold greater affinity for F-araCTP than it did for F-dCTP, though E149Q only had 2-fold greater affinity for F-araCTP (Table 3.3). These results differed from those using CTP analogues with 2'-OH groups in alternating axial (*i.e.*, 'ribo') and equatorial (*i.e.*, 'arabino') positions. Both wild-type and E149Q variants were more strongly inhibited by CTP than araCTP, suggesting that the 2'-arabino-OH group is unable to act in the same role as the 2'-arabino-F of F-araCTP or dF-dCTP (Table 3.3).

3.3.4 CTPS-Catalyzed Conversion of dF-dUTP into dF-dCTP

Since the geminal difluoro groups on dF-dCTP greatly enhanced its binding to *Ec*CTPS, we addressed whether 2',2'-difluorine substitutions would increase the binding of the deaminated variant of dF-dCTP (*i.e.*, dF-dUTP). We discovered that wild-type *Ec*CTPS catalyzed a reaction with dF-dUTP that resulted in pronounced product inhibition; however, E149D was not inhibited during the reaction (Figure 3.7). We confirmed the generation of dF-dCTP from dF-dUTP by ESI-MS (Figure 3.8), ¹⁵N- NMR spectroscopy (Figure 3.9), and RP-HPLC analysis (Figure 3.10). Though wild-type *Ec*CTPS was strongly inhibited by the dF-dCTP being generated, precluding the determination of a k_{cat} or K_{m} for the reaction, we determined that the efficiency of the reaction was approximately 6-fold lower than with UTP ($k_{\text{cat}}/K_{\text{m}} = 4.1 \pm 0.2 \text{ mM}^{-1}\text{s}^{-1}$) (Table 3.4). E149D, however, could catalyze the NH₃- and Gln-dependent reactions without being affected by product inhibition. The maximal rate of dF-dCTP generation ($V_{\text{max}}/[E]_{\text{T}} = 2.1 \pm 0.3 \text{ s}^{-1}$) was similar to that of UTP-dependent generation of CTP by E149D (Tables 3.1 and 3.3), and the catalytic efficiency of the Gln-dependent reaction ($k_{\text{cat}}/K_{\text{m}} = 5 \pm 1 \text{ mM}^{-1}\text{s}^{-1}$) was the same as it was using wild-type CTPS (Table 3.4). Surprisingly, no difference in affinity for dF-dUTP ($[S]_{0.5} = 0.26 \pm 0.07 \text{ mM}$) was observed with respect to UTP ($[S]_{0.5} = 0.31 \pm 0.03 \text{ mM}$), suggesting that the 2',2'-difluorine substitutions had no effect on binding affinity -

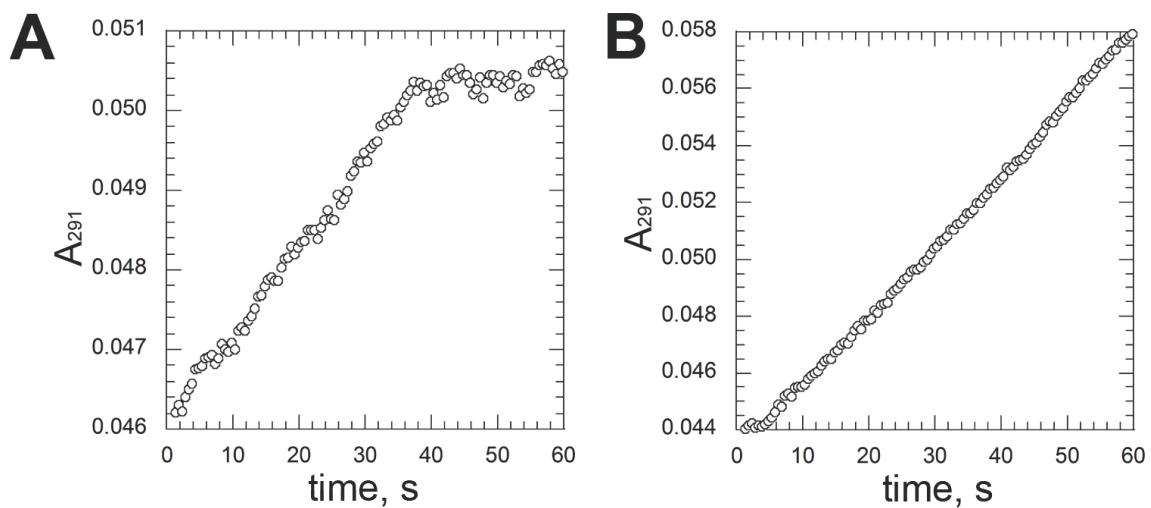


Figure 3.7. Steady-state progress curves for wild-type (A) and E149D (B) CTPS-catalyzed conversion of dF-dUTP to dF-dCTP. Both CTPSs were incubated under standard assay conditions with dF-dUTP (1.0 mM) prior to initiation of the reaction with NH_4Cl (150 mM). Reaction progress was monitored at $\lambda = 291$ nm for 60 s at 37 °C.

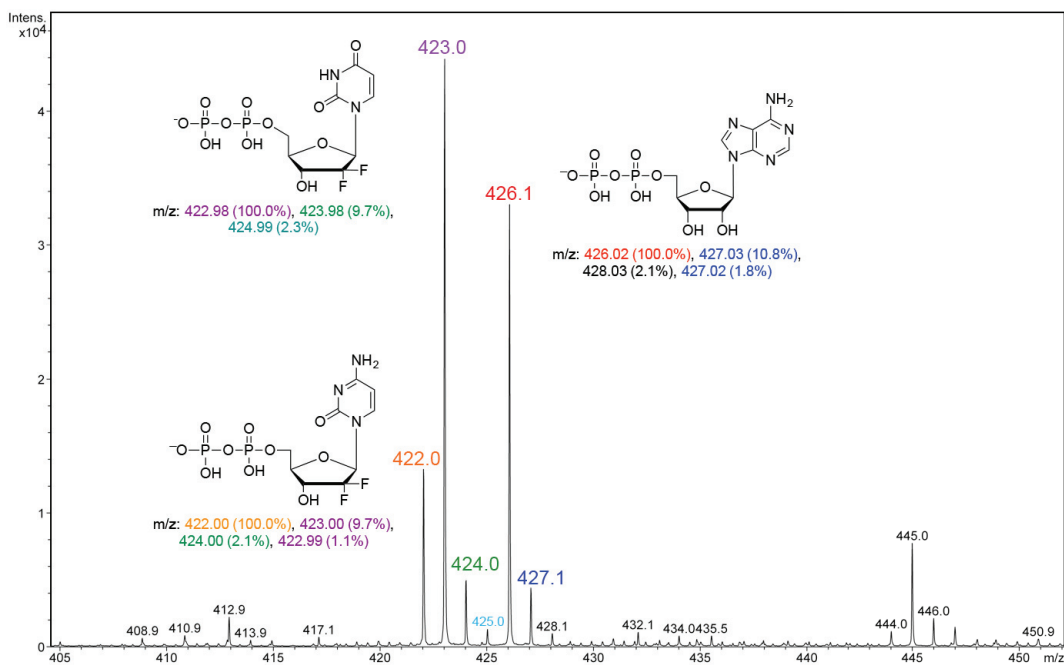


Figure 3.8. ESI-MS analysis of the nucleoside diphosphate species present in the E149D *Ec*CTPS reaction mixture, when dF-dUTP was employed as a substrate. The predominant nucleotide species detected were singly-charged nucleoside diphosphates. dF-dCDP, dF-dUDP, and ADP were detected at 422.0, 423.0, and 426.1 m/z , respectively.

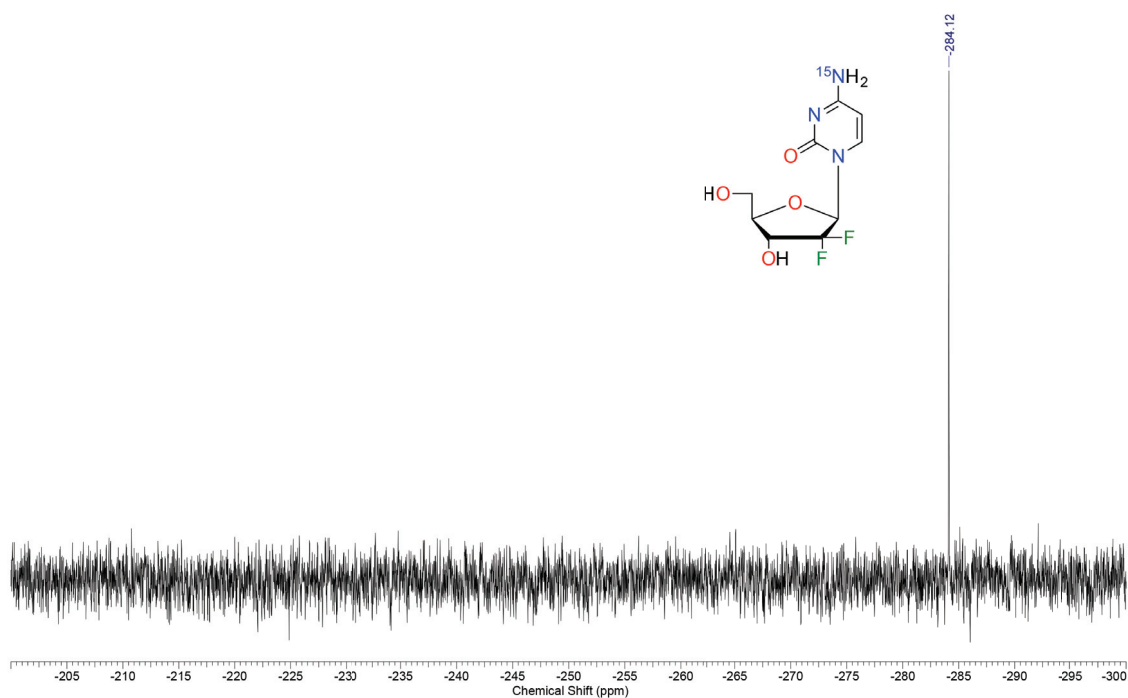


Figure 3.9. INEPT proton decoupled ^{15}N -NMR spectrum of the E149D-catalyzed conversion of dF-dUTP to dF-dCTP (solvent = DMSO-d_6). The spectrum is referenced to $\text{CH}_3^{15}\text{NO}_3$ (external standard, δ 0.0); $^{15}\text{NH}_4\text{Cl}$ has a chemical shift of $\delta -352.5$. The observed chemical shift for $4\text{-}^{15}\text{N}$ -dF-dCTP ($\delta -284.12$) is in agreement with the value of $\delta -287.7$ reported for $4\text{-}^{15}\text{N}$ -cytidine.

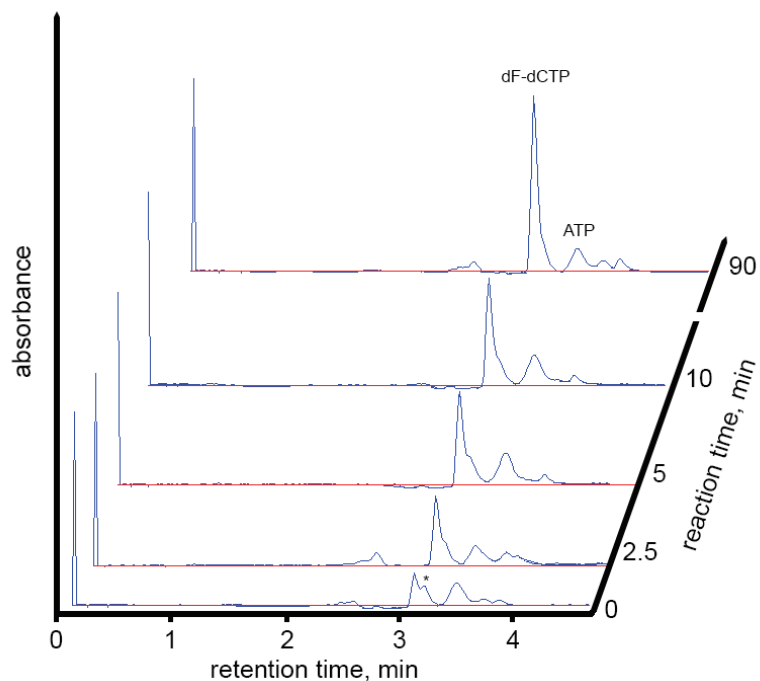


Figure 3.10. RP-HPLC chromatograms showing wild-type CTPS-catalyzed conversion of dF-dUTP to dF-dCTP. At 0, 2.5, 5, 10, and 90 min, 20 μ L injections of the CTPS reaction mixture were separated on a Synergi Polar-RP column and eluted under isocratic conditions using degassed phosphate buffer (20 mM, pH 2.7) at a flow rate of 1.0 mL/min. CTPS (6.0 μ M), dF-dUTP (1.0 mM), and ATP (1.0 mM) in assay buffer (70 mM HEPES, pH 8.0, containing 10 mM MgCl₂ and 0.5 mM EGTA) were pre-incubated at 37 °C for 2 min prior to initiating the reaction by addition of NH₄Cl (150 mM). Peaks corresponding to dF-dCTP, ATP, and dF-dUTP (*) are labelled. UV absorbance was monitored at 291 nm using a Waters 486 absorbance detector.

Table 3.4. Kinetic parameters for CTPS-catalyzed conversion of dF-dUTP into dF-dCTP^a

Varied substrate	NH ₃ source	Kinetic parameter ^b	CTPS variant	
			Wild-type	E149D
dF-dUTP	NH ₄ Cl	[S] _{0.5} (mM)	-	0.47 ± 0.02
		$V_{\max}/[E]_{\Gamma}$ (s ⁻¹)	-	0.43 ± 0.01
		n	-	1.8 ± 0.3
dF-dUTP	L-Gln	[S] _{0.5} (mM)	-	0.26 ± 0.07
		$V_{\max}/[E]_{\Gamma}$ (s ⁻¹)	-	2.1 ± 0.3
		n	-	1.2 ± 0.2
L-Gln		K_m (mM)	-	0.24 ± 0.02
		k_{cat} (s ⁻¹)	-	1.1 ± 0.2
		k_{cat}/K_m (mM ⁻¹ s ⁻¹)	4.1 ± 0.2	5 ± 1

^a See Appendix Figure A.3 for corresponding initial velocity plots.

^b Values are the averages of three experiments ± SDs.

with E149D (Table 3.4).

3.4 DISCUSSION

3.4.1 Potent Inhibition of CTPS by dF-dCTP

CTPS is a target of gemcitabine for the treatment of human cancers, but we chose to use recombinant CTPS from *E. coli* as a model enzyme for our investigation because it is the best characterized homologue. Additionally, *Ec*CTPS shares a high degree of structural and functional conservation with CTPSs from other organisms, including the two human CTPS variants (Figure 3.1). This kinetic analysis of the inhibition of *Ec*CTPS by dF-dCTP provided an inhibition constant (K_i), which was 30-fold lower than that previously reported for CTP (Scheit & Linke, 1982). The parabolic inhibition suggested that *Ec*CTPS binds two dF-dCTP molecules which may induce disadvantageous conformational changes in the adjacent, unbound, subunits. Because CTPS is a tetramer that exhibits half-of-the-sites reactivity (Levitzki *et al.*, 1971), there is assumed to be an extensive network of inter-subunit cross talk that regulates the catalytic events at one region from another. This type of inter-domain communication has been evoked for other ligands of the enzyme, but it is difficult to rationalize without a solved structure with dF-dCTP bound to the enzyme. Considering the lack of structures available, we docked a 3D model of dF-dCTP into a CTPS structure, which suggested dF-dCTP that binds similarly to CTP (Figure 3.4C). Our model for *Ec*CTPS with bound dF-dCTP as well as the structure of *Ec*CTPS with bound CTP (Endrizzi *et al.*, 2005) show three subunits interacting with the nucleotide triphosphate through multiple inter-digitating loops. If there is a structural transformation upon binding dF-dCTP that is transduced through these loops, then two dF-dCTP molecules may also inhibit unbound subunits of a *Ec*CTPS tetramer (Endrizzi *et al.*,

2005). Alternatively, CTP is known to cause *Ec*CTPS filament formation as an additional mode of catalytic regulation, and dF-dCTP may induce the same effect that could further inactivate unbound subunits if they too interact with filamentous *Ec*CTPS (see **Chapter 4**).

3.4.2 Structural Considerations for dF-dCTP Inhibition

The X-ray crystal structure of *Ec*CTPS bound to CTP shows a putative bifurcated H-bond between the 3'- and 2'-OH groups by Glu 149 (*E. coli* numbering) (Endrizzi *et al.*, 2005). Additionally, a study of the CTPS from *C. glutamicum* corroborates the importance of the Glu (that is homologous to Glu 149 in *E. coli*) residue in CTP binding since Ala substitution reduced the affinity of the enzyme for CTP (Zhu *et al.*, 2014). Surprisingly, we found that E149A was catalytically inactive in *E. coli*, but E149D was incapable of binding CTP or dF-dCTP. We initially thought that E149D was a conservative substitution since it also had an acidic side-chain, but the inability of this variant to bind CTP analogues revealed the sensitivity of the enzyme to changes in the location of the acidic group. E149Q disrupted the enzyme's ability to bind UTP, but not CTP or dF-dCTP. Previous analyses of the X-ray crystal structure of *Ec*CTPS with bound CTP suggested that Glu 149 was negatively charged, and its side-chain formed a bifurcated hydrogen bond with the ribose of CTP. However, the fact that E149Q could bind CTP and dF-dCTP suggested that Glu 149 may be protonated. The inability of E149D to bind dF-dCTP or CTP indicated that Glu 149 is important for their binding, but the E149Q variant afforded evidence that Gln is a tolerable substitute at this position. Furthermore, IC₅₀ studies using 2'-substituted CTP analogues revealed the importance of the 2'-OH-ribo group in the binding of CTP as araCTP did not inhibit either wild-type or E149Q *Ec*CTPSs. We assert that Glu 149 interacts with both the 2'-OH-ribo group of CTP and the 2'-F-ribo group of dF-dCTP based

on the inability of E149D to bind either inhibitor. If Glu 149 is negatively charged, then replacement of Glu 149 with Gln should have decreased the affinity of the enzyme for CTP; however, little change in CTP binding was observed and E149Q exhibited the same trend in binding the CTP/dF-dCTP analogues as wild-type *Ec*CTPS. These results were consistent with the 2'-F-*ribo* group making a limited contribution to binding, and signify that Glu 149 may be protonated in this site. This is further supported by the inability of *Ec*CTPS to bind araCTP or dCTP (Scheit & Linke, 1982). E149Q did exhibit slightly greater affinity for all fluorinated derivatives of CTP, relative to the wild-type enzyme, possibly owing to Glu 149 being protonated and acting as a dipole with a partial positive charge pointing towards the electronegative fluorines. Alternatively, Glu 149 may only become protonated in the presence of the fluorine substituents, whereas E149Q already has a sidechain that can act as a H-bond donor or acceptor for interaction with the 2'- and 3'-fluorine groups. Certainly, there can be other effects obscuring the exact role of Glu 149 in interacting with dF-dCTP such as the pucker conformation of the ribose ring which can change the position of the *ribo* and *arabino* substituents.

The crystal structure of *Ec*CTPS with bound CTP revealed that CTP assumes a C2'-*endo* conformation when bound, whereas dF-dCTP appears to prefer the C3'-*endo* conformation as suggested by structural studies on dF-dC incorporated into nucleic acids and in solution (Konerding *et al.*, 2002; Thibaudeau *et al.*, 1998). The C2'-*endo* conformation would position the 2'-F-*ribo* group to interact with Glu 149, and the 2'-F-*arabino* substituent would be positioned to interact with the polypeptide backbone of the Q114-V115-I116 loop on an adjacent subunit (Figure 3.4). In this conformation, the highly polarized C-F bond would likely interact with the carbonyl group of Ile 116 (approximately

2.7 Å away) through a dipolar interaction, but might also interact with the backbone amide NH group of Ile 116 (3.8 Å away), the side-chain amide group of Gln 114 (3.7 Å away), and/or form a hydrophobic interaction with the Ile 116 side chain.

The ability of C-F bonds to interact through H-bonding effects is debated, and interactions between organofluorines and proteins is more likely to arise from dipolar interactions (Dunitz & Taylor, 1997). The observed 12-fold decrease in the IC₅₀ value for dF-dCTP relative to F-dCTP is in accord with the expectation that the polarity of the C-F bonds increases with each fluorine substitution at the 2'-position (Wiberg & Rablen, 1993). Clearly, the 2'-F-*arabino* substituent of F-araCTP and dF-dCTP is responsible for much of the enhanced affinity of CTPS for dF-dCTP, and suggests that the 2'-F-*ribo* interaction is a less significant contributor to the enhanced affinity. Interaction of the 2'-F-*arabino* group with the aforementioned Q-V-I loop could also give rise to enhanced inter-subunit communication since the loop originates from another subunit in the tetramer than that of Glu 149. CTPS is highly cooperative with respect to binding of its nucleotide ligands (Levitzki & Koshland, 1969, 1971, 1972a; Levitzki *et al.*, 1971), but exactly how this occurs requires further illumination. The C3'-*endo* conformer docked similarly to the C2'-*endo* conformer (Figure 3.11), suggesting that these interactions may be retained in either conformation, but an X-ray crystal structure would lend more insight into the specific interactions between the geminal 2'-fluorine atoms and the protein. Unfortunately, few crystal structures of any CTPS homologues in the CTP-bound state have been solved, and none show UTP in an active conformation.

3.4.3 CTPS-Catalyzed Conversion of dF-dUTP into dF-dCTP

The exact binding mode of UTP in CTPS is debateable; molecular models place it in a discrete binding pocket near the γ -phosphate of ATP (Endrizzi *et al.*, 2004, 2005) and

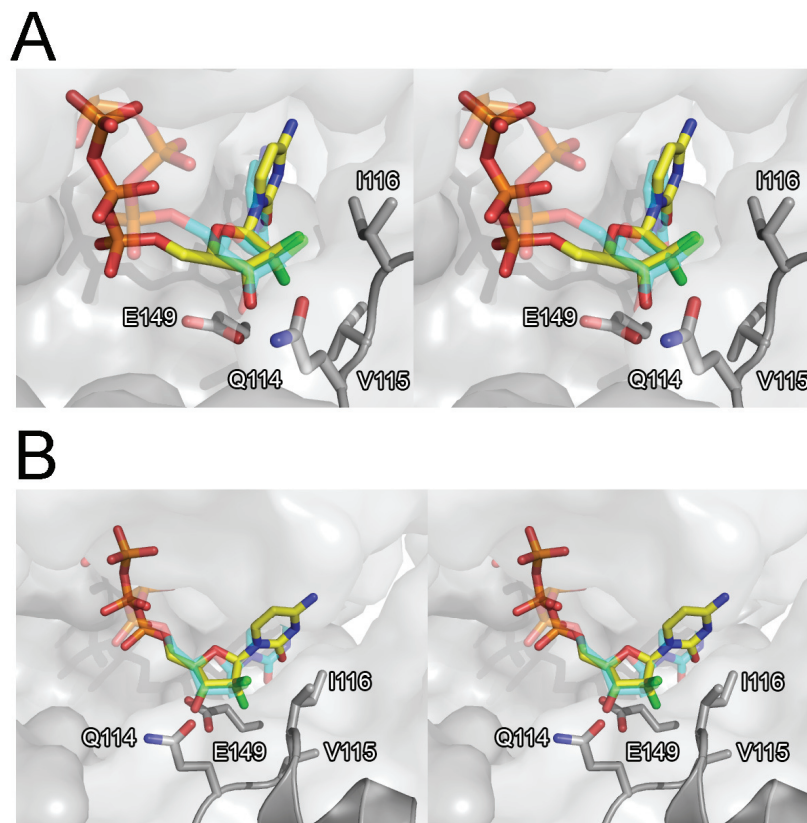


Figure 3.11. *EcCTPS* docked with dF-dCTP in the C3'-*endo* conformation (yellow sticks) super-positioned with the C2'-*endo* conformer (cyan sticks). Panel A and B are derived from the same structure, but panel B is rotated to clearly show the position of the inhibitor relative to Glu 149.

a structure of *Mt*CTPS had UTP co-crystallized in the CTP site (Mori *et al.*, 2015). Because the geminal 2'-fluorine substituents endowed dF-dCTP with increased affinity for *Ec*CTPS, we investigated whether the same substituents would increase the affinity of *Ec*CTPS for dF-dUTP. When *Ec*CTPS was incubated with dF-dUTP and substrates, an increase in absorbance at 291 nm was observed indicating that a reaction similar to the amination of CTP was occurring. Indeed, the reaction with dF-dUTP resulted in pronounced product inhibition and product analysis confirmed that dF-dCTP was being generated (Figures 3.8, 3.9, and 3.10). Conveniently, E149D was unable to bind dF-dCTP which afforded us the opportunity to perform kinetic analyses on the dF-dUTP-dependent reaction and determine the affinity of E149D for dF-dUTP. The geminal 2'-fluorines did not enhance the binding of dF-dUTP to E149D, unlike what was previously observed for dF-dCTP and wild-type CTPS.

The ability of CTPS to catalyze the conversion of dF-dUTP, with no difference in affinity for the analogue, suggests that the ribose and pyrimidine groups of UTP and CTP do indeed occupy different binding pockets as suggested by Endrizzi *et al.* (2004, 2005). Consequently, CTPS may have an important role in gemcitabine metabolism. E149D is just one mutant CTPS that can bind UTP and catalyze CTP production without product inhibition; other such mutations have been characterized for CTPS *in vitro* and *in vivo*. When Glu 161 (homologous to Glu 155 in *Ec*CTPS; Figure 3.4) in the CTPSs from *S. cerevisiae*, Chinese hamster ovary cells, and humans was mutated to Lys, the enzyme became resistant to product inhibition by CTP (Ostrander *et al.*, 1998; Whelan *et al.*, 1993; Whelan *et al.*, 1994). The inability of several well-characterized CTPS mutants to bind, but still generate CTP from UTP, is indicative of CTPS having two distinct binding pockets

for the respective nucleoside moieties. The mechanism through which UTP and CTP compete is likely mediated by a shared 5'-triphosphate binding site, as first suggested by the X-ray crystal structure of *Ec*CTPS with bound CTP (Endrizzi *et al.*, 2005). As such, the structure for *Mt*CTPS with UTP bound in the CTP orientation (Mori *et al.*, 2015) is likely an artefact, or implies that this homologue does not discriminate between the two nucleotides. The latter possibility is improbable due to the high conservation of sequence and structure between CTPSs from prokaryotes and eukaryotes. Moreover, the binding orientation of CTP positions the C-4 carbon of the uracil ring away from the γ -phosphate of ATP and NH_3 . A recent cryo-EM study on human CTPS shows UTP bound in an orientation that places the uracil ring towards the opening of the NH_3 tunnel and γ -phosphate of ATP (Lynch *et al.*, 2017), and superposition of this structure with another showing bound CTP reveals a shared 5'-triphosphate site (Figure 1.9). These structural data support the inference that UTP and CTP, while competitors for the same site, have different binding determinants for their respective nucleoside moieties. The discrimination between UTP and CTP has functional implications for CTPS in the regeneration of cytidine-based therapeutics.

Cytidine deaminases catalyze the deamination of cytidine nucleotides, the reverse of the CTPS reaction, and increased deaminase activity is associated with resistance to cytidine-based therapies such as araC and gemcitabine. For example, by deaminating gemcitabine, cytidine deaminases can reduce the efficacy of the drug by over 500-fold by converting dF-dC into the less potent dF-dU (Rudin *et al.*, 2011). Paradoxically, increased CTPS activity may theoretically contribute to resistance to these drugs due to an increase in the intracellular CTP levels that would compete for therapeutic targets. If this

mechanism is true, a lack of product inhibition arising from a mutation would further increase the intracellular CTP load and out-compete dF-dCTP for its targets. However, the intracellular concentration of dF-dUTP is often higher than that of dF-dCTP following gemcitabine treatment (Veltkamp & Kloeker-Rhoades, 2008; S. A. Veltkamp *et al.*, 2008), and the recycling of dF-dUTP - especially by a mutant CTPS that is resistant to feedback inhibition - might constitute a sensitizing mechanism through which deamination is mitigated by the CTPS-catalyzed regeneration of the more pharmacologically active dF-dCTP (Figure 3.12).

3.4.4 Conclusions

Gemcitabine is an effective chemotherapy agent used to treat various cancers, but the development of resistance to this drug is common (Bergman *et al.*, 2002; Geller *et al.*, 2017). Here, we used CTPS from *E. coli* as a model for understanding how dF-dCTP inhibits the enzyme *in vitro* due to its structural and functional similarities with the human homologues. We then established a structure-activity relationship for dF-dCTP using different 2'-substituted CTP analogues. dF-dCTP inhibited *Ec*CTPS with an apparent K_i of $3.0 \pm 0.1 \mu\text{M}$ making it one of the highest-affinity inhibitors identified for the enzyme. Furthermore, binding of dF-dCTP was reliant on an active site glutamate residue (Glu 149), and the ability of the residue to interact with the 2'-*ribo* substituent. Despite the apparent requirement for this interaction, *Ec*CTPS exhibited higher affinity for a 2'-*arabino*-F-substituted analogue (F-*ara*CTP) than one with only a 2'-*ribo*-F group indicating that much of the affinity for dF-dCTP is owing to the 2'-*arabino*-F substituent. Additionally, 2',2'-difluoro groups did not increase the affinity of the enzyme for dF-dUTP, and CTPS may be able to recycle 'inactivated' dF-dCTP by catalyzing the amination of dF-dUTP. Thus, CTPS is a potentially critical player in gemcitabine pharmacology *in vivo* since it is both

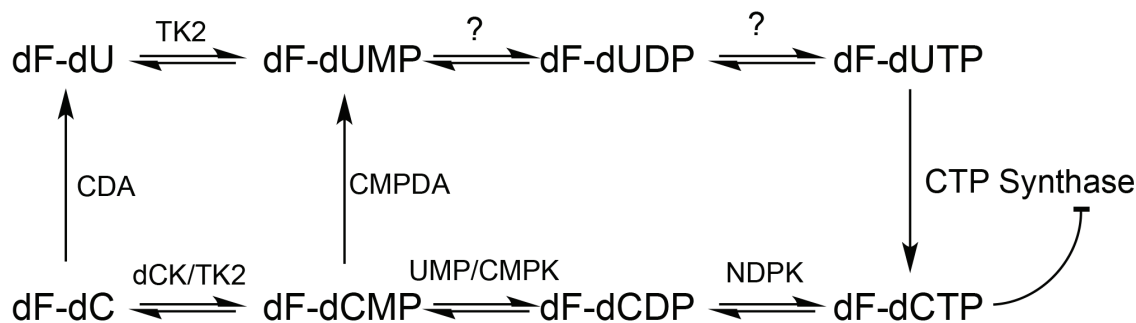


Figure 3.12. Proposed model for gemcitabine metabolism. Gemcitabine (dF-dC) and dF-dU are converted into their respective 5'-monophosphate derivatives by deoxycytidine kinase (dCK) and/or thymidine kinase 2 (TK2). Further phosphorylation of dF-dCMP into dF-dCDP and dF-dCTP is catalyzed by UMP/CMP kinase (UMP/CMPK) and nucleoside diphosphate kinase (NDPK), respectively. Catalysts of the dF-dUMP phosphorylation cascade are unidentified. Cytidine deaminase and CMP deaminase (CMPDA) catalyze the deamination reactions for the conversion of dF-dC and dF-dCMP, respectively, yielding dF-dU, and dF-dUMP, respectively. Regeneration of dF-dCTP from dF-dUTP is catalyzed by the amidoligase activity of CTP synthase, resulting in product inhibition (bar-headed arrow). (Mini *et al.*, 2006)

inhibited by dF-dCTP and can regenerate the active drug metabolite from the more abundant dF-dUTP catabolite.

CHAPTER 4 GEMCITABINE-5'-TRIPHOSPHATE INDUCES CTP SYNTHASE

FILAMENT FORMATION

Reproduced in part with permission from – McCluskey, G.D. and Bearne, S.L. (2018) "Biophysical Analysis of Bacterial CTP Synthase Filaments Formed in the Presence of the Chemotherapeutic Metabolite Gemcitabine-5'-triphosphate" J. Mol. Biol. 2836(18): 30102-5. © 2018. This manuscript version is made available under the CC-BY-NC-ND 4.0 license <http://creativecommons.org/licenses/by-nc-nd/4.0/>.

4.1 INTRODUCTION

Regulation of CTPS by CTP is not restricted to competition with UTP for the synthase active site. CTP causes CTPS to polymerize into elongated filaments though the physiological role of the filaments has not been clearly delineated. CTPS filaments in *E. coli* are product-bound and inactive (Barry *et al.*, 2014), while those made up from human CTPSs form in the presence of the NTP substrates (UTP and ATP) (Lynch *et al.*, 2017). The physiological role of CTPS filament formation in other species is poorly understood, but a growing number of studies suggest that many metabolic enzymes can form filamentous structures in situations where catalytic activity must be finely-tuned (Aughey & Liu, 2015; Beaty & Lane, 1983; Eisenberg & Tomkins, 1968; Frey *et al.*, 1975; Kim *et al.*, 2005; Petrovska *et al.*, 2014).

*Ec*CTPS filaments are the best-characterized homologues, but very little is yet known about the function of these filaments or the structural determinants for their formation. Upon binding CTP, *Ec*CTPS polymerizes into elongated filaments consisting of catalytically inactive tetramers (Barry *et al.*, 2014). Informed by the cryo-EM structures of the *Ec*CTPS filament, a mutational study on Glu 155 demonstrated the importance of CTP binding and a putative local H-bonding network that work to stabilize tetramer nucleation (Barry *et al.*, 2014; Lynch *et al.*, 2017). Having demonstrated that dF-dCTP

inhibits *Ec*CTPS with a parabolic competitive mode of inhibition in **Chapter 3**, we sought to determine to what extent this anti-tumour drug metabolite could also stimulate filament formation. Rudimentary modelling of dF-dCTP into the active site suggested that the binding mechanism is similar to that of CTP, but that dF-dCTP has additional interactions between the 2'-*arabino*-F and an interdigitating Q-V-I loop on another subunit. We hypothesized that the increased affinity owing to this novel, but putative, interaction might enhance filament formation. Indeed, we found that dF-dCTP was able to promote *Ec*CTPS filament formation similarly to CTP, but at lower concentrations, as assayed by transmission electron microscopy (TEM) and dynamic light scattering (DLS). UTP was effective in preventing and reversing filament formation, and surprisingly high concentrations of dF-dCTP were required to mitigate the filament inhibiting effects of UTP. Additionally, recent work suggested that Phe 227, located in the binding pocket for the cytosine ring of CTP, mediates an important interaction with CTP that rearranges the H-bonding pattern at the active site to give rise to stable filaments, but no functional evidence was provided (Lynch *et al.*, 2017). We investigated the roles of Glu 149 and Phe 227 to see whether CTP and dF-dCTP, neither of which are bound by E149D, share a similar mechanism in *Ec*CTPS filament formation, and whether Phe 227 is required for filament stability. Interestingly, the E149D and F227A variants were incapable of forming dF-dCTP- or CTP-induced filaments, but the F227L variant could with limited efficacy compared to wild-type *Ec*CTPS.

4.2 EXPERIMENTAL

4.2.1 General

Gemcitabine-5'-triphosphate was purchased from Jena Bioscience (Jena, Germany). Sample viscosity and refractive index were determined using a Rheosense μ VISC (San Ramon, CA, USA) and a Mettler Toledo Refracto 30GS refractometer (Mississauga, ON, Canada), respectively.

4.2.2 Transmission Electron Microscopy

Polymerization of *Ec*CTPS was assessed by TEM using an adapted protocol (Barry *et al.*, 2014). Recombinant *Ec*CTPS variants (15 μ M) were incubated in assay buffer (70 mM HEPES, pH 8.0, 10 mM Mg_2Cl , 0.5 mM EGTA) and either CTP (1.0 mM) or dF-dCTP (100 μ M) for 30 min at 37 °C. Samples were then diluted 10-fold in assay buffer containing 50% glycerol before being deposited on Formvar-coated carbon grids (TAAB Laboratories, Berkshire, UK) for uranyl acetate (0.7% w/v) staining. Negative stain transmission electron micrographs were obtained using a JEOL 1230 transmission electron microscope.

4.2.3 Dynamic Light Scattering

Light scattering measurements were conducted using a BI-200SM goniometer and laser scattering system fitted with a Brookhaven Mini-L30 diode laser (637 nm, 30 mW; Brookhaven Instruments, Holtsville, NY, USA). CTPS assay buffer and NTP stock solutions were filtered through 0.02- μ m Anotop 10 Plus filters (GE Healthcare Life Sciences, Germany) and pre-equilibrated at 37 °C prior to addition of recombinant *Ec*CTPS (3.0 μ M). The enzyme-NTP solution was promptly filtered through a 0.22- μ m nylon syringe filter (Chromatographic Specialties, Brockville, ON, Canada) into a Suprasil quartz cuvette (75 x 10 mm; Hellma Analytics, Plainview, NY, USA). The filtered sample was

equilibrated at 37 °C for 10 min prior to measurements recorded at an angle of 60° for a total duration of 2 min at 37 °C. Autocorrelation functions were fitted using a non-negative least squares (NNLS) algorithm (Brookhaven Instruments DLS software v. 5.89) to determine the intensity- and number-weighted size distributions of *Ec*CTPS oligomers and/or filaments.

4.2.4 Calculations

Calculation of *Ec*CTPS filament size was carried out using an adapted protocol for rod-like scatterers (Berne & Pecora, 2000; Hou *et al.*, 2012; Seils & Pecora, 1995; Tracy & Pecora, 1992). The Brookhaven instrument control software recorded the intensity of scattered light along the scattering vector as a function of time, and the resulting autocorrelation function was fitted with eqn. 4.1 to determine the decay times (τ) for *Ec*CTPS particles in solution. The decay times were then converted into decay rates (Γ) using eqn. 4.2. The scattering vector (q) was determined using eqn. 4.3, in which the refractive index (R_I) of the solution was 1.336, scattering angle (θ) was fixed at 60°, and the wavelength (λ) was 637 nm. The magnitude of q remained constant given that measurements were recorded at a fixed wavelength and angle. Furthermore, the temperature of the assays was fixed at 310 K, and the viscosity (η) did not change from 0.713 mPa•s under any of the conditions tested. The self-diffusion coefficient of a scatterer (D) was calculated using eqn. 4.4. For small spherical particles, the diffusion coefficient is directly proportional to the hydrodynamic diameter (d_H), as described by the Stokes-Einstein equation (eqn. 4.5). However, utilization of the Stokes-Einstein equation is not appropriate for large or rod-shaped particles (Tracy & Pecora, 1992), such as those observed for previous CTPS polymerization experiments (Barry *et al.*, 2014). Instead, we

applied theory developed by Pecora (Berne & Pecora, 2000; Hou *et al.*, 2012; Seils & Pecora, 1995; Tracy & Pecora, 1992) in which D was separated into translational and rotational diffusion coefficients. This transformation allows for the derivation of a reduced Stokes-Einstein equation for rod-like particles in solution which has been employed to describe FtsZ filaments (Hou *et al.*, 2012). By determining the decay time for a non-polymerized unit of *Ec*CTPS (*i.e.*, a tetramer), we numerically determined the number of tetramers (n) present in an *Ec*CTPS filament using its own decay time, as described by eqn 4.6.

$$G(\tau) = \exp\left(-\frac{t}{\tau}\right) \quad (4.1)$$

$$\Gamma = \frac{1}{\tau} \quad (4.2)$$

$$q = \frac{4\pi R_I}{\lambda} \sin\left(\frac{\theta}{2}\right) \quad (4.3)$$

$$D = \frac{\Gamma}{q^2} \quad (4.4)$$

$$d_H = \frac{k_B T}{3\pi\eta D} \quad (4.5)$$

$$\frac{\tau_{tet}}{\tau_{fil}} = \frac{\ln(n) + 0.316 + \frac{0.583}{n} + \frac{0.05}{n^2}}{n} \quad (4.6)$$

4.2.5 Effects of UTP on Filament Assembly

The ability of UTP to prevent CTP- and dF-dCTP-induced filament formation was examined by equilibrating *Ec*CTPS with a saturating concentration of UTP prior to addition of dF-dCTP. Samples for TEM were prepared as previously described in **section 4.2.2**, but with UTP (1.0 mM) added prior to the addition of CTP or dF-dCTP during the initial incubation at 37 °C for 30 min. For DLS analyses, independent samples of *Ec*CTPS (3.0 μM) in assay buffer containing ATP (1.0 mM) and UTP (1.0 mM), with or without either CTP (0, 50, 100, 200, 300, 600, 1000, or 10000 μM) or dF-dCTP (50, 100, 200, or

300 μM), were incubated at 37 °C for 10 min. DLS measurements were then recorded as previously described in **section 4.2.3** to determine the mean d_H value for populations of *EcCTPS* particles in these samples.

Alternatively, the ability of UTP to bind and promote filament disassembly was analyzed by DLS. *EcCTPS* (3.0 μM) was combined with assay buffer containing ATP (2.0 mM) with either CTP (1.0 mM) or dF-dCTP (100 μM) in a syringe fitted with a 0.22- μm nylon filter and filtered into the DLS cell. A control sample was prepared similarly, but with buffer instead of either cytidine analogue. All reagents were equilibrated at 37 °C prior to addition of *EcCTPS*, and measurements of mean scattering intensity were recorded once every second for 20 min. An equilibrium-state DLS measurement of the d_H was obtained for these samples following the 20-min incubation to assess particle size. Filament disassembly was then initiated by the addition of filtered UTP (1.0 mM), and the scattering intensity and equilibrium-state d_H measurements were recorded once more, as previously described.

4.2.6 Kinetic Characterization of *EcCTPS* Variants

EcCTPS activity was measured using the continuous spectrophotometric assay and data analysis methods described in **section 2.4**. Unvaried ligands were held at saturating concentrations in accord with Table 2.2, unless otherwise stated. *EcCTPS* (10-30 $\mu\text{g}/\text{mL}$) was pre-incubated at 37 °C for 2 min with saturating concentrations of every ligand, with one of NH_4Cl (0–150 mM), Gln (0-6.0 mM), GTP (0–1.0 mM), UTP (0-2.0 mM), or ATP (0-2.0 mM) varied. Due to the onset of NH_4Cl -dependent substrate inhibition for F227A and F227L, eqn. 4.7 was fitted to the data. All kinetic parameters were determined in triplicate with average values reported \pm the standard deviations (SD).

$$v_i = \frac{V_{\max}[\text{NH}_3]}{K_m + [\text{NH}_3] + \frac{[\text{NH}_3]^2}{K'}} \quad (4.7)$$

4.2.7 GF-HPLC

The ability of wild-type, E149D, F227A and F227L variants to form tetramers was evaluated using GF-HPLC as described in **section 2.8**. Wild-type and mutant *EcCTPS*s (0.5 mg/mL, 20- μ L injection volume) were eluted under isocratic conditions with assay buffer (70 mM HEPES, pH 8.0, 10 mM MgCl₂, 0.5 mM EGTA) containing saturating concentrations of ATP and UTP (both = 1.0 mM) at a flow rate of 0.5 mL/min on a Yarra SEC-3000 column (3 μ m, 7.80 mm \times 300 mm, Phenomenex, Torrance, CA, USA). Protein oligomers were detected by native protein fluorescence.

4.2.8 Circular Dichroism

Circular dichroism (CD) spectra for wild-type, E149D, F227A, and F227L *EcCTPS* variants (0.2 mg/mL in 2 mM Tris SO₄, pH 8.0, 10 mM MgSO₄) were obtained as described in **section 2.7**. Measurements were performed at a constant temperature of 37 °C.

4.3 RESULTS

4.3.1 Effects of dF-dCTP on *EcCTPS* Filaments

Binding of CTP causes large-scale filament formation by *EcCTPS* since dF-dCTP ostensibly inhibits *EcCTPS* through a similar mechanism to CTP, we investigated whether the drug metabolite could also induce *EcCTPS* filament formation. We initially replicated the TEM results of Barry *et al.* (2014) using recombinant His₆-tagged *EcCTPS* (15 μ M) and either CTP (1.0 mM) or dF-dCTP (100 μ M). Incubation of *EcCTPS* with CTP induced filament formation, as expected, and incubation with dF-dCTP also yielded filaments of comparable length and distribution (Figure 4.1A).

Interestingly, clustered filaments were detected in the absence of either cytidine analogue, but were generally dissimilar to those induced by the addition of CTP or dF-dCTP (Figure 4.2). GF-HPLC experiments showed that *Ec*CTPS eluted primarily as a lower molecular weight population in the absence of UTP and ATP, but the apparent molecular weights increased upon addition of UTP and ATP (both 1.0 mM), ATP alone (2 mM), and ATP and CTP (2.0 mM ATP; 1.0 mM CTP) (Figure 4.3). GF-HPLC detection was insensitive to species >480 kDa, consistent with the molecular weight of octameric *Ec*CTPS; therefore, larger aggregates or filaments could not be resolved. Instead, DLS was utilized to explore the effects of CTP and dF-dCTP on specific populations of *Ec*CTPS oligomers. Initially, we conducted DLS experiments on *Ec*CTPS in the absence of NTPs due to the observation of filaments in samples lacking either cytidine-derived NTP (Figure 4.2). A ~1.5 μ M threshold concentration required for *Ec*CTPS filament formation was previously determined by Barry *et al.* (2016); therefore, we utilized an enzyme concentration of 3.0 μ M for DLS experiments because it is greater than the threshold but not so great that it exceeded the detection capacity of the DLS apparatus or caused non-specific protein aggregation. Three populations of *Ec*CTPS were detected in the absence of NTPs with hydrodynamic diameters of 10, 83, and 330 nm (Figure 4.4). Upon addition of ATP and UTP, *Ec*CTPS tetramers ($d_H \approx 11$ nm) made up the highest proportion of species present in the sample, but some larger particles remained (Figure 4.4B). Because the larger species appear unresponsive to NTPs, and may diffuse similarly to larger, cytidine-induced filaments, we chose to focus primarily on the effects of CTP and dF-dCTP on the tetrameric *Ec*CTPS ($d_H \approx 12 - 14$ nm; Table 4.1).

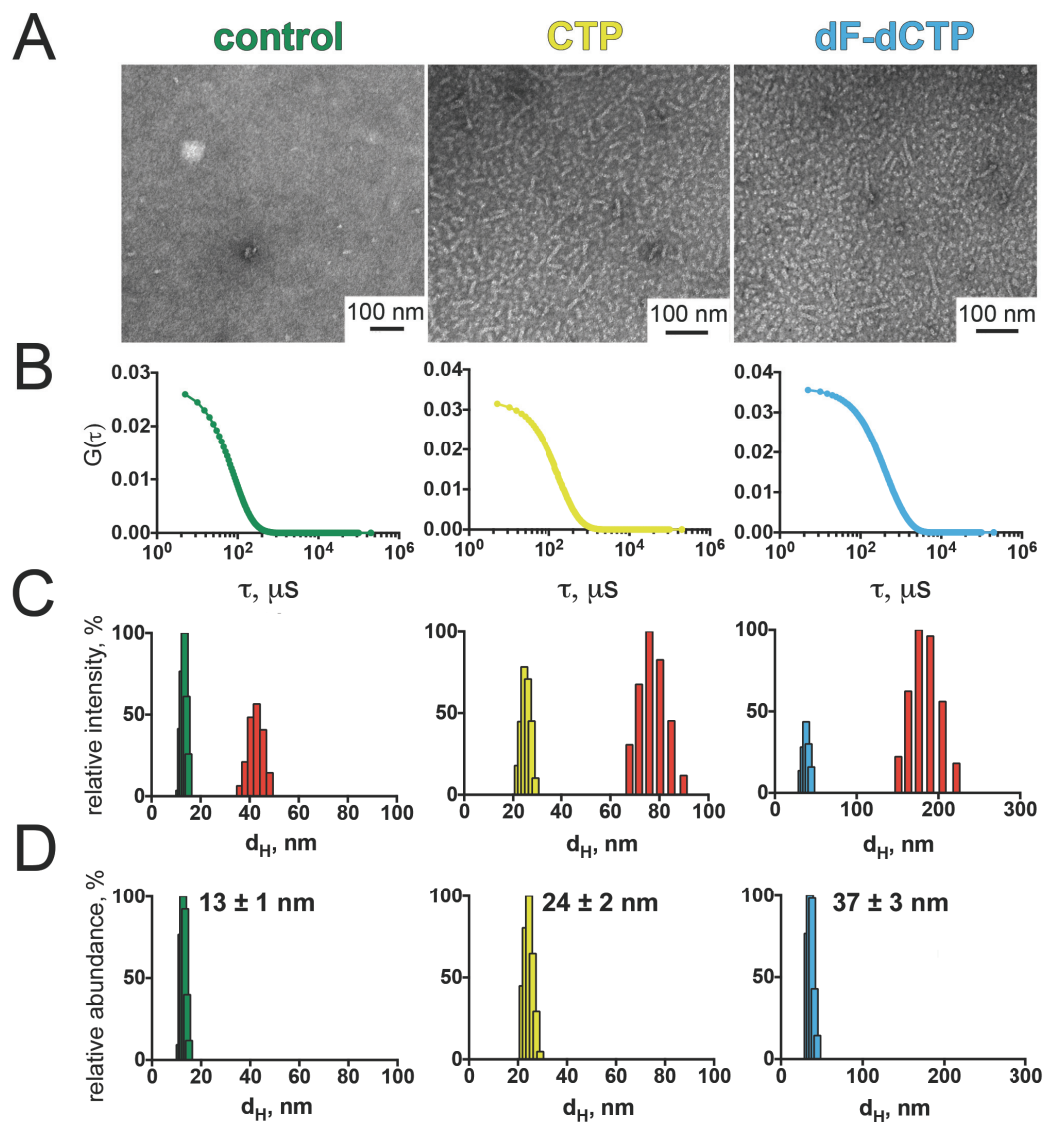


Figure 4.1. Detection of wild-type *EcCTPS* filaments by TEM and DLS. (A) Representative transmission electron micrographs of wild-type *EcCTPS* (15 μ M) incubated in assay buffer containing ATP (2.0 mM, control) and either CTP (1.0 mM) or dF-dCTP (100 μ M). Samples were incubated for 30 min at 37 $^{\circ}$ C prior to staining with uranyl acetate (0.7% w/v) and imaged using transmission electron microscopy. (B) NNLS fits to the autocorrelation functions from DLS analyses of wild-type *EcCTPS* (3.0 μ M) incubated with ATP (2.0 mM, green) and CTP (1.0 mM, yellow) or dF-dCTP (100 μ M, cyan). (C) Intensity- and (D) number-weighted distributions of *EcCTPS* derived from the NNLS fits in panel B. Relative scattering intensities are represented as a percentage of the most abundant population. The mean hydrodynamic diameters (d_H) \pm SD were determined using the decay times shown in Table 4.1. (See **section 4.2** for more detailed experimental methods)



Figure 4.2. Representative transmission electron micrograph of *EcCTPS* aggregates in the absence of ligands. Wild-type *EcCTPS* (15 μM) was incubated in assay buffer for 37 $^{\circ}\text{C}$ for 30 min prior to 10-fold dilution with assay buffer containing 50% glycerol.

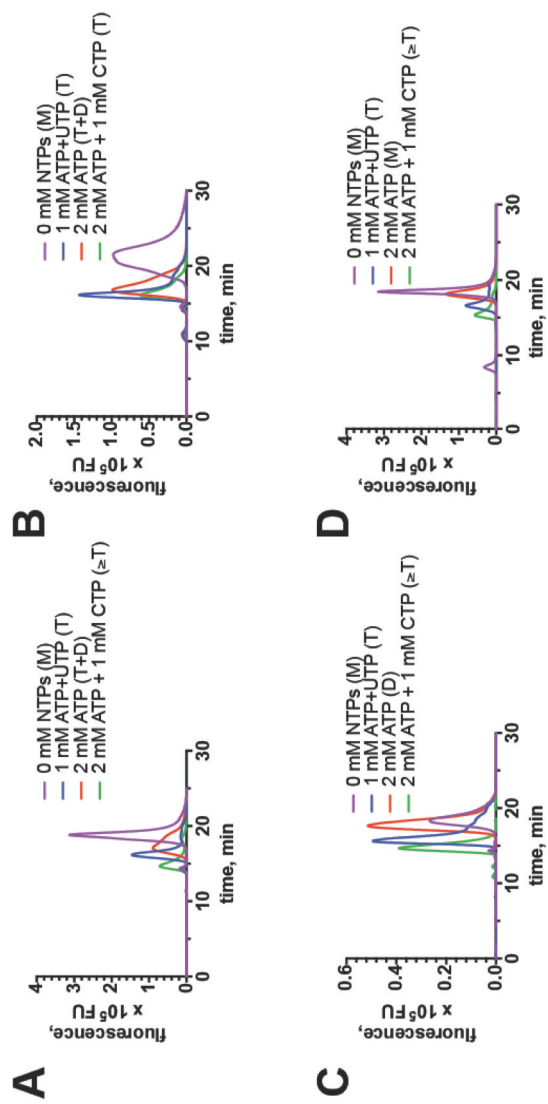


Figure 4.3. GF-HPLC analysis of wild-type (A), E149D (B), F227A (C), and F227L (D) *EcCTPS* variants. *EcCTPS*s (0.5 mg/mL, 20- μ L injection volume) were eluted under isocratic conditions with assay buffer containing no NTPs (violet), 1.0 mM ATP and UTP (blue), 2.0 mM ATP (red), or 2.0 mM ATP and 1.0 mM CTP (green). Chromatograms are representative images from three independent experiments. See [section 2.8](#) for more detailed experimental methods. M = monomer, D = dimer, T= tetramer, and \geq T includes tetrameric and higher order species.

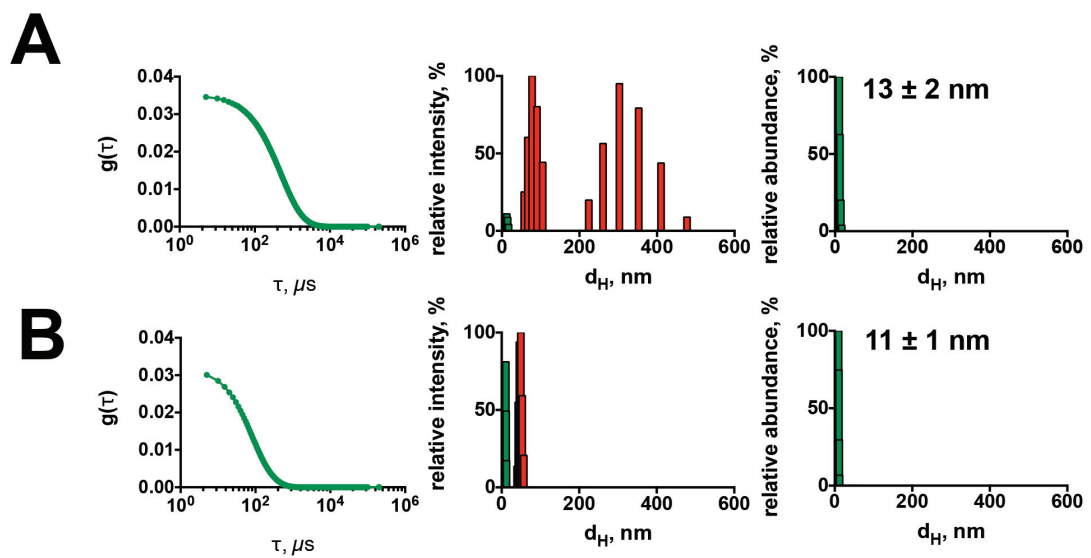


Figure 4.4. ATP and UTP limit the large-scale aggregation of wild-type *EcCTPS*. DLS measurements for wild-type *EcCTPS* equilibrated in assay buffer containing either no ligands (A), or 1.0 mM ATP and UTP (B). NNLS fits to the autocorrelation functions and mean hydrodynamic diameters (d_H) \pm SD, weighted by intensity and number, were extracted using Brookhaven Instruments DLS software v. 5.89.

Table 4.1. Length and diffusive properties for wild-type and mutant *Ec*CTPSSs equilibrated with ATP (control), and CTP or dF-dCTP.

	wild-type			E149D			F227A			F227L		
	control ^c	CTP ^d	dF-dCTP ^e	control ^c	CTP ^d	dF-dCTP ^e	control ^c	CTP ^d	dF-dCTP ^e	control ^c	CTP ^d	dF-dCTP ^e
τ , μs	121 \pm 9	230 \pm 17	331 \pm 31	108 \pm 13	113 \pm 10	101 \pm 12	122 \pm 11	113 \pm 9	124 \pm 9	109 \pm 18	199 \pm 28	164 \pm 18
Γ , $\times 10^3 \text{ s}^{-1}$	8.3 \pm 0.6	4.4 \pm 0.3	3.0 \pm 0.3	9.3 \pm 1.1	8.9 \pm 0.8	9.9 \pm 1.1	8.3 \pm 0.7	8.8 \pm 0.7	8.1 \pm 0.6	9.2 \pm 1.5	5.0 \pm 0.7	6.1 \pm 0.7
D , nm s^{-1}	48 \pm 4	25 \pm 2	17 \pm 2	53 \pm 7	51 \pm 5	57 \pm 7	48 \pm 4	51 \pm 4	47 \pm 3	53 \pm 9	29 \pm 4	35 \pm 4
d_H , nm	13 \pm 1	24 \pm 2	37 \pm 3	12 \pm 1	13 \pm 1	11 \pm 1	12.9 \pm 1	12.5 \pm 1	13.7 \pm 1	12 \pm 2	22 \pm 3	18 \pm 2
n CTPS tetramers	1	3	6	1	1	1	1	1	1	1	2	2
\sim filament length, nm^a	12	28	53	12	12	12	12	12	12	12	20	20

^a Calculated from the determined value of n using eqn. 12; ^b Calculated using eqn. 6 with n rounded to the nearest integer; ^c [ATP] = 2 mM, [CTP] = 1 mM, [ATP] = 2 mM, [dF-dCTP] = 100 μM .

The effects of CTP and dF-dCTP on filament formation in solution were assessed by incubating *EcCTPS* with ATP (2.0 mM) and either CTP (1.0 mM) or dF-dCTP (100 μ M) at 37 °C for 10 min. Following equilibration, DLS measurements were recorded, resulting in the detection of particles of mean hydrodynamic diameter of 24 ± 2 nm and 37 ± 3 nm for CTP and dF-dCTP, respectively (Table 4.1). These d_H values were approximately 2- and 3-fold higher than when *EcCTPS* was equilibrated with ATP (2.0 mM) (Table 4.1; Figure 4.1B-C). Applying Pecora's model for rod-like scatterers to our data, we calculated the mean number of tetramers (n) present in CTP- and dF-dCTP-induced filaments to be 3 and 6, respectively (Table 4.1). These values were then used to estimate actual filament length in accordance with eqn. 4.6 where L_n is the length of cryo-EM filaments with n tetramers (12 nm, from point-to-point measurement), and 3.9 nm is the mean length per tetramer that is lost due to interlocking of subunits in the *EcCTPS* filament structure. Using this approach, we estimated the mean length of CTP- and dF-dCTP-induced filaments to be approximately 28 and 53 nm, respectively (Table 4.1).

4.3.2 Effects of UTP on *EcCTPS* Filaments

Although mounting evidence shows that the nucleoside moieties of UTP and CTP are bound at two distinct pockets on *EcCTPS* (Endrizzi *et al.*, 2004, 2005; Lynch *et al.*, 2017) (also supported by evidence in **Chapter 3**), both ligands compete for the same 5'-triphosphate binding site with similar affinities ($[S]_{0.5}^{UTP} = 110 \pm 10 \mu\text{M}$; $IC_{50}^{CTP} = 81 \pm 8 \mu\text{M}$; Tables 4.2 and 4.3, respectively). On the other hand, dF-dCTP is bound by *EcCTPS* with a much higher affinity ($IC_{50}^{dF-dCTP} = 1.2 \pm 0.1 \mu\text{M}$), owing to the 2'-*arabino*-F substituent (discussed in **section 3.4.2**). To further support that dF-dCTP inhibits *EcCTPS* and induces filament formation through a similar mechanism to CTP, we examined the

Table 4.2. Kinetic parameters for wild-type and mutant *Ec*CTPS variants.

experiment	kinetic parameter ^{a,d}		CTPS variant		
	Wild-type		E149D	F227A	F227L
NH ₃ -dependent CTP formation	K_m (mM)	2.15 ± 0.14	1.9 ± 0.9	1.70 ± 0.32	0.768 ± 0.155
	k_{cat} (s ⁻¹)	9.50 ± 0.53	1.2 ± 0.3	3.2 ± 0.50	4.17 ± 0.49
	k_{cat}/K_m (mM ⁻¹ s ⁻¹)	4.43 ± 0.12	0.73 ± 0.39	1.88 ± 0.06	5.48 ± 0.46
	K'	–	–	4.7 ± 1.3	4.4 ± 1.6
L-Gln-dependent CTP formation ^{b,c}	K_m (mM)	0.24 ± 0.02	0.15 ± 0.03	0.26 ± 0.025	0.27 ± 0.015
	k_{cat} (s ⁻¹)	6.0 ± 0.4	2.9 ± 0.3	3.6 ± 0.16	4.7 ± 0.29
	k_{cat}/K_m (mM ⁻¹ s ⁻¹)	24.7 ± 0.7	20 ± 4	13.6 ± 1.16	17.2 ± 1.05
GTP-dependent CTP formation	K_A (mM)	0.032 ± 0.01	0.14 ± 0.03	0.1 ± 0.01	0.09 ± 0.01
	k_{act} (s ⁻¹)	7.1 ± 0.3	3.7 ± 0.1	3.5 ± 0.2	5.8 ± 0.2
	k_o (s ⁻¹)	0.5 ± 0.09	0.4 ± 0.03	0.3 ± 0.05	0.4 ± 0.1
UTP-dependent CTP formation ^{b,d}	$[S]_{0.5}$ (mM)	0.11 ± 0.01	0.31 ± 0.03	0.23 ± 0.01	0.14 ± 0.01
	$V_{max}/[E]_T$ (s ⁻¹)	4.2 ± 0.2	4.2 ± 0.3	4.3 ± 0.2	4.9 ± 0.2
	n	1.8 ± 0.1	0.7 ± 0.1	1.7 ± 0.1	1.8 ± 0.1
ATP-dependent CTP formation ^{b,d}	$[S]_{0.5}$ (mM)	0.18 ± 0.04	0.25 ± 0.03	0.29 ± 0.04	0.25 ± 0.01
	$V_{max}/[E]_T$ (s ⁻¹)	5.6 ± 0.2	3.5 ± 0.2	3.8 ± 0.2	4.9 ± 0.1
	n	1.5 ± 0.2	2.2 ± 0.4	2.5 ± 0.3	2.5 ± 0.3

^a Values are the average of three experiments ± SD

^b Using L-Gln as the substrate ([Gln] = 6 mM)

^c [GTP] = 0.25 mM; ^d [ATP] = 1.0 mM

^d [UTP] = 1.0 mM

^e See Appendix Figure A.4 for corresponding initial velocity plots.

Table 4.3. IC₅₀ values for the inhibition of wild-type and mutant *Ec*CTPS variants by CTP and dF-dCTP^a

	IC ₅₀ , μM ^{b,c}			
	CTP	<i>n</i>	dF-dCTP	<i>n</i>
wild-type	81 ± 8	1.1 ± 0.2	1.2 ± 0.1	1.4 ± 0.1
E149D	– ^d	–	– ^d	–
F227A	30 ± 2	1.5 ± 0.1	1.3 ± 0.3	1.5 ± 0.4
F227L	340 ± 5	1.12 ± 0.04	1.9 ± 0.2	1.1 ± 0.2

^a See Appendix Figure A.5 for corresponding v_i/v_o plots.

^b Values are the averages of three experiments ± SD

^c [UTP] = [UTP]_{0.5}/2

^d No significant inhibition observed.

dF-dCTP concentrations $\leq 200 \mu\text{M}$ - yielding populations of tetramers with $d_H \approx 13 \text{ nm}$ (Figure 4.5B). When the same experiment was performed with CTP, the addition of UTP (1.0 mM) prevented *EcCTPS* filament assembly at all CTP concentrations $\leq 1000 \mu\text{M}$ (Figure 4.5C).

To investigate the ability of UTP to bind and disassemble *EcCTPS* filaments, we induced polymerization with CTP and dF-dCTP, followed by addition of UTP. Raw scattering intensity (measured over 20 min) increased upon addition of either cytidine-derived NTP relative to control (Figure 4.6A), though the window for determining the initial rates of polymerization had apparently passed before scattering could be measured. Moreover, the addition of UTP (1.0 mM) decreased scattering intensities over the next 20-min measurement consistent with disassembly of *EcCTPS* filaments (Figure 4.6A). DLS measurements were recorded before and after the addition of UTP under each condition to determine whether the decreased scattering intensity over time correlated with a reduction in mean d_H . Prior to addition of UTP, the mean d_H for CTP- and dF-dCTP-induced filaments were $29 \pm 7 \text{ nm}$ and $41 \pm 9 \text{ nm}$, respectively, compared to the control sample of $14 \pm 2 \text{ nm}$ (Figure 4.6B). Following addition of UTP, however, the d_H values for CTP- and dF-dCTP-containing samples reduced to $15 \pm 2 \text{ nm}$ and $15 \pm 3 \text{ nm}$, respectively, while the control d_H remained at $14 (\pm 3) \text{ nm}$. Another control experiment was also performed to ensure that the decrease in scattering intensity and/or d_H was not caused by dilution due to the addition of UTP, in which the UTP-containing solution was substituted for an equal volume of assay buffer. No significant changes in raw scattering intensity or d_H were observed following addition of buffer (Figure 4.7). These data, combined with the observations discussed in **Chapter 3**, indicate that CTP and dF-dCTP share similar

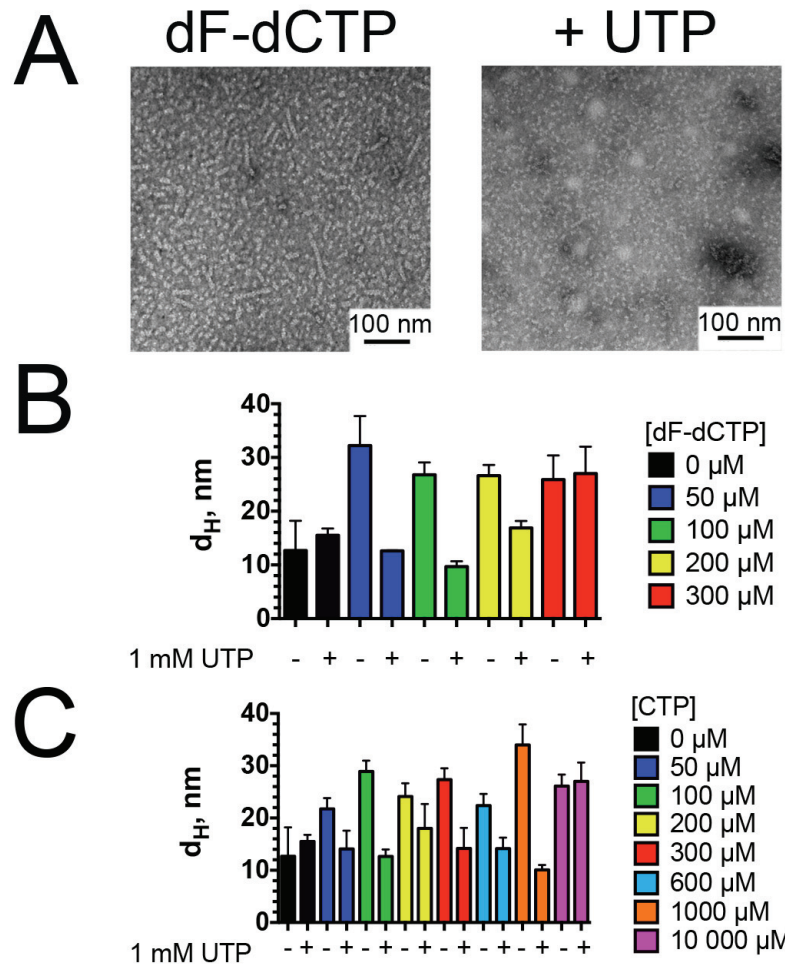


Figure 4.5. Inhibition of filament formation by UTP. (A) Representative transmission electron micrographs of wild-type EcCTPS (15 μ M) incubated in assay buffer containing dF-dCTP (100 μ M) with or without UTP (1.0 mM). Samples were diluted, stained, and imaged as described in **section 4.2.2**. The mean hydrodynamic diameters (d_H) \pm SD for wild-type *EcCTPS* incubated in assay buffer containing ATP (2.0 mM) with or without UTP (1.0 mM) and the indicated concentration of either dF-dCTP (B) or CTP (C).

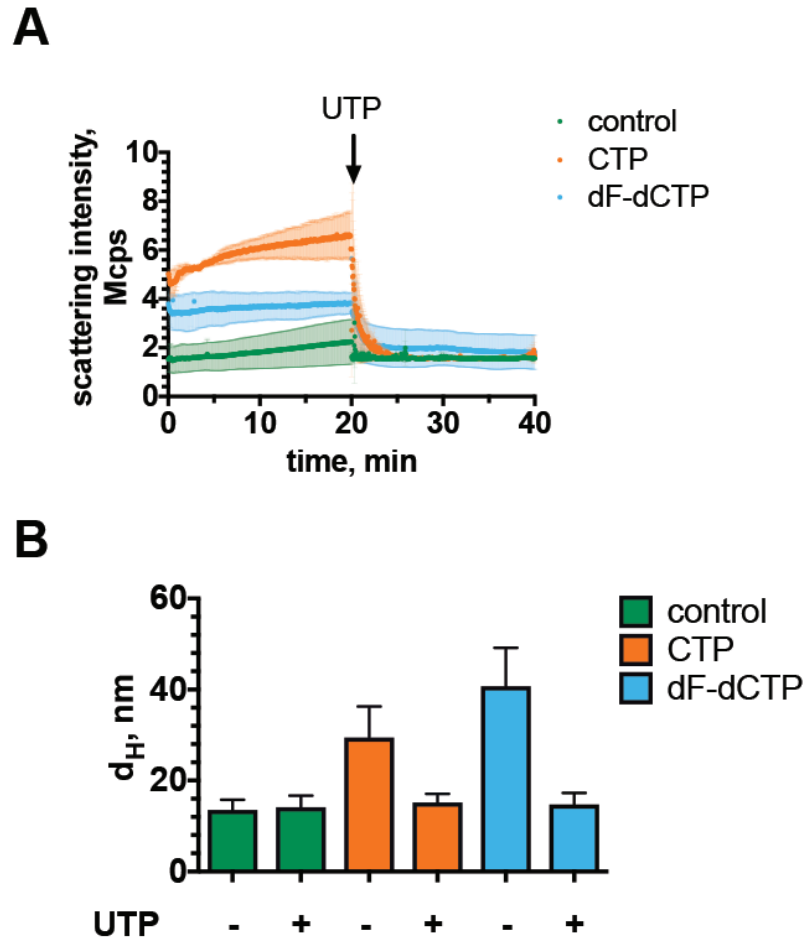


Figure 4.6. UTP-dependent disassembly of *Ec*CTPS filaments. (A) Scattering intensity was measured for *Ec*CTPS (3.0 μ M) in the presence of ATP (2.0 mM, control) with either CTP (1.0 mM) or dF-dCTP (100 μ M) over 20 min. UTP (1.0 mM) was then added and scattering intensities were recorded for another 20 min. (B) Equilibrium-state measurements of mean hydrodynamic diameters (d_H) obtained for the samples described in panel (A) before (-) and after (+) addition of UTP. Data are the average of three independent trials \pm SD.

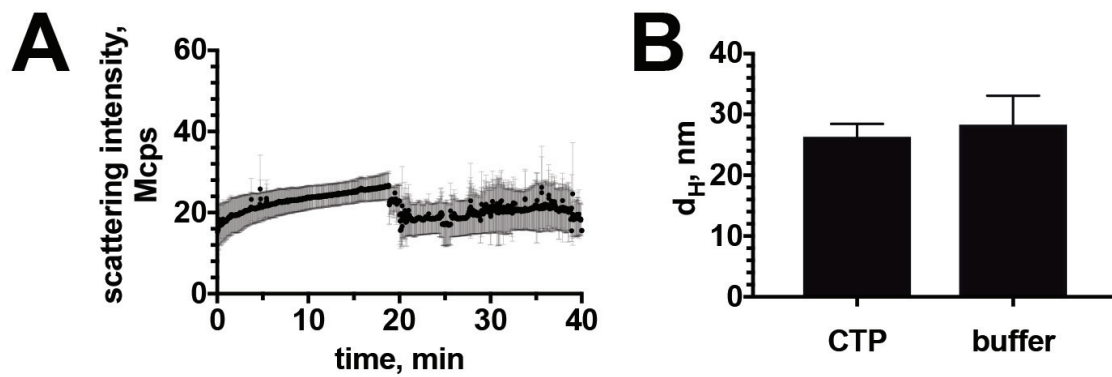


Figure 4.7. Dilution by assay buffer does not cause *EcCTPS* filament disassembly. **(A)** Scattering intensity was measured for *EcCTPS* (3.0 μM) in the presence of ATP (2.0 mM, control) with CTP (1.0 mM) over 20 min. Assay buffer (50 μL) was then added and scattering intensities were recorded for another 20 min. **(B)** Equilibrium-state measurements of mean hydrodynamic diameters (d_{H}) obtained for the samples described in panel **(A)** before (-) and after (+) addition of assay buffer. Data are the average of three independent trials \pm SD.

mechanisms for *Ec*CTPS inhibition *and* filament formation.

4.3.3 Structural Determinants for CTP- and dF-dCTP-Induced *Ec*CTPS Filament Formation

Using the available structural information for *Ec*CTPS with bound CTP, and the model of dF-dCTP bound in the active site (Figures 3.3 and 3.10), we probed the structural determinants for CTP- and dF-dCTP-induced filament formation. As discussed in **Chapter 3**, Glu 149 is required for the recognition of the 3'- and 2'-substituents of cytidine-derived nucleotide triphosphates (Table 3.2); therefore, we investigated the importance of this residue for *Ec*CTPS filament formation in the presence of CTP and dF-dCTP. E149D exhibited similar kinetic efficacy to wild-type *Ec*CTPS, with no major changes in the apparent affinities for GTP, UTP, or ATP ($K_A^{\text{GTP}} = 0.14 \pm 0.03$ mM; $[S]_{0.5}^{\text{UTP}} = 0.31 \pm 0.03$ mM; $[S]_{0.5}^{\text{ATP}} = 0.25 \pm 0.03$ mM) (Table 4.2). TEM experiments revealed that E149D was unable to form filaments in the presence of either nucleotide (Figure 4.9). In GF-HPLC experiments, E149D eluted with ATP (2.0 mM) and CTP (1.0 mM) at the same time as wild-type *Ec*CTPS with ATP and UTP (both 1.0 mM), indicating that the mutant *Ec*CTPS could not oligomerize beyond a tetramer. However, higher-order species were detected for wild-type *Ec*CTPS by GF-HPLC when CTP was present (Figure 4.3). E149D was also incapable of forming CTP- or dF-dCTP-induced filaments under DLS conditions, suggesting that recognition of CTP by Glu 149 is necessary for filament formation (Table 4.1, Figure 4.8). We did, however, detect signal corresponding to the same high- d_H species (red bars, Figure 4.8) observed in the experiments with wild-type *Ec*CTPS (red bars, Figure 4.4) in the absence of ligands indicating that higher-order species form independently of CTP and dF-dCTP.

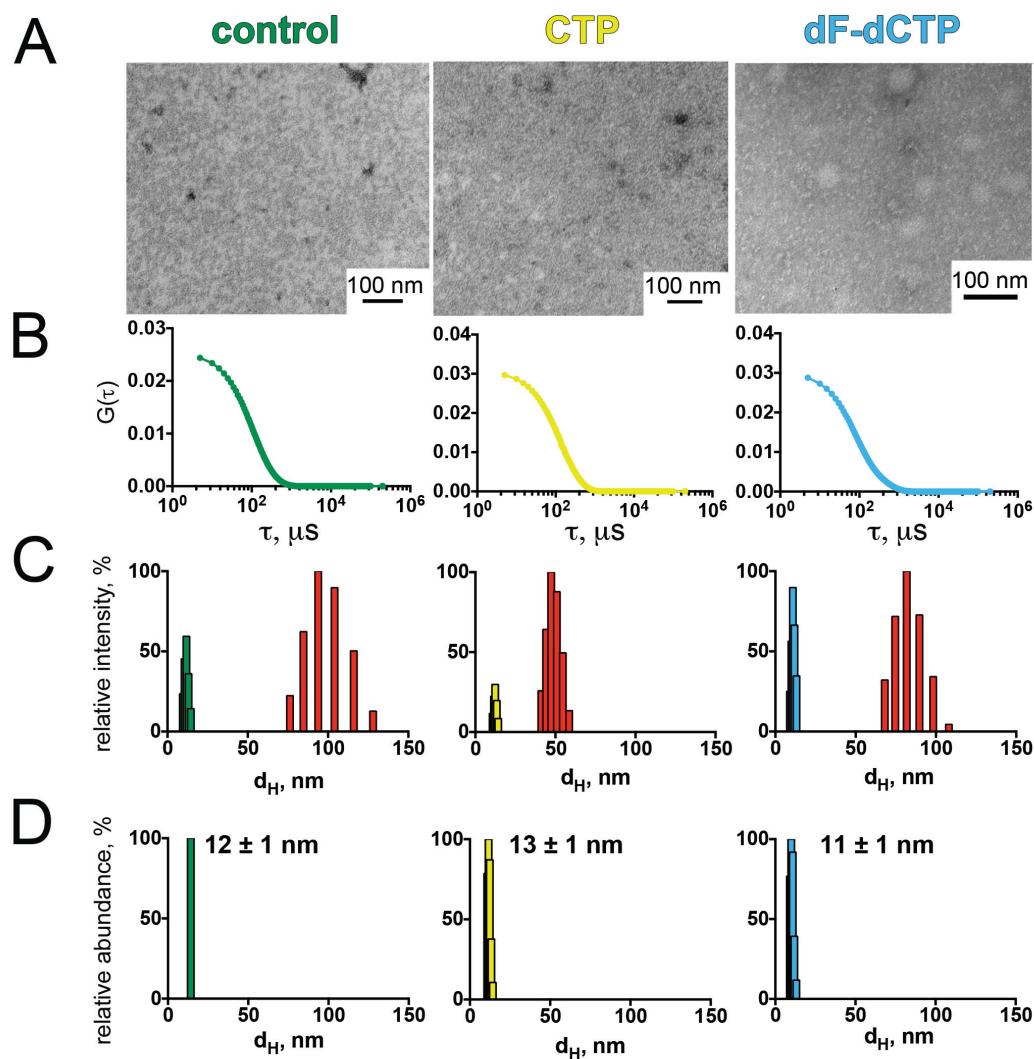


Figure 4.8. Detection of E149D *EcCTPS* filaments by TEM and DLS. (A) Representative transmission electron micrographs of E149D *EcCTPS* (15 μ M) incubated in assay buffer containing ATP (2.0 mM, control) and either CTP (1.0 mM) or dF-dCTP (100 μ M). Samples were incubated for 30 min at 37 $^{\circ}$ C prior to staining with uranyl acetate (0.7% w/v) and imaged using transmission electron microscopy. (B) NNLS fits to the autocorrelation functions from DLS analyses of E149D *EcCTPS* (3.0 μ M) incubated with ATP (2.0 mM, green) and CTP (1.0 mM, yellow) or dF-dCTP (100 μ M, cyan). (C) Intensity- and (D) number-weighted distributions of *EcCTPS* derived from the NNLS fits in panel B. Relative scattering intensities are represented as a percentage of the most abundant population. The mean hydrodynamic diameters (d_H) \pm SD were determined using the decay times shown in Table 4.1.

Recognition of the cytosine ring may also be an important requirement for cytidine-dependent filament formation, and recent structural analyses have invoked Phe 227 as an important CTP-binding determinant that stabilizes *Ec*CTPS filaments (Lynch *et al.*, 2017). Lynch *et al.* (2017) asserted that Phe 227 forms an edge-on interaction with the cytosine ring of CTP that rearranges the H-bond network in *Ec*CTPS to stabilize the filament conformation. To test the possibility that Phe 227 is important for *Ec*CTPS filament formation, we constructed F227A and F227L *Ec*CTPS variants and characterized their kinetic parameters. F227A and F227L exhibited the same affinity for Gln ($K_m = 0.26 \pm 0.03$ and 0.27 ± 0.02 mM, respectively), and both variants had similar catalytic efficiencies ($k_{cat}/K_m = 14 \pm 1$ and 17 ± 1 mM⁻¹s⁻¹, respectively) to wild-type *Ec*CTPS (Table 4.2). Importantly, no major defects in the apparent binding affinities (*i.e.*, $[S]_{0.5}$ and K_A values) for GTP, UTP, or ATP were observed for F227A ($K_A^{GTP} = 0.10 \pm 0.01$ mM; $[S]_{0.5}^{UTP} = 0.23 \pm 0.01$ mM; $[S]_{0.5}^{ATP} = 0.29 \pm 0.04$ mM) or F227L ($K_A^{GTP} = 0.09 \pm 0.01$ mM; $[S]_{0.5}^{UTP} = 0.14 \pm 0.01$ mM; $[S]_{0.5}^{ATP} = 0.25 \pm 0.01$ mM) relative to wild-type *Ec*CTPS (Table 4.2), suggesting that the NTP-binding sites were not structurally perturbed. Circular dichroism spectrometry also showed no major differences in protein secondary structure between wild-type and mutant *Ec*CTPSs (Figures 3.4 and 4.9).

Despite the proposed interaction between Phe 227 and the cytosine ring, F227A was inhibited by both CTP ($IC_{50} = 30 \pm 2$ μ M) and dF-dCTP ($IC_{50} = 1.3 \pm 0.3$ μ M) (Table 4.3). The affinity for CTP was 3-fold greater than observed for wild-type *Ec*CTPS while the affinity for dF-dCTP was unchanged with respect to wild-type *Ec*CTPS. F227L was also inhibited by CTP ($IC_{50} = 340 \pm 5$ μ M) 3-fold *less* than the wild-type variant, but F227L was also inhibited by dF-dCTP similarly to wild-type and F227A variants ($IC_{50} = 1.9 \pm 0.2$

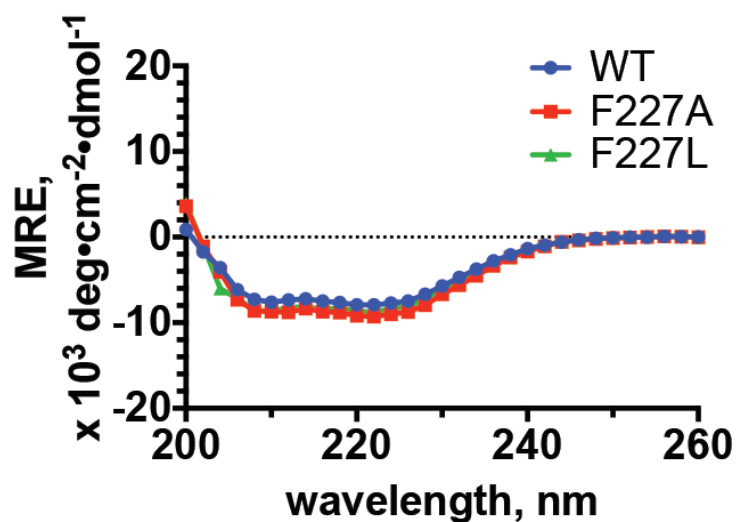


Figure 4.9. Circular dichroism spectra for wild-type (blue), F227A (red), F227L (green) CTPS variants. CD spectra were obtained at 37 °C using purified recombinant enzyme (0.2 mg/mL in 2 mM Tris-SO₄ buffer, pH 8.0, containing 10 mM MgSO₄) between 190 and 260 nm with a 0.1-cm light-path. Spectra were truncated at 200 nm due to a lack of buffer transparency.

μM) (Table 4.3). These results signified that the proposed edge-on interaction between Phe 227 and the cytosine ring is not required for binding, but might still be required for the putative H-bond rearrangement that stabilizes *Ec*CTPS filaments.

Despite both Phe 227 variants having similar affinities to dF-dCTP, the two mutants differed in their ability to form filaments. TEM analysis revealed that F227A was primarily tetrameric, with a lower proportion of higher-order species present compared to wild-type *Ec*CTPS with dF-dCTP (Figure 4.10). F227A eluted in a similar pattern to wild-type *Ec*CTPS in GF-HPLC experiments (Figure 4.3), wherein CTP appeared to cause a shift in molecular weight towards what is estimated to be the octamer. However, DLS analyses revealed that the vast majority of F227A was tetrameric when equilibrated under the same conditions (Table 4.1; Figure 4.10). Both CTP and dF-dCTP were unable to significantly induce filament formation by F227A (Table 4.1), supporting the potential role for Phe 227 in stabilizing the enzyme in a filament-competent state. The F227L variant formed larger particles with respect to F227A, but few were similar to those observed with wild-type *Ec*CTPS (Figure 4.11). The GF-HPLC analysis of the F227L yielded similar results to F227A (Figure 4.3), but the DLS results differed in that a greater proportion of F227L formed filaments in both CTP- and dF-dCTP-dependent manners (Table 4.1; Figure 4.11). However, the mean d_H values for F227L were smaller than those of wild-type *Ec*CTPS in the presence of the cytidine analogues (Table 4.1). We estimated that F227L was mostly octameric when bound to CTP or dF-dCTP, after applying Pecora's model to the DLS data, indicating that F227L was unable to stabilize the nucleation of extended filaments.

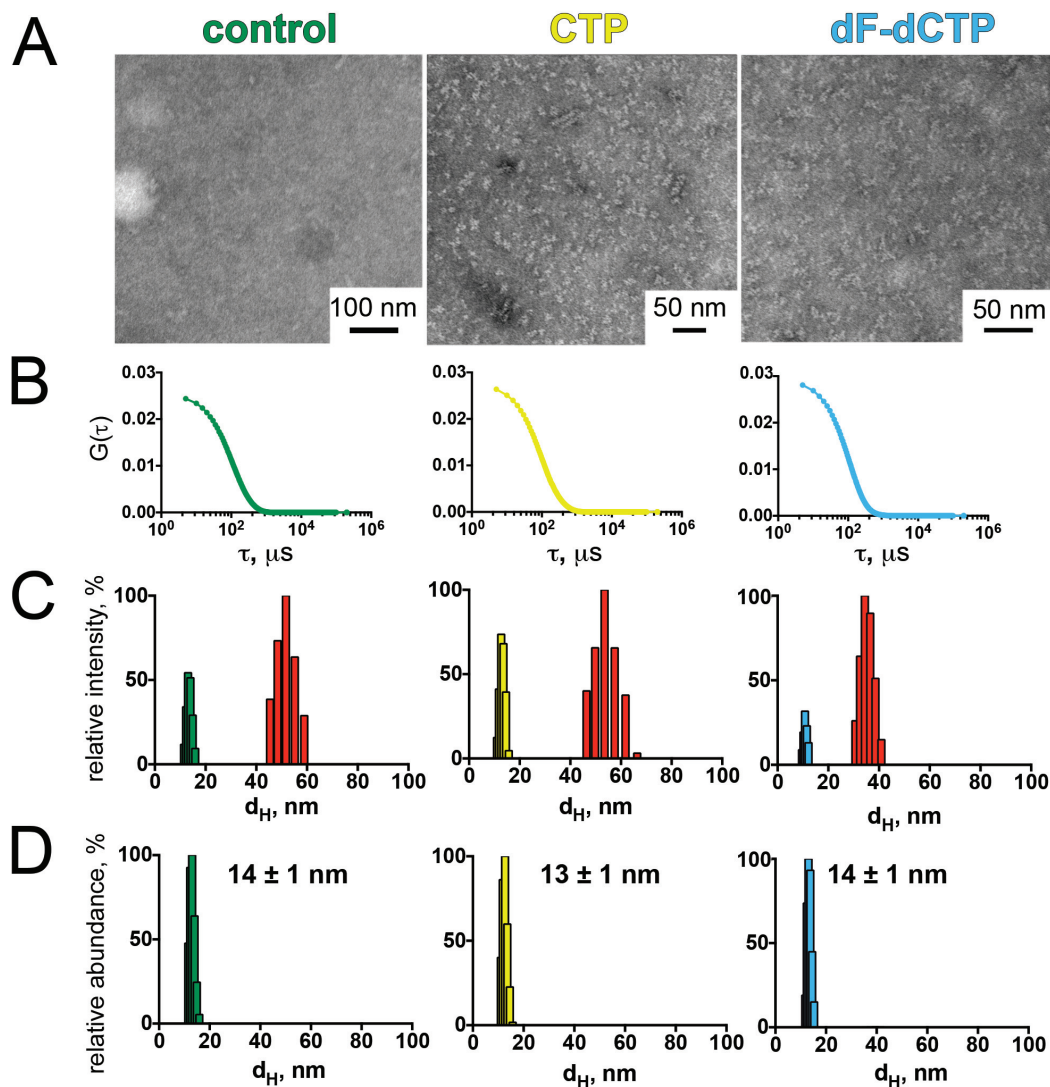


Figure 4.10. Detection of F227A *EcCTPS* filaments by TEM and DLS. **(A)** Representative transmission electron micrographs of F227A *EcCTPS* (15 μ M) incubated in assay buffer containing ATP (2.0 mM, control) and either CTP (1.0 mM) or dF-dCTP (100 μ M). Samples were incubated for 30 min at 37 $^{\circ}$ C prior to staining with uranyl acetate (0.7% w/v) and imaged using transmission electron microscopy. **(B)** NNLS fits to the autocorrelation functions from DLS analyses of F227A *EcCTPS* (3.0 μ M) incubated with ATP (2.0 mM, green) and CTP (1.0 mM, yellow) or dF-dCTP (100 μ M, cyan). **(C)** Intensity- and **(D)** number-weighted distributions of *EcCTPS* derived from the NNLS fits in panel B. Relative scattering intensities are represented as a percentage of the most abundant population. The mean hydrodynamic diameters (d_H) \pm SD were determined using the decay times shown in Table 4.1.

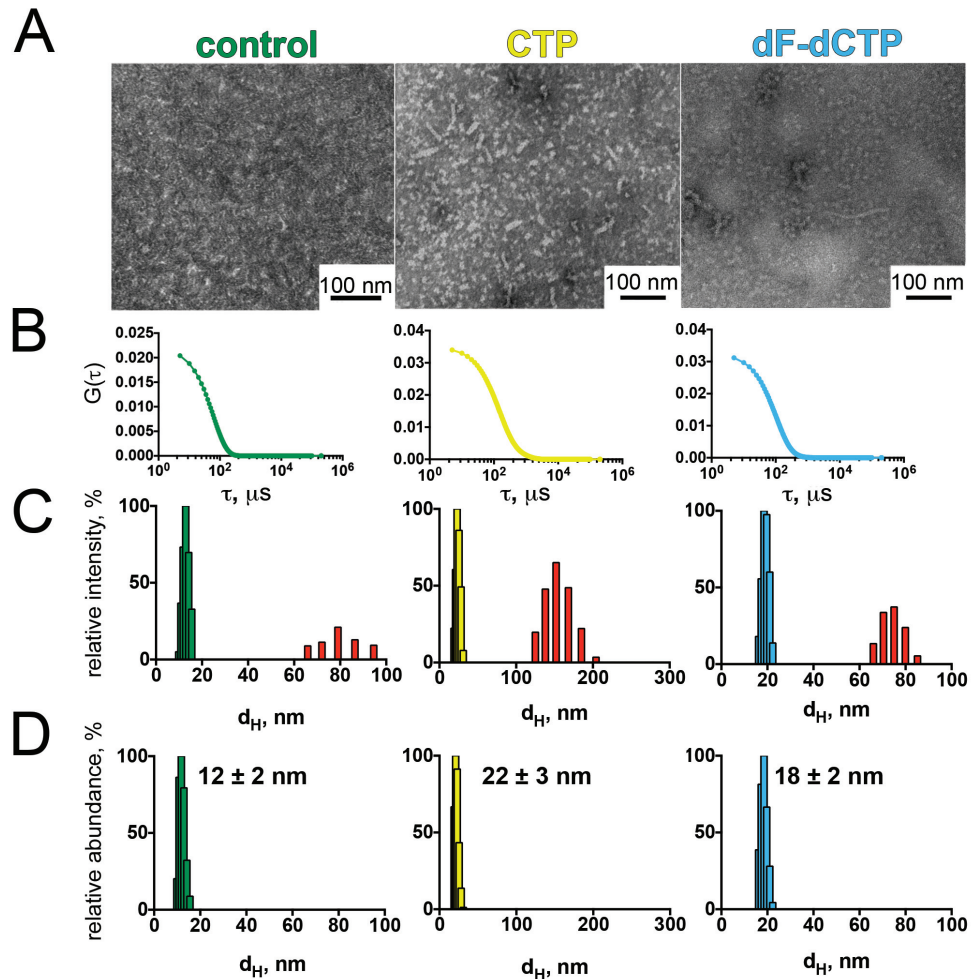


Figure 4.11. Detection of F227L *EcCTPS* filaments by TEM and DLS. (A) Representative transmission electron micrographs of F227L *EcCTPS* (15 μ M) incubated in assay buffer containing ATP (2.0 mM, control) and either CTP (1.0 mM) or dF-dCTP (100 μ M). Samples were incubated for 30 min at 37 $^{\circ}$ C prior to staining with uranyl acetate (0.7% w/v) and imaged using transmission electron microscopy. (B) NNLS fits to the autocorrelation functions from DLS analyses of F227L *EcCTPS* (3.0 μ M) incubated with ATP (2.0 mM, green) and CTP (1.0 mM, yellow) or dF-dCTP (100 μ M, cyan). (C) Intensity- and (D) number-weighted distributions of *EcCTPS* derived from the NNLS fits in panel B. Relative scattering intensities are represented as a percentage of the most abundant population. The mean hydrodynamic diameters (d_H) \pm SD were determined using the decay times shown in Table 4.1.

4.4 DISCUSSION

4.4.1 dF-dCTP Induces *Ec*CTPS Filament Formation

CTP has already been demonstrated to induce polymerization of *Ec*CTPS into inactive filaments (Barry *et al.*, 2014; Lynch *et al.*, 2017), but the mechanism by which this happens is unclear. CTPS filaments have been detected in multiple organisms, including humans, but only the prokaryotic variants are demonstrably inactive and bound to CTP. Instead of being CTP-induced, human CTPS filaments appear to bind the NTP substrates, UTP and ATP. Structural investigation of the human CTPS filaments revealed the importance of a short helical insertion in the GATase domain that forms inter-tetramer contacts when the tetramer is bound to UTP and ATP (Lynch *et al.*, 2017). Such adornments on GATase enzymes have been attributed to a host of evolutionarily divergent protein-protein interactions across a wide range of phyla (Plach *et al.*, 2017). CTPSs from *Drosophila* sp. and *Saccharomyces* sp. also form filaments, but it is unclear whether these filaments resemble the prokaryotic or human variants as the evolutionary origins and physiological function of these filaments have not been determined. In fact, CTPS filaments in yeast appear to consist of inactive enzyme, and filament formation is largely dependent on CTP and allosteric sites suggesting a similarity to the *Ec*CTPS filaments. Additionally, some eukaryotic CTPSs such as the CTPS1 from *Trypanosoma* sp. lack the helical insertion that is proposed to mediate active filament formation (Figure 1.10). This observation casts serious doubt on either the role of the insertion or the dichotomy between eukaryotic and prokaryotic CTPSs that suggests activity is a defining characteristic of eukaryotic CTPS filaments. Here, we characterized the filament-promoting effects of dF-

dCTP on the prokaryotic CTPS filaments from *E. coli*, the most well-characterized CTPS filaments that form in the presence of CTP.

Initial TEM experiments on *EcCTPS* indicated that dF-dCTP was capable of inducing filament formation like CTP. However, large tangles of filamentous CTPS were occasionally observed in nearly all TEM images (with or without NTPs), and their origin is not known. DLS analysis also demonstrated dF-dCTP-induced filament formation, but again populations of large species that were unresponsive to NTPs were detected. The nature of these larger species is unclear, but they may represent another population of polymeric *EcCTPS* that forms independently of substrates or CTP and dF-dCTP. The size distribution of this population was wide, suggesting that there may be some degree of non-specific protein-protein interactions that leads to higher molecular weight species that may arise due to concentration-dependent effects. We cannot discount the possibility that *EcCTPS* can form stable filamentous aggregates that are either monomeric, dimeric, or tetrameric in nature in the absence of ligands. Inactive filaments of dimeric CTPS have been detected in *Saccharomyces cerevisiae*, though further biochemical validation of these data is required (Noree *et al.*, 2014; Noree *et al.*, 2010). Nevertheless, similar observations of higher-order species were reported in previous light scattering studies on vimentin, wherein a small percentage of vimentin polymers were observed prior to induction of assembly (Lopez *et al.*, 2016). This may be a property of intrinsically 'sticky' proteins, and not necessarily representative of our attempts to characterize a *bona fide* ligand-dependent effect. For these reasons, we focused only on the changes in diffusion ($\equiv d_H$) of smaller, CTP- and dF-dCTP-responsive species.

dF-dCTP was able to induce *Ec*CTPS filament formation at a lower concentration than CTP, but filaments induced by both cytidine analogues appeared similar in size when analyzed by TEM. That dF-dCTP was able to induce filament formation at a concentration that was 10-fold lower than with CTP is unsurprising due to the greater affinity of the difluorinated NTP for *Ec*CTPS (see **Chapter 3**). DLS results were in accord with the observations in TEM experiments. Similar to what was previously observed in size-exclusion chromatography experiments (Levitzki & Koshland, 1972a), addition of ATP (2 mM) was sufficient to induce *Ec*CTPS tetramerization ($d_H = 13 \pm 1$ nm). The d_H of the control sample (tetramer) was consistent with point-to-point measurements of a tetramer in the cryo-EM structure (PDB: 5U3C, (Lynch *et al.*, 2017)); however, the fidelity of these measurements is expected to diminish as filament length increases and the apparent particle shape becomes more elliptical. Because the Stokes-Einstein equation is not applicable to non-spherical particles, corrections were made for more accurate inference of the dimensions of the rod-like polymers observed in TEM experiments. Applying Pecora's model for rod-like scatterers to these data, we estimated the mean length of CTP- and dF-dCTP-induced *Ec*CTPS filaments to be approximately 28 and 53 nm, respectively. These observations suggest that dF-dCTP is able to promote formation of longer *Ec*CTPS filaments than CTP, but because of a persistent aggregate species that was seemingly unresponsive to either cytidine analogue we cannot discount the possibility that some cytidine-responsive filaments diffuse similarly to the tangles detected by TEM. In this case, the aggregates may confound interpretation of DLS data and obscure observation of the larger cytidine-induced filaments due to similarities in diffusion. Regardless, the DLS method we developed was successful in monitoring the response of smaller *Ec*CTPS

species to CTP and dF-dCTP, which allowed for further assessment of the NTP-responsiveness of the filaments.

4.4.2 UTP Prevents Filament Formation and Disassembles Pre-Formed Filaments

UTP and CTP compete for the same 5'-triphosphate binding site resulting in UTP-dependent dispersion of pre-formed, CTP-induced *EcCTPS* filaments (Barry *et al.*, 2014). To elaborate on the effects of UTP on cytidine-induced *EcCTPS* filaments, we incubated *EcCTPS* with fixed concentrations of CTP or dF-dCTP, with or without a saturating concentration of UTP. Incubation of *EcCTPS* with UTP prevented dF-dCTP-induced filament formation, as detected by TEM. DLS analyses agreed with the TEM data in that UTP at 1.0 mM was capable of preventing the filament-inducing effects of a range of dF-dCTP concentrations $\leq 200 \mu\text{M}$, but this could be overcome when the CTP analogue concentration was increased to 300 μM . A similar trend was observed in the presence of CTP, but CTP-induced filament formation was prevented at $[\text{CTP}] \leq 1000 \mu\text{M}$ owing to its lower affinity for *EcCTPS*. The observation that higher concentrations of dF-dCTP (300 μM) were required for filament formation in the presence of UTP (1.0 mM), but not inhibition ($K_i = 3.0 \pm 0.1 \mu\text{M}$), indicated that the parabolic competitive inhibition observed for *EcCTPS* in the presence of dF-dCTP did not likely arise directly from filament formation (proposed in **section 3.4.1**).

The physiological role of *EcCTPS* filaments hasn't yet been established, but multiple lines of evidence have demonstrated that they are inactive, suggesting a mechanism for further regulation of enzymatic activity (Aughey & Liu, 2015; Barry *et al.*, 2014; Noree *et al.*, 2014; Wang *et al.*, 2015). Reduced catalytic activity in filamentous *EcCTPS* might arise from obstruction of conformational changes such that the GATase domain is no longer able to catalyze the generation of ammonia and/or effect its transfer to

the synthase domain. This model was put forth by Barry *et al.* (2014), and suggested that Gln and GTP were not able to induce an oft-evoked, but never observed, GATase domain rotation that stimulates Gln hydrolysis and shortens the NH₃ tunnel (Barry *et al.*, 2014; Endrizzi *et al.*, 2004). Alternatively, members of the same group proposed that *EcCTPS* filaments adopt a conformation that cannot bind UTP, and that the filaments are inactivated by conformational selection against substrates (Lynch *et al.*, 2017). Informed by the cryo-EM structure of CTP-induced *EcCTPS* filaments, cysteine cross-links were engineered to lock the enzyme in a filamentous state that could bind CTP, but was unable to bind UTP (Lynch *et al.*, 2017). However, the cross-links were designed based on a structure of *EcCTPS* that was already in a CTP-bound conformation and may not be representative of the wild-type enzyme. Their earlier work refuted this possibility; polymerization studies demonstrated that CTP stimulated the formation of filaments and addition of an equimolar concentration of UTP caused a reduction in scattered light indicating UTP-dependent disassembly of CTP-induced filaments (Barry *et al.*, 2014). Unfortunately, these scattering experiments were not designed to calculate particle size in the solution being examined.

Conversely, we tested whether UTP could bind and effect the disassembly of *EcCTPS* filaments in the presence of CTP and dF-dCTP using DLS. *EcCTPS* filament formation was pre-induced by addition of CTP or dF-dCTP and the raw scattering intensity was measured over a 20-min incubation. Both cytidine analogues caused increased scattering, relative to the control (ATP only). Addition of UTP caused a similar reduction in scattering intensity as was observed by Barry *et al.* (2014), and was consistent with a decrease in the mean d_H of the samples containing CTP and dF-dCTP. Addition of UTP did not change the d_H of the control sample, nor did adding buffer in place of UTP. These

data indicated that the UTP/CTP-binding site is accessible in the filaments, and that either CTP or dF-dCTP can be displaced by a high enough concentration of UTP to effect depolymerization. Unfortunately, our methods were insufficient to determine the exact mechanism by which depolymerization occurs; however, two potential models are plausible. UTP may only be able to bind the terminal tetramer of an *Ec*CTPS filament, inducing a sequential disassembly of the filament (Figure 4.12A). Alternatively, UTP may bind a protomer from within the filament and cause a structural disruption that bifurcates the filament at the bound tetramer (Figure 4.12B); however, this latter possibility would eventually require UTP to bind a terminal protomer to effect complete disassembly of the filament. The former hypothesis may explain why the cross-linked *Ec*CTPS filaments cannot bind UTP, especially since the cross-links were engineered based on the internal tetramer geometry.

4.4.3 Sensing the Cytosine Ring is Important for Filament Formation

*Ec*CTPS filament formation is dependent on occupation of the CTP-binding site by CTP or dF-dCTP, but how their binding is transduced into promoting polymerization is unclear. Our previous studies on the inhibition of *Ec*CTPS by dF-dCTP, and characterization of a mutant enzyme that could not bind CTP analogues provided us with a tool for probing the structural determinants for dF-dCTP-induced filament formation. Unfortunately, no structure of *Ec*CTPS with bound dF-dCTP exists, but the biochemical data (discussed in **Chapter 3**) support the hypothesis that the drug is bound similarly to CTP. Subsequently, we used the available structure of *Ec*CTPS filaments bound to CTP (PDB:5U3C, (Lynch *et al.*, 2017)) to inform our studies of the structural determinants of CTP and dF-dCTP-induced filament formation.

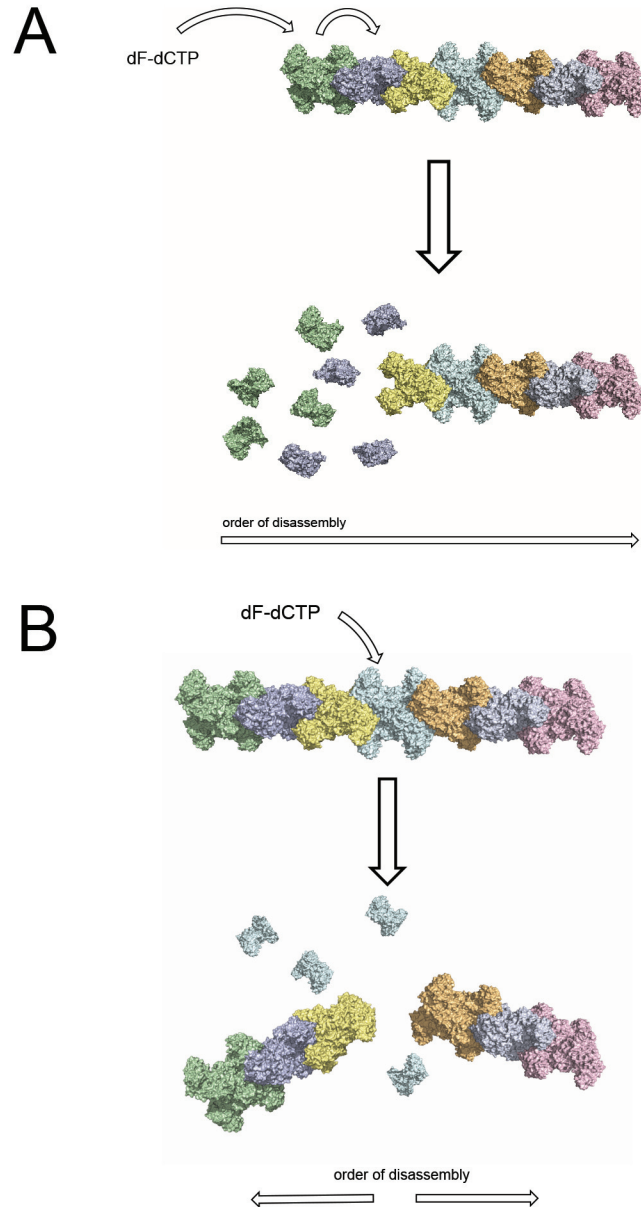


Figure 4.12. Potential mechanisms for UTP-dependent *EcCTPS* filament disassembly. (**A**) 'Exo' disruption wherein UTP binds the terminal tetramers on the filament and effects unidirectional disassembly, or (**B**) 'endo' disruption wherein UTP binds a tetramer within the filament and causes it to depolymerize.

The X-ray crystal structure of *Ec*CTPS suggests that Glu 149 binds the 3'-OH and 2'-OH of CTP through a bifurcated H-bond, which was supported by the observation that E149D could not bind CTP analogues. We deployed E149D again to further support the evidence that filament formation requires binding of CTP or dF-dCTP. TEM, DLS, and GF-HPLC experiments all demonstrated the inability of E149D to form CTP- or dF-dCTP-induced filaments. This is further evidence that recognition of CTP or dF-dCTP by Glu 149 is required for filament formation, though we cannot rule out the possibility that both CTP/dF-dCTP binding and filament formation have been disrupted separately by this substitution. That UTP competes with the cytidine analogues to effect filament disassembly is compelling evidence that occupation of the CTP binding site is the most important determinant for filament formation (discussed in **section 4.4.2**). Intriguingly, some higher-order species of E149D were detected by DLS, further indicating that the aggregates observed at higher d_H in the DLS experiments formed independently of CTP and dF-dCTP.

Two X-ray crystal structures of *Ec*CTPS, solved with bound CTP (PDB:2AD5 (Endrizzi *et al.*, 2005), and 5TKV (Lynch *et al.*, 2017)), suggest a role for Phe 227 in binding CTP. Phe 227 is located in the CTP binding pocket, and was claimed to form an edge-on interaction with the cytosine ring (Lynch *et al.*, 2017). Phe 227 has been co-crystallized with CTP in two different conformations: one in which the residue packs against the cytosine ring and one in which it is rotated 7.5 Å away from the ring. Baldwin and co-workers (2017) identified a putative H-bond network that changes orientation depending on the position of Phe 227 (Figure 4.13). CTP, and presumably dF-dCTP, are bound at the intersection of three subunits that may provide a scaffold for the three subunits

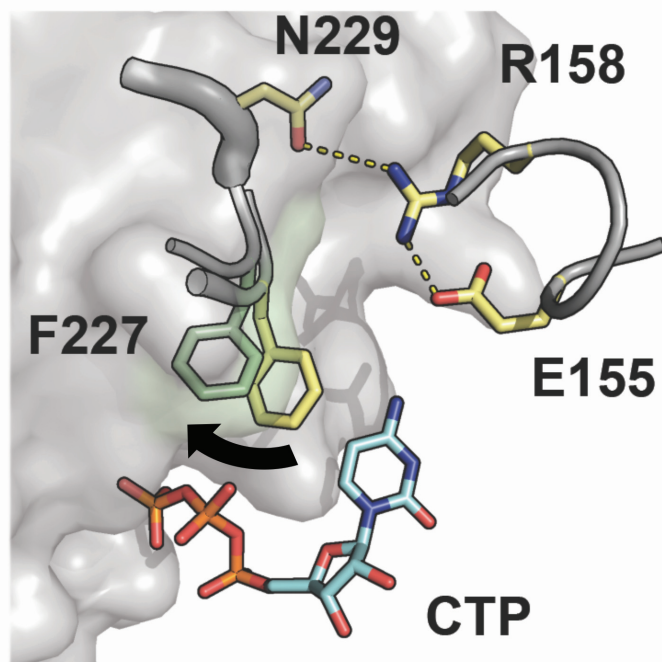


Figure 4.13. Putative role for Phe 227. Partial view of the CTP-binding site showing the proposed recognition of CTP (cyan sticks) by Phe 227 (yellow PDB: 5TKV; green PDB: 2AD5) and the putative H-bonding network (PDB: 5TKV). Rotation of Phe 227 is indicated by the black arrow. Image was adapted from Lynch *et al.* (2017), and rendered using PyMOL v. 1.9.2.0 (DeLano, 2002).

to interact.

This putative role for CTP may explain how it induces CTPS tetramerization in the absence of UTP and ATP (Pappas *et al.*, 1998). Stabilized by Glu 155, Arg 158 interacts with Asn 229 on an adjacent subunit when Phe 227 is packed against the cytosine ring, causing a conformational change similar to that observed in cryo-EM models of *Ec*CTPS filaments (Lynch *et al.*, 2017). When Phe 227 is not packed against the cytosine ring, Arg 158 and Asn 229 are separated by 5.6 Å and the helices upon which they reside are positioned such that important filament contacts are obviated (Lynch *et al.*, 2017). The importance of this H-bonding network was indirectly supported by substitution of Glu 155 with Lys (E155K) which reduced product inhibition by CTP and hindered *Ec*CTPS filament formation similar to E149D (Barry *et al.*, 2014). Here, we constructed Ala (F227A) and Leu (F227L) variants to directly explore the role of Phe 227 in *Ec*CTPS filament stabilization.

Replacement of Phe 227 with Leu was assumed to be a well-tolerated mutation, since CTPS from *Trypanosoma brucei* (*Tb*CTPS) has a Leu mutation at the homologous position (Figure 4.14), though whether *Tb*CTPS is product-inhibited is unknown (Fijolek *et al.*, 2007; Hofer *et al.*, 2001). Alternatively, if the assumptions made by Baldwin and co-workers (2017) are accurate, F227A would not bind CTP or dF-dCTP, resulting in an inability of this variant to form filaments should Phe 227 be necessary for binding these NTPs. Neither the F227A nor F227L substitutions were significantly detrimental to catalysis of CTP production, and CD spectroscopy showed no gross alterations of secondary structure with respect to wild-type *Ec*CTPS (Figure 4.9). F227A and F227L *Ec*CTPSs were both inhibited by dF-dCTP to a similar extent indicating that the high

<i>T. brucei</i>	CRSENRLTPDAKEKLSNLCGVRSGDIVSAPNVSCLYEVPVVFTKDGLVDRLVEKLRLVKR	298
<i>H. sapiens</i> CTPS1	CRCSNPLDTSVKEKISMFCHEVEPEQVICVHDVSSIYRVPLLLLEEQGVVDYFLRRLDLPIE	275
<i>E. coli</i>	CRSDRAVPANERAKIALFCNVPEKAVISLKDVDISIYKIPGLLKSQGLDDYICKRFSLNCP	269
<i>M. tuberculosis</i>	LRCDRDVPEALKNKIALMCDVDIDGVISTPDAPSIYDIPKVLHREELDAFVVRRLNLPFR	281
<i>T. thermophilus</i>	LRSARPVPEEVRKVALFTNVRPGHVFSSPTVEHLYEVPLLLLEEQGLGRAVERALGLEAV	280
<i>S. solfataricus</i>	GRATLPLDDETRRKIALFTNVKVDHIVSSYDVETSIEVPIILESQKLVSKILSRLKLEDR	271
	* . : : * : : : * : . . * : * : : : : . : *	

Figure 4.14. Protein sequence alignment for structurally characterized CTP synthases. The amino acid sequences of CTPSs from *Trypanosoma brucei* (taxid:5691), *Homo sapiens* (taxid:9606), *Escherichia coli* (taxid:562), *Mycobacterium tuberculosis* (taxid:1773), *Thermus thermophilus* (taxid:274), and *Sulfolobus solfataricus* (taxid:2287) were aligned using Clustal Omega (Sievers & Higgins, 2014). Residues at position 227 (*E. coli* numbering) are highlighted in yellow.

affinity of *Ec*CTPS for dF-dCTP is unrelated to Phe 227. On the other hand, the two Phe 227 variants were inhibited differently by CTP. F227A and F227L were inhibited 3-fold stronger and 3-fold weaker than wild-type, respectively, when CTP was used as the inhibitor. It is unclear why F227A and F227L would have different apparent affinities for CTP and not dF-dCTP, but perhaps the putative interactions between the 2'-*arabino*F and the Q-V-I loop compensate for the disruption in cytidine binding observed for F227L.

While both Phe 227 mutants were able to bind CTP and dF-dCTP, their capacity to form large-scale cytidine-induced filaments was hampered. DLS measurements indicated that F227A was unable to form oligomers larger than a tetramer; however, GF-HPLC and TEM showed that some octameric species were present though they may not be abundant in solution. F227L had a greater ability to form higher-order structures, but the sizes of F227L 'filaments' were smaller than those observed for wild-type *Ec*CTPS. These data indicate that the phenyl ring of Phe 227 is not critical for binding CTP or dF-dCTP, but does appear to play a vital role in filament formation. Instead of being an obligate binding determinant for CTP or its analogues, Phe 227 may 'sense' cytosine in the binding pocket leading to the stabilization of a filament-competent state. The limited capacity for the isopropyl side-chain of F227L, but not the methyl group of F227A, to substitute for the phenyl ring suggests that the interaction between *Ec*CTPS and the cytosine ring is primarily hydrophobic in nature. Whether the F227A and F227L substitutions caused a disruption of the H-bonding network between Glu 155, Arg 158, and Asn 229 cannot be confirmed without further structural investigation, but our data do lend some biochemical support for the hypothesis.

4.4.4 Conclusions

Mounting evidence suggests that many metabolic enzymes are regulated by filament formation, or some form of polymeric assembly (Aughey & Liu, 2015; Beaty & Lane, 1983; Eisenberg & Tomkins, 1968; Frey *et al.*, 1975; Kim *et al.*, 2005; Petrovska *et al.*, 2014). Knowing how polymerization is induced and regulates enzymatic activity is critical for our understanding of cellular physiology. DLS provided a platform for probing the biophysical characteristics of *Ec*CTPS filaments and should be considered as a technique that can augment studies on non-amyloid enzyme filaments. Here, we continued our investigation into how dF-dCTP inhibits *Ec*CTPS and demonstrated that it can mimic the filament-inducing properties of the enzymatic product, CTP. Although unsurprising given the known effects of CTP on filament formation, this result highlights the potential for nucleoside therapeutics to affect the filamentous states of enzymes. Furthermore, our DLS studies, in combination with traditional TEM and GF-HPLC techniques, furnish the first functional evidence that Phe 227 is important for filament formation.

CHAPTER 5 INVESTIGATION OF CTP SYNTHASE NH₃ CHANNELLING

5.1 INTRODUCTION

CTPS coordinates the hydrolysis of glutamine with the ligation of nascent NH₃ to an ATP-activated 4-P-UTP intermediate, all of which must be properly synchronized to ensure that CTP is produced efficiently. Like the other GATase enzymes, with the exception of the glucosamine-6P synthase (GlmS) (Mouilleron *et al.*, 2006; Teplyakov *et al.*, 2001), CTPS can also utilize exogenous NH₃ as a substrate, though the mechanism is less understood. The entry site for exogenous NH₃ has not been conclusively identified, but NH₃-dependent CTP generation is inhibited by the allosteric effector GTP suggesting that they may share a common binding site (MacDonnell *et al.*, 2004). Conversely, GTP is an allosteric activator of the GATase reaction (Levitzki & Koshland, 1969) that induces a conformational change stabilizing the tetrahedral intermediate formed during Gln hydrolysis (Bearne *et al.*, 2001).

While the NH₃ tunnel is not completely obstructed in the absence of GTP, since exogenous NH₃ can be utilized without it, the conformational change caused by GTP might also widen the tunnel to provide nascent NH₃ with a more facile route to the synthase domain. The NH₃ tunnel, starting in the GATase domain, is partially formed by the residues surrounding the catalytic triad that catalyzes the hydrolysis reaction (Zalkin, 1985). The tunnel continues to a constriction formed by 3 residues - Pro 54, His 57, and Val 60 - at the maw of the synthase domain that may comprise an NH₃ gate. According to high-resolution crystal structures and molecular models of the tunnel, the constriction is only ~2.4 Å in diameter (Endrizzi *et al.*, 2004), despite the molecular diameter of NH₃ being closer to 4 Å (Kammeyer & Whitman, 1972). Taking this into account, the tunnel

captured in X-ray diffraction studies must undergo a conformational change to allow for the effective transfer of NH₃ to the synthase domain, or the constriction is an artefact of the crystallization conditions. The proximity of the gate to the putative GTP binding site suggests a possible role for GTP in regulating opening of the NH₃ gate, thus coupling spatially distant reactions by modulating the inter-domain flow of NH₃.

The gate is highly conserved (Figure 5.1) and forms the boundary between GATase and synthase domains, suggesting that it may be a vital component for the coordination between the two domains. Using a site-directed mutagenesis approach, we investigated the role of Val 60, located at the most constricted part of the tunnel, in NH₃ channelling by *Ec*CTPS. Val 60 at the putative NH₃ gate was substituted by five amino acids (Ala, Cys, Asp, Trp, and Phe) to disrupt inter-domain NH₃ transport, and revealed the exquisite sensitivity of the enzyme to changes at the interface between its two domains. Alkylation of the V60F variant with DON, mimicking the glutamyl-enzyme intermediate, relieved inhibition of exogenous NH₃-dependent catalysis, indicating that the tunnel may open during glutamine hydrolysis.

5.2 EXPERIMENTAL

5.2.1 General

All chemicals, unless otherwise stated, were purchased from Sigma-Aldrich Canada Ltd. (Oakville, ON, Canada).

5.2.2 Assay of CTP production

The rate of CTP production was measured using the continuous spectrophotometric assay described in **section 2.4**. Enzyme (10 – 30 µg/mL, wild-type, V60A, V60C, V60D, V60W, and DON-V60F; 120-400 µg/mL V60F) and nucleotides (Table 2.2) were pre-

```

EcCTPS imkldpyinvdpgtmspiqhgevfvtedgaetdldlghyerfirtkmsrrnfttgriys 97
TbCTPS sikidpyinmdaglmspyehgevyvlddggevdldlgnyerwmsvqlrrehnittgkvyq 120
LlCTPS vqkfdpylnidpgtmspyqhgevfvtddgaetdldlghyerfidinlnkysnvtsgkvys 97
TtCTPS aikidpyvnvdagtmrpyehgevfvtadgaetdldighyerfldmdlsrgnnttgqvyl 106
HsCTPS1 sikidpyinidagtfspehgevfvlldggevdlldlgnyerfldirltkdnnlttgkiyq 95
SsCTPS avkidpyinvdagtmnpymhgevfvtedgaetdldlghyerfmdvnmkynnitagkvyf 97
ScCTPS sikidpymnidagtm脾ehgecfvlldggetdldlgnyerylgvtltkdhnittgkiys 95
SpCTPS sikidpymnidagtm脾ehgevfvlndggevdlldlgnyerylnvtlthdnnittgkvys 95
MtCTPS mqkldpylnvdpgtmnpfqhgevfvtedgaetldvghyerfldrnlpgsanvttgqvys 103
***** * . * *** . * * * * * * * * *

```

Figure 5.1. Partial sequence alignment of some biochemically characterized CTPSs. Amino acid sequence alignment of a portion of 9 representative CTPSs containing a putative NH₃ tunnel. Invariant residues (*) and residues showing conservation between groups of strongly (:) or weakly (.) similar properties are indicated. Val 60 (green, *E. coli* numbering), Pro 54 (blue), and His 57 (blue) are highlighted. In descending order the proteins included in the alignment are as follows: *Escherichia coli* (taxid:562), *Trypanosoma brucei* (taxid:5691), *L. lactis* (taxid:1358), *Thermus thermophilus* (taxid:274), *Homo sapiens* (taxid:9606), *Sulfolobus solfataricus* (taxid:2287), *Saccharomyces cerevisiae* (taxid:4932), *Schizosaccharomyces pombe* (taxid:4896), and *Mycobacterium tuberculosis* (taxid:83332). Alignment rendering was conducted using Clustal Omega (Sievers & Higgins, 2014).

incubated at 37 °C, followed by addition of the NH₃ source (NH₄Cl, NH₄OAc, or Gln) to initiate the reaction. For reactions using NH₄Cl or NH₄OAc (5.0 – 150 mM), KCl or NaOAc were used, respectively, to maintain an ionic strength of 0.15 M. For reactions using Gln (0.05 – 6.0 mM, wild-type, V60A, V60C, and V60D; 2-50 mM, V60F), GTP was present as saturating concentrations, unless otherwise stated (Table 2.2). Values of K_M , k_{cat} , and k_{cat}/K_M were determined by fitting of eqn 2.1 to the initial velocity data. The dependence of CTP production on GTP (0 – 2.0 mM) was measured with either Gln (6.0 mM, wild-type, V60A, V60C, and V60D; 50 mM, V60F) or NH₄OAc (150 mM DON-V60F). The values of k_{act} , K_A , and k_o were determined by fitting of eqn 2.2 to the initial velocity data. The dependence of CTP production on UTP (0 – 2.0 mM, wild-type; 0 – 4.0 mM, V60A, V60C, V60D, V60F, and DON-V60F; 0 – 5.0 mM, V60W) and ATP (0 – 4.0 mM) was examined with either Gln (6.0 mM, wild-type, V60A, V60C, and V60D; 50 mM, V60F) or NH₄OAc (150 mM, V60W and DON-V60F). All kinetic experiments with DON-V60F were conducted in the presence of a saturating concentration of GTP (1.0 mM), unless otherwise stated. Eqn 2.3 was fit to the initial velocity data using non-linear regression analysis to estimate the values of $V_{max}/[E]_T$, $[S]_{0.5}$, and n .

5.2.3 Coupling Ratio Determinations

GATase activities of the wild-type and Val 60 variants were assayed by measuring the levels of Gln and Glu derivatized by *o*-phthaldialdehyde (OPA) using RP-HPLC, as described previously (Iyengar & Bearne, 2002; Lunn & Bearne, 2004). Assays were conducted in assay buffer containing saturating concentrations of the appropriate ligands (Gln, GTP, ATP, and UTP) (Table 2.2), and enzyme (3.0 – 5.0 µg/mL, wild-type V60A, V60C, V60D, and V60W; 20 – 30 µg/mL, V60F) in a total volume of 1.0 mL. To investigate the integrity of the NH₃ tunnel, the coupling efficiency between the GATase

and synthase active sites was calculated using eqn. 5.1. To investigate the 'bottleneck' effect of V60F, Gln hydrolysis and CTP production were determined using RP-HPLC and UV/vis spectroscopy, respectively, as described above except with saturating, near K_m , and sub-saturating concentrations of Gln. The coupling ratio was also determined at saturating concentrations of Gln, but with the concentration of GTP reduced to 0.006 mM for wild-type CTPS and 0.08 mM for V60F (*i.e.*, $[GTP] \approx K_A/5$). For these GATase assays, the concentrations of wild-type CTPS were 3.5 $\mu\text{g/mL}$ (at saturating [Gln]), 6.9 $\mu\text{g/mL}$ (at near K_m of Gln), 4.0 $\mu\text{g/mL}$ (at sub-saturating [Gln]), and 3.9 $\mu\text{g/mL}$ (at sub-saturating [GTP]); and the concentrations of V60F were 10.0 $\mu\text{g/mL}$ (at saturating [Gln]), 26.0 $\mu\text{g/mL}$ (at near K_m of Gln), 23.7 $\mu\text{g/mL}$ (at sub-saturating [Gln]), and 19.5 $\mu\text{g/mL}$ (at sub-saturating [GTP]).

$$\text{coupling ratio} = \frac{(v_i/[E]_T)_{\text{CTP production}}}{(v_i/[E]_T)_{\text{Glu production}}} \quad (5.1)$$

5.2.4 Assay of N^4 -OH-CTP Production

Competition between nascent and exogenous nitrogen sources was investigated using Gln as the source of nascent NH_3 , and $\text{NH}_2\text{OH}\cdot\text{HOAc}$ as the exogenous nitrogen donor. $\text{NH}_2\text{OH}\cdot\text{HCl}$ was converted to the acetate salt (Higuchi & Barnstein, 1956) to avoid inhibition by chloride ions. Utilization of Gln or NH_2OH results in the conversion of UTP to either CTP or N^4 -OH-CTP, which can be measured individually by monitoring the change in absorbance at 291 nm where, $\Delta\epsilon_{291} = 1338 \text{ M}^{-1}\text{cm}^{-1}$ (Long & Pardee, 1967) or $\Delta\epsilon_{291} = 4023 \text{ M}^{-1}\text{cm}^{-1}$ (Willemoës & Larsen, 2003), respectively, or measured simultaneously by monitoring the change in absorbance at 291 nm and 300 nm where $\Delta\epsilon_{300}$ for conversion of UTP to CTP is negligible and $\Delta\epsilon_{300} = 3936 \text{ M}^{-1} \text{ cm}^{-1}$ for the conversion of UTP to N^4 -hydroxy-CTP (N^4 -OH-CTP) (Willemoës, 2004; Willemoës & Larsen, 2003).

Unlike ammonium salts, no calculation is needed to account for the total concentration of the nucleophilic form of NH_2OH because it has a $\text{p}K_a$ well below pH 8.0 ($\text{p}K_a$ $^+\text{NH}_3\text{OH} = 6.03$, (Good, 1960)). In the presence of both Gln and $\text{NH}_2\text{OH}\cdot\text{HOAc}$, the initial rate of N^4 -OH-CTP formation was therefore calculated using $\Delta A_{300}/\Delta t$, while the initial rate of CTP formation was calculated using eqn. 5.2 (Willemoës, 2004).

$$v_i = \frac{\Delta[\text{CTP}]}{\Delta t} = \frac{\Delta A_{291} - 1.73\Delta A_{300}}{\Delta t \Delta \epsilon_{291}} \quad (5.2)$$

To determine whether Gln and/or GTP could enhance utilization of exogenous NH_2OH , wild-type, V60F, and DON-V60F *Ec*CTPSs were assayed as described above with saturating concentrations of the indicated nucleotides (Table 2.2). For wild-type *Ec*CTPS (40 $\mu\text{g}/\text{mL}$), the reaction was initiated by the addition of $\text{NH}_2\text{OH}\cdot\text{HOAc}$ (100 mM) alone or simultaneously with Gln (6.0 mM). Similarly, V60F and DON-V60F (110 – 125 $\mu\text{g}/\text{mL}$) reactions were initiated by the addition of $\text{NH}_2\text{OH}\cdot\text{HOAc}$ (25 mM) alone, or simultaneously with Gln (50 mM). The ionic strength was maintained at 0.10 M using NaOAc for all variants. For wild-type *Ec*CTPS, curves for CTP and N^4 -OH-CTP production are fits of eqns. 5.3 and 2.1, respectively, to the initial velocity data. Due to the presence of substrate inhibition with V60F, the curve describing N^4 -OH-CTP production was fit with eqn 5.4. Data are the average of three independent experiments \pm SD.

$$\frac{v_i}{[\text{E}]_T} = \frac{\text{IC}_{0.5}^n(v_0/[\text{E}]_T)}{\text{IC}_{0.5}^n + [\text{I}]^n} \quad (5.3)$$

$$\frac{v_i}{[\text{E}]_T} = \frac{k_{\text{cat}}[\text{S}]}{K_m + [\text{S}] + \frac{[\text{S}]^2}{K'}} \quad (5.4)$$

5.2.5 Derivatization of *Ec*CTPS with 6-Diazo-5-oxo-L-norleucine (DON)

To investigate whether acyl-enzyme formation can enhance exogenous NH_3 utilization, wild-type, V60A, and V60F *Ec*CTPSs (20 μM) were derivatized with DON

(2.0 mM) in assay buffer containing ATP, UTP, and GTP (all = 1.0 mM) (Levitzki & Koshland, 1971; Levitzki *et al.*, 1971). The reaction was incubated for 1 h at 37 °C prior to dialysis for 12 h against fresh assay buffer lacking NTPs. The resulting DON-modified variants were used immediately in kinetic assays, as described in **section 5.2.2**. The effects of GTP on exogenous NH₃ utilization were investigated using unmodified wild-type *EcCTPS* (WT), DON-modified wild-type *EcCTPS* (DON-CTPS), DON-V60A, and DON-V60F (10-30 µg/mL) in assay buffer containing saturating concentrations of ligands and NH₄OAc (150 mM) as the nitrogen donor. Inhibition curves were fit to the initial velocity data for WT, DON-CTPS, and DON-V60A in accord with eqn. 5.3. Activation of DON-V60F by GTP was analyzed using non-linear regression analysis by fitting of eqn. 2.2 to the initial velocity data.

5.2.6 Dynamic Light Scattering

The oligomerization state of wild-type and Val 60 *EcCTPS* variants was analyzed by DLS in a similar manner to that described in **section 4.2.3**. In brief, enzyme (1.0 µM) was mixed with saturating concentrations of UTP and ATP (Table 2.2) and filtered into a quartz cuvette. The enzyme-ligand solution was then equilibrated at 37 °C for 10 minutes prior to recording hydrodynamic diameter measurements for 2 min at 37 °C on a BI-200SM goniometer. Intensity-weighted d_H distributions were acquired by fitting of a NNLS algorithm to the autocorrelation functions using Brookhaven Instruments DLS software v. 5.89.

5.2.7 Gel Filtration-High Performance Liquid Chromatography

The oligomerization state of wild-type and Val 60 variants to form tetramers was evaluated using GF-HPLC, similarly described in **section 2.8**. Wild-type and mutant *EcCTPS*s (0.5 mg/mL, 20-µL injection volume) were eluted under isocratic conditions

with assay buffer (70 mM HEPES, pH 8.0, 10 mM MgCl₂, 0.5 mM EGTA) as the eluent containing saturating concentrations of UTP and ATP (Table 2.2) at a flow rate of 0.5 mL/min on a Yarra SEC-3000 column (3 μm, 7.80 mm x 300 mm, Phenomenex, Torrance, CA, USA). Wild-type and V60F variants were also eluted in buffer containing saturating concentrations of UTP and ATP with either Gln or a combination of Gln and GTP. DON-V60F was also eluted with buffer containing only GTP because alkylation blocks binding of Gln.

5.2.8 Tunnel Modelling and Molecular Dynamics (MD) Simulations

MD simulations were conducted on wild-type and V60F *Ec*CTPSs in order to gain structural insight into how the mutation might impact the overall protein structure, and how the tunnel might be constricted. Homology models for wild-type and V60F CTPSs were built using SWISS-MODEL (Guex & Peitsch, 1997) to remove all ligands and include missing residues that were not observed in the X-ray diffraction analysis of the original structure using a wild-type *Ec*CTPS structure as a template (PDB: 2AD5). The resulting 3D models were energy minimized prior to simulation using the steepest descent method (50,000 steps, 100 ps) and a force constant of 1,000 kJ mol⁻¹ nm⁻². Each model was solvated using an explicit 3-point water model (SPC/E) in a cubic solute-box (143 × 143 × 143 Å). Simulations were performed using GROMACS Version 5.0.4 with the GROMOS96 54a7 force field (Berendsen *et al.*, 1995). Temperature and pressure were maintained at 300 K and 1 atm, respectively. Bonds lengths were constrained using the LINCS (linear constraint solver) algorithm and all atoms of the system were subject to the dynamics simulation.

Initially, the V60F *Ec*CTPS model was simulated once for 10 ns with trajectory coordinates saved at 20 ps intervals. Wild-type and V60F *Ec*CTPS models were subsequently subjected to 100 ns simulations with no alterations to the other simulation parameters. Three-dimensional models of the NH₃ tunnel and statistical data were generated for the initial structures derived from the simulations, since the V60F constriction became too great to model later in the simulation. Specifically, Caver Analyst 1.0 (Petrek *et al.*, 2006) was used to generate a 3D tunnel that passes through the NH₃ gate using the starting coordinates 107 × 95 × 52 Å. The initial search area was set to 2 Å with a probe size of 0.6 Å, and all other settings were kept as defaults. For the wild-type structure (PDB: 2AD5), the same coordinates were used, but with a probe size of 1.2 Å.

5.2.9 Circular Dichroism

Circular dichroism (CD) spectra for wild-type and Val 60 *Ec*CTPS variants (0.2 mg/mL in 2 mM Tris SO₄, pH 8.0, 10 mM MgSO₄) were obtained as described in **section 2.7**. Measurements were performed at a constant temperature of 37 °C.

5.3 RESULTS

To explore the role of the putative NH₃ gate in coordinating CTPS catalysis, we mutated Val 60 to Phe at the most constricted point of the NH₃ tunnel with the anticipation that the increased steric bulk would block or impede the passage of NH₃ (Figure 5.2A). Initially, a substitution of the conserved His 57 residue with alanine (H57A) was constructed to interrogate the role of another NH₃ gate residue, but the resulting H57A *Ec*CTPS was inactive (discussed further in **Chapter 6**). Skylign (Wheeler *et al.*, 2014) was employed to construct a hidden Markov model (HMM) logo from an alignment of 5581 predicted CTP synthase protein sequences obtained from the Pfam database (Finn *et*

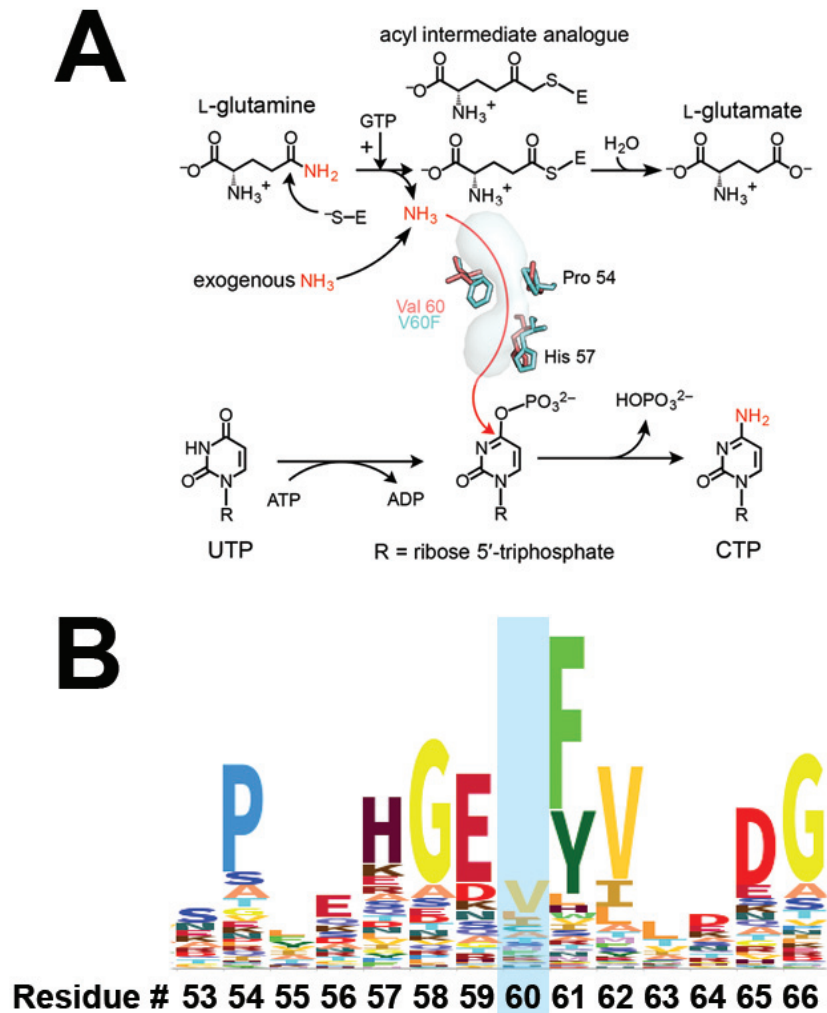


Figure 5.2. Catalytic mechanism and mutation strategy for inter-domain NH_3 channelling. **(A)** The catalytic mechanism of GTP-activated glutamine hydrolysis, subsequent transfer of NH_3 , and ATP-dependent amidoligation. The alternate alkyl-enzyme formed following treatment of *EcCTPS* with 6-diazo-5-oxo-L-norleucine (DON) is shown above the glutamyl-enzyme intermediate that forms transiently during Gln hydrolysis. Wild-type (red) and mutant (cyan) residues comprising the putative NH_3 gate are shown as sticks alongside a tunnel model (surface) to illustrate the constriction. The tunnel was modelled into the wild-type *EcCTPS* structure (PDB: 2AD5) using CAVER Analyst 1.0 (Petrek *et al.*, 2006). **(B)** Partial HMM logo for 5581 predicted CTP synthase protein sequences obtained from the Pfam database. Val 60 (*E. coli* numbering) is highlighted in blue. HMM logo was constructed using Skylign (Wheeler *et al.*, 2014).

al., 2000). Short alkyl (Leu, Ile, and Ala) and nucleophilic (Ser, Thr, and Cys) residues make up the majority of natural variants of Val 60 (*E. coli* numbering), while larger, aromatic, and acidic substitutions are not as abundant in the alignment (Figure 5.2B and Table 5.1). For comparison, we also substituted Val 60 with Ala, Cys, Asp, and Trp to examine the effects of some other side chains on catalysis. More 'natural' substitutions (V60A and V60C) were well-tolerated, while the less abundant substitutions (V60D, V60W, and V60F) were more disruptive to catalysis.

5.3.1 NH₃-dependent CTP Production

Current structural evidence indicates that NH₃ (diameter ≈ 4 Å) must pass through a 2.4 Å constriction that is partially formed by the Pro-His-Val gate. To determine whether the exogenous NH₃-dependent catalysis was impaired by mutagenesis, the ability of each Val 60 variant to utilize exogenous NH₃ as a substrate was examined. Conservative mutations (V60A and V60C) had little effect on utilization of NH₄Cl or NH₄OAc-derived NH₃, with both exhibiting the same catalytic rate as wild-type (Table 5.3). V60C, however, was less efficient (k_{cat}/K_m of $1.8 \pm 0.1 \text{ mM}^{-1}\text{s}^{-1}$, with both NH₃ sources) than wild-type (k_{cat}/K_m for NH₄Cl = $5.7 \pm 1.4 \text{ mM}^{-1}\text{s}^{-1}$, for NH₄OAc = $5.3 \pm 0.2 \text{ mM}^{-1}\text{s}^{-1}$) owing to a reduced affinity for exogenous NH₃, suggesting that a hydrophobic residue (*e.g.*, Val or Ala) is required for optimal tunnel and/or gate function. Consistent with this hypothesis, V60D had lower catalytic efficiency with exogenous NH₃ than wild-type and the conservative CTPS variants, though the K_m for NH₄Cl-derived NH₃ ($3.6 \pm 0.4 \text{ mM}$) was 2-fold higher than that for NH₄OAc-derived NH₃ ($1.6 \pm 0.5 \text{ mM}$) suggesting that the presence of Cl⁻ disrupted NH₃ binding. V60W had a similar K_m for NH₄OAc-derived NH₃ ($1.5 \pm 0.1 \text{ mM}$) to wild-type CTPS, but the turnover was approximately 5-fold lower ($k_{\text{cat}} = 1.6 \pm$

Table 5.1. Relative amino acid probabilities for position 60 (*E. coli* numbering).

Residue	Probability	Residue	Probability	Residue	Probability	Residue	Probability
V	0.339	T	0.049	K	0.024	N	0.018
L	0.086	S	0.02	E	0.023	P	0.016
I	0.081	M	0.037	R	0.021	H	0.015
C	0.067	F	0.034	G	0.02	D	0.011
A	0.066	Y	0.024	Q	0.02	W	0.007

Table 5.2. Relative amino acid probabilities for position 57 (*E. coli* numbering).

Residue	Probability	Residue	Probability	Residue	Probability	Residue	Probability
H	0.334	S	0.048	L	0.038	F	0.021
K	0.073	Q	0.045	V	0.035	P	0.019
E	0.063	D	0.04	I	0.027	M	0.016
R	0.053	T	0.04	G	0.025	C	0.007
A	0.05	N	0.039	Y	0.024	W	0.005

0.1 s⁻¹) (Table 5.3). Interestingly, V60F was unable to use any exogenous source of NH₃ unless GTP, normally an inhibitor of NH₃-dependent CTP catalysis (MacDonnell *et al.*, 2004), was added to the reaction mixture. Even with GTP, the activity of V60F was only detectable with NH₄OAc and was nearly 50-fold slower ($k_{\text{cat}} = 0.16 \pm 0.01 \text{ s}^{-1}$) than wild-type CTPS ($k_{\text{cat}} = 7.67 \pm 0.54 \text{ s}^{-1}$) (Table 5.3).

5.3.2 Gln-Dependent CTP Production

Likewise, the conservative substitutions had little effect on catalysis when Gln was the substrate, unlike V60D, V60W, and V60F. V60A and V60C had $k_{\text{cat}}/K_{\text{m}}$ values of 14.2 ± 0.9 and $21.6 \pm 4.1 \text{ mM}^{-1}\text{s}^{-1}$, respectively, similar to the wild-type efficiency of $24.7 \pm 0.7 \text{ mM}^{-1}\text{s}^{-1}$ (Table 5.3). Neither the affinity of V60A and V60C for glutamine ($K_{\text{m}} = 0.37 \pm 0.01 \text{ mM}$ and $0.24 \pm 0.04 \text{ mM}$, respectively) nor the turnover value ($k_{\text{cat}} = 5.2 \pm 0.2 \text{ s}^{-1}$ and $5.1 \pm 0.03 \text{ s}^{-1}$, respectively) differed significantly from the wild-type CTPS values ($K_{\text{m}} = 0.24 \pm 0.02 \text{ mM}$; $k_{\text{cat}} = 6.0 \pm 0.4 \text{ s}^{-1}$) (Table 5.3). On the other hand, V60D exhibited an 8-fold decrease in catalytic efficiency, and the Gln-dependent activity of V60W was too low to be measured reliably (Table 5.3). Despite the inability to utilize exogenous NH₃ effectively, V60F could utilize Gln as a substrate with a 7-fold decrease in activity ($k_{\text{cat}} = 0.82 \pm 0.06 \text{ s}^{-1}$) and 25-fold increase in K_{m} ($5.9 \pm 0.2 \text{ mM}$), relative to wild-type *Ec*CTPS (Table 5.3).

Because Gln-dependent catalysis requires GTP for full activity, the GTP-dependent kinetic parameters were measured for each mutant. Every substitution for Val 60 caused a reduction in GTP affinity, in accord with the putative GTP binding site being nearby. V60A and V60C had 5- and 4-fold reduced affinity for GTP, respectively, though the turnover rate (k_{cat}) was similar to wild-type *Ec*CTPS for both (Table 5.3). Notably, the K_{A} for GTP was 15- and 24-fold higher for V60D and V60F, respectively, indicating that the

Table 5.3. Kinetic parameters for exogenous and nascent NH_3 -dependent catalysis of wild-type and Val 60-substituted *Ec*CTPS variants.^{a,b}

Nitrogen source	Kinetic parameter ^c	<i>Ec</i> CTPS variant						
		Wild-type	V60A	V60C	V60D	V60W	V60F	DON-V60F
NH_4Cl -dependent CTP formation	K_M (mM)	1.7 ± 0.4	0.66 ± 0.1	3.3 ± 0.7	3.6 ± 0.4	4.1 ± 2.2	- ^d	1.6 ± 0.3 ^e
	k_{cat} (s ⁻¹)	9.4 ± 0.7	3.3 ± 0.2	5.7 ± 0.8	0.99 ± 0.07	0.95 ± 0.3	- ^d	1.2 ± 0.1 ^e
	k_{cat}/K_M (mM ⁻¹ s ⁻¹)	5.7 ± 1.3	5.1 ± 1.2	1.8 ± 0.1	0.3 ± 0.01	0.25 ± 0.05	- ^d	0.73 ± 0.1 ^e
NH_4OAc -dependent CTP formation	K_M (mM)	1.4 ± 0.1	0.61 ± 0.04	4.2 ± 0.2	1.6 ± 0.5	1.5 ± 0.1	0.94 ± 0.08 ^e	3.1 ± 0.13 ^e
	k_{cat} (s ⁻¹)	7.7 ± 0.5	3.12 ± 0.08	7.5 ± 0.2	1.1 ± 0.1	1.6 ± 0.1	0.16 ± 0.01 ^e	2.2 ± 0.2 ^e
	k_{cat}/K_M (mM ⁻¹ s ⁻¹)	5.3 ± 0.1	5.1 ± 0.2	1.8 ± 0.1	0.7 ± 0.2	1.1 ± 0.1	0.17 ± 0.01 ^e	0.72 ± 0.05 ^e
Gln-dependent CTP formation	K_M (mM)	0.24 ± 0.02	0.37 ± 0.01	0.24 ± 0.04	0.5 ± 0.1	- ^d	5.9 ± 0.2	- ^d
	k_{cat} (s ⁻¹)	6.0 ± 0.4	5.2 ± 0.2	5.14 ± 0.03	1.6 ± 0.2	- ^d	0.82 ± 0.06	- ^d
	k_{cat}/K_M (mM ⁻¹ s ⁻¹)	24.7 ± 0.7	14.2 ± 0.9	21.6 ± 4.1	2.9 ± 0.5	- ^d	0.14 ± 0.01	- ^d

^a See Appendix Figures A.6, A.7, A.8, A.9, A.10, A.11, and A.12 for corresponding initial rate plots.

^b See Table 2.2 for the saturating concentrations of unvaried ligands.

^c Values are the averages of three independent experiments ± SD.

^d Activity too low to be determined reliably.

^e Contained 1.0 mM GTP.

acidic and bulky aromatic substitutions were detrimental to catalysis. GTP-dependent kinetics could not be measured reliably for V60W because of the inability of this variant to utilize Gln as a substrate.

5.3.3 UTP- and ATP-Dependent kinetics

UTP and ATP are not only required as substrates, but also to promote tetramerization of the enzyme. Val 60 is located near the dimer-dimer interface, and may also be close enough to the amidoligase domain such that the Val 60 mutants might have impaired ability to bind the NTP substrates. UTP- and ATP-dependent kinetics were measured using Gln as the NH₃ source to explore this possibility, except for V60W where the inability to utilize Gln as a substrate necessitated the use of NH₄OAc instead. All variants had similar [S]_{0.5} values for ATP, with the exception of V60W which had 5-fold lower affinity relative to wild-type *EcCTPS* (Table 5.4). On the other hand, the UTP-binding site was apparently more sensitive to changes in the chemical environment at the gate. V60A, V60C, and V60D exhibited similar UTP-dependent catalytic proficiency, compared to wild-type *EcCTPS*, but substitution of Val 60 with a large, aromatic residue was detrimental to UTP binding (Table 5.4). The abilities of V60W and V60F to bind UTP were reduced 12- and 7-fold relative to wild-type *EcCTPS* ([S]_{0.5} = 0.10 ± 0.02 mM), respectively. These data indicate that less conservative substitutions for Val 60 had greater impact on the active sites than the 'natural' V60A and V60C mutations.

5.3.4 GATase Activity and Coupling Efficiencies

While the passage of *exogenous* NH₃ appeared to be blocked, V60F did permit *nascent* NH₃ to traverse the NH₃ tunnel to yield CTP, albeit at a much lower rate than wild-type *EcCTPS*. The depressed rate of Gln-dependent CTP formation could have arisen from the V60F mutation introducing a deformation in the tunnel leading to loss of nascent NH₃

Table 5.4. Kinetic parameters for NTP-dependent catalysis of wild-type and Val 60-substituted *Ec*CtPS variants.^{a,b}

Activator/Substrate	Kinetic parameter ^c	CTPS variant						
		Wild-type	V60A	V60C	V60D	V60W ^e	V60F	DON-V60F
GTP	K_A (mM)	0.032 ± 0.01	0.15 ± 0.03	0.13 ± 0.01	0.78 ± 0.09	- ^d	0.42 ± 0.04	0.31 ± 0.02
	k_{act} (s ⁻¹)	7.1 ± 0.3	5.9 ± 0.2	4.9 ± 0.2	1.31 ± 0.07	- ^d	1.01 ± 0.1	1.76 ± 0.03
	k_o	0.5 ± 0.09	0.17 ± 0.03	0.3 ± 0.09	0.15 ± 0.02	- ^d	- ^d	0.25 ± 0.05
UTP	$[S]_{0.5}$	0.10 ± 0.02	0.25 ± 0.02	0.15 ± 0.01	0.32 ± 0.05	1.2 ± 0.1	0.74 ± 0.08	1.0 ± 0.06
	$V_{max}/[E]_T$	6.18 ± 0.23	5.69 ± 0.11	5.10 ± 0.03	1.7 ± 0.2	1.4 ± 0.1	1.05 ± 0.12	1.86 ± 0.09
ATP	n	1.8 ± 0.24	1.37 ± 0.08	1.4 ± 0.1	1.42 ± 0.06	2.16 ± 0.15	1.65 ± 0.08	1.75 ± 0.06
	$[S]_{0.5}$	0.18 ± 0.04	0.22 ± 0.003	0.19 ± 0.03	0.29 ± 0.02	0.96 ± 0.12	0.3 ± 0.06	0.47 ± 0.005
	$V_{max}/[E]_T$	5.6 ± 0.2	5.56 ± 0.3	5.10 ± 0.1	1.5 ± 0.1	1.5 ± 0.07	0.99 ± 0.06	1.68 ± 0.06
	n	1.52 ± 0.22	1.29 ± 0.11	1.3 ± 0.1	1.54 ± 0.20	2.27 ± 0.08	2.0 ± 0.2	2.28 ± 0.14

^a See Appendix Figures A.6, A.7, A.8, A.9, A.10, A.11, and A.12 for corresponding initial rate plots.

^b See Table 2.2 for the saturating concentrations of unvaried ligands.

^c Values are the averages of three independent experiments ± SD.

^d Activity too low to be determined reliably.

^e NTP-dependent kinetics for V60W were measured with 150 mM NH₄OAc.

(*i.e.*, a leaky tunnel), or a more extensive effect on the GATase and/or synthase machinery. We tested the efficiency of NH₃ transport from the GATase domain to the synthase domain for the wild-type and Val 60-substituted *Ec*CTPSs by measuring the number of CTP molecules formed per molecule of NH₃. V60A, C, and D variants were all ~100% efficient indicating that the NH₃ tunnel was intact. However, V60D exhibited reduced overall GATase activity relative to wild-type *Ec*CTPS, which accounted for the lowered rate of CTP production using Gln as a substrate (Tables 5.2 and 5.4). Similarly, though we were unable to determine a coupling efficiency for V60W since the Gln-dependent CTP production was not measurable, the GATase activity for V60W was low ($k_{\text{cat}} = 0.08 \pm 0.02 \text{ s}^{-1}$) (Table 5.3). The relatively high rate of activity with exogenous NH₃, but poor catalysis of Gln hydrolysis, suggested that the GATase reaction was somehow compromised by the substitution.

V60F was the only Val 60 variant that exhibited a clear defect in NH₃ channelling. At saturating concentrations of Gln, V60F produced NH₃ at a rate 1.3-fold faster than the rate at which CTP was formed, a coupling efficiency of 75 (± 12) % (Table 5.5). This reduced coupling efficiency could arise from NH₃ leaking away from the tunnel or a 'bottleneck effect' in which a rapid build-up of NH₃ creates a blockage at the now-constricted gate. We slowed the GATase reaction down by reducing the concentration of Gln to explore this possibility. At concentrations of Gln near the K_m value, wild-type and V60F *Ec*CTPSs had coupling efficiencies of 98 (± 6) % and 105 (± 23) %, respectively, indicating that the rate of catalysis in the GATase domain was not substantially different from the overall rate of CTP generation (Table 5.6). The V60F substitution failed to block inter-domain coupling under sub-saturating conditions as well, since 100 (± 9) % of the

Table 5.5. Coupling efficiencies for wild-type and Val 60-substituted *Ec*CTPSs at saturating ligand concentrations^a.

	CTPS variant					
	Wild-type	V60A	V60C	V60D	V60W	V60F
CTP production ($v_i/[E]_T$, s^{-1}) ^b	6.0 ± 0.4	4.74 ± 0.24	5.14 ± 0.03	1.39 ± 0.16	- ^d	0.85 ± 0.12
Gln hydrolysis ($v_i/[E]_T$, s^{-1}) ^b	5.99 ± 0.23	3.8 ± 0.3	5.2 ± 0.7	1.27 ± 0.14	0.08 ± 0.02	1.14 ± 0.09
coupling efficiency ^c	1.00 ± 0.08	1.25 ± 0.1	0.99 ± 0.13	1.09 ± 0.15	N/A	0.75 ± 0.12

^a See Table 2.2 for saturating ligand concentrations.

^b Values are the averages of three independent experiments ± SD.

^c Coupling efficiency was calculated using eqn. 5.1

^d Activity too low to be detected

^e See Appendix Figure A.13 for representative kinetic plots.

Table 5.6. Coupling efficiencies for V60F *Ec*CTPS at non-saturating ligand concentrations.

	$[\text{Gln}] \approx K_m$		Sub-saturating $[\text{Gln}]$		Sub-saturating $[\text{GTP}]^b$	
CTP production ($v_i/[\text{E}]_T, \text{s}^{-1}$) ^c	3.32 ± 0.05	0.44 ± 0.03	0.33 ± 0.01	0.24 ± 0.01	1.44 ± 0.11	0.25 ± 0.02
Gln hydrolysis ($v_i/[\text{E}]_T, \text{s}^{-1}$) ^c	3.38 ± 0.2	0.42 ± 0.09	0.31 ± 0.01	0.24 ± 0.02	1.42 ± 0.02	0.27 ± 0.02
coupling efficiency ^d	0.98 ± 0.06	1.05 ± 0.23	1.06 ± 0.05	1.00 ± 0.09	1.01 ± 0.08	0.93 ± 0.08
$[\text{Gln}]$ (mM)	0.3	8	0.03	1.2	6	50

^a $[\text{GTP}] = 1.0 \text{ mM}$

^b $[\text{GTP}] \approx K_A/5$

^c Values are the averages of three independent experiments ± SD.

^d Coupling efficiency was calculated using eqn. 5.1

^e See Appendix Figure A.13 for representative kinetic plots.

nascent NH_3 was converted into CTP (Table 5.6). These data suggest that the V60F substitution did not introduce a leak, nor did it hinder the passage of nascent NH_3 , except slightly when the rate of NH_3 production was high. Moreover, this ‘bottleneck’ effect was also relieved by slowing the rate of NH_3 production through reduction in the concentration of GTP at saturating concentrations of Gln, which signified that an inability to deal with the rate of Gln hydrolysis was indeed the cause of the observed reduced NH_3 transfer (Table 5.6). Still, the rate of Gln hydrolysis catalyzed by V60F at saturating concentrations of Gln ($V_{\max}/[E]_{\text{T}} = 1.14 \pm 0.09 \text{ s}^{-1}$) was lower than that of wild-type ($V_{\max}/[E]_{\text{T}} = 5.99 \pm 0.23 \text{ s}^{-1}$) by ~ 5 -fold, indicating that the GATase reaction was also impaired by the V60F substitution (Table 5.5). The possibility that the V60F mutation introduces a pronounced alteration in structure could not be ruled out; though, circular dichroism spectroscopy of V60F showed no appreciable difference in the secondary structure relative to wild-type CTPS (Figure 5.3).

5.3.5 Utilization of NH_2OH

Evidently, *exogenous* NH_3 could not be utilized as a substrate by V60F in the absence of GTP, but *nascent* NH_3 was able to overcome the effect of the V60F substitution. We assessed whether Gln and/or GTP were capable of enhancing *exogenous* NH_3 -dependent catalysis using an approach similar to that described by Willemoes for studies on the activation of CTPS from *LICTPS* (Willemoes, 2004). In brief, NH_4OAc can be substituted by NH_2OH , resulting in the production of N^4 -OH-CTP, which absorbs at a higher wavelength than CTP allowing for the simultaneous determination of cytidine produced from nascent or exogenous nitrogen sources. However, we first had to establish that nascent (NH_3) and exogenous (NH_2OH) amines follow the same route in the *E. coli* homologue in order to draw a comparison between how the two sources are affected by

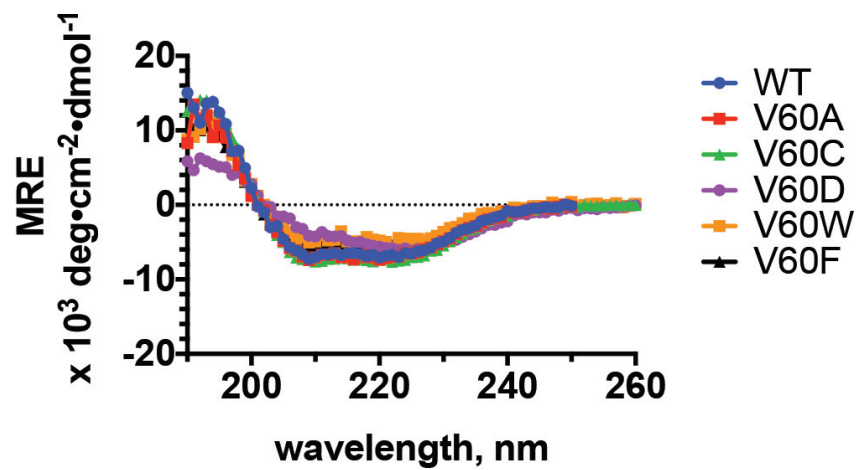


Figure 5.3. CD analysis of Val 60 *EcCTPS* variants. Circular dichroism spectra for wild-type (WT), V60A, V60C, V60D, V60W, and V60F *EcCTPS* variants were obtained at 37 °C using purified recombinant enzyme (0.2 mg/mL in 2 mM Tris-SO₄ buffer, pH 8.0, containing 10 mM MgSO₄) between 190 and 260 nm with a 0.1-cm light-path.

Gln. For wild-type *Ec*CTPS, CTP formation declined with a corresponding rise in *N*⁴-OH-CTP as the concentration of NH₂OH increased (Figure 5.4), suggesting that the two nucleophilic amines (NH₃ and NH₂OH) compete. When the same experiment was conducted using V60F, *N*⁴-OH-CTP formation was much slower, as might be expected due to the increased bulk of NH₂OH and the presumably obstructed tunnel; however, CTP formation from nascent NH₃ was strongly inhibited by increasing concentrations of NH₂OH, like wild-type *Ec*CTPS (Figure 5.4).

Having concluded that both nascent and exogenous amines likely take the same route to the synthase domain, we incubated V60F with NH₂OH in the presence and absence of GTP and/or Gln to determine whether the GTP binding and/or GATase activity enhances the passage of exogenous NH₂OH to the synthase domain. In the presence of a saturating concentration of Gln, the rate of *N*⁴-OH-CTP production was enhanced ~3-fold relative to NH₂OH alone (Figure 5.4). However, unlike when NH₄OAc was the exogenous amine, GTP was unable to enhance the utilization of the bulkier NH₂OH. Wild-type *Ec*CTPS did not exhibit any Gln- or GTP-dependent increase in NH₂OH utilization, consistent with the observation that the enzyme normally uses exogenous substrate whose passage to the synthase site is unimpeded (Figure 5.4).

5.3.6 Effects of Acyl-Enzyme Formation

Evidently, the utilization of exogenous NH₂OH by V60F increased upon addition of Gln, but whether it was Gln binding or hydrolysis that enhanced *N*⁴-OH-CTP production was ambiguous. Gln is hydrolysed at a basal rate in the absence of GTP; thus, either binding or hydrolysis of Gln may have enhanced NH₂OH utilization. During Gln hydrolysis, Cys 379 acts as the nucleophile forming a glutamyl-enzyme thioester intermediate that is subsequently hydrolyzed, yielding Glu and NH₃ (Bearne *et al.*, 2001;

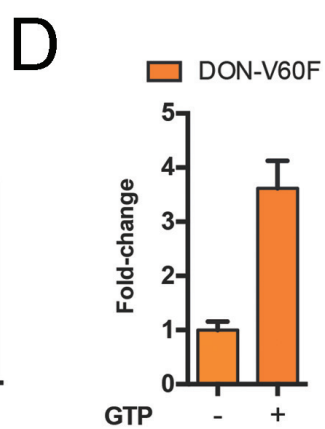
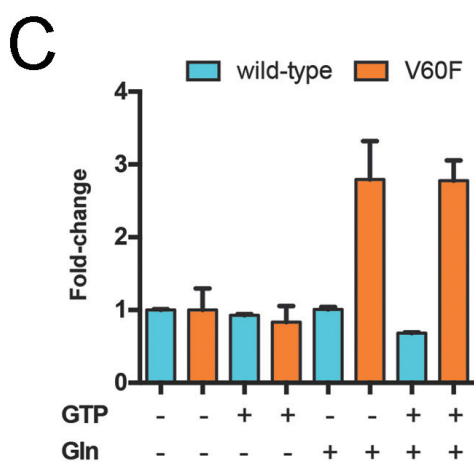
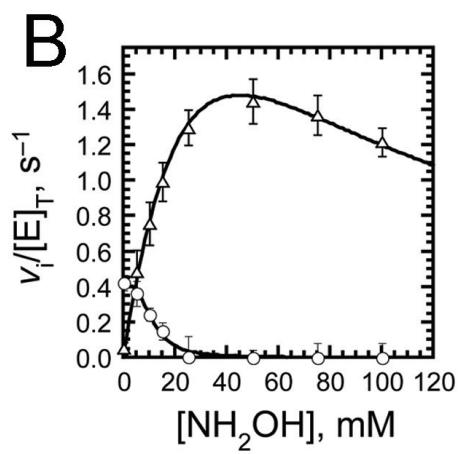
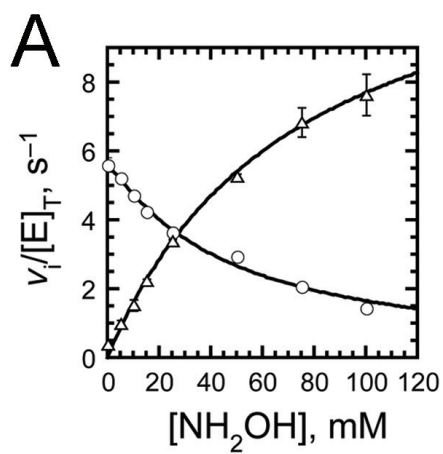


Figure 5.4. Competition between nascent NH_3 and NH_2OH and the activating effects of the GATase machinery on V60F. The rates of CTP (\circ) and N^4 -OH-CTP (Δ) production for wild-type (**A**) and V60F (**B**) *Ec*CTPS variants were measured in the presence of saturating concentrations of Gln (Table 2.2) and varied concentrations of $\text{NH}_2\text{OH}\cdot\text{HOAc}$ (0 - 100 mM). The ionic strength was maintained at 0.10 M with NaOAc. Curves for CTP production are fits of eqn. 5.3 to the initial velocity data, and curves for the production of N^4 -OH-CTP are fits of eqn. 5.4 to the initial velocity data. For N^4 -OH-CTP production by wild-type, the apparent values of K_m , k_{cat} , and k_{cat}/K_m were 74 ± 19 mM, 13.4 ± 2.4 s $^{-1}$, and 0.18 ± 0.01 mM $^{-1}$ s $^{-1}$, respectively. For N^4 -OH-CTP production by wild-type, the apparent values of K_m , k_{cat} , and K' were 36 ± 4 mM, 3.7 ± 0.2 s $^{-1}$, and 62 ± 11 mM, respectively. The values of IC_{50} were 46 ± 3 mM and 8.8 ± 1.1 mM for wild-type and V60F, respectively. The activating effects of the GATase components on wild-type (**C**, cyan), V60F (**C**, orange), or DON-V60F (**D**) *Ec*CTPSs were investigated by pre-incubating the enzymes with saturating concentrations of ATP and UTP before initiation of the reaction with NH_2OH (100 mM, wild-type; 25 mM, V60F and DON-V60F) and, where indicated, a saturating amount of Gln and/or GTP. Data are expressed as the relative change in $v_i/[\text{E}]_T$ upon treatment with the activating ligand with respect to the control sample (Gln and GTP = 0 mM or '-'). See section 5.2.3 for detailed methodology.

Zalkin, 1985). We covalently modified V60F with DON to mimick the glutamyl-enzyme intermediate (Figure 5.2A), and investigated whether alkylation enhanced exogenous nitrogen utilization. Despite having an inactivated GATase domain, the DON-modified enzyme retains the ability to utilize exogenous NH_3 as a substrate (Levitzki & Koshland, 1971; Levitzki *et al.*, 1971). Although NH_4OAc -dependent activity for DON-V60F was initially more active than V60F, GTP still activated the enzyme. Once a saturating concentration of GTP was reached, DON-V60F was 14-fold more active at utilizing exogenous NH_3 from NH_4OAc as a substrate ($k_{\text{cat}} = 2.2 \pm 0.2 \text{ s}^{-1}$) than unmodified V60F ($k_{\text{cat}} = 0.16 \pm 0.01 \text{ s}^{-1}$) under identical conditions (Table 5.3 and 5.4), suggesting that acyl-enzyme formation can enhance NH_3 utilization. Indeed, NH_2OH utilization was also enhanced, but unlike unmodified V60F, only in the presence of GTP (Figure 5.4B) suggesting that DON-V60F was not a perfect glutamyl-enzyme mimic. Neither was DON-V60F a complete 'rescue' as the values of k_{cat} were also 8- and 3.5-fold lower than wild-type CTPS using NH_4Cl and NH_4OAc , respectively, suggesting that activation by DON did not alleviate inhibition by Cl^- (Table 5.3).

The activation of NH_3 -dependent CTP production for V60F and DON-V60F was unexpectedly dependent on GTP, which is normally an inhibitor of this process (MacDonnell *et al.*, 2004). We examined the GTP-dependent inhibition of NH_3 -dependent catalysis by unmodified and modified (DON-CTPS) wild-type CTPSs as a contrast to the activating effects of GTP on DON-V60F. As reported previously (Levitzki *et al.*, 1971), GTP inhibited DON-CTPS ($\text{IC}_{50} = 0.08 \pm 0.02 \text{ mM}$) more effectively than the unmodified enzyme ($\text{IC}_{50} = 3.6 \pm 0.8 \text{ mM}$), but failed to completely ablate CTP production (Figure 5.5). While DON-CTPS had a higher apparent affinity for GTP compared to wild-type

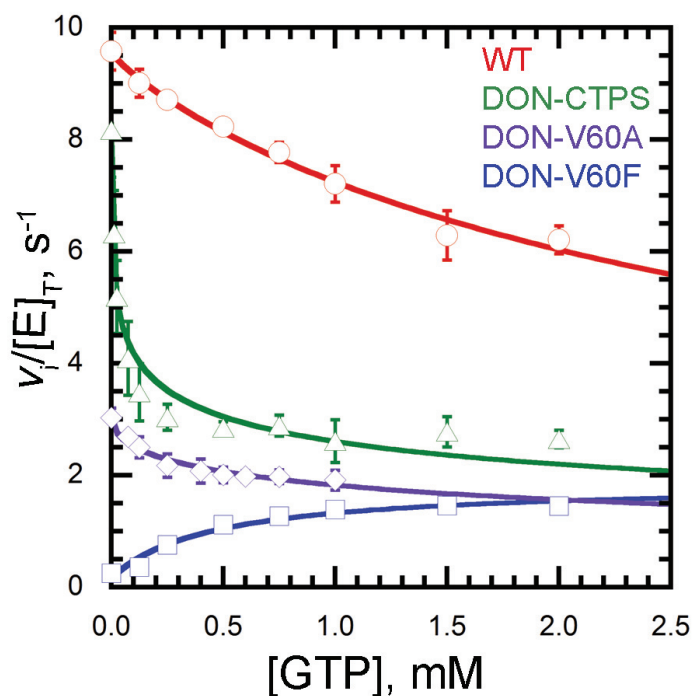


Figure 5.5. Effects of GTP on NH_3 -dependent CTP production catalyzed by *EcCTPS* variants. Unmodified wild-type (WT, red), modified wild-type (DON-CTPS, green), DON-V60A (violet), and DON-V60F (blue) were incubated with saturating concentrations of ATP, UTP, and NH_4OAc (Table 2.2) and increasing concentrations of GTP (0 – 2.0 mM). The data represent the average initial velocities from three independent experiments \pm SD. Curves for WT, DON-CTPS, and DON-V60A are fits of eqn. 5.5 to the initial velocity data. The IC_{50} values were 3.6 ± 0.8 mM (extrapolated) for WT, 0.08 ± 0.02 mM for DON-CTPS, and 2.2 ± 0.6 mM (extrapolated) for DON-V60A. Hill values for WT, DON-CTPS, and DON-V60A were 0.87 ± 0.09 , 0.56 ± 0.08 , and 0.50 ± 0.08 , respectively. In the case of DON-CTPS, the IC_{50} was calculated using $0 \leq [\text{GTP}] \leq 0.25$ mM. The curve for DON-V60F is a fit of eqn. 2.2 and kinetic parameters can be found in Table 5.4.

*Ec*CTPS, DON-V60F had only slightly stronger affinity for GTP relative to the unmodified V60F variant (Table 5.4). Together these data indicated that the greater rate enhancement observed for DON-V60F relative to unmodified V60F was likely due to conformational transitions arising from alkylation rather than an increase in affinity for GTP. Interestingly, DON-CTPS and DON-V60F exhibited similar activity with NH₄OAc at saturating concentrations of GTP ($v_i/[E]_T \approx 2.66 \text{ s}^{-1}$ and $v_i/[E]_T \approx 1.45 \text{ s}^{-1}$, respectively). Assuming this was coincidence, the GTP-dependent inhibition of a DON-V60A variant was also examined in the presence of NH₄OAc. While V60A normally has roughly 2-fold less activity utilizing NH₄OAc as an NH₃ source, DON-V60A still exhibited similar activity to the other modified variants at a saturating concentration of GTP (Figure 5.5). In effect, modification of V60F with DON was able to restore wild-type *Ec*CTPS catalytic activity under these assay conditions.

5.3.7 Effects of Salt

We conducted inhibition studies with chloride and acetate salts to ensure that the reduced ability of V60F to use exogenous NH₃ did not solely arise from chloride-mediated inhibition that was somehow alleviated by Gln and/or GTP. The possibility that high concentrations of chloride could inhibit V60F and DON-V60F was supported by their apparent inability to effectively utilize NH₄Cl as a source of exogenous NH₃. Additionally, V60D and V60W also exhibited reduced efficiency with NH₄Cl compared to NH₄OAc. Here, Gln-dependent CTP formation was measured with wild-type, V60A, V60C, V60D, and V60F incubated with varying concentrations (0 – 150 mM) of NaCl, KCl, or NaOAc (Figure 5.6). Wild-type and V60C CTPSs were not significantly inhibited by chloride or acetate, while V60A was inhibited by ~40% with 150 mM of either NaCl or KCl, and not greatly inhibited by acetate under the assay conditions (Figure 5.6). V60D and V60F,

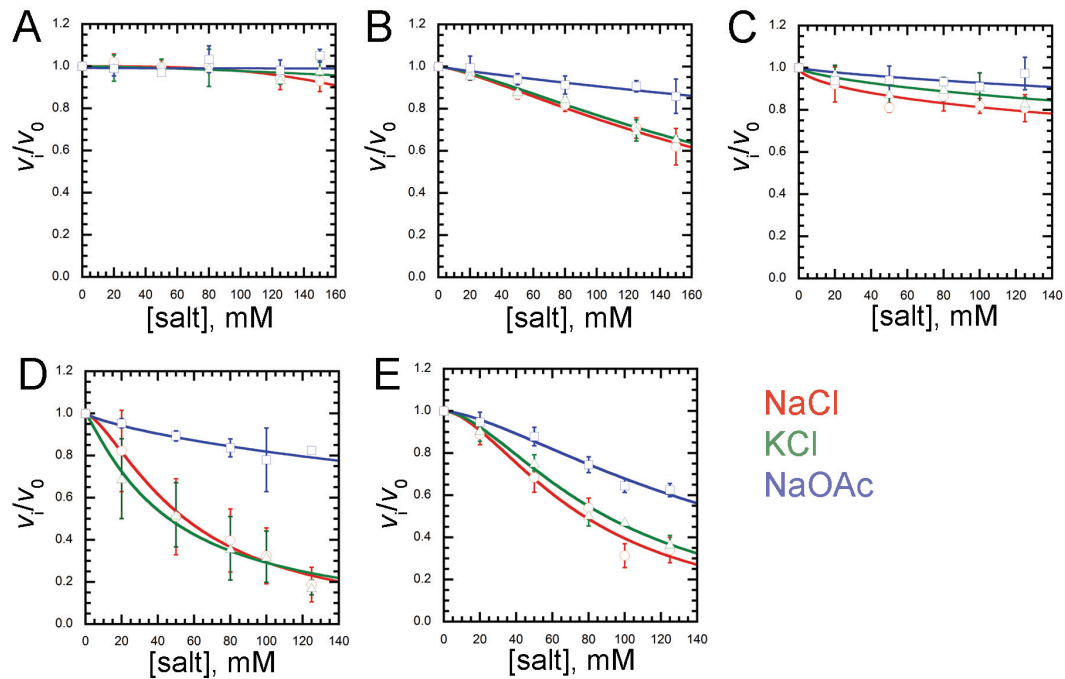


Figure 5.6. Inhibition of Gln-dependent CTP production by salts. The ability of NaCl (red), KCl (green), and NaOAc (blue) to inhibit Gln-dependent CTP formation by wild-type (A), V60A (B), V60C (C), V60D (D), and V60F (E) EcCTPS was assessed. Values of v_i/v_0 were determined from the observed velocity in the presence of the inhibitor (v_i) relative to the velocity in the absence of inhibitor (v_0). Samples contained saturating concentrations of ATP, UTP, GTP (in accord with Table 2.2), and the indicated concentration of inhibitor in assay buffer (70 mM HEPES, pH 8.0, 10 mM $MgCl_2$, 0.5 mM EGTA). Reactions were initiated using a saturating concentration of Gln as the substrate (Table 2.2). Curves are fits to the relative velocity data in accord with eqn. 2.4.

conversely, were nearly completely inhibited by NaCl and KCl (125 mM), while the equivalent concentration of NaOAc afforded 20 and 40% inhibition, respectively (Figure 5.6). Similar inhibitory effects were observed for NaCl and KCl indicating that inhibition by the cation was unlikely. Though the inability of V60W to catalyze Gln-dependent CTP production precluded a similar investigation of its sensitivity to Cl⁻, this variant was markedly more proficient with NH₄OAc than it was with NH₄Cl (Table 5.3). Together, these data support the hypothesis that the less-conservative Val 60 substitutions sensitized the enzyme to salt-dependent inhibition.

5.3.8 Effects of Val 60 Substitutions on Oligomerization

Bacterial CTPS is most active as a tetramer, and changing the chemical nature of Val 60 at the dimer-dimer interface may have altered the ability of the mutant enzymes to oligomerize, resulting in the diminished catalytic activity observed. Changing the hydrophobicity (V60F or V60W) or increasing acidity (V60D) in this region could have impaired assembly of the active tetramer - chiefly considering that most mutants exhibited diminished ability to bind ATP and/or UTP that drive the oligomerization process. Additionally, the sensitivity of these variants to Cl⁻ was similar to *Ll*CTPS, which has been shown not to form tetramers at high concentrations of NH₄Cl (Willemoës & Larsen, 2003). As such, the oligomerization state of each CTPS variant was analyzed by DLS and GF-HPLC using assay buffer containing saturating concentrations of UTP and ATP to induce tetramerization. For DLS assays, wild-type *Ec*CTPS was equilibrated without NTPs to detect the mean hydrodynamic diameter of a dimer in solution ($d_H = 8.1 \pm 3.3$ nm) as a control for non-tetramerized protein (Figure 5.7). The hydrodynamic diameter of *Ec*CTPS tetramers were measured in the presence of saturating concentrations of UTP and ATP with (15.1 ± 2.9 nm) or without GTP ($d_H = 15.1 \pm 3.8$ nm) to determine the hydrodynamic

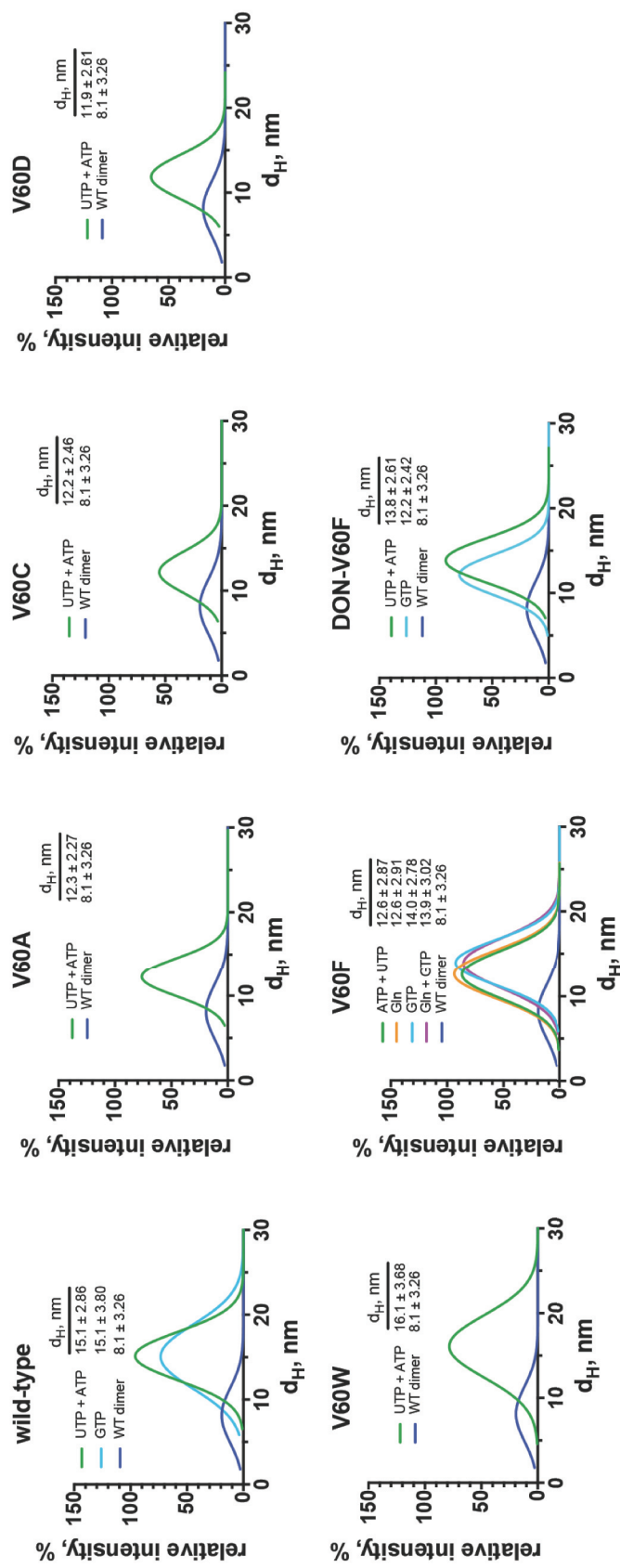


Figure 5.7. DLS results for Val 60 variants. DLS was used to determine the mean d_H for wild-type (WT) and mutant *Ec*CTPSs equilibrated with saturating concentrations of UTP and ATP at 37 °C (Table 2.2). Gln and/or GTP were also added, where indicated, as controls to ensure that GATase-mediated activation of V60F is not caused by increased tetramerization. Wild-type was also equilibrated without NTPs (WT dimer) to promote association of the dimeric species as a control for non-oligomerized enzyme. Data are represented as Gaussian fits to aggregate relative intensities from three experiments with the mean $d_H \pm SD$ indicated for each treatment. Detailed experimental methods can be found in **section 5.2.6**.

diameter of *Ec*CTPS tetramers under these conditions. In the presence of saturating concentrations of UTP and ATP, the V60A, V60C, V60D, and V60W mutants had hydrodynamic diameters of 12.3 ± 2.3 nm, 12.2 ± 2.5 nm, 11.9 ± 2.6 nm, and 16.1 ± 3.7 nm, respectively, indicating little or no change in oligomerization relative to wild-type *Ec*CTPS under the same conditions (Figure 5.7). V60F had only a slightly lower d_H compared to wild-type (12.6 ± 2.9 nm), and no increase was observed upon addition of Gln (50 mM) (Figure 5.7). While GTP induced a slight increase in d_H to 14.0 ± 2.8 nm, the enzyme only had a d_H of 13.9 ± 3.0 in the presence of both Gln and GTP suggesting that these activating ligands did not greatly impact oligomerization (Figure 5.7). Furthermore, DON-V60F, which is activated by GTP, did not exhibit any increase in d_H following addition of GTP (Figure 5.7).

When GF-HPLC was used to assess the oligomerization state of the *Ec*CTPS variants, wild-type, V60A, and V60C *Ec*CTPSs were present as tetramers at saturating concentrations of ATP and UTP, but V60W exhibited a reduced capacity to form a monodisperse population of tetramers (Figure 5.8). No tetrameric population was detected for V60D, despite the enzyme being active with exogenous NH_3 and Gln. Curiously, the proportion of monomeric wild-type *Ec*CTPS increased when Gln was introduced to the mobile phase, but this effect was abolished by addition of GTP. Contrary to the DLS results, V60F was detected as a monodisperse population of dimers in the presence of saturating concentrations of UTP and ATP, which shifted predominantly to monomers upon addition of Gln and GTP. DON-V60F behaved similarly, though more of the tetrameric species were present when only saturating concentrations of UTP and ATP were employed, and mostly tetramers were detected upon addition of GTP. Together these data

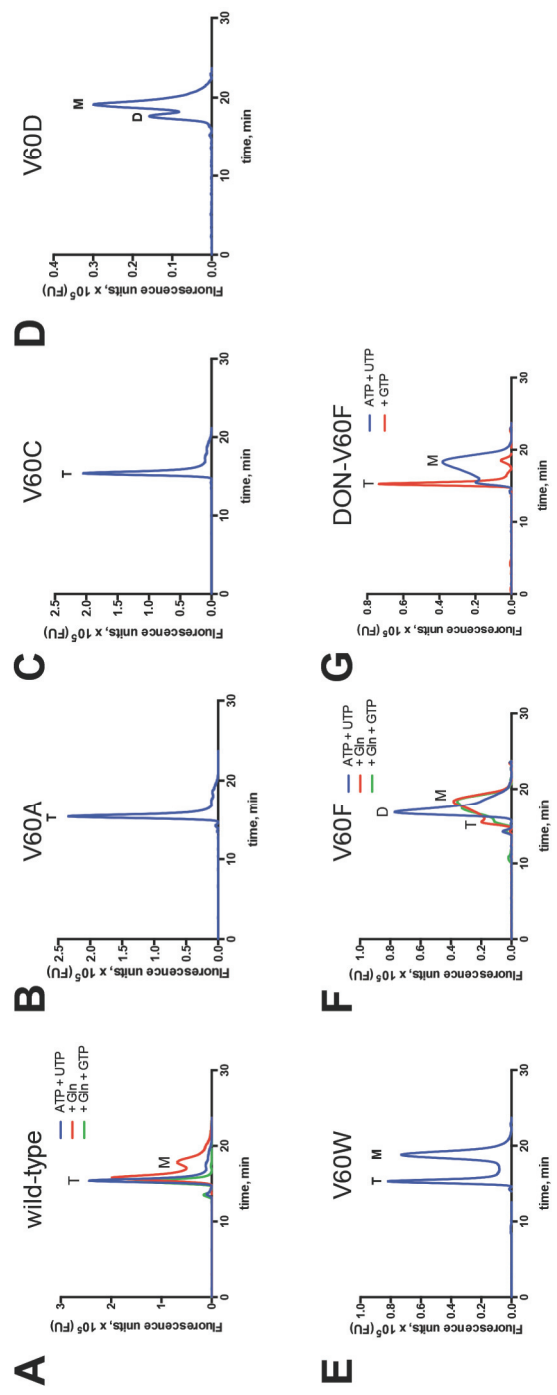


Figure 5.8. GF-HPLC analysis of wild-type and Val 60 *EcCTPS* variants. Wild-type (A), V60A (B), V60C (C), V60D (D), V60W (E), V60F (F), and DON-V60F (G) *EcCTPS*s (0.5 mg/mL, 20- μ L injection volume) were eluted at ambient temperature under isocratic conditions with assay buffer containing saturating concentrations of ATP and UTP (blue). Wild-type, V60F, and DON-V60F were also eluted with the same buffer containing saturating concentrations of Gln or a combination of Gln (6.0 mM, wild-type; 50 mM V60F) and GTP (0.25 mM, wild-type; 1.0 mM V60F and DON-V60F) together (green) where indicated. Chromatograms are representative of three independent experiments.

suggested that the Val 60 substitutions may have reduced the ability of *Ec*CTPS to undergo oligomerization. However, GF-HPLC is a non-equilibrium technique and the impaired ability of the variants to undergo full tetramerization appears to have been overcome under the equilibrium conditions of the DLS measurements (and, by extension, the kinetic assays).

5.3.9 Molecular Dynamics Simulations

The wide-ranging effects of Val 60 substitutions on NH₃ transport, GTP allostery, GATase activity, and oligomeric regulation are difficult to reconcile in the absence of structural data. X-ray crystal structures with CTPS in an 'active' conformation are few and far between, owing to the difficulties in crystallizing this enzyme, and none have been solved with bound GTP. To study the conformational dynamics of CTPS, we constructed a homology model for a V60F monomer in the absence of ligands, and simulated it *in silico* for 10 ns in the GROMOS96 54a7 force-field using GROMACS 5.0.4 (Berendsen *et al.*, 1995). The resulting simulation was then analyzed in the context of the previous kinetic characterizations.

CAVER Analyst 1.0 was employed to identify the tunnel connecting the GATase and synthase active sites (Petrek *et al.*, 2006). Interestingly, the V60F substitution resulted in a 50% tighter constriction in the putative NH₃ gate at 0 ns, relative to wild-type (PDB: 2AD5), that was quickly closed such that no tunnel could be identified due to the extent of the constriction (Figure 5.9). While the physiological relevance of a monomeric V60F in the absence of ligands may be dubious, it was encouraging to see that the overall geometry of the gate region was maintained with respect to wild-type CTPS (Figure 5.9). Investigation of the GATase active site and putative GTP-binding site also revealed a possible conformation of the *apo* structure. The catalytic triad of the GATase domain is

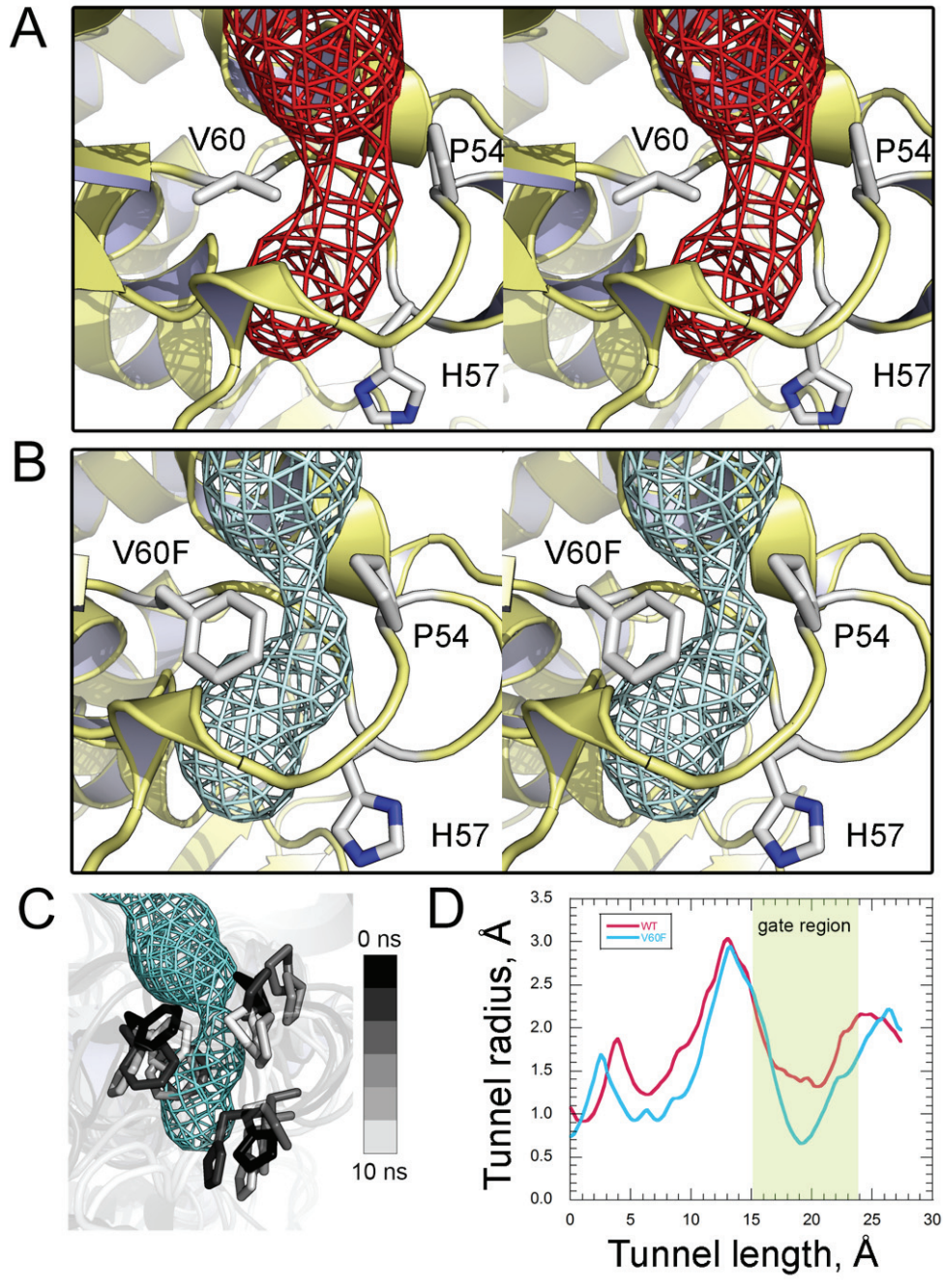


Figure 5.9. Structural model of the inter-domain NH₃ tunnel of wild-type and V60F *Ec*CTPS variants. Tunnels were modelled into the wild-type *Ec*CTPS crystal structure (**A**; PDB: 2AD5) and a V60F homology model (**B**) using CAVER Analyst 1.0 (Petrek *et al.*, 2006). The V60F homology model was constructed using SWISS-MODEL (Guex & Peitsch, 1997) using the wild-type crystal structure as a template. (**C**) The residues comprising the NH₃ gate of V60F at time = 0, 2, 4, 6, 8, and 10 ns were super-positioned with the V60F tunnel at time = 0 ns. Simulations were carried out in GROMACS 5.0.4. (**D**) The dimensions of the predicted NH₃ tunnels for wild-type (red) and V60F (cyan) *Ec*CTPSs were extracted using CAVER Analyst 1.0. The constricted region of the gate is highlighted in green. Three-dimensional renderings of protein structure were constructed using PyMOL v. 1.8.2.0 (DeLano, 2002).

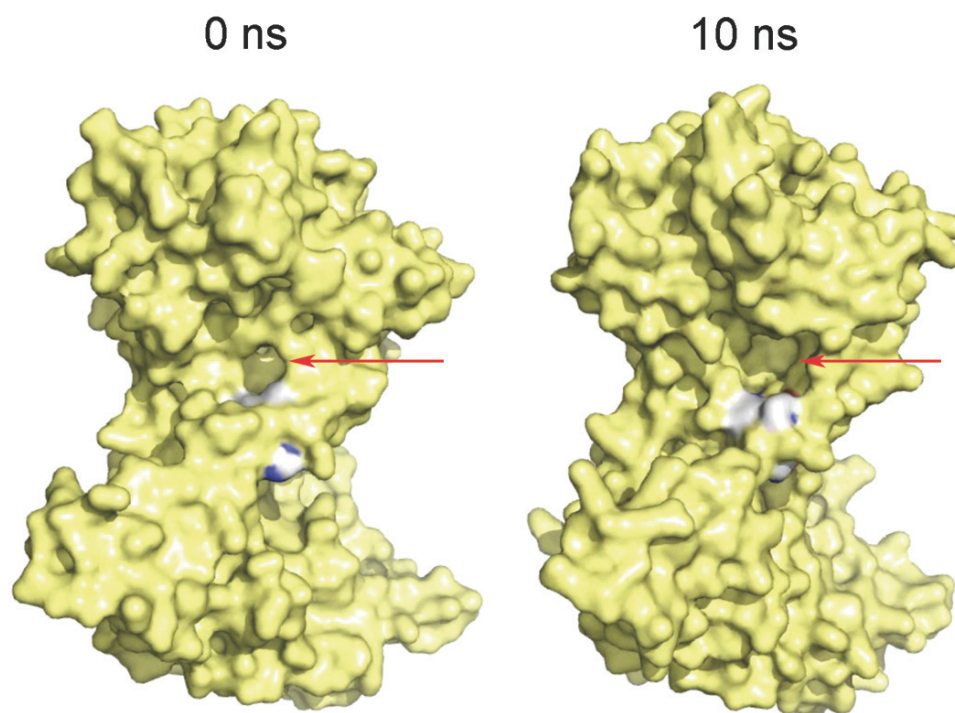


Figure 5.10. Surface model for the V60F homology model before and after 10 ns simulation. V60F homology model was constructed using SWISS-MODEL(Guex & Peitsch, 1997) and the wild-type crystal structure as a template (PDB 2AD5) (Endrizzi *et al.*, 2005). The model was simulated in GROMACS 5.0.4 (Berendsen *et al.*, 1995) for 10 ns. The GATase active site is marked by red arrows at time = 0 and 10 ns showing the 'closed' and 'open' states, respectively. Detailed experimental methods can be found in **section 5.2.4**.

buried within the core of the CTPS protein in X-ray crystal structures, but the domain opened and closed during the equilibration of the model in GROMACS (Figure 5.10). This observation indicated that there may be, at least, two conformational states for the GATase domain: one in which the face of the protein is open and then closes upon binding Gln and/or GTP. This appears to be the case, based on the X-ray structure for *Ss*CTPS in which the GATase active site is open (Figure 1.5); however, the *Ss*CTPS structure was only solved for dimeric enzyme (Lauritsen *et al.*, 2011). In any case, the possibility remained that any or all of these results were artefacts of performing a short simulation on a mutant CTPS monomer in the absence of ligands. We performed extended 100-ns simulations on both tetrameric V60F and wild-type *Ec*CTPS models for a more realistic sample size, though ligands were still omitted from the simulation. The quaternary structure of wild-type CTPS did not significantly change over the course of the simulation; however, two V60F protomers showed slight deviation in structure after 75 ns (Figure 5.11). Despite the apparent disturbance of quaternary structure *in silico*, the 'gate' remained surprisingly unperturbed suggesting that the V60F substitution may not grossly affect the local environment (Figure 5.11). Intriguingly, the phenyl ring in V60F was closer to His 57 for much of the simulation, relative to the Val side-chain present in wild-type *Ec*CTPS (Figure 5.12). This may have impacted either NH₃ channelling or the synthase domain (Figures 5.11 and 5.12).

5.4 DISCUSSION

Substitutions of conserved residues often have significant detrimental catalytic consequences for the enzyme being modified, which is partly why it was felt to be essential to construct multiple Val 60 mutant *Ec*CTPSs. Despite having substituted Val 60 with

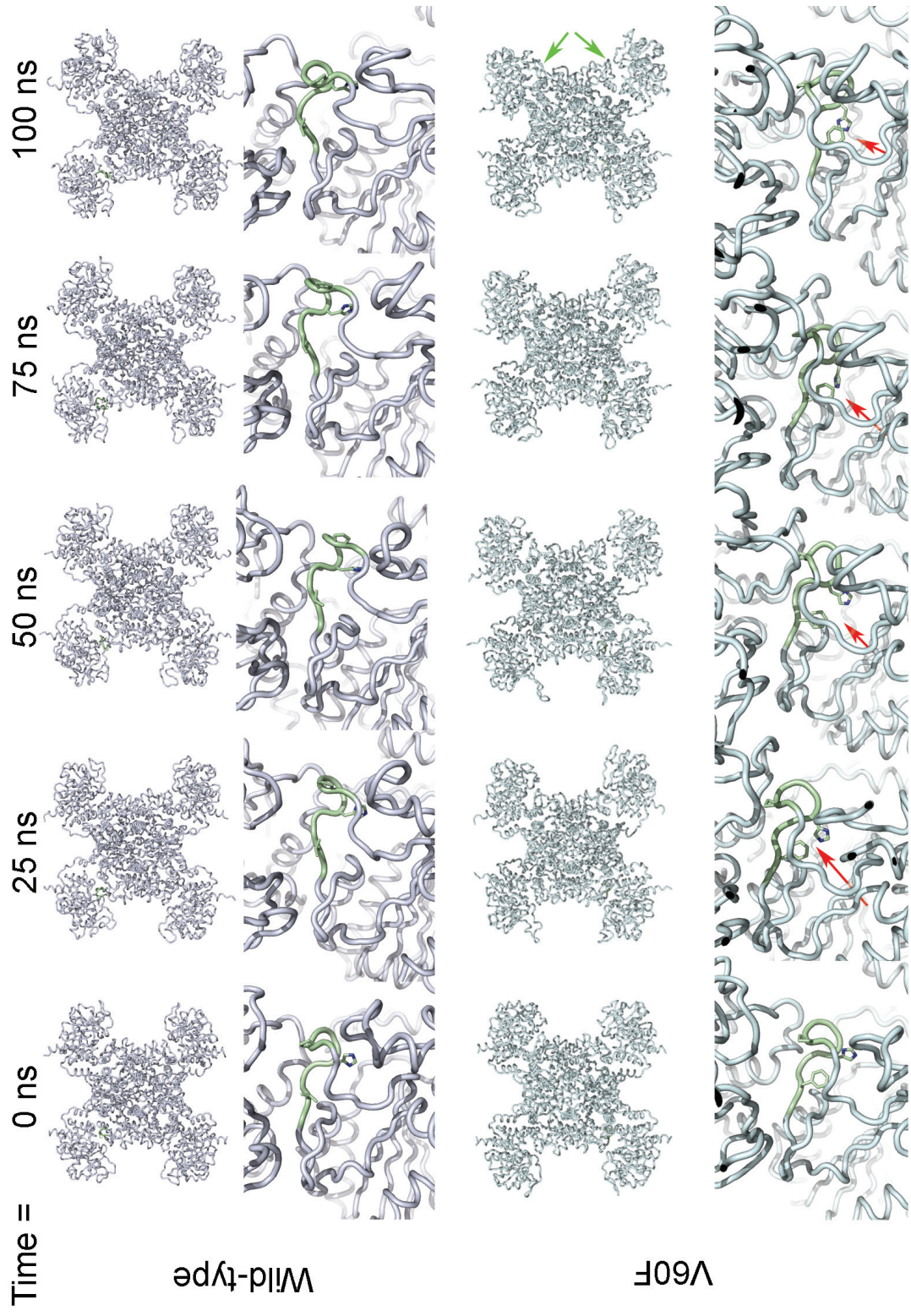


Figure 5.11. Snapshots of simulated wild-type and V60F *Ec*CTPS variants. Structural models for tetrameric wild-type (blue-white) and V60F (cyan) were constructed based on the *Ec*CTPS crystal structure (PDB: 2AD5)(Endrizzi *et al.*, 2005) and simulated for 100 ns using GROMACS 5.0.4 (Berendsen *et al.*, 1995). Snapshots of the tetramer and NH₃ gate (green) were taken at 0, 25, 50, 75, and 100 ns. Disruption of V60F quaternary structure is marked by green arrows. The interaction between His 57 and Phe 60 is marked by a red arrow. Detailed experimental methods can be found in **section 5.2.4**.

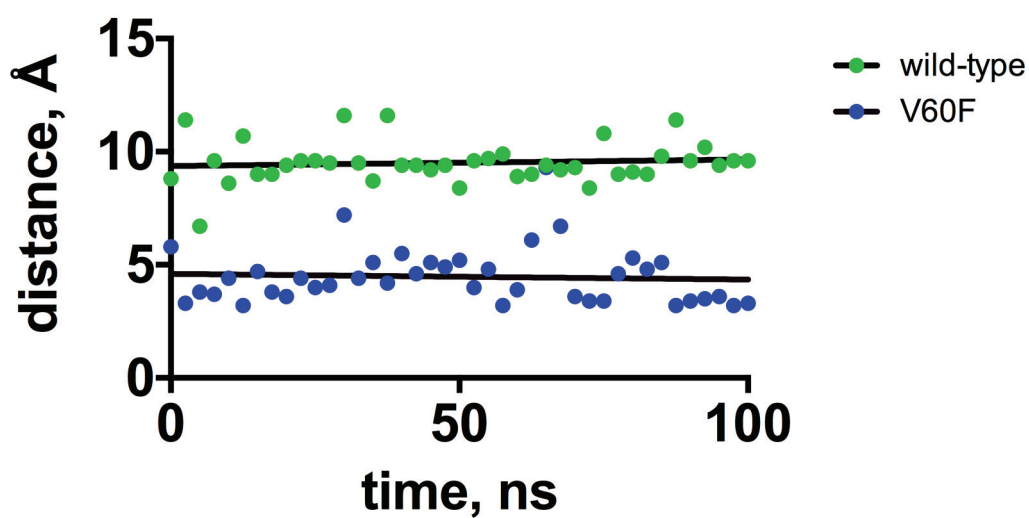


Figure 5.12. Distance between Val 60 (wild-type, green) or Phe 60 (V60F, blue) and His 57. Point-to-point measurements between the atoms in closest proximity for each side chain were determined manually using PyMOL (DeLano, 2002). Distance between the atoms was then plotted as a function of simulation time using the structures shown in Figure 5.11. Measurements were recorded every 2.5 ns.

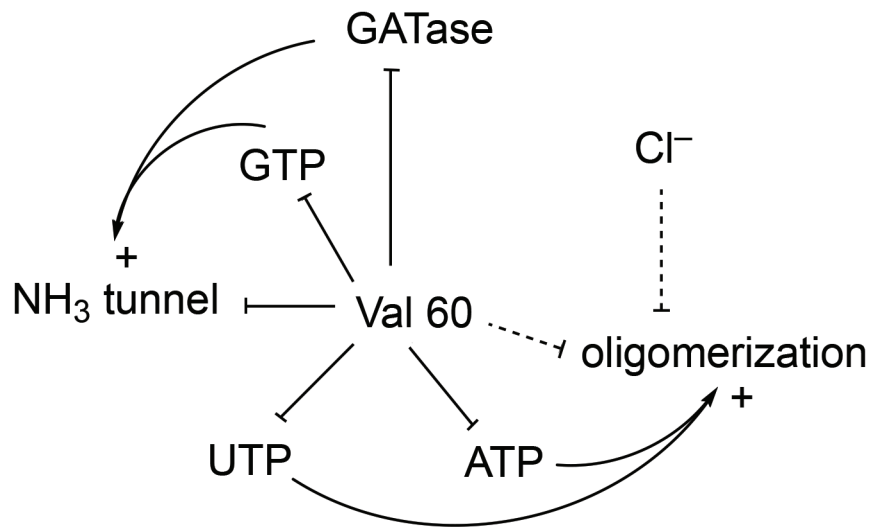


Figure 5.13. Effects of Val 60 mutation on EcCTPS enzymatic properties. Inhibitory effects are represented by bar-headed arrows and activating effects are shown as "+" signs. Confirmed links are represented by solid lines, whereas less consistent effects are shown with hashed lines.

naturally-occurring amino acid residues found in CTPS homologues, no Val 60 variant was completely unaffected and few exhibited similar defects. The varying impairments caused by Val 60 mutations and how these may be mitigated are summarized in Figure 5.13.

5.4.1 V60A and V60C

Of the five *Ec*CTPS mutants constructed, V60A and V60C were the most conservative mutations performed in accord with the HMM data (Figure 5.2). While no CTPS homologue with an Ala at this position has been biochemically characterized, the CTPS from *S. cerevisiae* contains a Cys at the homologous position and has been intensively studied (Figure 5.1) (Chang *et al.*, 2007; Chang & Carman, 2008; Choi & Carman, 2007; Choi *et al.*, 2003; Ostrander *et al.*, 1998; Pappas *et al.*, 1998; Park *et al.*, 2003). We anticipated that V60A and V60C would behave similarly to wild-type *Ec*CTPS due to the relatively high occurrence of Ala- and Cys-containing variants found nature, and the fact that *Sc*CTPS1 can utilize exogenous NH₃. As such, these variants served as important controls for the more 'radical' substitutions.

In keeping with our hypothesis, V60A and V60C catalyzed CTP production using exogenous NH₃ and Gln with near-wild-type proficiency. Both mutants had similar ability to utilize NH₄Cl- and NH₄OAc-derived NH₃, and no significant inhibition by Cl⁻ was observed, indicating that these conservative substitutions had only minor consequences on catalysis. Likewise, coupling between the GATase and synthase domains was 100% efficient at saturating concentrations of every ligand. V60A and V60C formed tetramers in both GF-HPLC and DLS experiments, and no structural deviation from wild-type *Ec*CTPS was observed by CD spectroscopy. Thus, no overriding structural perturbations were apparent following the substitutions, and the only significant defect was a ~4-fold decrease in affinity of both mutants for GTP. The lowered affinity for GTP can be

explained by the proximity of Val 60 to the putative GTP-binding site. An X-ray crystal structure of CTPS has not yet been solved with bound GTP, but molecular modelling (Endrizzi *et al.*, 2004, 2005) and kinetic analyses (MacDonnell *et al.*, 2004) point to a region between the GATase active site and the NH₃ gate as the putative GTP-binding site. The elevated activation constant describing the affinity of V60C for GTP (K_A) was equal to the normal saturating concentration of GTP required by *Sc*CTPS (Ostrander *et al.*, 1998; Pappas *et al.*, 1998), indicating that the substitutions were not wholly innocuous.

5.4.2 V60D and V60W

Catalysis of CTP production was hampered to a much greater extent when Val 60 was substituted by Asp (V60D) or Trp (V60W). NH₄Cl- and NH₄OAc-dependent catalysis by V60D was 19- and 7.5-fold less efficient than for wild-type *Ec*CTPS, respectively. The difference in efficiency between each ammonium salt was due to substantially higher inhibition by Cl⁻ than OAc. The V60D-catalyzed Gln-dependent reaction was also less efficient than wild-type; however, the rate was not significantly different from that with exogenous NH₃. Indeed, the production and transfer of nascent NH₃ through the tunnel was unimpaired with the V60D mutant since the GATase activity and CTP production were coupled with 100% efficiency. Together these data suggested that the Asp residue did not inhibit catalysis by blocking the NH₃ gate. V60D had much lower affinity for GTP than wild-type *Ec*CTPS (K_A was 25-fold higher), which supported the hypothesis that GTP is bound near Val 60. If Val 60 were to interact with GTP, then an acidic side-chain was expected to have a substantial effect on binding of a negatively charged and partially hydrophobic molecule like GTP, though, even at saturating concentrations of GTP, catalysis was still lower than wild-type. V60D had reduced GATase activity and a lower k_o value, indicating that impaired Gln hydrolysis likely caused the lower catalytic activity

relative to wild-type. Of all the Val 60 variants, the CD spectrum for V60D deviated the most relative to the wild-type *Ec*CTPS (Figure 5.3). Although this deviation was slight, it does imply some differences in secondary structure for this enzyme. Corresponding changes in the electrostatics of this region are a likely cause of the inability of V60D to form tetramers in the GF-HPLC assay.

The NH₃ gate is proximal to the dimer-dimer interface that mediates formation of the active tetramer. It stands to reason that radical change in the chemical environment in this area would disrupt oligomerization, though V60D did form tetramers in solution at 37 °C, as determined by DLS. GF-HPLC is a non-equilibrium technique that was performed at ambient temperature (~22 °C), and previous size-exclusion analyses of *Ec*CTPS determined that its oligomerization depends partly on temperature (Anderson, 1983). At room-temperature *Ec*CTPS is mostly dimeric until saturating concentrations of UTP and ATP are present (Anderson, 1983). CTPS has since been demonstrated to be much more tetrameric under equilibrative conditions (Robertson, 1995). V60D may also exhibit this behaviour, but with a reduced capacity to form tetramers relative to wild-type that is corrected once incubated at 37 °C under the conditions of the DLS experiments.

Of the five variants examined, V60W was the least effective at catalyzing Gln-dependent CTP production. V60W catalyzed NH₄Cl- and NH₄OAc-dependent reactions at similar rates as V60D, and exhibited the same salt-dependent inhibition. Unfortunately, the Gln-dependent activity was too low to be determined thereby precluding the same inhibition studies. However, there was a clear reduction in catalytic efficiency when NH₄Cl was the NH₃ donor relative to NH₄OAc. The reason for the ablated Gln-dependent reaction could have been inactivation of the GATase domain or a perforation in the tunnel

caused by the introduction of a much larger residue at the gate. A coupling efficiency could not be calculated for V60W, but the GATase domain was active enough to be characterized by measuring the production of Glu using RP-HPLC. V60W had an apparent activity that was 75-fold slower than wild-type *Ec*CTPS under the same conditions, and approximately 6-fold slower than the wild-type-catalyzed rate of CTP production when GTP is absent (k_0). These data indicate that the V60W substitution has a far-reaching effect on the GATase activity, but do not rule out a possible perforation in the tunnel.

Mutation of residues making up the NH₃ tunnel of another GATase enzyme, CPS, caused a leak in the tunnel (Kim & Raushel, 2004). The mutant CPS was unable to utilize Gln as a substrate, but could effectively catalyze the exogenous NH₃-dependent reaction indicating that nascent NH₃ was leaking out while exogenous NH₃ could diffuse in from bulk solvent. Though Gln hydrolysis was clearly impaired in the V60W mutant, our observation that no CTP production could be measured suggested that what little nascent NH₃ that was generated could not reach the synthase domain. Correspondingly higher rates of CTP production with exogenous NH₃ are consistent with the CPS result in that NH₃ from bulk solvent may be able to diffuse into such a perforation. Intriguingly, the CD spectrum for V60W was not appreciably different from the other Val 60 variants with the exception of V60D. V60W was able to form tetramers as determined using GF-HPLC, though the presence of an equally-populated monomeric species was also indicative of some disruption of tetramerization at ambient temperature. Nevertheless, V60W was found to be primarily tetrameric by DLS measurements in solution at 37 °C.

5.4.3 V60F

Substitutions of Val 60 were originally prepared to investigate how NH₃ is transported between domains because the constriction shown in CTPS crystal structures

appears too narrow for NH₃ to pass. Assuming there is a conformational change in the tunnel that governs NH₃ transport, we attempted to limit the scope of the gate to enable a kinetic interrogation of this mechanism. Remarkably, V60F had limited ability to catalyze CTP production when exogenous NH₃ was deployed as a substrate, but Gln-derived NH₃ was utilized much more effectively. Furthermore, GTP was required for exogenous NH₃ utilization despite normally inhibiting this reaction. The requirement for GTP, and putative proximity to Val 60, suggested that GTP induced a conformational change in the area to effect NH₃ transport. A model of V60F was constructed that agreed with the assertion that this variant had a constricted NH₃ gate due to the increased bulk of the Phe side-chain. Additionally, a 100 ns simulation of the tetrameric V60F showed that the aromatic side chain of the Phe residue interacted with the imidazole side chain of His 57 via an edge-on interaction for much of the simulation, which would have further blocked the tunnel exit. That nascent, but not exogenous, NH₃ could bypass this seemingly obstructed gate suggested that GATase activity was required to open the blockage. This notion is similar to observations with GlnS which cannot utilize exogenous NH₃ (Teplyakov *et al.*, 2001). Instead, GlnS has evolved an intrinsically blocked NH₃ tunnel that opens only during Gln hydrolysis (Mouilleron *et al.*, 2006).

Because the rate of Gln-dependent catalysis was reduced with respect to wild-type *EcCTPS*, coupling assays were conducted with V60F to determine whether lower activity was the result of a leak, a *bona fide* blockage, or reduced Gln hydrolysis. While there was a disparity in the rate of Gln-dependent activity relative to wild-type, 75% of nascent NH₃ formed in V60F was utilized in the synthase domain. This result suggests that 25% of NH₃ was indeed leaking out through a perforation; however, another possibility is that the tunnel

was 'clogged' by the rapid build-up of NH_3 at saturating [Gln]. When the concentrations of Gln were lowered to $\approx K_m$ or a sub-saturating amount, coupling efficiency increased such that 100% of the NH_3 produced in the GATase domain was utilized to generate CTP. This 'bottleneck' effect was also relieved following a reduction in [GTP], even at saturating [Gln], signifying that the impaired coupling when both GATase ligands are saturating may arise from a rapid build-up of NH_3 that the tighter gate cannot cope with.

Evidently, there was a disruption in the NH_3 tunnel of V60F that was relieved by Gln and/or GTP because Gln-dependent catalysis was faster than exogenous NH_3 -dependent catalysis. We tested whether Gln and/or GTP could increase the rate of CTP production from an exogenous nitrogen source. Since Gln- and NH_3 -derived CTP are indistinguishable in the product CTP, we employed NH_2OH as an exogenous amine to mimic exogenous NH_3 . Incubation of CTPS with NH_2OH results in the generation of N^4 -OH-CTP that absorbs UV light at a slightly higher wavelength than CTP, enabling the simultaneous kinetic analysis of Gln- and NH_2OH -dependent catalysis through product analysis. We first established that NH_2OH and nascent NH_3 compete for the same 4-P-UTP intermediate, since CTPS is a tetramer that exhibits half-of-the-sites reactivity with Gln (Levitzki *et al.*, 1971), but subunits lacking bound Gln might still react with exogenous amines (Willemoës, 2004). Levitski and Koshland (Levitzki & Koshland, 1971) concluded that exogenous NH_3 competes with nascent NH_3 derived from Gln based on the observation that the rates of CTP production at pH 9.25 were equal (but not additive) (Levitzki & Koshland, 1971). Willemoës and co-workers (2004) have directly demonstrated that exogenous and nascent amines compete for the same 4-P-UTP in *LICTPS*. When we performed the same experiment for wild-type and V60F *EcCTPSs*, CTP formation declined

with a corresponding rise in N^4 -OH-CTP as the concentration of NH_2OH increased, confirming that nascent NH_3 and NH_2OH also compete in *Ec*CTPS. The rate of N^4 -OH-CTP production was much slower with the V60F variant, possibly due to the increased bulk of NH_2OH and the presumably constricted tunnel. Consistent with the requirement for GATase activity for NH_3 channelling in V60F, N^4 -OH-CTP production was markedly enhanced in the presence of Gln. Though no GTP-dependent effect was observed, GTP may not be able to effect a great enough conformational change to enable translocation of the bulkier NH_2OH as it did with exogenous NH_3 .

5.4.4 DON-V60F

Evidently, Gln was more effective at promoting exogenous amine channelling through the constricted tunnel of V60F, but whether this was due to Gln binding or hydrolysis remained unclear. Gln is hydrolysed in the GATase domain at a basal rate when GTP is absent, and this slower process may be sufficient for enhancing inter-domain NH_3 transport in V60F. We mimicked the formation of the glutamyl-enzyme intermediate DON (Levitzki & Koshland, 1971) to determine whether an acyl-enzyme intermediate mimic could induce a conformational change in the tunnel. The resulting DON-V60F was able to catalyze CTP production using NH_4Cl and NH_4OAc , but still required GTP for activation. Unlike the unmodified V60F, DON-V60F also required GTP for enhanced NH_2OH utilization, which may be due to the static nature of the alkylation or GTP cannot open the gate wide enough in the absence of Gln or its mimic. Basal GATase activity may be sufficient for opening the V60F tunnel, but only when the full catalytic cycle is in progress instead of the first half-reaction that is mimicked by alkylation with DON. Nevertheless, alkylation of V60F at the GATase active site greatly enhanced NH_3 -dependent CTP production supporting the notion that GATase activity opens the tunnel.

That GTP activates NH_3 -dependent catalysis by V60F or DON-V60F at all is striking because GTP normally inhibits the utilization of exogenous NH_3 . Consequently, we also tested the effects of GTP on NH_3 -dependent CTP production for wild-type, DON-CTPS, and DON-V60A. DON modifications enhanced GTP binding and the inhibition of wild-type CTPS when exogenous NH_3 is employed as the nitrogen source, but never fully obviated CTP production entirely. DON-CTPS, DON-V60A, and DON-V60F had similar rates of CTP production at saturating [GTP] indicating that modification of V60F by DON, by and large, 'rescued' the enzyme by restoring near-wild-type levels of activity under these conditions. The slightly lower rates for the DON-V60A and DON-V60F variants with respect to DON-CTPS is likely due to the slight inhibitory effects of OAc^- . Although it seems counter-intuitive, given the disparate effects of GTP, it may be that V60F and DON-V60F are both inhibited by GTP - to the maximal extent to which this may occur - and the effect is not evident owing to the necessity of GTP in relieving the constriction within the NH_3 tunnel.

DON does not completely rescue the defects caused by the substitution, however, since the affinities for GTP, UTP, and ATP are not enhanced relative to unmodified V60F, and the enzyme is apparently still inhibited by Cl^- . V60F was strongly inhibited by Cl^- , but the activity with NH_4OAc was also negligible in the absence of GTP despite V60F retaining 60% Gln-dependent activity in the presence of OAc^- . Additionally, GF-HPLC analysis showed that both V60F and DON-V60F had diminished capability to form tetramers at ambient temperature. The addition of Gln and GTP induced limited tetramer formation in V60F, and GTP markedly enhanced DON-V60F tetramerization. For these reasons we cannot fully disregard the possibility that the enhanced activity arises from Gln-

or GTP-induced oligomerization into an active tetramer; however, no Gln-, GTP-, or DON-dependent effects on the size of V60F in solution at 37 °C were observed by DLS. Because DLS and kinetic assays were performed under identical conditions, it is more likely that V60F and DON-V60F are tetramers with blocked NH₃ tunnels.

CTPS exhibits half-of-the-sites reactivity (Levitzki *et al.*, 1971), which raises the question as to whether Gln or DON open the gate on the bound subunit, or whether there is a conformational change transduced across the tetramer that enhances exogenous NH₃ passage in the adjacent, unreacting protomer. However, competition between nascent NH₃ and NH₂OH suggests that Gln hydrolysis enhances exogenous amine utilization on the subunit in which it is bound. Additionally, the NH₃ tunnel is constrained to a single subunit, and does not feed into another to the best of our knowledge.

5.4.5 Conclusions

Several studies have been performed to understand how amidotransferases coordinate NH₃ transport with 'downstream' amidoligation reactions in a synthase domain, generally through site-directed mutagenesis and subsequent kinetic experimentation. CPS (Kim & Raushel, 2001, 2004; Mullins & Raushel, 1999), NadE (Chuenchor *et al.*, 2012), GlnS (Mouilleron *et al.*, 2006; Teplyakov *et al.*, 2001), FGAR-AT (Tanwar *et al.*, 2015), and ImGPS (Amaro *et al.*, 2005; Myers *et al.*, 2005) are just a few examples of amidotransferases that have been extensively studied and structurally characterized with respect to their ability to synchronize multiple reactions. The tunnel of NadE contains several aperture-like constrictions that open/close depending on what combination of ligands are bound, and mutation of a conserved Leu 489 to Phe reduced inter-domain coupling efficiency (Chuenchor *et al.*, 2012). Mutation (α P360A/ α H361A/ β R265A) of CPS resulted in a perforation of its NH₃ tunnel leading to a leak of nascent NH₃, but adequate

utilization of exogenous NH_3 (Kim & Raushel, 2004). Here, we obtained a result for a one-amino acid substitution that blocked the use of exogenous NH_3 , but retained Gln-dependent activity suggesting that GATase activity may affect the opening of the NH_3 gate.

Extensive mutational and kinetic experiments provided evidence that Val 60 is an important residue for GATase activity, NTP binding, inhibition by Cl^- , coupling between domains, and oligomerization (Figure 5.13). The lack of X-ray crystal structures leave us without direct observation of how Val 60 variants affect the overall conformation of *Ec*CTPS. The V60F variant had a slightly reduced coupling efficiency at maximal GATase activity that was ameliorated by slowing down the reaction; evidently V60F had a slight bottleneck in its NH_3 tunnel that could not effectively cope with the rapid build-up of nascent NH_3 . Kinetic experiments yielded support for Gln, or a combination of DON and GTP, causing a conformational change that opens a putative constriction introduced by substituting Val 60 with Phe. Molecular modelling and simulations on a V60F homology model provided little insight into the mechanistic effects of V60F, since a tunnel could only be modelled through the gate during the initial states of the simulation, presumably because the constriction became too tight. Extended simulations only emphasized the instability of the V60F tetramer. GF-HPLC analysis confirmed that non-conservative substitutions of Val 60 caused undue lability of the *Ec*CTPS tetramer, but equilibration in solution at 37 °C appeared to mitigate this effect in the DLS assays. We cannot discount that disruption of the tetramer could potentially contribute to the low activities observed for the Val 60 variants, but the bottleneck of V60F was observed under 'ideal' conditions indicating that NH_3 channelling was indeed impaired by the mutation. Though wild-type *Ec*CTPS does not require Gln hydrolysis to utilize exogenous NH_3 , and the tunnel may play more of a

'facilitator' role in NH_3 transfer (like FGAR-AT), we uncovered a mutant enzyme that required catalytic dynamics for inter-domain coordination.

CHAPTER 6 ANALYSIS OF THE UTP SITE

6.1 INTRODUCTION

CTPS has evolved a mechanism by which it can coordinate the catalysis of three chemical reactions together with perfect efficiency. Much of this coordination is enabled by the inter-domain NH₃ tunnel in combination with allosteric interactions that enhance catalysis at distal active sites. For example, the 4-P-UTP intermediate can stimulate GATase activity in concert with GTP (Willemoës & Sigurskjold, 2002), which might also open the Pro-His-Val gate at the constriction of the tunnel. The X-ray crystal structure of apo*Ec*CTPS revealed that the His 57, located at the gate, is mobile and can occupy two different conformations: 'open' and 'closed' (Endrizzi *et al.*, 2004). Electron density for His 57 was only detectable in the 'open' conformation upon crystallization of *Ec*CTPS with bound products (ADP and CTP; PDB: 2AD5)(Endrizzi *et al.*, 2005), which suggested that His 57 acts like a hatch that opens allowing nascent NH₃ through during catalysis.

Here, we mutated His 57 to Ala (H57A) to investigate the role of this residue in NH₃ channelling. Interestingly, when we substituted His 57 for Ala (H57A), the rate of CTP formation was below detectable levels for our assay. The H57A variant exhibited relatively high GATase activity, which suggested the possibility of a perforated tunnel but the ability to utilize exogenous NH₃ or NH₂OH as substrates was also poor. Though the defect could arise from a tunnel blockage or NH₃ channelling asynchrony, the lack of amidoligation by H57A opens the door to the possibility that His 57 acts as a catalytic residue.

Additionally, we interrogated the UTP site with pseudouridine-5'-triphosphate (ΨTP) to probe the possible role of Asp 70 in catalysis. This residue is positioned near the

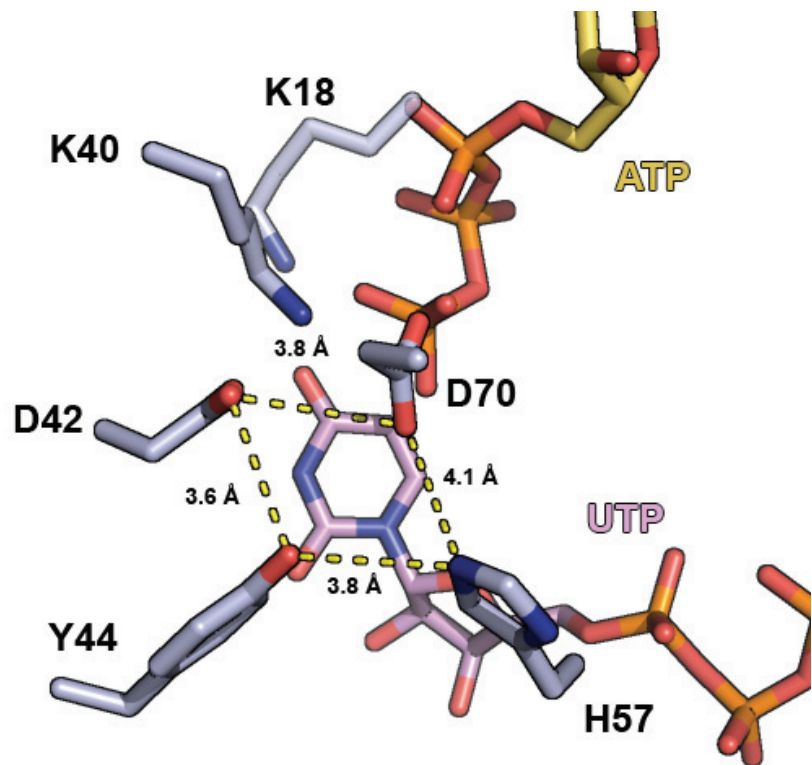


Figure 6.1. View of the UTP-binding site in *EcCTPS*. The X-ray structure for apo*EcCTPS* (PDB:1S1M) showing His 57 in the 'closed' position. Putative H-bonds are marked by hashed yellow lines with the bond lengths labelled. UTP (pink sticks) and ATP (yellow sticks) from the 6.1-Å resolution cryo-EM *HsCTPS* structure (PDB:5U03) are manually positioned beneath the *EcCTPS* structure for visualization purposes.

C-5 carbon on the uracil ring (Figure 6.1) of bound UTP, and Ψ TP retains many of the features of UTP but is protonated at the N-5 position that would lie adjacent to Asp 70. If Asp 70 acts as a catalytic base, perhaps activated by the nearby His 57 residue (Figure 6.1), then Ψ TP could act as a potent inhibitor by introducing an additional binding determinant.

6.2 EXPERIMENTAL

6.2.1 General

Ψ TP was purchased from TriLink Biotechnologies (San Diego, CA, USA), and all other chemicals were purchased from Sigma-Aldrich Canada Ltd. (Oakville, ON, Canada).

6.2.2 Analysis of N^4 -OH-CTP Production

The rate of NH_2OH -dependent N^4 -OH-CTP production was measured by monitoring the change in absorbance at $\lambda = 300$ nm using $\epsilon_{300} = 3936 \text{ M}^{-1} \text{ cm}^{-1}$, as described in **section 5.2.4**. In brief, H57A (300 $\mu\text{g}/\text{mL}$) was incubated in assay buffer (70 mM HEPES, pH 8.0, 10 mM MgCl_2 , 0.5 mM EGTA) containing GTP (1.0 mM) and ATP or UTP (both at 2.0 mM, except where otherwise stated) at 37 °C. Reactions were then initiated by addition of 150 mM $\text{NH}_2\text{OH}\cdot\text{HCl}$.

6.2.3 Analysis of GATase activity

The rates of Gln and Gln-OH hydrolysis for the H57A *Ec*CTPS variant were measured by RP-HPLC as described in **section 2.5**. H57A (12.5 $\mu\text{g}/\text{mL}$) was incubated with ATP (2.0 mM), UTP (2.0 mM), and GTP (1.0 mM) in a total volume of 1 mL of assay buffer (70 mM HEPES, pH 8.0, 10 mM MgCl_2 , 0.5 mM EGTA) at 37 °C. Reactions were initiated by addition of either Gln (6.0 mM) or Gln-OH (15 mM). Aliquots (20 μL) were removed and the amino acids derivatized by OPA for 1 min at ambient temperature at 0, 1, 3, 5, and 7 min time points before separation on a Synergi Fusion-RP column (4 μm ; 80 Å;

50 x 4.6 mm; Phenomenex, Torrance, CA, USA). Elution was performed under isocratic conditions using degassed 0.1 M NaOAc (pH 6.2):methanol:THF (800:190:10 v/v/v) mobile phase at a flow rate of 1.5 mL/min. Derivatives of Gln, Gln-OH, and Glu were detected using a Waters 474 scanning fluorescence detector ($\lambda_{\text{ex}} = 343 \text{ nm}$; $\lambda_{\text{em}} = 440 \text{ nm}$).

6.2.4 Inhibition by Ψ TP

IC_{50} values were determined by monitoring the rate of Gln-dependent CTP production using a concentration of UTP equal to $2 \cdot [S]_{0.5}$ (*i.e.*, 0.2 mM, wild-type; 0.6 mM E149D) and the indicated concentrations of Ψ TP (0 – 0.6 μ M). All other ligands were maintained at saturating concentrations (Table 2.2). Eqn 2.4 was fitted to the inhibition data by nonlinear regression analysis to obtain the IC_{50} and n values and the apparent K_i values were calculated in accord with eqn. 6.1.

$$K_i^{\text{app}} = \frac{IC_{50}^n}{1 + \left(\frac{[S]}{[S]_{0.5}}\right)^n} \quad (6.1)$$

6.3 RESULTS

6.3.1 H57A

As mentioned in **section 5.3**, we constructed a His 57 to Ala-substituted *Ec*CTPS to investigate the purported 'trap door' role of this residue in gating NH_3 transfer, but the levels of CTP production by the resulting H57A variant were below the detection threshold for our assay when Gln or NH_4Cl were employed as the NH_3 sources (data not shown). However, to push the reaction rate to a detectable level we increased the enzyme concentration and used $\text{NH}_2\text{OH} \cdot \text{HCl}$ as a source of exogenous nitrogen. For wild-type *Ec*CTPS, the turnover number ($V_{\text{max}}/[E]_{\text{T}}$) for $\text{NH}_2\text{OH} \cdot \text{HOAc}$ -dependent N^4 -OH-CTP generation was $13.4 \pm 2.4 \text{ s}^{-1}$ compared to $7.7 \pm 0.5 \text{ s}^{-1}$ for NH_4OAc -dependent CTP generation (Figure 5.4 and Table 5.3). NH_2OH -dependent N^4 -OH-CTP generation was

catalyzed by the H57A mutant, enabling us to estimate apparent kinetic parameters for UTP ($V_{\max}/[E]_T = 0.19 \text{ s}^{-1}$, $[S]_{0.5} = 0.56 \text{ mM}$, $n = 1.09$) and ATP ($V_{\max}/[E]_T = 0.17 \text{ s}^{-1}$, $[S]_{0.5} = 0.44 \text{ mM}$, $n = 1.45$) (Figure 6.2 and Table 6.1). Though it appeared that the H57A substitution disrupted the affinity of the variant for the NTP substrates relative to wild-type *EcCTPS*, a determination of these parameters for the wild-type enzyme using NH_2OH as the substrate also exhibited slightly perturbed values for UTP-dependent kinetic parameters relative to when Gln was used as the substrate ($V_{\max}/[E]_T = 7.08 \text{ s}^{-1}$, $[S]_{0.5} = 0.36 \text{ mM}$, $n = 1.65$) (Figure 6.3 and Table 6.1). These data indicated that the apparent lower affinity of the H57A mutant for ATP and UTP is due to NH_2OH , and the substitution did not severely impair catalysis by blocking the binding of NTP substrates.

Remarkably, the ability of the H57A variant to bind UTP was unperturbed with respect to wild-type *EcCTPS* when NH_2OH is the substrate despite the proximity of His 57 to the putative UTP-binding determinants in the active site. Because binding of NTP substrates was unaffected, we investigated whether GATase activity and/or inter-domain NH_3 channelling were inhibited for the H57A mutant. The turnover number for Gln hydrolysis was $2.0 \pm 0.21 \text{ s}^{-1}$, only 3-fold slower than that of wild-type *EcCTPS* ($v_i/[E]_T = 5.99 \pm 0.23 \text{ s}^{-1}$), indicating that there was minimal effect on GATase activity and that NH_3 channelling may be impaired (Figure 6.4A and Table 6.1). The H57A variant was not active enough to assay Gln-dependent CTP production, precluding coupling ratio determination, but could use NH_2OH . We tested whether Gln-OH, which is hydrolyzed to yield Glu and nascent NH_2OH , could be utilized as a substrate in order to determine the

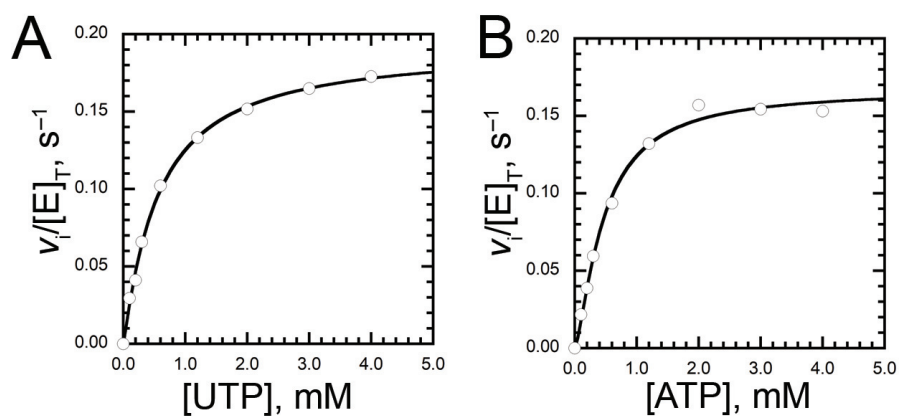


Figure 6.2. (A) UTP- and (B) ATP-dependent kinetics for the H57A variant. The H57A *Ec*CTPS was incubated with ATP and UTP (both 2.0 mM), and GTP (1.0 mM) before initiating the reaction with $NH_2OH \cdot HOAc$ (150 mM). Curves are fits of eqn. 2.3 to the data. Values for $V_{max}/[E]_T$, $[S]_{0.5}$, and n are $0.19 s^{-1}$, $0.56 mM$, and 1.09 for UTP, respectively, and $0.17 s^{-1}$, $0.44 mM$, and 1.45 for ATP, respectively. Data are for only one experiment.

Table 6.1. Kinetic parameters for wild-type and H57A *Ec*CTPS variants.

Reaction being assayed	Kinetic parameter	<i>Ec</i> CTPS variant	
		wild-type	H57A
Gln hydrolysis ^a	$v_i/[E]_T, s^{-1}$	5.99 ± 0.23	2.0 ± 0.21
Gln-OH hydrolysis ^b	$v_i/[E]_T, s^{-1}$	ND ^d	1.53
UTP-dependent CTP production ^{b,c}	$[S]_{0.5}, mM$	0.36	0.56
	$V_{max}/[E]_T, s^{-1}$	7.08	0.19
	n	1.65	1.09
ATP-dependent CTP production ^{b,c}	$[S]_{0.5}, mM$	ND ^d	0.17
	$V_{max}/[E]_T, s^{-1}$	ND ^d	0.44
	n	ND ^d	1.45

^a Values are the averages of three independent experiments \pm SD.

^b Values are from one experiment

^c $NH_2OH \cdot HCl$ (150 mM) was used as the nitrogen source.

^d Not determined.

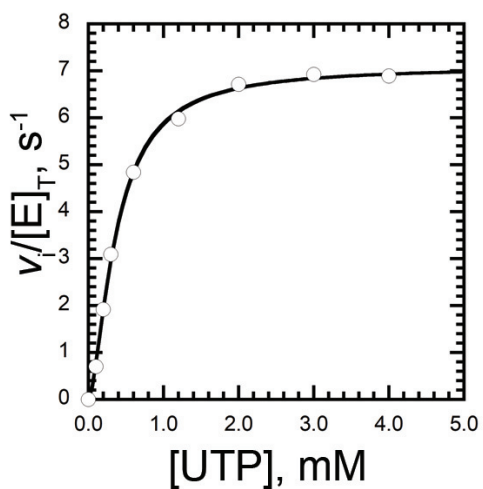


Figure 6.3. UTP-dependent kinetics for wild-type *EcCTPS*. The wild-type variant was incubated with the indicated concentration of UTP, ATP (1.0 mM), and GTP (0.25 mM) before initiating the reaction with $\text{NH}_2\text{OH}\cdot\text{HOAc}$ (150 mM). Curves are fits of eqn. 2.3 to the data. Values for $V_{\text{max}}/[E]_T$, $[S]_{0.5}$, and n are 7.08 s^{-1} , 0.36 mM, and 1.65, respectively. Data are for only one experiment.

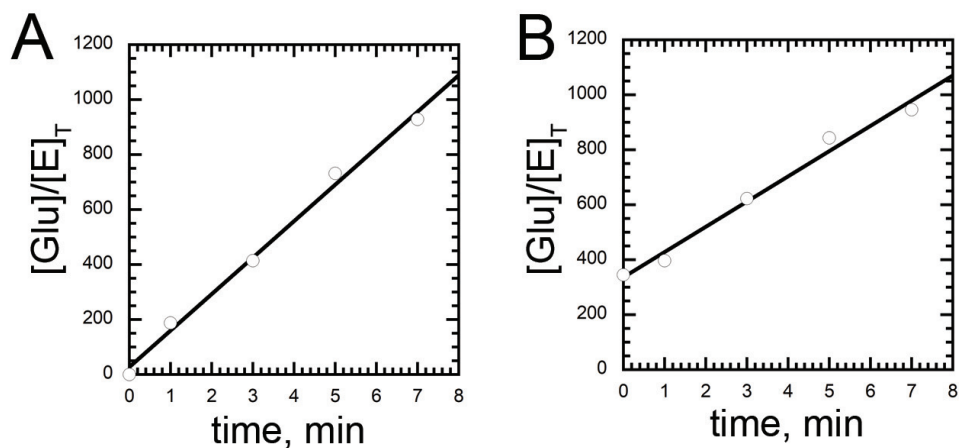


Figure 6.4. Kinetic determination of the Gln- and Gln-OH-dependent GATase activity of H57A *Ec*CTPS. For both experiments, the H57A enzyme was incubated with ATP (2.0 mM), UTP (2.0 mM), and GTP (1.0 mM) before initiating the reaction with either (A) Gln (6.0 mM) or (B) Gln-OH (15 mM). Values of $v_i/[E]_T$ for Gln and Gln-OH hydrolysis were $2.0 \pm 0.21 \text{ s}^{-1}$ and 1.53 s^{-1} , respectively. Data with Gln are representative of three independent experiments, whereas the data with Gln-OH employed as the substrate are for only one experiment.

efficiency of inter-domain coupling. The value of $v_i/[E]_T$ for H57A-catalyzed Gln-OH hydrolysis (1.53 s^{-1}) was comparable to that of Gln hydrolysis (Figure 6.4B and Table 6.1), but no Gln-OH-dependent N^4 -OH-CTP production was apparent. These results suggested that the H57A variant had a channelling defect and His 57 was not, necessarily, a catalytic residue. We cannot rule out that the H57A exhibits low catalytic activity due to 'misfiring' in which the enzyme has an intact tunnel, but is unable to properly synchronize the GATase and synthase reactions.

6.3.2 Inhibition of *Ec*CTPS by Ψ TP

While the hypothesis that His 57 is a catalytic base in the amidoligase reaction no longer appeared valid, investigation of the UTP-binding site produced some interesting observations. UTP is phosphorylated to form a 4-P-UTP intermediate (Levitzi & Koshland, 1971; von der Saal *et al.*, 1985) that is flanked by two Lys residues, but also lies adjacent to a Tyr and two Asp residues (Figure 6.1). Asp 42 is positioned such that it is a reasonable candidate to serve as a Brønsted catalyst for deprotonation of N-3 and subsequent attack of the O-4 onto the γ -phosphate of ATP. Furthermore, Asp 70 could act as a Brønsted base that deprotonates the 4-phosphocarbinolamine intermediate formed following the attack of NH_3 on the 4-P-UTP intermediate (Figure 6.1). We tested whether Ψ TP would inhibit *Ec*CTPS, anticipating that the protonated N-3 and N-5 groups (UTP numbering) on its pyrimidine ring might interact strongly with these residues (Figure 6.5). Ψ TP was not a substrate (data not shown) but was capable of inhibiting wild-type *Ec*CTPS ($\text{IC}_{50} = 0.12 \pm 0.01 \text{ mM}$, $K_i^{\text{app}} = 0.041 \pm 0.011 \text{ mM}$) with 2-fold greater apparent affinity than UTP ($[\text{S}]_{0.5} = 0.11 \pm 0.01 \text{ mM}$) (Figure 6.6A and Table 3.2). To confirm that Ψ TP was bound in the 'UTP orientation', and not in the CTP pocket, we tested the inhibition of

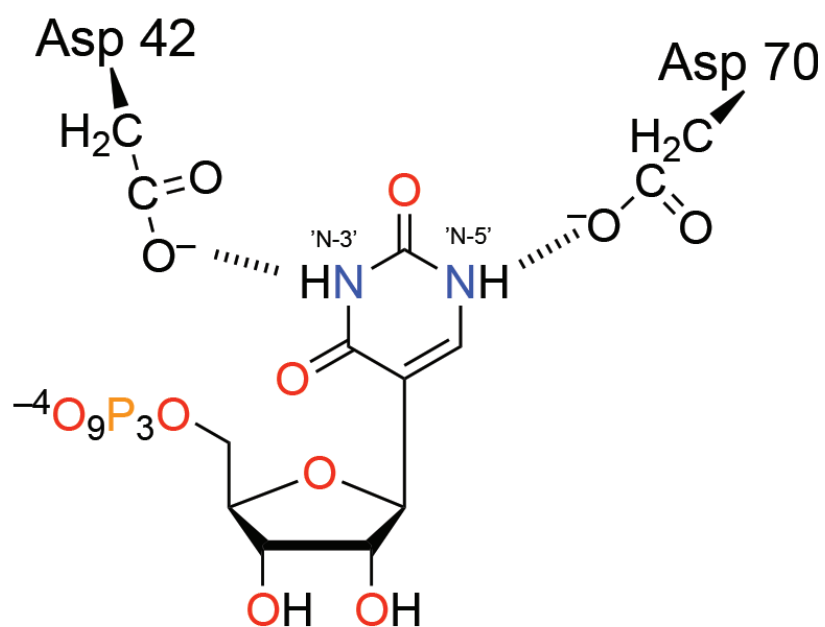


Figure 6.5. Proposed binding interactions with the pyrimidine ring of ΨTTP at the active site of *Ec*CTPS. UTP numbering was used to label the pyrimidine nitrogen groups for sake of consistency. The roles of Asp 42 and Asp 70 in catalysis of CTP generation have not been confirmed.

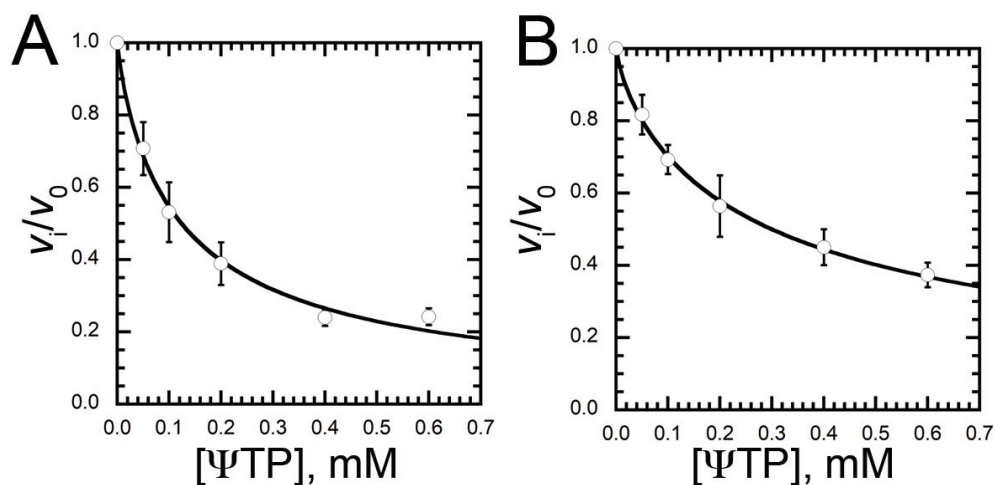


Figure 6.6. Inhibition of *EcCTPS*s by Ψ TP. The ability of Ψ TP to inhibit Gln-dependent CTP formation by wild-type (A) and E149D *EcCTPS* variants was assessed. Values of v_i/v_0 were determined from the observed velocity in the presence of the inhibitor (v_i) relative to the velocity in the absence of inhibitor (v_0). Samples contained saturating concentrations of ATP (1.0 mM), GTP (0.25 mM), $2 \times [S]_{0.5}^{UTP}$ (0.2 mM, wild-type; 0.6 mM E149D), and the indicated concentration of inhibitor in assay buffer. Reactions were initiated using a saturating concentration of Gln as the substrate (6.0 mM). Curves are fits to the relative velocity data in accord with eqn. 2.4. IC_{50} values were 0.12 ± 0.01 mM and 0.30 ± 0.01 mM for wild-type and E149D variants, respectively.

the E149D variant since it cannot bind cytidine analogues. The E149D *Ec*CTPS was inhibited by Ψ TTP with similar potency to the wild-type enzyme ($IC_{50} = 0.30 \pm 0.01$ mM, $K_i^{app} = 0.10 \pm 0.02$ mM; $[S]_{0.5}^{UTP} = 0.31 \pm 0.03$ mM) (Figure 6.6B and Table 3.2). Though the interaction with *Ec*CTPS was not very strong, Ψ TTP was an inhibitor that bound slightly better than UTP indicating that there is an enhanced interaction with the enzyme.

6.4 DISCUSSION

Together these experiments on the H57A mutant and Ψ TTP produced some intriguing results, but ultimately led to dead ends. While His 57 is highly conserved, Ala residues are apparently present at this position in some CTPSs in nature (Table 5.2). That said, the vast majority of residues in this position contain polar side chains, which supports the notion that His 57 is involved in catalysis in some manner. There is the possibility, however, that the predicted CTPS sequences are either not perfectly aligned or annotated. Alternatively, Ala-containing CTPSs may have entirely different structuring in this region that permit catalytic activity without the defects of the single residue-substituted H57A variant. Alternatively, inactivity of the H57A *Ec*CTPS could result for multiple reasons. Inhibition of the GATase domain is unlikely, but mutagenesis studies on the nearby Val 60 showed how Gln hydrolysis could be impaired by changes in the NH_3 gate. Due to the lack of activity in the synthase domain, the lack of catalysis by the H57A variant could be any permutation of defects preceding amidoligation (GATase, channelling, etc.). Fortunately, GATase activity could be measured, which revealed that the hydrolysis of Gln was only modestly impaired relative to wild-type. Though it couldn't catalyze the Gln-OH-dependent reaction, the H57A variant was capable of catalyzing N^4 -OH-CTP generation when exogenous NH_2OH was used as the substrate. This was compelling evidence that

H57A has a perforated tunnel, like the triple Ala-substituted of CPS (Kim & Raushel, 2004); however, NH_2OH is also a much stronger nucleophile than NH_3 , which could also account for the increased reactivity (Edwards & Pearson, 1962). In this case, the lone pairs of electrons on the oxygen would help stabilize a positive charge on the $\text{R}^+\text{NH}_2\text{:O:H}$ intermediate (R being the C-4 position of UTP in this case, Figure 6.7). This would also yield the tetrahedral intermediate more quickly than NH_3 due to the increased acidity of NH_2OH relative to NH_3 ($\text{p}K_a = 6.03$ and 9.24 for $^+\text{NH}_3\text{OH}$ and NH_4^+ , respectively)(Good, 1960; Lunn & Bearne, 2004). Unfortunately, there is no clear answer as to why the H57A variant is inactive, and there will likely not be one until more detailed structural data for CTPS with bound UTP and/or intermediates are available.

Because ΨTP contains an N-5 (UTP numbering) proton adjacent to Asp 70, we tested whether this change would enhance the interaction with *Ec*CTPS. Initially, we tested whether ΨTP was a substrate for wild-type *Ec*CTPS, but no activity was detected. However, ΨTP was a reasonably strong inhibitor of the reaction binding with two-fold tighter apparent affinity than UTP. To ensure that ΨTP was not bound in the CTP binding pocket, inhibition studies were also carried out using the E149D variant, which cannot bind CTP. Similar to what we report for the wild-type *Ec*CTPS, E149D had 3-fold tighter apparent affinity for ΨTP than for UTP. This result confirmed that ΨTP was likely not binding at the CTP site, and that substitution of C-5 position with nitrogen slightly enhanced interaction with the enzyme. Though ΨTP maintains a similar H-bonding pattern as UTP, the introduction of an sp^2 hybridized C-1 carbon would lock the rotation of the pyrimidine ring. In this scenario, the slightly tighter binding of ΨTP relative to UTP could be due to conformational selection in which the entropy barrier is lower because the ring

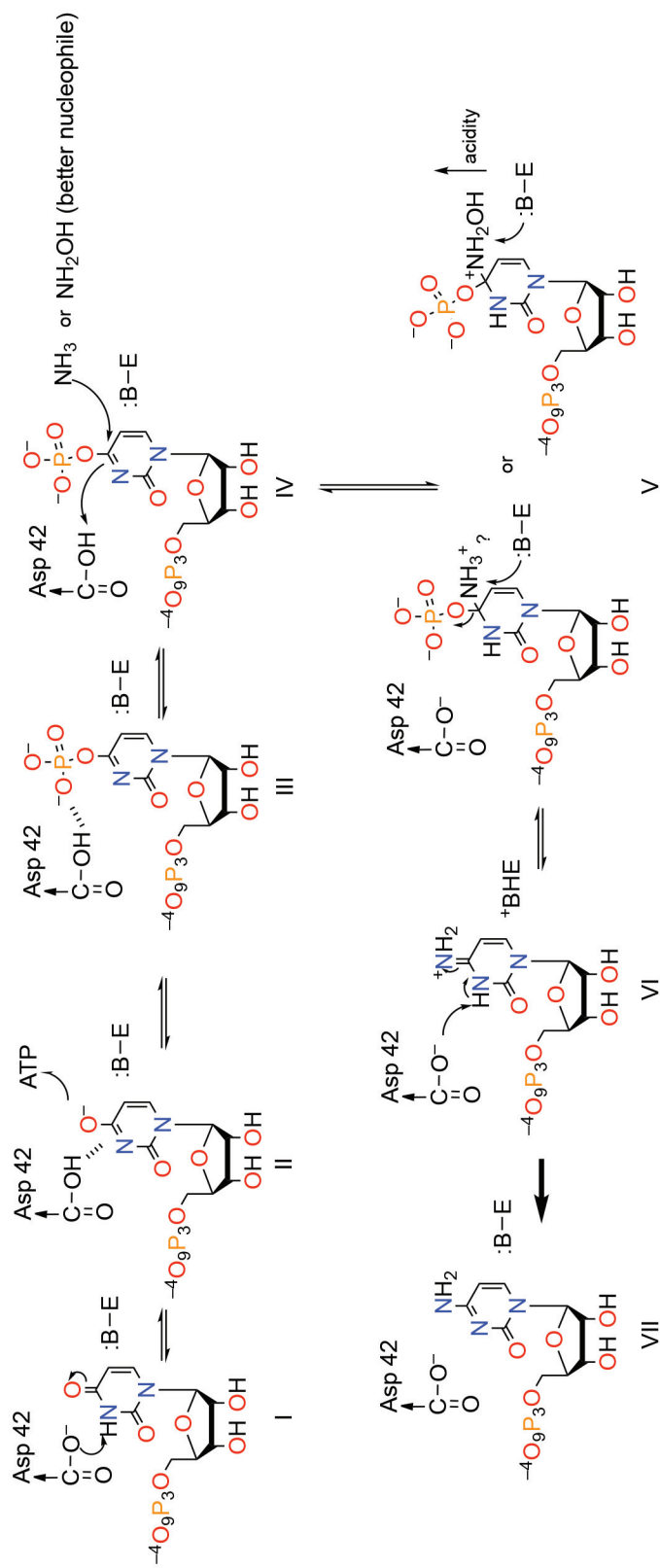


Figure 6.7. Hypothetical mechanism for the amidoligation reaction.

(I) A general base (possibly Asp 42) deprotonates the N-3 position resulting in iminolate formation (II) and attack on the γ -phosphate of ATP (III). The iminolate and 4P-UTP intermediates may be partially stabilized by H-bonding with the now-protonated general base catalyst (hashed lines). NH_3 attacks the C-4 position and the N-3 atom abstracts a proton from the general base catalyst (IV) forming a tetrahedral intermediate (V). Somehow the recently ligated NH_3 is deprotonated leading to liberation of inorganic phosphate and formation of the intermediate shown in panel VI. Another deprotonation event (VI) leads to CTP generation and the catalytic residues are restored to their ground state by an unknown mechanism (VII).

is already in a more favourable conformation. Unfortunately, due to a lack of information as to how CTPS binds UTP in general, let alone Ψ TP, we cannot draw any more conclusions from these experiments at this time.

CHAPTER 7 CONCLUSIONS

7.1 GEMCITABINE-5'-TRIPHOSPHATE AND CTP SYNTHASE

Heinemann *et al.* (1995) successfully demonstrated that treatment of cells with dF-dC caused dF-dCTP-dependent depletion of CTP pools, but direct inhibition of CTPS was never demonstrated. The inhibition studies presented in **Chapter 3** provide an estimate of the degree by which *Ec*CTPS is inhibited by dF-dCTP *in vitro*, supporting the findings of Heinemann *et al.* (1995). dF-dCTP was capable of inhibiting *Ec*CTPS by a parabolic competitive mode of inhibition. Rudimentary docking of a dF-dCTP model into the CTPS synthase domain showed little difference from the conformation of *Ec*CTPS with bound CTP that had been solved by X-ray crystallography. However, the previous structural data (Endrizzi *et al.*, 2004, 2005) in conjunction with our model did provide a reasonable framework to investigate how dF-dCTP is bound with such high affinity. CTP analogues with a 2'-*arabino* fluorine group were much more effective at inhibiting *Ec*CTPS than the compound containing only a 2'-*ribo* fluorine. Based on the limited structural information at hand, we rationalized that interactions between the 2'-*arabino* fluorine and an interdigitating, hydrophobic loop are the most likely contributors to the enhanced affinity observed for these analogues. Furthermore, site-directed mutagenesis experiments shed some light on how CTP and its analogues are bound by *Ec*CTPS. Substitution of Glu 149, a putative CTP-binding determinant, with Gln afforded a variant that was capable of binding CTP analogues despite previous assertions that the carboxylate of Glu 149 is a charged H-bond acceptor of the 3'- and 2'-OH groups of the ribose. Surprisingly, the more conservative E149D substitution disrupted the binding of CTPS and its analogues. Not only did this highlight how CTPS must recognize the ribose of CTP and its analogues, but

the ability of the E149D variant to catalyze CTP production revealed functional evidence that *Ec*CTPS discriminates between the nucleoside moieties of UTP and CTP. We capitalized on the unique properties of the E149D mutant by testing whether dF-dUTP, the so-called 'inactive' catabolite of gemcitabine, is bound with greater affinity than UTP. Incubation of wild-type *Ec*CTPS with dF-dUTP resulted in the rapid onset of product inhibition, but studies using the E149D variant showed that dF-dUTP was bound with the same affinity as UTP. Furthermore, wild-type and E149D *Ec*CTPSs catalyzed the conversion of dF-dUTP into dF-dCTP, presenting a new putative paradigm for gemcitabine metabolism *in vivo*.

A growing number of studies have recently demonstrated that CTPS forms filamentous structures *in vitro* and *in vivo*. During the nascent period of CTPS filament investigation, many seemingly opposing theories were presented, including the assertion that GATase activity mediates filament formation (Ingerson-Mahar *et al.*, 2010). Later it became apparent that prokaryotic CTPS filaments were induced by the product, CTP, so we investigated whether dF-dCTP may also mediate filament formation. Unlike previous studies that used right-angle fluorescence counting or immunofluorescence, we developed a DLS assay to characterize the populations of supramolecular *Ec*CTPS structures. On the whole, dF-dCTP induced the formation of slightly longer *Ec*CTPS filaments, which could be disassembled by addition of UTP. Surprisingly, higher concentrations of dF-dCTP were required to induce filament formation than were necessary for inhibition in the presence of UTP, which ruled out polymerization as a mediator of the previously observed parabolic competitive inhibition.

The inability of the E149D variant to form filaments in a dF-dCTP-dependent manner confirmed that the mechanism of dF-dCTP-induced polymerization was likely similar to that of CTP. The presence of other higher-order species in both wild-type and E149D samples revealed the presence of an as-of-yet unknown higher-order population that does not respond to NTPs. We were also able to test the hypothesis that Phe 227, located in the CTP-binding pocket, is necessary for binding CTP and rearranging a H-bond network to promote filament formation (Lynch *et al.*, 2017). Substitution of Phe 227 with Ala and Leu residues revealed that the Phe residue is not required for binding CTP (or dF-dCTP), but was necessary for large-scale filament formation. Interestingly, it seems that the phenyl ring of Phe 227 is required for *sensing* the cytosine ring, and inducing a conformational change that facilitates filament formation. The observation that CTPS is inhibited by dF-dCTP, which subsequently induces enzyme polymerization, reveals new insight into gemcitabine pharmacology and may help inform future studies into the mechanism of the drug or its analogues.

7.2 NH₃ CHANNELLING

All GATase family enzymes are inherently complex due to the synchronization of multiple reactions, often between multiple domains and/or subunits. Though CTPS has a relatively simple NH₃ tunnel (compared to CPS, for example), *Ec*CTPS was extremely sensitive to mutations at the putative NH₃ gate. Site-directed mutagenesis of a conserved residue, Val 60, that is located between the two catalytic domains in *Ec*CTPS resulted in a wide range of impacts on catalysis. Even conservative mutations of Val 60 (V60A and V60C) inhibited binding of GTP despite not having overly detrimental effects on overall CTP generation. However, V60D, V60W, and V60F variants had various effects on

multiple enzymatic processes. V60D exhibited reduced GATase activity, but an equally low ability to catalyze CTP production from exogenous sources of NH₃. The latter observation implied that the synthase domain and/or the structure of the NH₃ tunnel were impaired. Furthermore, the affinity of the V60D mutant for GTP was far lower than observed for wild-type *EcCTPS*. That the affinity for GTP of the V60D variant was impacted is not too surprising, if GTP binds nearby. However, catalysis could also be inhibited at saturating concentrations of GTP because the substitution blocks GTP-mediated conformational changes. On the other hand, V60W could not effectively catalyze Gln-dependent CTP production and the affinities of this variant for UTP and ATP were an order of magnitude lower relative to wild-type *EcCTPS*. The extremely low GATase activity likely accounts for the diminished overall catalytic activity; however, the V60W substitution may have also introduced a leak in the NH₃ tunnel allowing nascent NH₃ out and exogenous NH₃ in. This would account for why V60W still exhibits relatively high turnover numbers when exogenous NH₃ sources are used in lieu of Gln.

Of all the Val 60 substitutions, V60F was the most interesting, and most complicated. Somehow, the bulkier V60W substitution did not greatly impact the utilization of exogenous NH₃, but the slightly less bulky V60F completely prevented use of NH₄Cl and impaired the use of NH₄OAc. Likewise, V60W had a much greater impact on the GATase activity than the V60F substitution did. While the V60F variant exhibited enhanced utilization of exogenous NH₃ in the presence of Gln or DON, we cannot state for *certain* the reason for this effect. *EcCTPS* structures often show that the UTP- and ATP-binding cleft is open to solvent, which may be where exogenous NH₃ or NH₂OH enter the active site instead of through the tunnel. Though competition between nascent NH₃ and

exogenous NH_2OH suggested that nascent and exogenous amines take the same route to the synthase domain, competition is ultimately measured by CTP production. Thus, we cannot conclusively distinguish between substrate passing through the tunnel or entering the synthase site directly.

Gln and/or GTP may influence the conformation of the synthase domain such that NH_3 or NH_2OH can more effectively access the 4-P-UTP intermediate, and perhaps the V60F constriction is not being opened as we propose. Furthermore some mutations in CTPS sensitize the enzyme to inhibition by Cl^- or disrupt tetramerization resulting in lower activity than expected. Consequently, any disruption to *Ec*CTPS catalysis that is introduced by use of site-directed mutagenesis could be affecting any one of a range of enzymatic processes. Ultimately, the most parsimonious explanation is often the best. We have determined that Gln or DON and GTP can both increase the utilization of exogenous NH_3 in a tunnel defective mutant (V60F), which may result from conformational changes that relieve a constriction in the gate.

7.3 FUTURE WORK

Despite the difficulty in studying a complex multi-reaction, multimeric enzyme, there are still valuable avenues left for CTPS study. Previous attempts at inhibiting CTPS with analogues of the 4-P-UTP intermediate failed to yield significant inhibition (Taylor *et al.*, 2008). Upon investigating the amidoligase site, it stands to reason that a highly negative charged 4-phosphonyl-UTP may not bind because the N-3 position is not protonated (similar to the intermediate in panel IV of Figure 6.7). Perhaps Asp 42 (or another active site residue) can only bind the 4-P-UTP intermediate following proton abstraction, and the presumably negatively charged ground state is unable to bind anionic

inhibitors. In such a mechanism, Asp 42 would then be protonated and may form a hydrogen bond to partially stabilize the negative charge on the UTP transition states, which otherwise won't happen if there is no proton at N-3. Currently very little is known about the amidoligase mechanism, and there are several seemingly important residues in close proximity to one another (Figure 6.1). While the H57A variant was inactive, and the reasons for this remain unclear, I think that a classical approach could help to delineate the amidoligase mechanism. If His 57 plays an active role in the amidoligase reaction, activity of the H57A *Ec*CTPS mutant may be restored upon addition of exogenous imidazole. This chemical rescue approach has been employed for His to Ala mutations in the past, and is also applicable to Lys and Arg mutations (using NH_3 and guanidinium hydrochloride) (Carter & Wells, 1987; Toney & Kirsch, 1989). I am also curious as to how substitutions for Asp 42, Tyr 44, and Asp 70 change the catalytic proficiency of *Ec*CTPS; however, it would be difficult to tell whether inactivation of the enzyme is due to disruptions in structure or catalysis. Moreover, substitution of Asp 42 with Asn may allow binding of 4-phosphono-UTP, which should bind with high enough affinity to be assayed by isothermal titration calorimetry, if it is indeed an effective intermediate analogue. Hopefully, now that cryo-EM has been used to characterize an ostensibly low-populated UTP-bound state for *Hs*CTPS (given that previous X-ray studies first suggested that it binds in the CTP pocket), there can now be more serious investigations into how the substrate is bound and/or reacts with the enzyme. This goes for GTP as well since the exact location of its binding site on the enzyme remains inconclusive.

Another curious aspect of *Ec*CTPS is its domain organization, which is thought to have arisen from a gene fusion event that coupled GATase activity to the amidoligation

reaction. The enzyme is a bi-lobular assembly of two otherwise discrete subunits connected by a partially-disordered linker (Endrizzi *et al.*, 2004). I think there is merit in cleaving the linker and observing how this impacts CTPS activity and oligomerization. Though the primary structure of an extant CTPS would be utilized, this would essentially re-create a model for the extinct, two-subunit CTPS. Similar studies on ImGPS were performed using an ancestral reconstruction of the enzyme that retained the ability to oligomerize and effect catalysis (Reisinger *et al.*, 2013). Later studies also demonstrated how GATase structures have evolved specific interactions with synthase domains or other protomers to form higher-order structures (Plach *et al.*, 2017). How this evolution in CTPS took place presents the interesting question of how it became a single polypeptide and required tetramerization for full activity. Furthermore, CTPS is the only GATase identified to-date to be allosterically modulated by GTP. Since the interaction with GTP appears to be mediated by the GATase-synthase interface, and GTP happens to be structurally similar to the three other NTPs that bind to CTPS, evolution of this allostery may be tied to the evolution of the GATase-synthase association and 'molecular rheostatic' regulation of intracellular NTP pools.

REFERENCES

- Abeles, R. H., & Beck, W. S. (1967). The mechanism of action of cobamide coenzyme in the ribonucleotide reductase reaction. *Journal of Biological Chemistry*, 242(16), 3589-3593.
- Ali, J. A., Creek, D. J., Burgess, K., Allison, H. C., Field, M. C., Mäser, P., & De Koning, H. P. (2013). Pyrimidine salvage in *Trypanosoma brucei* bloodstream forms and the trypanocidal action of halogenated pyrimidines. *Molecular Pharmacology*, 83(2), 439-453. doi:10.1124/mol.112.082321
- Amaro, R. E., Myers, R. S., Davisson, V. J., & Luthey-Schulten, Z. A. (2005). Structural elements in IGP synthase exclude water to optimize ammonia transfer. *Biophysical Journal*, 89(1), 475-487.
- Anderson, P. M. (1983). CTP synthetase from *Escherichia coli*: an improved purification procedure and characterization of hysteretic and enzyme concentration effects on kinetic properties. *Biochemistry*, 22(13), 3285-3292. doi:10.1021/bi00282a038
- Aughey, G. N., & Liu, J. L. (2015). Metabolic regulation via enzyme filamentation. *Critical Reviews in Biochemistry and Molecular Biology*, 51(4), 282-293. doi:10.3109/10409238.2016.1172555
- Baker, C., Banson, J., Bollinger, J., Stubbe, J., Samano, V., Robins, M., Lippert, B., Jarvi, E., & Resvick, R. (1991). 2'-Deoxy-2'-methylencytidine and 2'-deoxy-2', 2'-difluorocytidine 5'-diphosphates: potent mechanism-based inhibitors of ribonucleotide reductase. *Journal of Medicinal Chemistry*, 34(6), 1879-1884. doi:10.1021/jm00110a019
- Bakovic, M., Fullerton, M. D., & Michel, V. (2007). Metabolic and molecular aspects of ethanolamine phospholipid biosynthesis: the role of CTP:phosphoethanolamine cytidyltransferase (Pcyt2). *Biochemistry and Cell Biology = Biochimie et Biologie Cellulaire*, 85(3), 283-300. doi:10.1139/o07-006
- Bapiro, T. E., Frese, K. K., Courtin, A., Bramhall, J. L., Madhu, B., Cook, N., Neesse, A., Griffiths, J. R., Tuveson, D. A., Jodrell, D. I., & Richards, F. M. (2014). Gemcitabine diphosphate choline is a major metabolite linked to the Kennedy pathway in pancreatic cancer models in vivo. *British Journal of Cancer*, 111(2), 318-325. doi:10.1038/bjc.2014.288
- Barry, R. M., Bitbol, A.-F. F., Lorestani, A., Charles, E. J., Habrian, C. H., Hansen, J. M., Li, H.-J. J., Baldwin, E. P., Wingreen, N. S., Kollman, J. M., & Gitai, Z. (2014). Large-scale filament formation inhibits the activity of CTP synthetase. *eLife*, 3. doi:10.7554/eLife.03638

- Bearne, S. L., Hekmat, O., & Macdonnell, J. E. (2001). Inhibition of Escherichia coli CTP synthase by glutamate gamma-semialdehyde and the role of the allosteric effector GTP in glutamine hydrolysis. *The Biochemical Journal*, 356(Pt 1), 223-232.
- Beatty, N. B., & Lane, M. D. (1983). The polymerization of acetyl-CoA carboxylase. *Journal of Biological Chemistry*, 258(21), 13051-13055.
- Berendsen, H. J. C., van der Spoel, D., & van Drunen, R. (1995). GROMACS: a message-passing parallel molecular dynamics implementation. *Computer Physics Communications*, 91(1-3), 43-56.
- Bergman, A. M., Pinedo, H. M., & Peters, G. J. (2002). Determinants of resistance to 2', 2'-difluorodeoxycytidine (gemcitabine). *Drug Resistance Updates*, 5(1), 19-33.
- Berne, B. J., & Pecora, R. (2000). *Dynamic light scattering: with applications to chemistry, biology, and physics*. New York, NY: Courier Corporation.
- Bloom, C. R., Kaarsholm, N. C., Ha, J., & Dunn, M. F. (1997). Half-site reactivity, negative cooperativity, and positive cooperativity: quantitative considerations of a plausible model. *Biochemistry*, 36(42), 12759-12765. doi:10.1021/bi970762f
- Burns, K. E., Xiang, Y., Kinsland, C. L., McLafferty, F. W., & Begley, T. P. (2005). Reconstitution and biochemical characterization of a new pyridoxal-5'-phosphate biosynthetic pathway. *Journal of the American Chemical Society*, 127(11), 3682-3683. doi:10.1021/ja042792t
- Carter, P., & Wells, J. A. (1987). Engineering enzyme specificity by "substrate-assisted catalysis". *Science*, 237(4813), 394-399. doi:10.1126/science.3299704
- Chang, C., Jeng, Y., Peng, M., Keppeke, G., Sung, L., & Liu, J. (2017). CTP synthase forms the cytoophidium in human hepatocellular carcinoma. *Experimental Cell Research*, 361(2), 292-299.
- Chang, C. C., Lin, W. C., Pai, L. M., Lee, H. S., Wu, S. C., Ding, S. T., Liu, J., & Sung, L. (2015). Cytoophidium assembly reflects upregulation of IMPDH activity. *Journal of Cell Science*, 128(19), 3550-3555. doi:10.1242/jcs.175265
- Chang, Y.-F. F., Martin, S. S., Baldwin, E. P., & Carman, G. M. (2007). Phosphorylation of human CTP synthetase 1 by protein kinase C: identification of Ser(462) and Thr(455) as major sites of phosphorylation. *Journal of Biological Chemistry*, 282(24), 17613-17622. doi:10.1074/jbc.M702799200

- Chang, Y. F., & Carman, G. M. (2008). CTP synthetase and its role in phospholipid synthesis in the yeast *Saccharomyces cerevisiae*. *Progress in Lipid Research*, 47(5), 333-339.
- Chen, K., Zhang, J., Tastan, Ö., Deussen, Z., Siswick, M., & Liu, J. (2011). Glutamine analogs promote cytoophidium assembly in human and *Drosophila* cells. *Journal of Genetics and Genomics*, 38(9), 391-402.
- Chittur, S. V., Klem, T. J., Shafer, C. M., & Davisson, V. J. (2001). Mechanism for acivicin inactivation of triad glutamine amidotransferases. *Biochemistry*, 40(4), 876-887. doi:10.1021/bi0014047
- Choi, M.-G. G., & Carman, G. M. (2007). Phosphorylation of human CTP synthetase 1 by protein kinase A: identification of Thr455 as a major site of phosphorylation. *Journal of Biological Chemistry*, 282(8), 5367-5377. doi:10.1074/jbc.M610993200
- Choi, M.-G. G., Park, T.-S. S., & Carman, G. M. (2003). Phosphorylation of *Saccharomyces cerevisiae* CTP synthetase at Ser424 by protein kinases A and C regulates phosphatidylcholine synthesis by the CDP-choline pathway. *Journal of Biological Chemistry*, 278(26), 23610-23616. doi:10.1074/jbc.M303337200
- Chuenchor, W., Doukov, T. I., Resto, M., Chang, A., & Gerratana, B. (2012). Regulation of the intersubunit ammonia tunnel in *Mycobacterium tuberculosis* glutamine-dependent NAD⁺ synthetase. *Biochemical Journal*, 443(2), 417-426.
- de Korte, D., Haverkort, W. A., Gennip, A. H., & Roos, D. (1985). Nucleotide profiles of normal human blood cells determined by high-performance liquid chromatography. *Analytical Biochemistry*, 147(1), 197-209.
- DeLano, W. L. (2002). Pymol: An open-source molecular graphics tool. *CCP4 Newsletter On Protein Crystallography*, 40, 82-92.
- Dowhan, W., Bogdanov, M., & Mileykovskaya, E. (2008). Functional roles of lipids in membranes *Biochemistry of Lipids, Lipoproteins and Membranes (Fifth Edition)*: Elsevier.
- Dunitz, J. D., & Taylor, R. (1997). Organic fluorine hardly ever accepts hydrogen bonds. *Chemistry-A European Journal*, 3(1), 89-98. doi:10.1002/chem.19970030115
- Edwards, J. O., & Pearson, R. G. (1962). The factors determining nucleophilic reactivities. *Journal of the American Chemical Society*, 84(1), 16-24. doi:10.1021/ja00860a005

- Eisenberg, H., & Tomkins, G. M. (1968). Molecular weight of the subunits, oligomeric and associated forms of bovine liver glutamate dehydrogenase. *Journal of Molecular Biology*, 31(1), 37-49.
- Endrizzi, J. A., Kim, H., Anderson, P. M., & Baldwin, E. P. (2004). Crystal structure of *Escherichia coli* cytidine triphosphate synthetase, a nucleotide-regulated glutamine amidotransferase/ATP-dependent amidoligase fusion protein and homologue of anticancer and antiparasitic drug targets. *Biochemistry*, 43(21), 6447-6463. doi:10.1021/bi0496945
- Endrizzi, J. A., Kim, H., Anderson, P. M., & Baldwin, E. P. (2005). Mechanisms of product feedback regulation and drug resistance in cytidine triphosphate synthetases from the structure of a CTP-inhibited complex. *Biochemistry*, 44(41), 13491-13499. doi:10.1021/bi051282o
- Fijolek, A., Hofer, A., & Thelander, L. (2007). Expression, purification, characterization, and in vivo targeting of trypanosome CTP synthetase for treatment of African sleeping sickness. *Journal of Biological Chemistry*, 282(16), 11858-11865. doi:10.1074/jbc.M611580200
- Finn, R. D., Bateman, A., Clements, J., Coghill, P., Eberhardt, R. Y., Eddy, S. R., Heger, A., Hetherington, K., Holm, L., Mistry, J., Sonnhammer, E. L., Tate, J., & Punta, M. (2000). The Pfam protein families database. *Nucleic Acids Research*, 28, D222-230.
- Frey, T. G., Eisenberg, D., & Eiserling, F. A. (1975). Glutamine synthetase forms three- and seven-stranded helical cables. *Proceedings of the National Academy of Sciences of the United States of America*, 72(9), 3402-3406.
- Geller, L. T., Barzily-Rokni, M., Danino, T., Jonas, O. H., Shental, N., Nejman, D., Gavert, N., Zwang, Y., Cooper, Z. A., Shee, K., Thaiss, C. A., Reuben, A., Livny, J., Avraham, R., Frederick, D. T., Ligorio, M., Chatman, K., Johnston, S. E., Mosher, C. M., Brandis, A., Fuks, G., Gurbatri, C., Gopalakrishnan, V., Kim, M., Hurd, M. W., Katz, M., Fleming, J., Maitra, A., Smith, D. A., Skalak, M., Bu, J., Michaud, M., Trauger, S. A., Barshack, I., Golan, T., Sandbank, J., Flaherty, K. T., Mandinova, A., Garrett, W. S., Thayer, S. P., Ferrone, C. R., Huttenhower, C., Bhatia, S. N., Gevers, D., Wargo, J. A., Golub, T. R., & Straussman, R. (2017). Potential role of intratumor bacteria in mediating tumor resistance to the chemotherapeutic drug gemcitabine. *Science (New York, N.Y.)*, 357(6356), 1156-1160. doi:10.1126/science.aah5043
- Good, N. E. (1960). Activation of the Hill reaction by amines. *Biochimica et Biophysica Acta*, 40, 502-517.

- Goto, M., Omi, R., Nakagawa, N., Miyahara, I., & Hirotsu, K. (2004). Crystal structures of CTP synthetase reveal ATP, UTP, and glutamine binding sites. *Structure (London, England : 1993)*, *12*(8), 1413-1423. doi:10.1016/j.str.2004.05.013
- Guex, N., & Peitsch, M. C. (1997). SWISS - MODEL and the Swiss - Pdb Viewer: an environment for comparative protein modeling. *Electrophoresis*, *18*(15), 2714-2723. doi:10.1002/elps.1150181505
- Hatse, S., De Clercq, E., & Balzarini, J. (1999). Role of antimetabolites of purine and pyrimidine nucleotide metabolism in tumor cell differentiation. *Biochemical Pharmacology*, *58*(4), 539-555.
- Heinemann, V., Schulz, L., Issels, R., & Plunkett, W. (1995). Gemcitabine: a modulator of intracellular nucleotide and deoxynucleotide metabolism. *Seminars in Oncology*, *22*(4 Suppl 11), 11-18.
- Heinemann, V., Xu, Y., Chubb, S., Sen, A., Hertel, L., Grindey, G., & Plunkett, W. (1992). Cellular elimination of 2', 2'-difluorodeoxycytidine 5'-triphosphate: a mechanism of self-potential. *Cancer Research*, *52*(3), 533-539.
- Higgins, M. J., Graves, P. R., & Graves, L. M. (2007). Regulation of human cytidine triphosphate synthetase 1 by glycogen synthase kinase 3. *Journal of Biological Chemistry*, *282*(40), 29493-29503. doi:10.1074/jbc.M703948200
- Higuchi, T., & Barnstein, C. H. (1956). Hydroxylammonium acetate as carbonyl reagent. *Analytical Chemistry*, *28*(6), 1022-1025. doi:10.1021/ac60114a028
- Hofer, A., Steverding, D., Chabes, A., Brun, R., & Thelander, L. (2001). Trypanosoma brucei CTP synthetase: a target for the treatment of African sleeping sickness. *Proceedings of the National Academy of Sciences of the United States of America*, *98*(11), 6412-6416. doi:10.1073/pnas.111139498
- Honeywell, R., Ruiz van Haperen, V., Veerman, G., Smid, K., & Peters, G. (2015). Inhibition of thymidylate synthase by 2', 2'-difluoro-2'-deoxycytidine (Gemcitabine) and its metabolite 2', 2'-difluoro-2'-deoxyuridine. *The International Journal of Biochemistry & Cell Biology*, *60*, 73-81.
- Hou, S., Wiczorek, S. A., Kaminski, T. S., Ziebac, N., Tabaka, M., Sorto, N., Foss, M., Shaw, J., Thanbichler, M., Weibel, D., Nieznanski, K., Holyst, R., & Garstecki, P. (2012). Characterization of Caulobacter crescentus FtsZ protein using dynamic light scattering. *Journal of Biological Chemistry*, *287*(28), 23878-23886.

- Huang, P., Chubb, S., Hertel, L. W., Grindey, G. B., & Plunkett, W. (1991). Action of 2', 2'-difluorodeoxycytidine on DNA synthesis. *Cancer Research*, 51(22), 6110-6117.
- Ingerson-Mahar, M., Briegel, A., Werner, J. N., Jensen, G. J., & Gitai, Z. (2010). The metabolic enzyme CTP synthase forms cytoskeletal filaments. *Nature Cell Biology*, 12(8), 739-746. doi:10.1038/ncb2087
- Iyengar, A., & Bearne, S. L. (2002). An assay for cytidine 5'-triphosphate synthetase glutaminase activity using high performance liquid chromatography. *Analytical Biochemistry*, 308(2), 396-400.
- Iyengar, A., & Bearne, S. L. (2003). Aspartate-107 and leucine-109 facilitate efficient coupling of glutamine hydrolysis to CTP synthesis by Escherichia coli CTP synthase. *The Biochemical journal*, 369(Pt 3), 497-507. doi:10.1042/BJ20021110
- Kammeyer, C. W., & Whitman, D. R. (1972). Quantum mechanical calculation of molecular radii. I. Hydrides of elements of periodic groups IV through VII. *The Journal of Chemical Physics*, 56(9), 4419-4421. doi:10.1063/1.1677883
- Kang, G. J., Cooney, D. A., Moyer, J. D., Kelley, J. A., Kim, H., Marquez, V. E., & Johns, D. G. (1989). Cyclopentenylcytosine triphosphate. Formation and inhibition of CTP synthetase. *Journal of Biological Chemistry*, 264(2), 713-718.
- Kassel, K. M., Au, D. R. a. R., Higgins, M. J., Hines, M., & Graves, L. M. (2010). Regulation of human cytidine triphosphate synthetase 2 by phosphorylation. *Journal of Biological Chemistry*, 285(44), 33727-33736. doi:10.1074/jbc.M110.178566
- Kaufman, E. R. (1984). Resistance to 5-fluorouracil associated with increased cytidine triphosphate levels in V79 Chinese hamster cells. *Cancer research*, 44(8), 3371-3376.
- Kaushik, M., Basu, K., Benoit, C., Cirtiu, C., Vali, H., & Moores, A. (2015). Cellulose Nanocrystals as Chiral Inducers: Enantioselective Catalysis and Transmission Electron Microscopy 3D Characterization. *Journal of the American Chemical Society*, 137(19), 6124-6127. doi:10.5772/60985
- Kemp, A. J., Lyons, S. D., & Christopherson, R. I. (1986). Effects of acivicin and dichloroallyl lawsone upon pyrimidine biosynthesis in mouse L1210 leukemia cells. *Journal of Biological Chemistry*, 261(32), 14891-14895.

- Kim, J., & Raushel, F. M. (2001). Allosteric Control of the Oligomerization of Carbamoyl Phosphate Synthetase from *Escherichia coli*. *Biochemistry*, *40*(37), 11030-11036. doi:10.1021/bi011121u
- Kim, J., & Raushel, F. M. (2004). Perforation of the tunnel wall in carbamoyl phosphate synthetase derails the passage of ammonia between sequential active sites. *Biochemistry*, *43*(18), 5334-5340. doi:10.1021/bi049945+
- Kim, S. Y., Kim, Y. W., Hegerl, R., Cyrklaff, M., & Kim, I. S. (2005). Novel type of enzyme multimerization enhances substrate affinity of oat β -glucosidase. *Journal of structural biology*, *150*(1), 1-10.
- Kizaki, H., Ohsaka, F., & Sakurada, T. (1982). Role of GTP in CTP synthetase from Ehrlich ascites tumor cells. *Biochemical and Biophysical Research Communications*, *108*(1), 286-291.
- Klem, T. J., & Davisson, V. J. (1993). Imidazole glycerol phosphate synthase: the glutamine amidotransferase in histidine biosynthesis. *Biochemistry*, *32*(19), 5177-5186. doi:10.1021/bi00070a029
- Konerding, D., James, T. L., Trump, E., Soto, A. M., Marky, L., & Gmeiner, W. (2002). NMR structure of a gemcitabine-substituted model Okazaki fragment. *Biochemistry*, *41*(3), 839-846. doi:10.1021/bi015678l
- Koshland, D. E., & Levitzki, A. (1974). 16. CTP Synthetase and Related Enzymes *The Enzymes* (Vol. 10, pp. 539-559): Elsevier.
- Koshland, D. E., Némethy, G., & Filmer, D. (1966). Comparison of experimental binding data and theoretical models in proteins containing subunits. *Biochemistry*, *5*(1), 365-385. doi:10.1021/bi00865a047
- Kroep, J., Loves, W., van der Wilt, C., Alvarez, E., Talianidis, I., Boven, E., Braakhuis, B., van Groeningen, C., Pinedo, H., & Peters, G. (2002). Pretreatment deoxycytidine kinase levels predict in vivo gemcitabine sensitivity. *Molecular Cancer Therapeutics*, *1*(6), 371-376.
- Kucuk, Z. Y., Zhang, K., Filipovich, L., & Bleasing, J. (2016). CTP synthase 1 deficiency in successfully transplanted siblings with combined immune deficiency and chronic active EBV infection. *Journal of Clinical Immunology*, *36*(8), 750-753. doi:10.1007/s10875-016-0332-z

- Langdon, W. Y., Hartley, J. W., Klinken, S. P., Ruscetti, S. K., & Morse, H. C. (1989). v-cbl, an oncogene from a dual-recombinant murine retrovirus that induces early B-lineage lymphomas. *Proceedings of the National Academy of Sciences of the United States of America*, 86(4), 1168-1172.
- Lauritsen, I., Willemoës, M., Jensen, K. F., Johansson, E., & Harris, P. (2011). Structure of the dimeric form of CTP synthase from *Sulfolobus solfataricus*. *Acta Crystallographica. Section F, Structural Biology Communications*, 67(2), 201-208.
- Levitcki, A., & Koshland, D. E. (1969). Negative cooperativity in regulatory enzymes. *Proceedings of the National Academy of Sciences of the United States of America*, 62(4), 1121-1128.
- Levitcki, A., & Koshland, D. E. (1971). Cytidine triphosphate synthetase. Covalent intermediates and mechanisms of action. *Biochemistry*, 10(18), 3365-3371. doi:10.1021/bi00794a008
- Levitcki, A., & Koshland, D. E. (1972a). Ligand-induced dimer-to-tetramer transformation in cytosine triphosphate synthetase. *Biochemistry*, 11(2), 247-253. doi:10.1021/bi00752a016
- Levitcki, A., & Koshland, D. E. (1972b). Role of an allosteric effector. Guanosine triphosphate activation in cytosine triphosphate synthetase. *Biochemistry*, 11(2), 241-246.
- Levitcki, A., Stallcup, W. B., & Koshland, D. E. (1971). Half-of-the-sites reactivity and the conformational states of cytidine triphosphate synthetase. *Biochemistry*, 10(18), 3371-3378.
- Lieberman, I. (1956). Enzymatic amination of uridine triphosphate to cytidine triphosphate. *Journal of Biological Chemistry*, 222(2), 765-775.
- Liu, G., Jin, C., & of Chemistry, J.-C. (2004). CMP-N-Acetylneuraminic Acid Synthetase from *Escherichia coli* K1 Is a Bifunctional Enzyme IDENTIFICATION OF MINIMAL CATALYTIC DOMAIN FOR SYNTHETASE ACTIVITY AND NOVEL FUNCTIONAL DOMAIN FOR PLATELET-ACTIVATING FACTOR ACETYLHYDROLASE ACTIVITY. *Journal of Biological Chemistry*. doi:10.1074/jbc.M400143200
- Liu, J. L. (2010). Intracellular compartmentation of CTP synthase in *Drosophila*. *Journal of Genetics and Genomics*, 37(5), 281-296.

- Long, C. W., & Pardee, A. B. (1967). Cytidine triphosphate synthetase of *Escherichia coli* B I. Purification and kinetics. *Journal of Biological Chemistry*, *242*(20), 4715-4721.
- Lopez, C. G., Saldanha, O., Huber, K., & Köster, S. (2016). Lateral association and elongation of vimentin intermediate filament proteins: A time-resolved light-scattering study. *Proceedings of the National Academy of Sciences of the United States of America*, *113*(40), 11152-11157.
- Lunn, F. A., & Bearne, S. L. (2004). Alternative substrates for wild - type and L109A *E. coli* CTP synthases. *The FEBS Journal*, *271*(21), 4204-4212. doi:10.1111/j.1432-1033.2004.04360.x
- Lynch, E. M., Hicks, D. R., Shepherd, M., Endrizzi, J. A., Maker, A., Hansen, J. M., Barry, R. M., Gitai, Z., Baldwin, E. P., & Kollman, J. M. (2017). Human CTP synthase filament structure reveals the active enzyme conformation. *Nature Structural & Molecular Biology*, *24*(6), 507-514. doi:10.1038/nsmb.3407
- MacDonnell, J. E., Lunn, F. A., & Bearne, S. L. (2004). Inhibition of *E. coli* CTP synthase by the “positive” allosteric effector GTP. *Biochimica et Biophysica Acta*, *1699*(1-2), 213-220.
- Martin, E., Palmic, N., Sanquer, S., Lenoir, C., Hauck, F., Mongellaz, C., Fabrega, S., Nitschké, P., Esposti, M. D., Schwartzentruber, J., Taylor, N., Majewski, J., Jabado, N., Wynn, R. F., Picard, C., Fischer, A., Arkwright, P. D., & Latour, S. (2014). CTP synthase 1 deficiency in humans reveals its central role in lymphocyte proliferation. *Nature*, *510*(7504), 288-292. doi:10.1038/nature13386
- Massiere, F., & Badet-Denisot, M. A. (1998). The mechanism of glutamine-dependent amidotransferases. *Cellular and Molecular Life Sciences ...*, *54*(3), 205-222. doi:10.1007/s000180050145
- McCluskey, G. D., Mohamady, S., Taylor, S. D., & Bearne, S. L. (2016). Exploring the Potent Inhibition of CTP Synthase by Gemcitabine-5'-Triphosphate. *ChemBioChem*, *17*(23), 2240-2249. doi:10.1002/cbic.201600405
- Mini, E., Nobili, S., Caciagli, B., Landini, I., & Mazzei, T. (2006). Cellular pharmacology of gemcitabine. *Annals of Oncology*, *17*(5), 7-12. doi:10.1093/annonc/mdj941

- Mori, G., Chiarelli, L. R., Esposito, M., Makarov, V., Bellinzoni, M., Hartkoorn, R. C., Degiacomi, G., Boldrin, F., Ekins, S., de Jesus Lopes Ribeiro, A. L., Marino, L. B., Centárová, I., Svetlíková, Z., Blaško, J., Kazakova, E., Lepioshkin, A., Barilone, N., Zanoni, G., Porta, A., Fondi, M., Fani, R., Baulard, A. R., Mikušová, K., Alzari, P. M., Manganelli, R., de Carvalho, L. P., Riccardi, G., Cole, S. T., & Pasca, M. R. (2015). Thiophenecarboxamide derivatives activated by EthA kill Mycobacterium tuberculosis by inhibiting the CTP synthetase PyrG. *Chemistry & Biology*, 22(7), 917-927.
- Mouilleron, S., Badet-Denisot, M. A., & Golinelli-Pimpaneau, B. (2006). Glutamine binding opens the ammonia channel and activates glucosamine-6P synthase. *Journal of Biological Chemistry*, 281(7), 4404-4412.
- Mullins, L. S., & Raushel, F. M. (1999). Channeling of ammonia through the intermolecular tunnel contained within carbamoyl phosphate synthetase. *Journal of the American Chemical Society*, 121(15), 2803-2804. doi:10.1021/ja990063l
- Myers, R. S., Amaro, R. E., Luthey-Schulten, Z. A., & Davisson, V. (2005). Reaction coupling through interdomain contacts in imidazole glycerol phosphate synthase. *Biochemistry*, 44(36), 11974-11985. doi:10.1021/bi050706b
- Noree, C., Monfort, E., Shiau, A. K., & Wilhelm, J. E. (2014). Common regulatory control of CTP synthase enzyme activity and filament formation. *Molecular Biology of the Cell*, 25(15), 2282-2290. doi:10.1091/mbc.E14-04-0912
- Noree, C., Sato, B. K., Broyer, R. M., & Wilhelm, J. E. (2010). Identification of novel filament-forming proteins in *Saccharomyces cerevisiae* and *Drosophila melanogaster*. *The Journal of Cell Biology*, 190(4), 541-551. doi:10.1083/jcb.201003001
- Oliveira de Souza, J., Dawson, A., & Hunter, W. N. (2017). An Improved Model of the *Trypanosoma brucei* CTP Synthetase Glutaminase Domain-Acivicin Complex. *ChemMedChem*, 12(8), 577-579. doi:10.1002/cmdc.201700118
- Oliver, J. C., Gudihal, R., Burgner, J. W., Pedley, A. M., Zwierko, A., Davisson, V., & Linger, R. (2014). Conformational changes involving ammonia tunnel formation and allosteric control in GMP synthetase. *Archives of Biochemistry and Biophysics*, 545, 22-32.
- Ostrander, D. B., O'Brien, D. J., Gorman, J. A., & Carman, G. M. (1998). Effect of CTP synthetase regulation by CTP on phospholipid synthesis in *Saccharomyces cerevisiae*. *Journal of Biological Chemistry*, 273(30), 18992-19001.

- Pappas, A., Yang, W. L., Park, T. S., & of Chemistry, C.-G. M. (1998). Nucleotide-dependent tetramerization of CTP synthetase from *Saccharomyces cerevisiae*. *Journal of Biological Chemistry*. doi:10.1074/jbc.273.26.15954
- Park, T. S., O'Brien, D. J., & Carman, G. M. (2003). Phosphorylation of CTP synthetase on Ser36, Ser330, Ser354, and Ser454 regulates the levels of CTP and phosphatidylcholine synthesis in *Saccharomyces cerevisiae*. *Journal of Biological Chemistry*, 278(23), 20785-20794. doi:10.1074/jbc.M301394200
- Park, T. S., Ostrander, D. B., Pappas, A., & Carman, G. M. (1999). Identification of Ser424 as the protein kinase A phosphorylation site in CTP synthetase from *Saccharomyces cerevisiae*. *Biochemistry*, 38(27), 8839-8848. doi:10.1021/bi990784x
- Pence, H. E., & Williams, A. (2010). ChemSpider: an online chemical information resource. *ChemSpider: an online chemical information resource*. doi:10.1021/ed100697w
- Petrek, M., Otyepka, M., Banás, P., Kosinová, P., Koca, J., & Damborský, J. (2006). CAVER: a new tool to explore routes from protein clefts, pockets and cavities. *BMC Bioinformatics*, 7(316), 1-9.
- Petrovska, I., Nüske, E., Munder, M. C., Kulasegaran, G., Malinovska, L., Kroschwald, S., Richter, D., Fahmy, K., Gibson, K., Verbavatz, J., & Alberti, S. (2014). Filament formation by metabolic enzymes is a specific adaptation to an advanced state of cellular starvation. *eLife*, 3, e02409.
- Plach, M. G., Semmelmann, F., Busch, F., Busch, M., Heizinger, L., Wysocki, V. H., Merkl, R., & Sterner, R. (2017). Evolutionary diversification of protein-protein interactions by interface add-ons. *Proceedings of the National Academy of Sciences of the United States of America*, 114(40), E8333-E8342. doi:10.1073/pnas.1707335114
- Plunkett, W., Huang, P., Searcy, C. E., & Gandhi, V. (1996). Gemcitabine: preclinical pharmacology and mechanisms of action. *Seminars in Oncology*, 23(5 Suppl 10), 3-15.
- Politi, P. M., Xie, F., Dahut, W., Ford, H., & chemotherapy ..., K.-J. A. (1995). Phase I clinical trial of continuous infusion cyclopentenyl cytosine. *Cancer Chemotherapy and Pharmacology*, 36(6), 513-23.
- Raushel, F. M., Thoden, J. B., & Holden, H. M. (1999). The amidotransferase family of enzymes: molecular machines for the production and delivery of ammonia. *Biochemistry*, 38(25), 7891-7899. doi:10.1021/bi990871p

- Raushel, F. M., Thoden, J. B., & Holden, H. M. (2003). Enzymes with molecular tunnels. *Accounts of Chemical Research*, 36(7), 539-548. doi:10.1021/ar020047k
- Reisinger, B., Sperl, J., Holinski, A., Schmid, V., Rajendran, C., Carstensen, L., Schlee, S., Blanquart, S., Merkl, R., & Sterner, R. (2013). Evidence for the existence of elaborate enzyme complexes in the Paleoarchean era. *Journal of the American Chemical Society*, 136(1), 122-129. doi:10.1021/ja4115677
- Richardson, K. A., Vega, T. P., Richardson, F. C., Moore, C., Rohloff, J., Tomkinson, B., Bendele, R., & Kuchta, R. (2004). Polymerization of the triphosphates of AraC, 2', 2'-difluorodeoxycytidine (dFdC) and OSI-7836 (T-araC) by human DNA polymerase α and DNA primase. *Biochemical Pharmacology*, 68(12), 2337-2346.
- Rishavy, M. A., Cleland, W. W., & Lusty, C. J. (2000). ^{15}N isotope effects in glutamine hydrolysis catalyzed by carbamyl phosphate synthetase: evidence for a tetrahedral intermediate in the mechanism. *Biochemistry*, 39(24), 7309-7315.
- Robertson, J. G. (1995). Determination of subunit dissociation constants in native and inactivated CTP synthetase by sedimentation equilibrium. *Biochemistry*, 32(22), 7533-7541. doi:10.1021/bi00022a029
- Rudin, D., Li, L., Niu, N., Kalari, K. R., Gilbert, J. A., Ames, M., & Wang, L. (2011). Gemcitabine cytotoxicity: interaction of efflux and deamination. *Journal of Drug Metabolism and Toxicology*, 2(107), 1-10.
- Ruiz van Haperen, V., Veerman, G., Vermorken, J., & Peters, G. J. (1993). 2', 2'-Difluoro-deoxycytidine (gemcitabine) incorporation into RNA and DNA of tumour cell lines. *Biochemical Pharmacology*, 46(4), 762-766.
- Sakamoto, K., Ishibashi, Y., Adachi, R., Matsumoto, S., Oki, H., Kamada, Y., Sogabe, S., Zama, Y., Sakamoto, J., & Tani, A. (2017). Identification of cytidine-5-triphosphate synthase1-selective inhibitory peptide from random peptide library displayed on T7 phage. *Peptides*, 94, 56-63.
- Sambrook, J., & Russell, D. W. (2006). Preparation and Transformation of Competent E. coli Using Calcium Chloride. *CSH protocols*, 2006(1). doi:10.1101/pdb.prot3932
- Scheit, K. H., & Linke, H. J. (1982). Substrate specificity of CTP synthetase from Escherichia coli. *The FEBS Journal*, 126(1), 57-60. doi:10.1111/j.1432-1033.1982.tb06745.x

- Schimmel, K. J. M., Gelderblom, H., & Guchelaar, H. (2007). Cyclopentenyl cytosine (CPEC): an overview of its in vitro and in vivo activity. *Current Cancer Drug Targets*, 7(5), 504-509.
- Seils, J., & Pecora, R. (1995). Dynamics of a 2311 base pair superhelical DNA in dilute and semidilute solutions. *Macromolecules*, 28(3), 661-673. doi:10.1021/ma00107a001
- Seydoux, F., Malhotra, O. P., & Bernhard, S. A. (1974). Half-site reactivity. *CRC Critical Reviews in Biochemistry*, 2(2), 227-257.
- Shukla, S. K., Purohit, V., Mehla, K., Gunda, V., Chaika, N. V., Vernucci, E., King, R. J., Abrego, J., Goode, G. D., Dasgupta, A., Illies, A. L., Gebregiworgis, T., Dai, B., Augustine, J. J., Murthy, D., Attri, K. S., Mashadova, O., Grandgenett, P. M., Powers, R., Ly, Q. P., Lazenby, A. J., Grem, J. L., Yu, F., Matés, J. M. M., Asara, J. M., Kim, J.-W. W., Hankins, J. H., Weekes, C., Hollingsworth, M. A., Serkova, N. J., Sasson, A. R., Fleming, J. B., Oliveto, J. M., Lyssiotis, C. A., Cantley, L. C., Berim, L., & Singh, P. K. (2017). MUC1 and HIF-1alpha signaling crosstalk induces anabolic glucose metabolism to impart gemcitabine resistance to pancreatic cancer. *Cancer Cell*, 32(1), 71-87.
- Sievers, F., & Higgins, D. G. (2014). Clustal omega. *Current Protocols in Bioinformatics*, 48, 1-16. doi:10.1002/0471250953.bi0313s48
- Snapp, E. L., Hegde, R. S., Francolini, M., Lombardo, F. J., Colombo, S., Pedrazzini, E., Borgese, N., & Lippincott-Schwartz, J. (2003). Formation of stacked ER cisternae by low affinity protein interactions. *Journal of Cell Biology*, 163(2), 257-269.
- Steeves, C. H., & Bearne, S. L. (2011). Activation and inhibition of CTP synthase from *Trypanosoma brucei*, the causative agent of African sleeping sickness. *Bioorganic & Medicinal Chemistry Letters*, 21(18), 5188-5190. doi:10.1016/j.bmcl.2011.07.054
- Strochlic, T. I., Stavrides, K. P., Thomas, S. V., Nicolas, E., O'Reilly, A. M., & Peterson, J. R. (2014). Ack kinase regulates CTP synthase filaments during *Drosophila* oogenesis. *EMBO Reports*, 15(11), 1184-1191. doi:10.15252/embr.201438688
- Sundler, R., & Akesson, B. (1975). Regulation of phospholipid biosynthesis in isolated rat hepatocytes. Effect of different substrates. *Journal of Biological Chemistry*, 250(9), 3359-3367.

- Tamborini, L., Pinto, A., Smith, T. K., Major, L. L., Iannuzzi, M. C., Cosconati, S., Marinelli, L., Novellino, E., Lo Presti, L., Wong, P. E., Barrett, M. P., De Micheli, C., & Conti, P. (2012). Synthesis and biological evaluation of CTP synthetase inhibitors as potential agents for the treatment of African trypanosomiasis. *ChemMedChem*, 7(9), 1623-1634. doi:10.1002/cmdc.201200304
- Tanwar, A. S., Sindhikara, D. J., Hirata, F., & Anand, R. (2015). Determination of the Formylglycinamide Ribonucleotide Amidotransferase Ammonia Pathway by Combining 3D-RISM Theory with Experiment. *ACS Chemical Biology*, 10(3), 698-704. doi:10.1021/cb501015r
- Taylor, S. D., Lunn, F. A., & Bearne, S. L. (2008). Ground State, Intermediate, and Multivalent Nucleotide Analogue Inhibitors of Cytidine 5' - Triphosphate Synthase. *ChemMedChem*, 3(12), 1853-1857. doi:10.1002/cmdc.200800236
- Tepljakov, A., Obmolova, G., Badet, B., & Badet-Denisot, M. A. (2001). Channeling of ammonia in glucosamine-6-phosphate synthase. *Journal of Molecular Biology*, 313(5), 1093-1102.
- Thibaudeau, C., Plavec, J., & Chattopadhyaya, J. (1998). A new generalized karplus-type equation relating vicinal proton-fluorine coupling constants to H-C-F torsion angles. *The Journal of Organic Chemistry*, 63(15), 4967-4984. doi:10.1021/jo980144k
- Toney, M. D., & Kirsch, J. F. (1989). Direct Brønsted analysis of the restoration of activity to a mutant enzyme by exogenous amines. *Science*, 243(4897), 1485-1488. doi:10.1126/science.2538921
- Toschi, L., Finocchiaro, G., Bartolini, S., Gioia, V., & Cappuzzo, F. (2005). Role of gemcitabine in cancer therapy. *Future Oncology*, 1(1), 7-17. doi:10.1517/14796694.1.1.7
- Tracy, M. A., & Pecora, R. (1992). Dynamics of rigid and semirigid rodlike polymers. *Annual Review of Physical Chemistry*, 43, 525-557.
- Trott, O., & Olson, A. J. (2010). AutoDock Vina: improving the speed and accuracy of docking with a new scoring function, efficient optimization, and multithreading. *Journal of Computational Chemistry*, 31(2), 455-461. doi:10.1002/jcc.21334
- Trück, J., Kelly, D. F., Taylor, J. M., Kienzler, A. K., Lester, T., Seller, A., Pollard, A., & Patel, S. (2016). Variable phenotype and discrete alterations of immune phenotypes in CTP synthase 1 deficiency: Report of 2 siblings. *The Journal of Allergy and Clinical Immunology*, 138(6), 1722-1725.

- Veltkamp, S., Pluim, D., van Eijndhoven, M., Bolijn, M., Ong, F., Govindarajan, R., Unadkat, J., Beijnen, J., & Schellens, J. (2008). New insights into the pharmacology and cytotoxicity of gemcitabine and 2', 2'-difluorodeoxyuridine. *Molecular Cancer Therapeutics*, 7(8), 2415-2425. doi:10.1158/1535-7163.MCT-08-0137
- Veltkamp, S. A., Jansen, R. S., Callies, S., Pluim, D., Visseren-Grul, C. M., Rosing, H., & Kloeker-Rhoades, S., Andre, V. A., Beijnen, J. H., Slapak, C. A., Schellens, J. H. (2008). Oral administration of gemcitabine in patients with refractory tumors: a clinical and pharmacologic study. *Clinical Cancer Research*. doi:10.1158/1078-0432.CCR-07-4521
- Veltkamp, S. A., Pluim, D., van Eijndhoven, M., Bolijn, M., Ong, F., Govindarajan, R., Unadkat, J., Beijnen, J., & Schellens, J. (2008). New insights into the pharmacology and cytotoxicity of gemcitabine and 2', 2'-difluorodeoxyuridine. *Molecular Cancer Therapeutics*, 7(8), 2415-2425. doi:10.1158/1535-7163.MCT-08-0137
- Verschurr, A. C. (2007). Cytidine triphosphate synthetase (CTP synthetase) as a druggable target in cancer. *Drugs Future*, 32(12), 1071.
- Verschuur, A. C., Van Gennip, A. H., Brinkman, J., Voûte, P., & van Kuilenburg, A. (2000). Cyclopentenyl cytosine induces apoptosis and secondary necrosis in a T-lymphoblastic leukemic cell-line. *Advances in Experimental Medicine and Biology*, 486, 319-325.
- von der Saal, W., Anderson, P. M., & Villafranca, J. J. (1985). Mechanistic investigations of Escherichia coli cytidine-5'-triphosphate synthetase. Detection of an intermediate by positional isotope exchange experiments. *Journal of Biological Chemistry*, 260(28), 14993-14997.
- Wang, J., Lohman, G., & Stubbe, J. (2007). Enhanced subunit interactions with gemcitabine-5'-diphosphate inhibit ribonucleotide reductases. *Proceedings of the National Academy of Sciences of the United States of America*, 104(36), 14324-14329. doi:10.1073/pnas.0706803104
- Wang, P., Lin, W., Tsai, Y., Cheng, M., Lin, Y.-H. H., Tseng, S., Chakraborty, A., & Pai, L. (2015). Regulation of CTP Synthase Filament Formation During DNA Endoreplication in Drosophila. *Genetics*, 201(4), 1511-1523. doi:10.1534/genetics.115.180737
- Weng, M., Makaroff, C. A., & Zalkin, H. (1986). Nucleotide sequence of Escherichia coli pyrG encoding CTP synthetase. *Journal of Biological Chemistry*, 261(12), 5568-5574.

- Weng, M. L., & Zalkin, H. (1987). Structural role for a conserved region in the CTP synthetase glutamine amide transfer domain. *Journal of Bacteriology*, *169*(7), 2023-2028. doi:10.1128/jb.169.7.3023-3028.1987
- Wheeler, T. J., Clements, J., & Finn, R. D. (2014). Skylign: a tool for creating informative, interactive logos representing sequence alignments and profile hidden Markov models. *BMC Bioinformatics*, *15*, 7. doi:10.1186/1471-2105-15-7
- Whelan, J., Phear, G., Yamauchi, M., & Meuth, M. (1993). Clustered base substitutions in CTP synthetase conferring drug resistance in Chinese hamster ovary cells. *Nature Genetics*, *3*(4), 317-322. doi:10.1038/ng0493-317
- Whelan, J., Smith, T., Phear, G., Rohatiner, A., Lister, A., & Meuth, M. (1994). Resistance to cytosine arabinoside in acute leukemia: the significance of mutations in CTP synthetase. *Leukemia*, *8*(2), 264-265.
- Wiberg, K. B., & Rablen, P. R. (1993). Origin of the stability of carbon tetrafluoride: negative hyperconjugation reexamined. *Journal of the American Chemical Society*, *115*, 614-625. doi:10.1021/ja00055a034
- Wilkins, M., Gasteiger, E., Bairoch, A., Sanchez, J., Williams, K., Appel, R., & Hochstrasser, D. (2005). Protein identification and analysis tools on the ExPASy server. *Methods in Molecular Biology*, *112*, 521-552. doi:10.1385/1-59259-890-0:571
- Willemoës, M. (2004). Competition between ammonia derived from internal glutamine hydrolysis and hydroxylamine present in the solution for incorporation into UTP as catalysed by *Lactococcus lactis* CTP synthase. *Archives of Biochemistry and Biophysics*, *424*(1), 105-111. doi:10.1016/j.abb.2004.01.018
- Willemoës, M., & Larsen, S. (2003). Substrate inhibition of *Lactococcus lactis* cytidine 5'-triphosphate synthase by ammonium chloride is enhanced by salt-dependent tetramer dissociation. *Archives of Biochemistry and Biophysics*, *413*(1), 17-22.
- Willemoës, M., & Sigurskjold, B. W. (2002). Steady-state kinetics of the glutaminase reaction of CTP synthase from *Lactococcus lactis*. The role of the allosteric activator GTP incoupling between glutamine hydrolysis and CTP synthesis. *European Journal of Biochemistry*, *269*(19), 4772-4779.
- Williams, J. C., Kizaki, H., Weber, G., & Morris, H. P. (1978). Increased CTP synthetase activity in cancer cells. *Nature*, *271*(5640), 71-73. doi:10.1038/271071a0

- Yang, W. L., & Carman, G.M. (1996). Phosphorylation and regulation of CTP synthetase from *Saccharomyces cerevisiae* by protein kinase A. *Journal of Biological Chemistry*, 271(46), 28777-28783.
- Yang, W. L., Bruno, M.E., & Carman, G.M. (1996). Regulation of yeast CTP synthetase activity by protein kinase C. *Journal of Biological Chemistry*, 271(19), 11113-11119. doi:10.1074/jbc.271.19.11113
- Yang, W. L., McDonough, V. M., Ozier-Kalogeropoulos, O., Adeline, M. T., Flocco, M. T., & Carman, G. M. (1994). Purification and characterization of CTP synthetase, the product of the URA7 gene in *Saccharomyces cerevisiae*. *Biochemistry*, 33(35), 10785-10793.
- Zalkin, H. (1985). CTP synthetase. *Methods in Enzymology*, 113, 282-287.
- Zalkin, H. (1993). The amidotransferases. *Advances in Enzymology - and Related Areas of Molecular Biology*, 66, 203-309.
- Zalkin, H., Argos, P., Narayana, S. V., Tiedeman, A. A., & Smith, J. (1985). Identification of a trpG-related glutamine amide transfer domain in *Escherichia coli* GMP synthetase. *Journal of Biological Chemistry*, 260(6), 3350-3354.
- Zalkin, H., & Smith, J. L. (1998). Enzymes utilizing glutamine as an amide donor. *Advances in Enzymology - and Related Areas of Molecular Biology*, 72, 87-144.
- Zhu, M., Sun, W., Wang, Y., Meng, J., Zhang, D., Guo, T., Ouyang, P., Ying, H., & Xie, J. (2014). Engineered cytidine triphosphate synthetase with reduced product inhibition. *Protein Engineering, Design & Selection*, 27(7), 225-233.

APPENDIX A

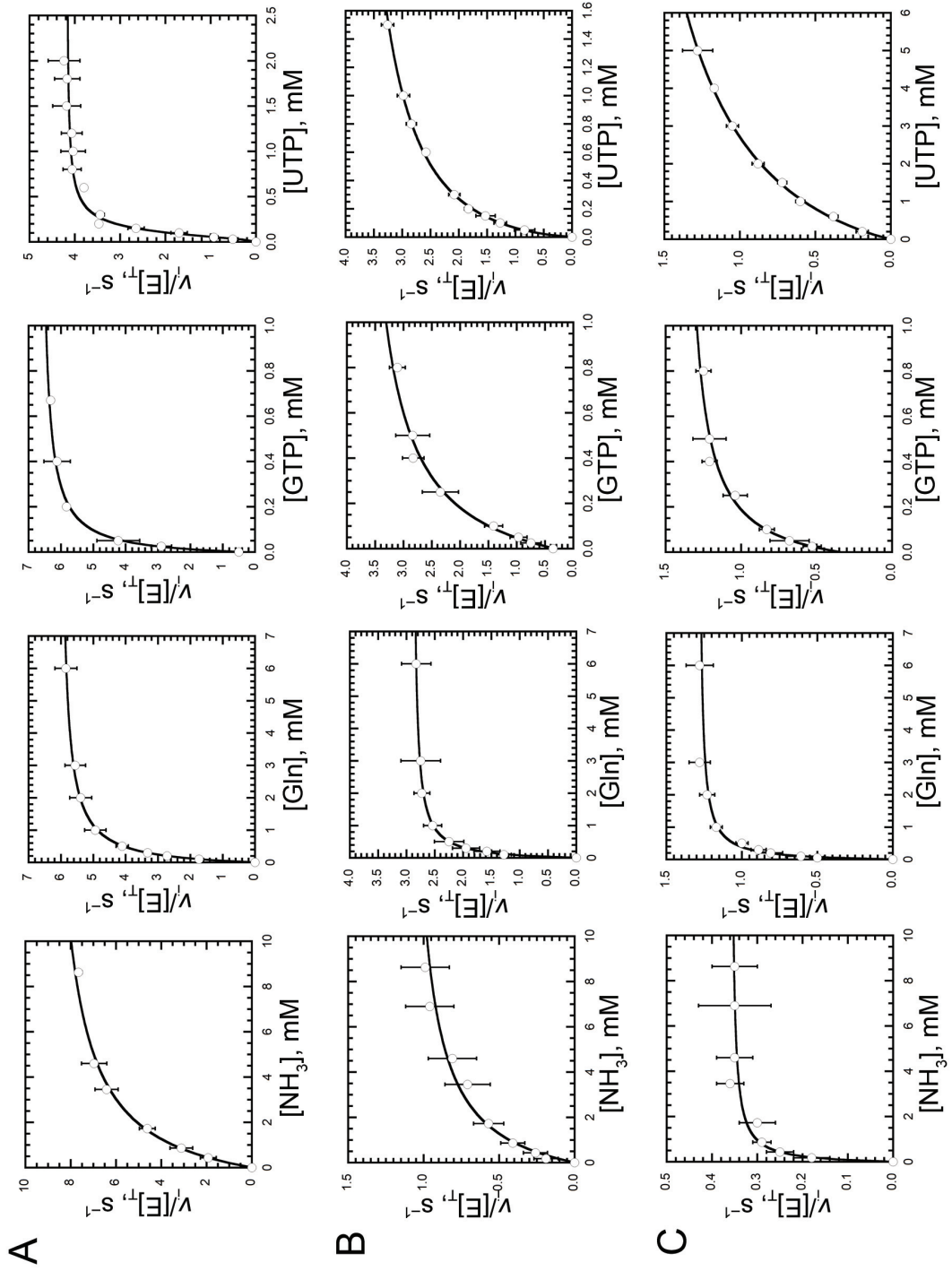


Figure A.1. Steady-state kinetic characterization of wild-type (A), E149D (B), and E149Q (C) *EcCTPS* variants. The kinetic parameters for NH₃-, glutamine-, GTP-, and UTP-dependent CTP production were measured for each indicated *EcCTPS* variant with saturating concentrations of ligands, except where indicated (Table 2.2). These data represent the average of three independent experiments \pm SD and are fitted to eqn. 2.1, 2.2, and 2.3, as stated in **section 2.4**. Values for K_m , k_{cat} , k_{cat}/K_m , $[S]_{0.5}$, $V_{max}/[E]_T$, n , K_A , k_{act} and k_o are given in Table 3.2.

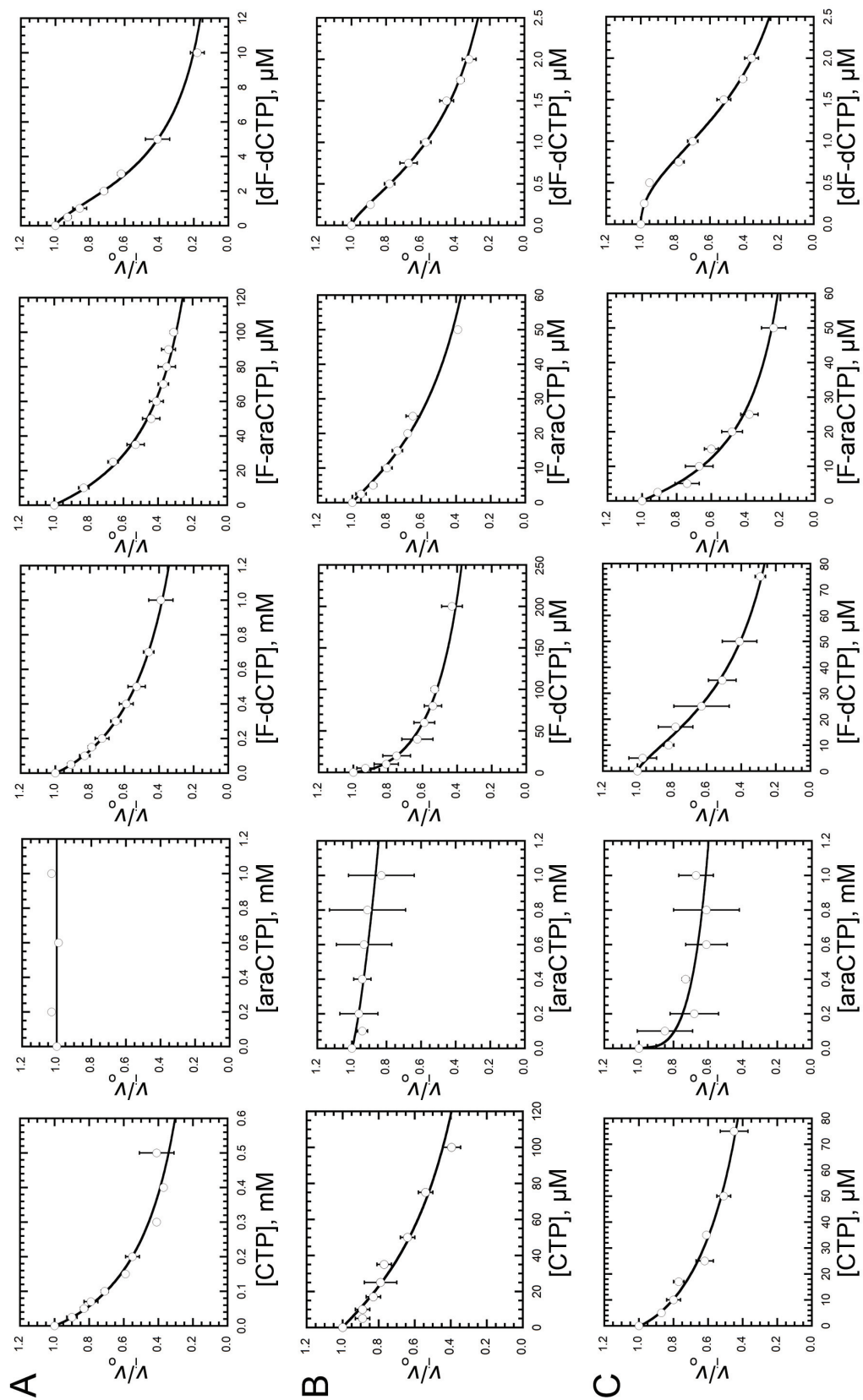


Figure A.2. Inhibition of wild-type and E149Q variants by CTP and analogues. Inhibition of wild-type was measured at [UTP] = 0.20 mM (**A**) and 0.05 mM (**B**), and inhibition of the E149Q variant was measured at [UTP] = 0.05 mM (**C**). Values of v_i/v_0 were determined from the observed velocity in the presence of the inhibitor (v_i) relative to the velocity in the absence of inhibitor (v_0). Data are the averages from three independent experiments \pm SD fitted with eqn. 2.4 as described in **section 2.6**. IC_{50} values are given in table 3.3

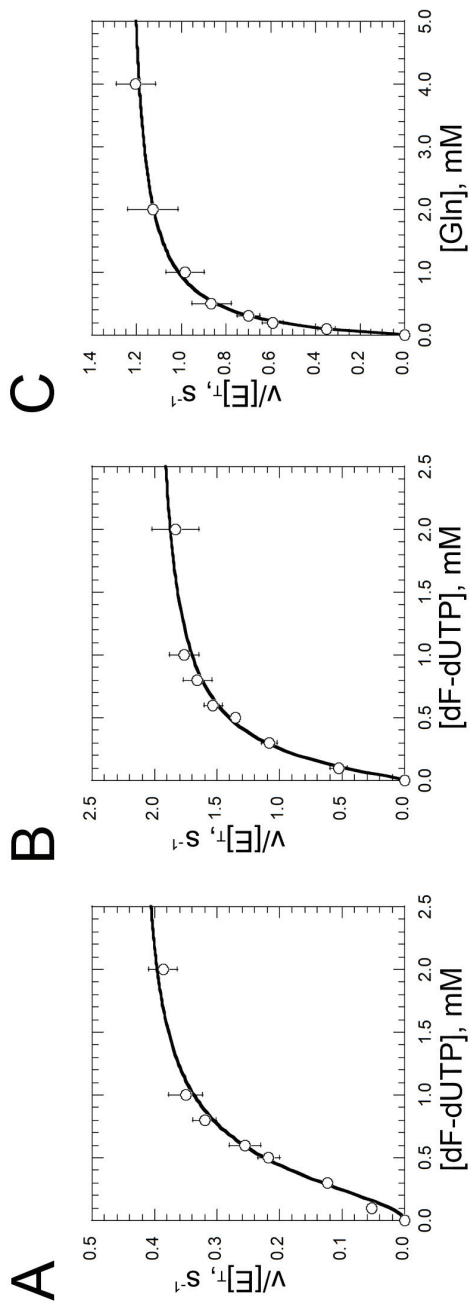


Figure A.3. Steady-state kinetic characterization of the E149D *Ec*CTPS-catalyzed conversion of dF-dUTP to dF-dCTP. The E149D variant (20 – 30 $\mu\text{g}/\text{mL}$) was incubated with ATP (1.0 mM) and varying concentrations of dF-dUTP (0.1 – 2.0 mM) prior to initiating the reaction with either 150 mM NH_4Cl (**A**) or 6.0 mM Gln (**B**). Determination of the Gln-dependent kinetic parameters (**C**) was conducted using a saturating concentration of ATP (1.0 mM), dF-dUTP (1.0 mM), GTP (0.25 mM) and varying concentrations of Gln (0.1 – 4.0 mM). GTP (1.0 mM) was present in all reactions in which Gln was the source of NH_3 . For NH_4Cl -dependent kinetics, the ionic strength of the reaction was maintained at 150 mM using KCl. The data are the average initial velocities (\pm SD) from three independent experiments. The average data from three independent experiments were plotted (\pm SD) and fitted to eqns. 2.3 and 2.1, as stated in **section 2.4**. Values of $[\text{S}]_{0.5}$, $V_{\text{max}}/[\text{E}]_{\text{T}}$, n , K_{m} , k_{cat} , and $k_{\text{cat}}/K_{\text{m}}$, are given in Table 3.4.

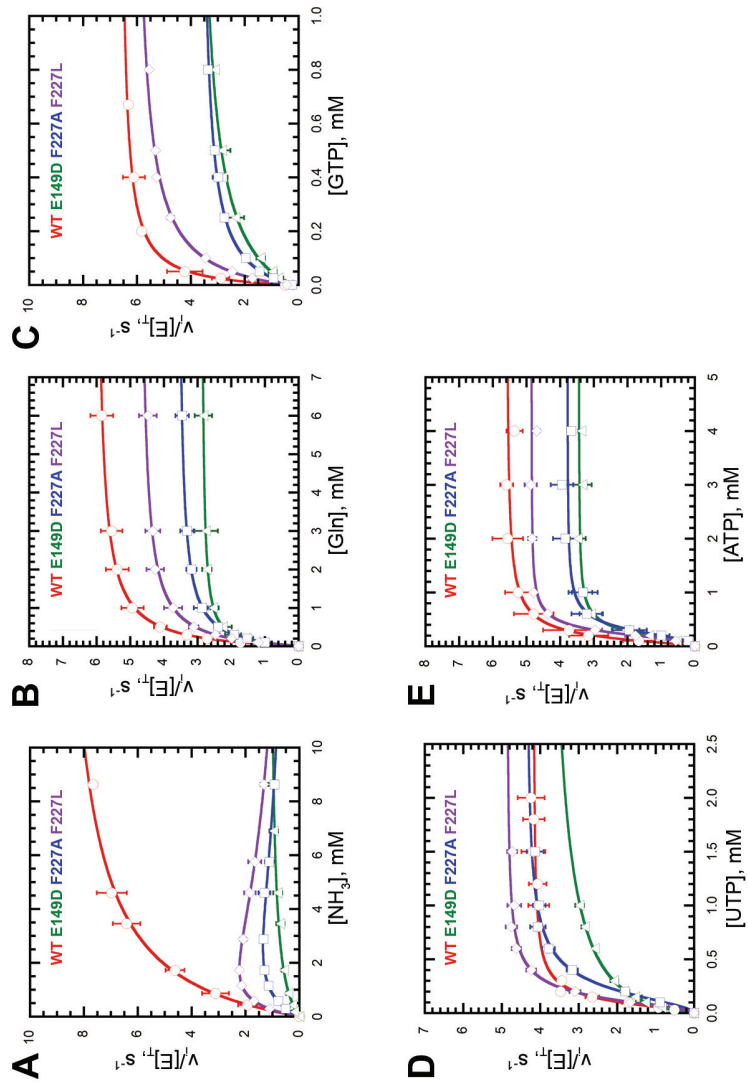


Figure A.4. Steady-state kinetic characterization of wild-type (WT, red), E149D (green), F227A (blue), and F227L (violet) *Ec*CTPS variants. The rate of NH₃- (A), glutamine- (B), GTP- (C), UTP- (D), and ATP- (E) dependent CTP formation was measured for wild-type *Ec*CTPS

in assay buffer with saturating concentrations of ATP (1.0 mM), UTP (1.0 mM), GTP (0.25 mM), and glutamine (6.0 mM), unless stated

otherwise. These data represent the average of three independent experiments \pm SD. Data were fitted to eqns. 2.1, 2.2, 2.3, and 4.7 as stated in **sections 2.4** and **4.2.6**. Values of K_m , k_{cat} , k_{cat}/K_m , K' , $[S]_{0.5}$, $V_{max}/[E]_T$, n , K_A , k_{act} and k_o are given in Table 4.2.

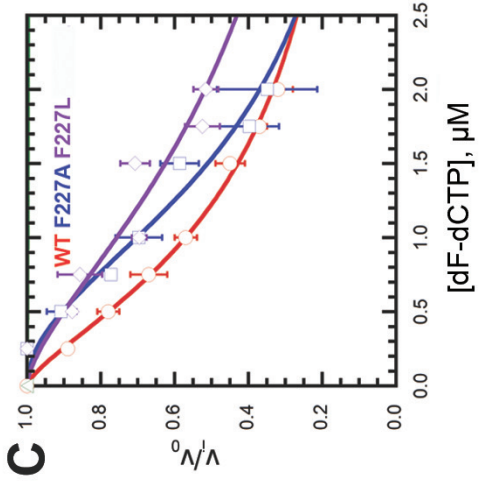
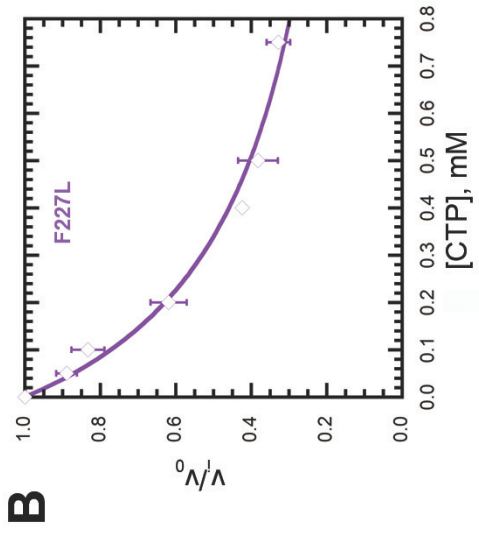
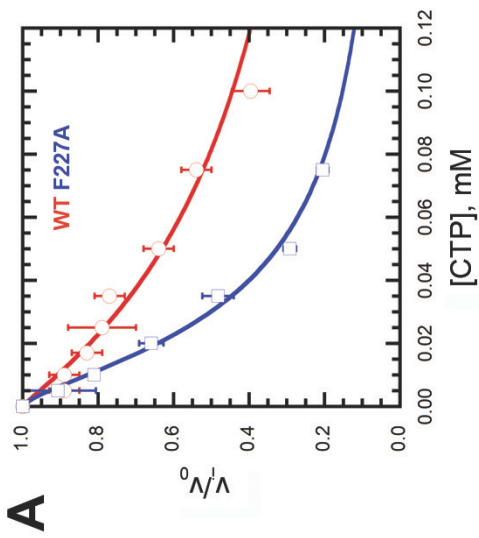


Figure A.5. Inhibition of wild-type (WT, red), F227A (blue), and F227L (violet) *Ec*CTPS variants by CTP (**A** and **B**) and dF-dCTP (**C**). Values of v_i/v_o were determined from the observed velocity in the presence of the inhibitor (v_i) relative to the velocity obtained in the absence of inhibitor (v_o). The average data from three independent experiments were plotted (\pm SD) and fitted to eqn. 2.4 as stated in **section 2.6**. Corresponding IC_{50} and n values are given in Table 4.3 and the apparent lack of inhibition by CTP and dF-dCTP is shown in Figure 3.6.

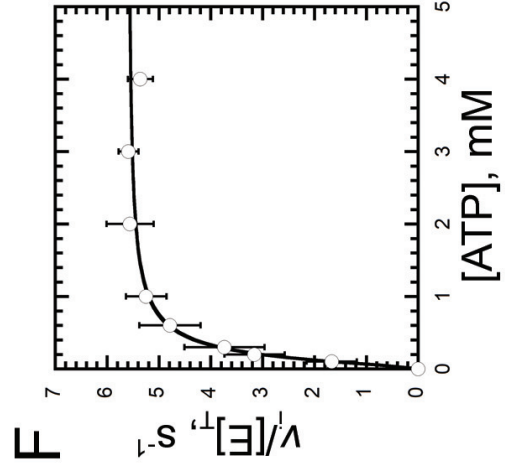
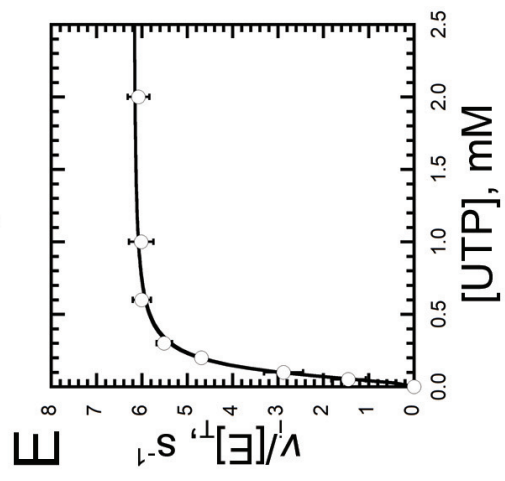
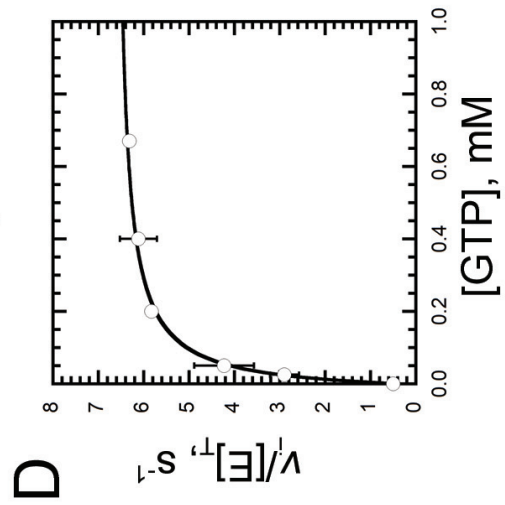
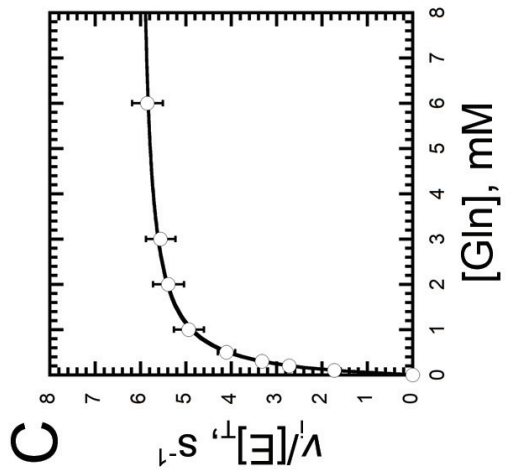
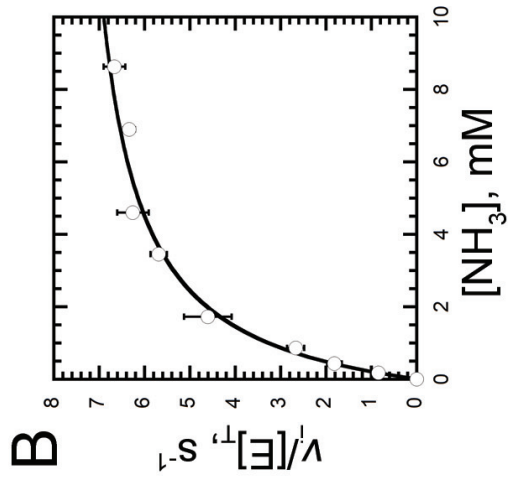
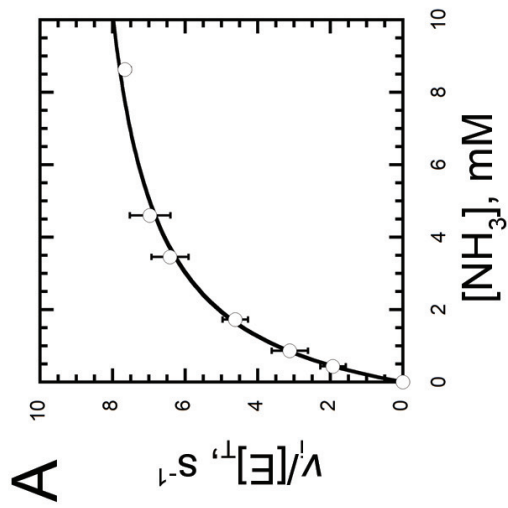


Figure A.6. Steady-state kinetic characterization of wild-type *Ec*CTPS. The kinetic parameters for (A) NH_4Cl -, (B) NH_4OAc -, (C) glutamine-, (D) GTP-, (E) UTP-, and (F) ATP-dependent CTP production. Reactions were performed with wild-type *Ec*CTPS with saturating concentrations of ligands, except where indicated (Table 2.2). These data are the averages of three independent experiments \pm SD and are fitted to eqn. 2.1, 2.2, and 2.3, as stated in **section 2.4**. Values for K_m , k_{cat} , k_{cat}/K_m , $[\text{S}]_{0.5}$, $V_{\text{max}}/[\text{E}]_{\text{T}}$, n , K_A , k_{act} and k_o are given in Tables 5.2 and 5.3. Additional experimental details are found in **section 5.2.2**.

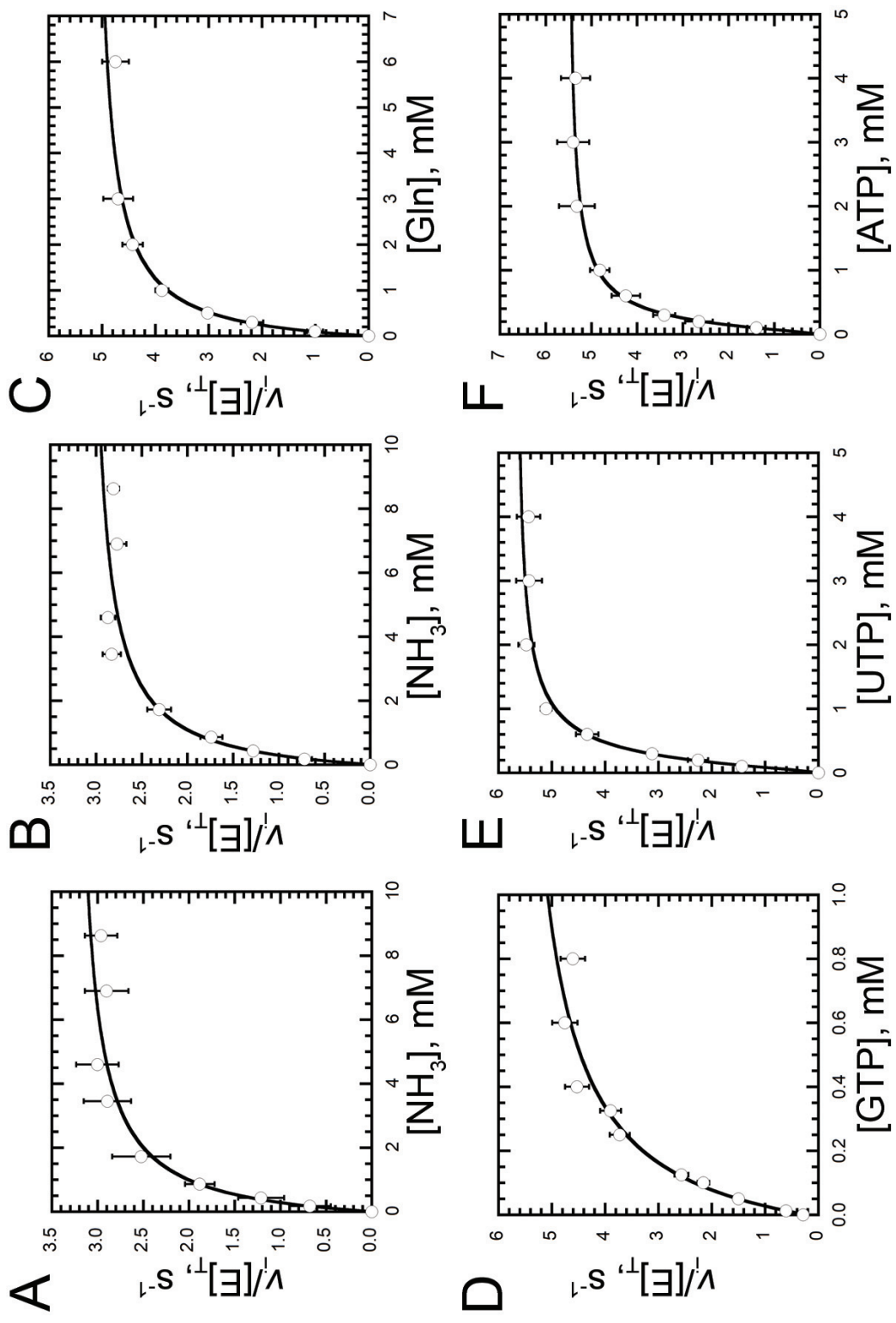


Figure A.7. Steady-state kinetic characterization of V60A *Ec*CTPS. The kinetic parameters for (A) NH_4Cl -, (B) NH_4OAc -, (C) glutamine-, (D) GTP-, (E) UTP-, and (F) ATP-dependent CTP production. Reactions were performed with V60A *Ec*CTPS with saturating concentrations of ligands, except where indicated (Table 2.2). These data are the averages of three independent experiments \pm SD and are fitted to eqn. 2.1, 2.2, and 2.3, as stated in **section 2.4**. Values for K_m , k_{cat} , k_{cat}/K_m , $[\text{S}]_{0.5}$, $V_{\text{max}}/[\text{E}]_T$, n , K_A , k_{act} and k_o are given in Tables 5.2 and 5.3. Additional experimental details are found in **section 5.2.2**.

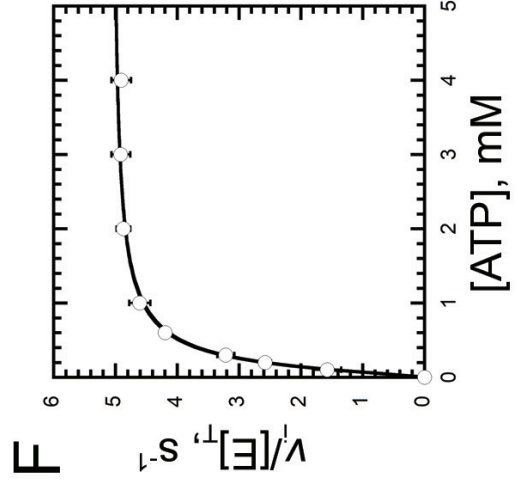
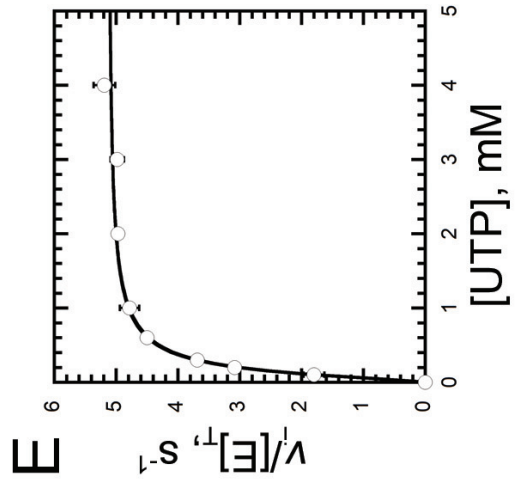
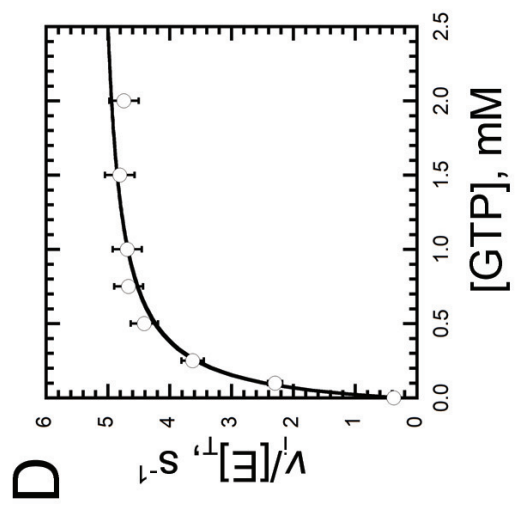
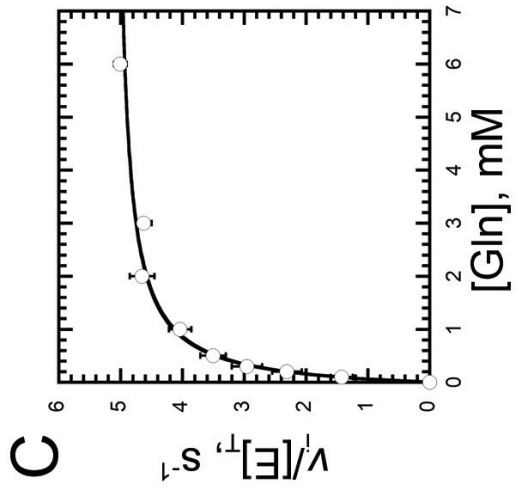
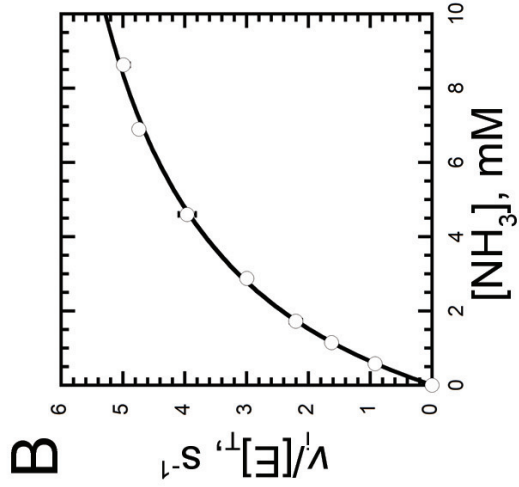
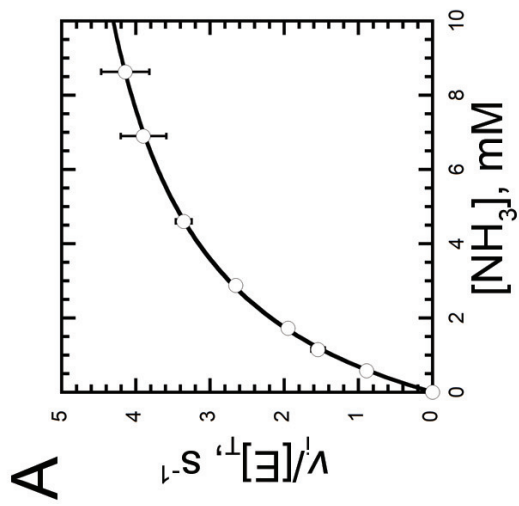


Figure A.8. Steady-state kinetic characterization of V60C *Ec*CTPS. The kinetic parameters for (A) NH₄Cl-, (B) NH₄OAc-, (C) glutamine-, (D) GTP-, (E) UTP-, and (F) ATP-dependent CTP production. Reactions were performed with V60C *Ec*CTPS with saturating concentrations of ligands, except where indicated (Table 2.2). These data are the averages of three independent experiments \pm SD and are fitted to eqn. 2.1, 2.2, and 2.3, as stated in **section 2.4**. Values for K_m , k_{cat} , k_{cat}/K_m , $[S]_{0.5}$, $V_{max}/[E]_T$, n , K_A , k_{act} and k_o are given in Tables 5.2 and 5.3. Additional experimental details are found in **section 5.2.2**.

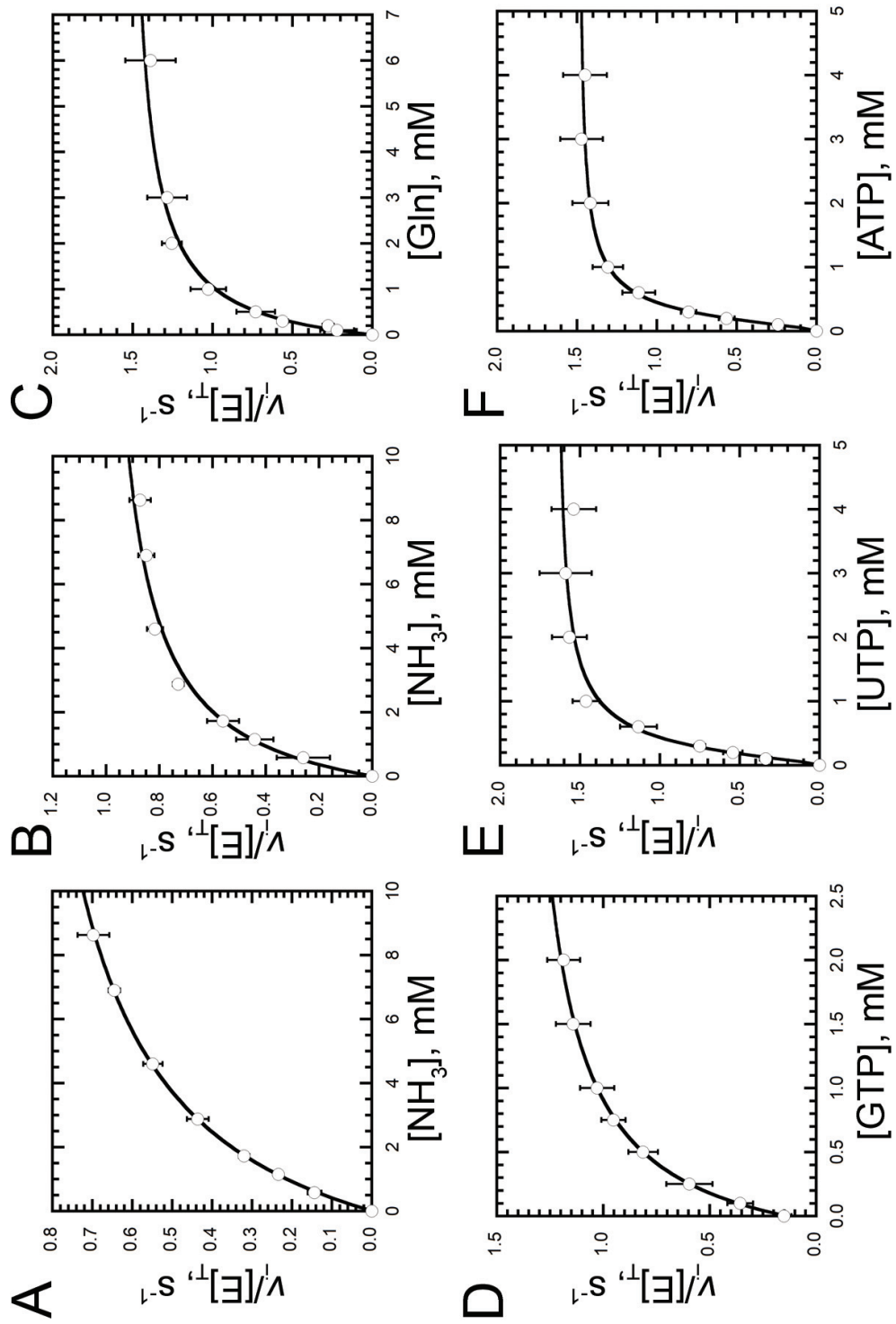


Figure A.9. Steady-state kinetic characterization of V60D *Ec*CTPS. The kinetic parameters for (A) NH_4Cl -, (B) NH_4OAc -, (C) glutamine-, (D) GTP-, (E) UTP-, and (F) ATP-dependent CTP production. Reactions were performed with V60D *Ec*CTPS with saturating concentrations of ligands, except where indicated (Table 2.2). These data are the averages of three independent experiments \pm SD and are fitted to eqn. 2.1, 2.2, and 2.3, as stated in **section 2.4**. Values for K_m , k_{cat} , k_{cat}/K_m , $[\text{S}]_{0.5}$, $V_{\text{max}}/[\text{E}]_{\text{T}}$, n , K_A , k_{act} and k_o are given in Tables 5.2 and 5.3. Additional experimental details are found in **section 5.2.2**.

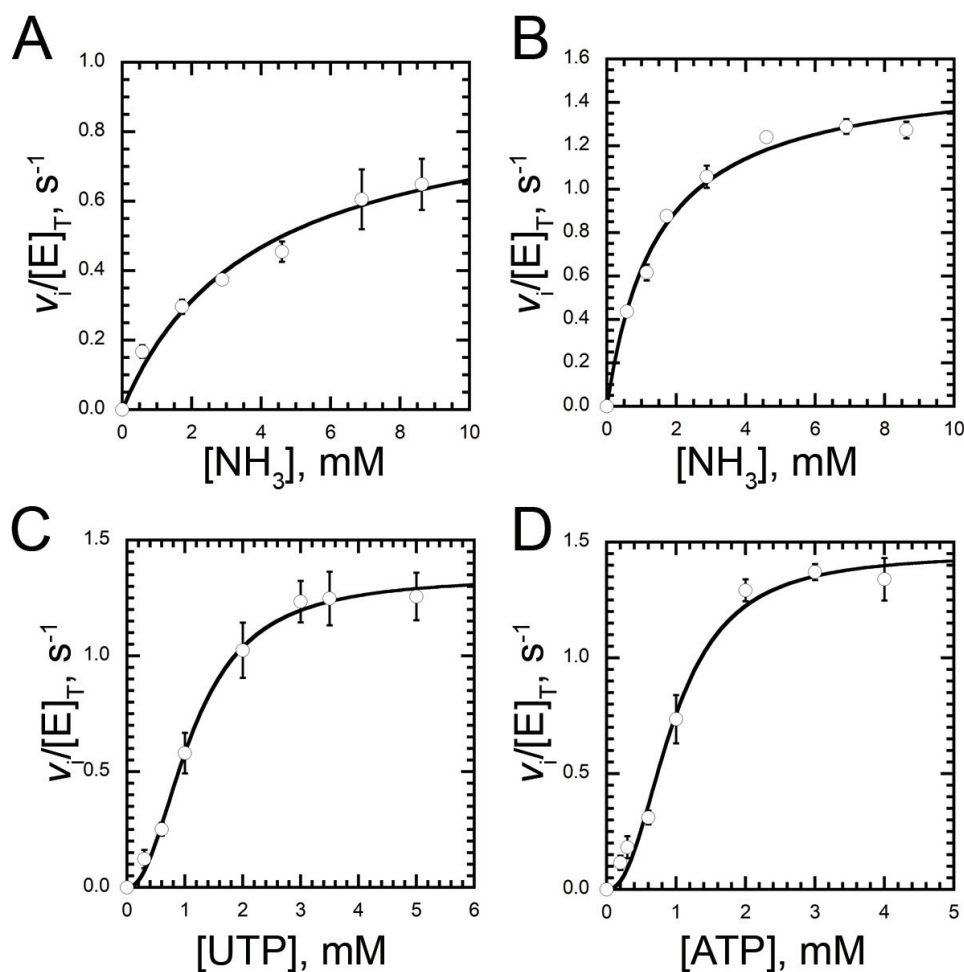


Figure A.10. Steady-state kinetic characterization of V60W *EcCTPS*. The kinetic parameters for (A) NH_4Cl -, (B) NH_4OAc -, (C) UTP-, and (D) ATP-dependent CTP production. Reactions were performed with V60W *EcCTPS* with saturating concentrations of ligands, except where indicated (Table 2.2). UTP- and ATP-dependent kinetics were monitored using NH_4OAc (150 mM) as the substrate. These data are the averages of three independent experiments \pm SD and are fitted to eqn. 2.1 and 2.3, as stated in **section 2.4**. Values for K_m , k_{cat} , k_{cat}/K_m , $[\text{S}]_{0.5}$, $V_{\text{max}}/[E]_T$, n , K_A , k_{act} and k_o are given in Tables 5.2 and 5.3. Additional experimental details are found in **section 5.2.2**.

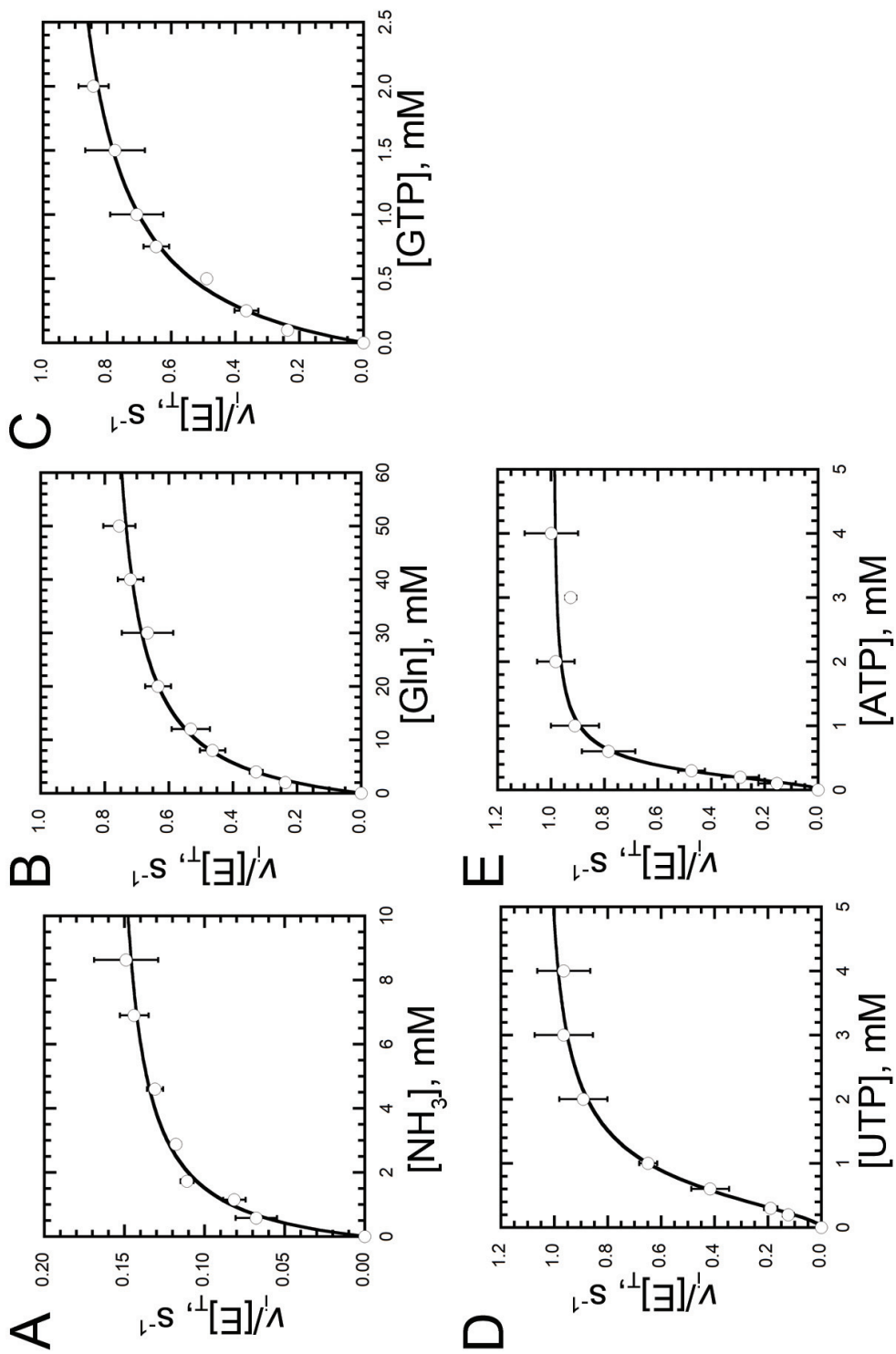


Figure A.11. Steady-state kinetic characterization of V60F *Ec*CTPS. The kinetic parameters for (A) NH₄OAc-, (B) glutamine-, (C) GTP-, (D) UTP-, and (E) ATP-dependent CTP production. Reactions were performed with V60F *Ec*CTPS with saturating concentrations of ligands, except where indicated (Table 2.2). NH₄OAc-dependent kinetics were assayed in the presence of GTP (1.0 mM). These data are the averages of three independent experiments \pm SD and are fitted to eqn. 2.1, 2.2, and 2.3, as stated in **section 2.4**. Values for K_m , k_{cat} , k_{cat}/K_m , $[S]_{0.5}$, $V_{max}/[E]_T$, n , K_A , and k_{act} are given in Tables 5.2 and 5.3. Additional experimental details are found in **section 5.2.2**.

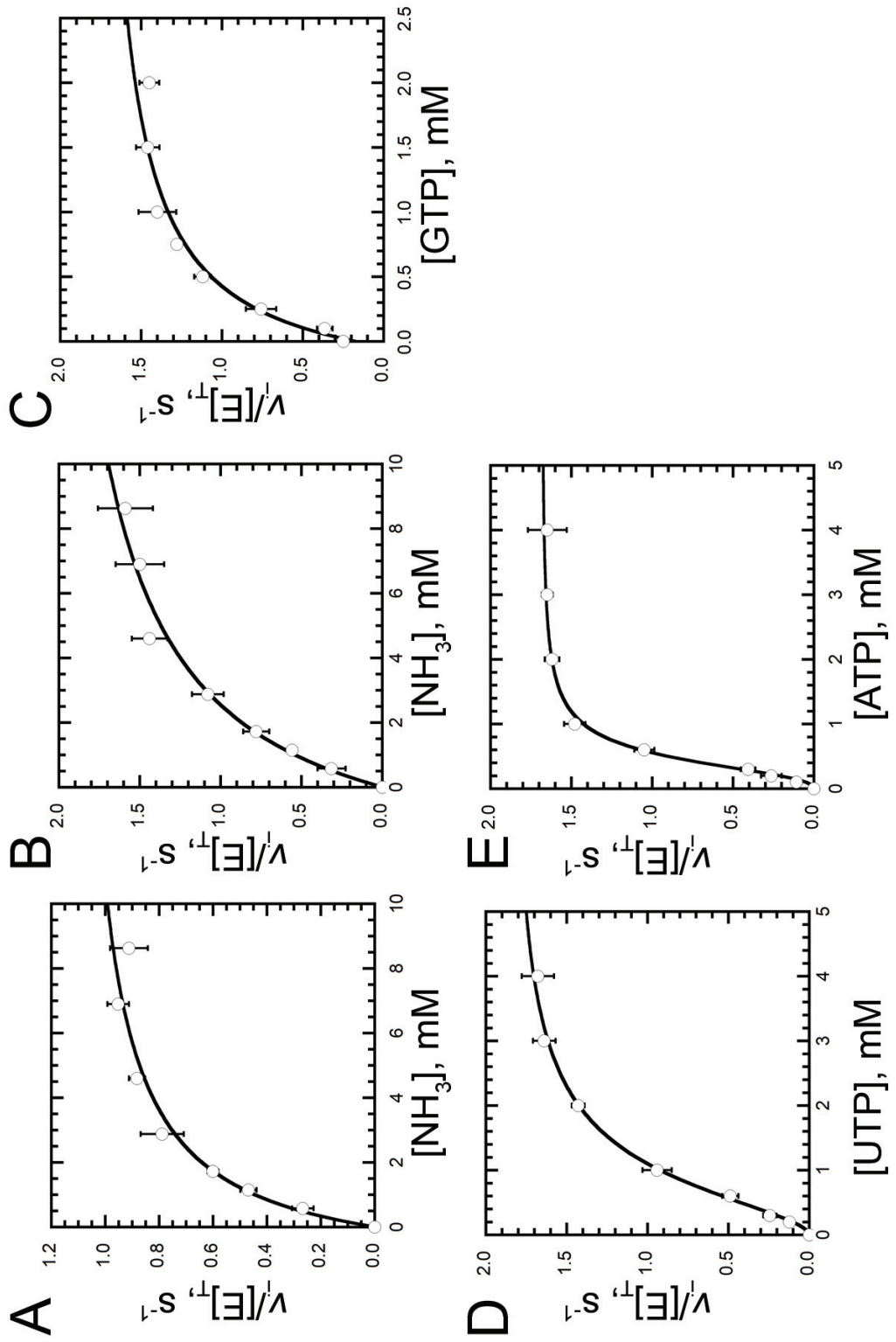


Figure A.12. Steady-state kinetic characterization of DON-V60F *Ec*CTPS. The kinetic parameters for (A) NH₄Cl-, (B) NH₄OAc-, (C) glutamine-, (D) GTP-, (E) UTP-, and (F) ATP-dependent CTP production. Reactions were performed with DON-V60F *Ec*CTPS with saturating concentrations of ligands, except where indicated (Table 2.2). NH₄Cl- and NH₄OAc-dependent kinetics were assayed in the presence of GTP (1.0 mM). UTP- and ATP-dependent kinetics were assayed using NH₄OAc (150 mM) as the substrate. These data are the averages of three independent experiments \pm SD and are fitted to eqn. 2.1, 2.2, and 2.3, as stated in **section 2.4**. Values for K_m , k_{cat} , k_{cat}/K_m , $[S]_{0.5}$, $V_{max}/[E]_T$, n , K_A , k_{act} and k_o are given in Tables 5.2 and 5.3. Additional experimental details are found in **section 5.2.2**.

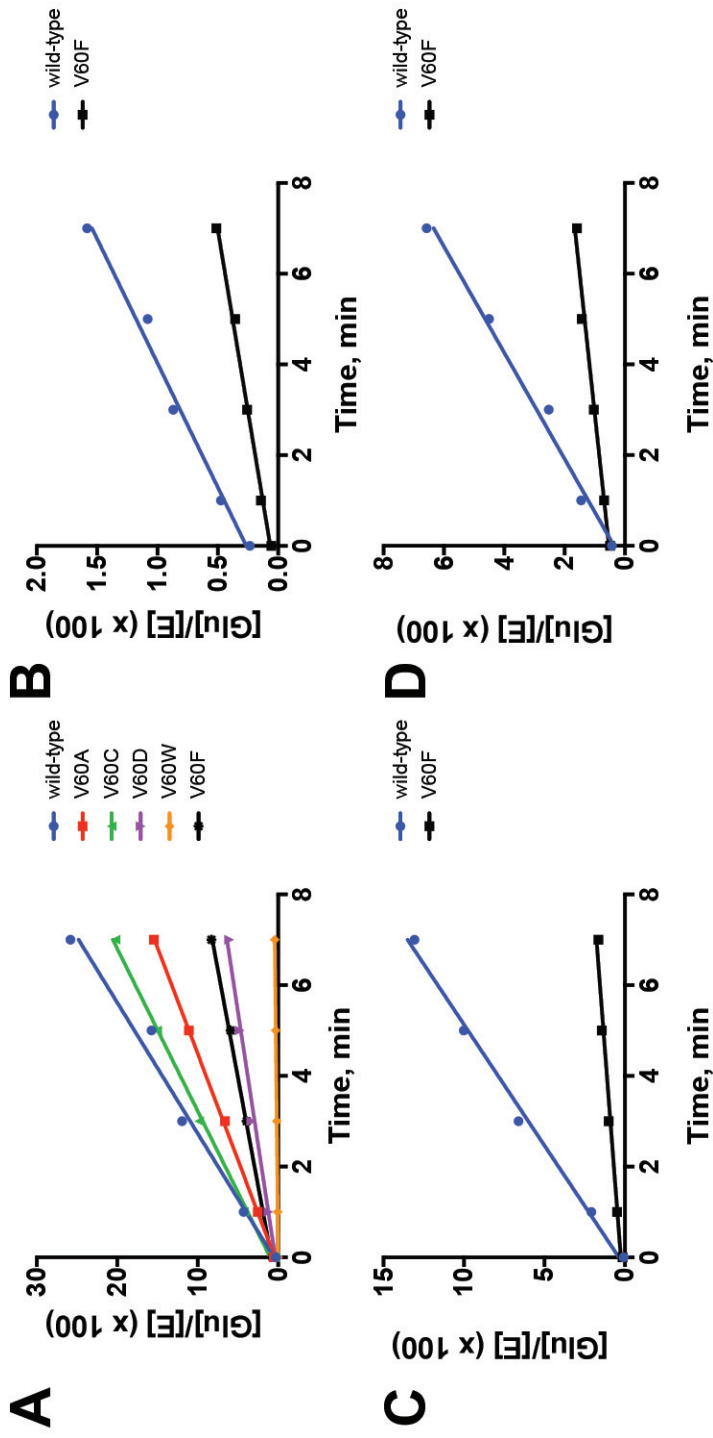


Figure A.13. Kinetic determination of the GATase activity for wild-type and Val 60-substituted *EcCTPS* variants. Glutamate production was measured at concentrations of Gln that were saturating (**A**), near K_m (**B**), and sub-saturating (**C**), as well as saturating concentrations of Gln but with GTP reduced 5-fold below the K_A (0.006 mM, wild-type; 0.06 mM, V60F). Ligand concentrations were otherwise kept at saturation unless otherwise stated. Values of $v_i/[E]_T$ were determined from the slopes of the lines, and are provided in Tables 5.4 and 5.5. Plots are representative of three independent experiments. Additional experimental details are found in **section 5.2.3**.

APPENDIX B

JOHN WILEY AND SONS LICENSE TERMS AND CONDITIONS

Feb 15, 2018

This Agreement between Mr. Gregory McCluskey ("You") and John Wiley and Sons ("John Wiley and Sons") consists of your license details and the terms and conditions provided by John Wiley and Sons and Copyright Clearance Center.

License Number	4290331064596
License date	Feb 15, 2018
Licensed Content Publisher	John Wiley and Sons
Licensed Content Publication	ChemBioChem
Licensed Content Title	Exploring the Potent Inhibition of CTP Synthase by Gemcitabine-5'-Triphosphate
Licensed Content Author	Gregory D. McCluskey, Samy Mohamady, Scott D. Taylor, Stephen L. Bearne
Licensed Content Date	Nov 16, 2016
Licensed Content Pages	10
Type of use	Dissertation/Thesis
Requestor type	Author of this Wiley article
Format	Print and electronic
Portion	Full article
Will you be translating?	No
Title of your thesis / dissertation	Investigation of Inhibition, Filament Formation, and Inter-Domain Ammonia Channelling of CTP Synthase
Expected completion date	Mar 2018
Expected size (number of pages)	250
Requestor Location	Mr. Gregory McCluskey 1521 LeMarchant St 9C Halifax, NS B3H3R3 Canada Attn: Mr. Gregory McCluskey
Publisher Tax ID	EU826007151
Total	0.00 CAD
Terms and Conditions	

TERMS AND CONDITIONS

This copyrighted material is owned by or exclusively licensed to John Wiley & Sons, Inc. or one of its group companies (each a "Wiley Company") or handled on behalf of a society with which a Wiley Company has exclusive publishing rights in relation to a particular work (collectively "WILEY"). By clicking "accept" in connection with completing this licensing transaction, you agree that the following terms and conditions apply to this transaction (along with the billing and payment terms and conditions established by the Copyright Clearance Center Inc., ("CCC's Billing and Payment terms and conditions"), at the time that you opened your RightsLink account (these are available at any time at <http://myaccount.copyright.com>).

Terms and Conditions

- The materials you have requested permission to reproduce or reuse (the "Wiley Materials") are protected by copyright.
- You are hereby granted a personal, non-exclusive, non-sub licensable (on a stand-alone basis), non-transferable, worldwide, limited license to reproduce the Wiley Materials for the purpose specified in the licensing process. This license, **and any CONTENT (PDF or image file) purchased as part of your order**, is for a one-time use only and limited to any maximum distribution number specified in the license. The first instance of republication or reuse granted by this license must be completed within two years of the date of the grant of this license (although copies prepared before the end date may be distributed thereafter). The Wiley Materials shall not be used in any other manner or for any other purpose, beyond what is granted in the license. Permission is granted subject to an appropriate acknowledgement given to the author, title of the material/book/journal and the publisher. You shall also duplicate the copyright notice that appears in the Wiley publication in your use of the Wiley Material. Permission is also granted on the understanding that nowhere in the text is a previously published source acknowledged for all or part of this Wiley Material. Any third party content is expressly excluded from this permission.
- With respect to the Wiley Materials, all rights are reserved. Except as expressly granted by the terms of the license, no part of the Wiley Materials may be copied, modified, adapted (except for minor reformatting required by the new Publication), translated, reproduced, transferred or distributed, in any form or by any means, and no derivative works may be made based on the Wiley Materials without the prior permission of the respective copyright owner. **For STM Signatory Publishers clearing permission under the terms of the [STM Permissions Guidelines](#) only, the terms of the license are extended to include subsequent editions and for editions in other languages, provided such editions are for the work as a whole in situ and does not involve the separate exploitation of the permitted figures or extracts**, You may not alter, remove or suppress in any manner any copyright,

trademark or other notices displayed by the Wiley Materials. You may not license, rent, sell, loan, lease, pledge, offer as security, transfer or assign the Wiley Materials on a stand-alone basis, or any of the rights granted to you hereunder to any other person.

- The Wiley Materials and all of the intellectual property rights therein shall at all times remain the exclusive property of John Wiley & Sons Inc, the Wiley Companies, or their respective licensors, and your interest therein is only that of having possession of and the right to reproduce the Wiley Materials pursuant to Section 2 herein during the continuance of this Agreement. You agree that you own no right, title or interest in or to the Wiley Materials or any of the intellectual property rights therein. You shall have no rights hereunder other than the license as provided for above in Section 2. No right, license or interest to any trademark, trade name, service mark or other branding ("Marks") of WILEY or its licensors is granted hereunder, and you agree that you shall not assert any such right, license or interest with respect thereto
- NEITHER WILEY NOR ITS LICENSORS MAKES ANY WARRANTY OR REPRESENTATION OF ANY KIND TO YOU OR ANY THIRD PARTY, EXPRESS, IMPLIED OR STATUTORY, WITH RESPECT TO THE MATERIALS OR THE ACCURACY OF ANY INFORMATION CONTAINED IN THE MATERIALS, INCLUDING, WITHOUT LIMITATION, ANY IMPLIED WARRANTY OF MERCHANTABILITY, ACCURACY, SATISFACTORY QUALITY, FITNESS FOR A PARTICULAR PURPOSE, USABILITY, INTEGRATION OR NON-INFRINGEMENT AND ALL SUCH WARRANTIES ARE HEREBY EXCLUDED BY WILEY AND ITS LICENSORS AND WAIVED BY YOU.
- WILEY shall have the right to terminate this Agreement immediately upon breach of this Agreement by you.
- You shall indemnify, defend and hold harmless WILEY, its Licensors and their respective directors, officers, agents and employees, from and against any actual or threatened claims, demands, causes of action or proceedings arising from any breach of this Agreement by you.
- IN NO EVENT SHALL WILEY OR ITS LICENSORS BE LIABLE TO YOU OR ANY OTHER PARTY OR ANY OTHER PERSON OR ENTITY FOR ANY SPECIAL, CONSEQUENTIAL, INCIDENTAL, INDIRECT, EXEMPLARY OR PUNITIVE DAMAGES, HOWEVER CAUSED, ARISING OUT OF OR IN CONNECTION WITH THE DOWNLOADING, PROVISIONING, VIEWING OR USE OF THE MATERIALS REGARDLESS OF THE FORM OF ACTION, WHETHER FOR BREACH OF CONTRACT, BREACH OF WARRANTY, TORT, NEGLIGENCE, INFRINGEMENT OR OTHERWISE (INCLUDING, WITHOUT LIMITATION, DAMAGES BASED ON LOSS OF PROFITS, DATA, FILES, USE, BUSINESS OPPORTUNITY OR CLAIMS OF THIRD PARTIES),

AND WHETHER OR NOT THE PARTY HAS BEEN ADVISED OF THE POSSIBILITY OF SUCH DAMAGES. THIS LIMITATION SHALL APPLY NOTWITHSTANDING ANY FAILURE OF ESSENTIAL PURPOSE OF ANY LIMITED REMEDY PROVIDED HEREIN.

- Should any provision of this Agreement be held by a court of competent jurisdiction to be illegal, invalid, or unenforceable, that provision shall be deemed amended to achieve as nearly as possible the same economic effect as the original provision, and the legality, validity and enforceability of the remaining provisions of this Agreement shall not be affected or impaired thereby.
- The failure of either party to enforce any term or condition of this Agreement shall not constitute a waiver of either party's right to enforce each and every term and condition of this Agreement. No breach under this agreement shall be deemed waived or excused by either party unless such waiver or consent is in writing signed by the party granting such waiver or consent. The waiver by or consent of a party to a breach of any provision of this Agreement shall not operate or be construed as a waiver of or consent to any other or subsequent breach by such other party.
- This Agreement may not be assigned (including by operation of law or otherwise) by you without WILEY's prior written consent.
- Any fee required for this permission shall be non-refundable after thirty (30) days from receipt by the CCC.
- These terms and conditions together with CCC's Billing and Payment terms and conditions (which are incorporated herein) form the entire agreement between you and WILEY concerning this licensing transaction and (in the absence of fraud) supersedes all prior agreements and representations of the parties, oral or written. This Agreement may not be amended except in writing signed by both parties. This Agreement shall be binding upon and inure to the benefit of the parties' successors, legal representatives, and authorized assigns.
- In the event of any conflict between your obligations established by these terms and conditions and those established by CCC's Billing and Payment terms and conditions, these terms and conditions shall prevail.
- WILEY expressly reserves all rights not specifically granted in the combination of (i) the license details provided by you and accepted in the course of this licensing transaction, (ii) these terms and conditions and (iii) CCC's Billing and Payment terms and conditions.
- This Agreement will be void if the Type of Use, Format, Circulation, or Requestor Type was misrepresented during the licensing process.

- This Agreement shall be governed by and construed in accordance with the laws of the State of New York, USA, without regards to such state's conflict of law rules. Any legal action, suit or proceeding arising out of or relating to these Terms and Conditions or the breach thereof shall be instituted in a court of competent jurisdiction in New York County in the State of New York in the United States of America and each party hereby consents and submits to the personal jurisdiction of such court, waives any objection to venue in such court and consents to service of process by registered or certified mail, return receipt requested, at the last known address of such party.

WILEY OPEN ACCESS TERMS AND CONDITIONS

Wiley Publishes Open Access Articles in fully Open Access Journals and in Subscription journals offering Online Open. Although most of the fully Open Access journals publish open access articles under the terms of the Creative Commons Attribution (CC BY) License only, the subscription journals and a few of the Open Access Journals offer a choice of Creative Commons Licenses. The license type is clearly identified on the article.

The Creative Commons Attribution License

The [Creative Commons Attribution License \(CC-BY\)](#) allows users to copy, distribute and transmit an article, adapt the article and make commercial use of the article. The CC-BY license permits commercial and non-

Creative Commons Attribution Non-Commercial License

The [Creative Commons Attribution Non-Commercial \(CC-BY-NC\)License](#) permits use, distribution and reproduction in any medium, provided the original work is properly cited and is not used for commercial purposes.(see below)

Creative Commons Attribution-Non-Commercial-NoDerivs License

The [Creative Commons Attribution Non-Commercial-NoDerivs License](#) (CC-BY-NC-ND) permits use, distribution and reproduction in any medium, provided the original work is properly cited, is not used for commercial purposes and no modifications or adaptations are made. (see below)

Use by commercial "for-profit" organizations

Use of Wiley Open Access articles for commercial, promotional, or marketing purposes requires further explicit permission from Wiley and will be subject to a fee.

Further details can be found on Wiley Online

Library <http://olabout.wiley.com/WileyCDA/Section/id-410895.html>

Other Terms and Conditions:

v1.10 Last updated September 2015

Questions? customercare@copyright.com or +1-855-239-3415 (toll free in the US) or +1-978-646-2777.